US Army Corps of Engineers

Performance Evaluation of the New Orleans and Southeast Louisiana Hurricane Protection System

Final Report of the Interagency Performance Evaluation Task Force

Volume VIII – Engineering and Operational Risk and Reliability Analysis

June 2008

DRAFT FINAL

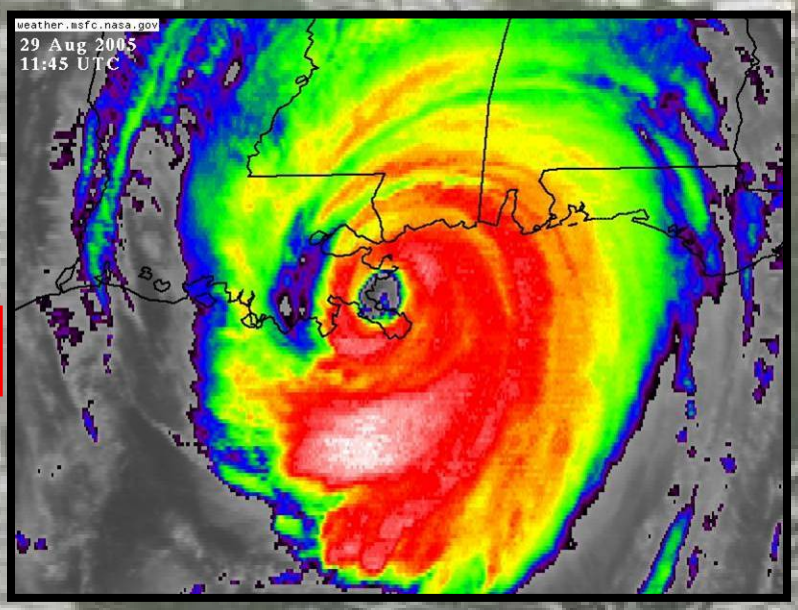

Volume I – Executive Summary and Overview
Volume II – Geodetic Vertical and Water Level Datums
Volume III – The Hurricane Protection System
Volume IV – The Storm
Volume V – The Performance – Levees and Floodwalls
Volume VI – The Performance – Interior Drainage and Pumping
Volume VII – The Consequences
Volume VIII – Engineering and Operational Risk and Reliability Analysis
Volume IX – General Appendices

Volume VIII
Engineering and Operational Risk and Reliability Analysis

Contents

Executive Summary VIII-1

Why Use Risk Assessment? VIII-1
What Is Risk? VIII-2
Why Use Risk Assessment for Hurricane Protection? VIII-2
What Risk Assessment Is Not VIII-3
Mission of the IPET Risk Team VIII-3
Risk Assessment Process VIII-5
Risk Assessment of New Orleans and Vicinity VIII-6
Results VIII-6

Risk Team Members VIII-8

Co-Leads VIII-8
Headquarters Liaison VIII-8
Members VIII-8

Scope of the Assessment VIII-10

Overview VIII-12

Risk Analysis Methodology VIII-14

Initial Assumptions and Constraints VIII-14
Defining the HPS VIII-15
Analysis Boundaries *VIII-18*
Physical Description of the HPS *VIII-19*
Classifying the Components of the HPS *VIII-20*
HPS Model for Risk Analysis *VIII-35*

Hazard Definition VIII-45

Estimation of Probabilities of Maximum Surges VIII-45
JPM-Optimal Sampling (JPM-OS) VIII-51
Construction of Extended Storm Tracks for Wave Predictions VIII-53
The Effect of Time Variations in the Parameter Set *VIII-54*
Estimation of Maximum Wave Conditions VIII-68
Construction of Surge Hydrographs VIII-68
Filtering of Hydrographs *VIII-69*
Calculating Duration Parameters *VIII-72*
Estimating Wave Hydrographs *VIII-79*
Investigating the Effects of Climate Variability on Surge Levels *VIII-79*

Risk Modeling VIII-82
Event Tree Development VIII-82
Initiating Event VIII-83
Gates and Closures Events VIII-84
Overtopping Events VIII-84
Breaching Events VIII-85
Breach Parameters VIII-86
Breach without Overtopping VIII-86
Breach During an Overtopping Event VIII-87
Rainfall and Pumping Events VIII-87
Branch and Sub-Basin Water Volumes VIII-93
Sub-basin Interflow VIII-94
Reliability Analysis VIII-96
Failure and Failure Modes VIII-96
HPS Systems Definition VIII-97
Reaches VIII-98
Fragility Curves VIII-98
Uncertainties VIII-99
Geological Profile and Soil Conditions *VIII-102*
Soil Engineering Properties *VIII-103*
Uncertainty Model *VIII-104*
Spatial Variation *VIII-107*
Measurement Noise *VIII-108*
Statistical Error *VIII-109*
Measurement Model Bias (systematic error) *VIII-109*
Fragility Curves VIII-109
No Overtopping *VIII-110*
Best Estimate Calculations *VIII-111*
Uncertainty in Realized Factor of Safety *VIII-112*
Seepage *VIII-113*
Length Effect *VIII-113*
Wave Runup *VIII-114*
I-Wall Fragility, No Overtopping *VIII-115*
Levee and I-Wall Fragility, With Overtopping *VIII-116*
Transitions and Point Structures *VIII-117*
Pumping Stations *VIII-117*
Consequences VIII-118
Life Loss Estimation VIII-119
Direct Property Loss Estimation VIII-119
Uncertainty Analysis VIII-122
Uncertainty Taxonomy VIII-122
Approach VIII-123
Hurricane Analysis Uncertainty VIII-125

Hurricane Surge/Wave Model Uncertainty VIII-127
Reliability Analysis Uncertainty VIII-128
Uncertainty Quantification VIII-130
Conclusion of the Uncertainty Analysis VIII-132

Risk Analysis Results VIII-133

50-Year Flood Event VIII-134
Flood Risk *VIII-134*
Life Loss Risk *VIII-134*
Property Loss Risk *VIII-134*
100-Year Flood Event VIII-135
Flood Risk *VIII-135*
Life Loss Risk *VIII-135*
Property Loss Risk *VIII-136*
500-Year Flood Event VIII-136
Flood Risk *VIII-136*
Life Loss Risk *VIII-137*
Property Loss Risk *VIII-137*
Summary of Results VIII-138

Conclusions VIII-140

References VIII-203

Appendix 1. Terminology

Appendix 2. New Orleans East Basin

Appendix 3. Jefferson Basin

Appendix 4. St. Charles Basin

Appendix 5. Plaquemines Basin

Appendix 6. St. Bernard Basin

Appendix 7. Orleans Basin

Appendix 8. Hazard Analysis

Appendix 9. Risk Methodology

Appendix 10. Reliability Modeling

Appendix 11. Uncertainty Analysis

Appendix 12. Consequences

Appendix 13. Risk Analysis Results

Appendix 14. Hurricane Protection System

Appendix 15. Computational Methodology

Executive Summary

Volume VIII (*Engineering and Operational Risk and Reliability Analysis*) of the Interagency Performance Evaluation Taskforce (IPET) report provides an overview of the risk assessment performed to determine the vulnerability of New Orleans and vicinity to flooding from hurricanes and to estimate the difference in risk, by location, for the pre-Katrina hurricane protection system (HPS) conditions and the post-Katrina (June 2007) HPS conditions. The risk assessment process, its application, and a presentation and discussion of results are presented in detail in the Appendices.

It is important to note that this effort involved developing and applying a prototype method to estimate risk for a large, complex, and geographically distributed system. In many respects, this is a first effort of its kind and represents the beginning of what is possible in the future. Efforts have been made to develop a logical and effective method that provides information useful for informing stakeholders of potential risks and for supporting investment decisions for risk reduction. The method is intended to generate reasonable and useful results; however, it should be understood that the results of any application of a large set of sophisticated models to a complex issue such as hurricane protection comes with associated uncertainty. An effort has been made to quantify that uncertainty, step by step through the process, to allow users of this information to better understand its limits.

Why Use Risk Assessment?

Risk is a concept that influences much of our lives but remains an emerging tool in many areas of water resources management. The insurance industry uses risk to set rates, businesses assess market risk, and the financial and stock markets are literally real-time risk assessments from millions of individuals who participate in the market. In water resources, risk has primarily been a tool applied to dam safety. Although similar, application of risk methods to a hurricane protection system such as the one in New Orleans is more complex because of the large geographical area, hundreds of miles of different types of structures, a wide range of conditions (soils, elevations, etc.), and the complex nature of hurricanes and the forces they can generate. It is important that the term risk and the way it is used in this study are clearly defined. One of the most difficult issues with risk is communicating the information itself.

A significant part of the Risk Team's effort was focused on developing a systems risk assessment of the capability of the HPS with regard to future hurricanes. The objective is to understand the risk to health and safety of people and property in New Orleans and vicinity. To put the current level of risk in perspective, the IPET assessment examined risk for the HPS as it

existed before Katrina and for the HPS after repairs and initial upgrades were accomplished by June 2007. This is the first time an engineering-based risk assessment has been used to look at such a large, geographically distributed, and complex water protection system. As such, this is a prototype effort and the methods and results should be considered prototypes.

What Is Risk?

People use the term "risk" in different ways. In this analysis for New Orleans, risk is defined as the chance of failure of a component of the HPS happening during a storm event, multiplied by the consequences of that failure. In New Orleans, failure leads to flooding, and the consequences of that flooding are loss of life and loss of property. High risk can exist due to being very vulnerable to flooding or from having the potential to incur catastrophic losses of lives or economic value when flooding occurs. An example of areas of high risk would be one that has poor protection, a large population, and many structures prone to flooding.

According to the National Highway Transportation Safety Administration (using 2004 data), an individual in the United States has an annual risk of losing his or her life in a traffic accident of 0.00015, which is 15 fatalities per 100,000 residents, or 1.4 fatalities for every 100 million miles traveled, under current patterns of driving. The chance of being in an accident is much greater, since not every accident involves fatalities. Statistics like this represent averages and are not necessarily representative of the risk one faces. For example, in Louisiana there are 2.03 fatalities per 100 million miles driven, making it higher risk than the national average. Within Louisiana, New Orleans has a traffic fatality risk 50 percent higher than Baton Rouge. These numbers are influenced by the amount of traffic, the condition and safety of the roads, traffic management, and simply reflect the history of accidents in the region.

We as individuals accept risk every time we get into a car. We also make risk-based decisions. We know that our risk is reduced in some vehicles compared to others. Air bags and seat belts, while not preventing accidents, reduce injury and deaths when an accident occurs. We can buy a safer car and buckle up when we drive. We can also choose to use public transport, which has a lower rate of fatalities-per-mile than do cars.

The situation is the same with hurricane protection. Risk can be reduced by having stronger physical protection and, thereby, reducing the probability of flooding; or by managing development in areas that have a high chance of being flooded, thereby reducing the consequences of flooding. We can also make personal choices such as living in an area with a lower chance of flooding, elevating our homes so the consequences of flooding are less, or having an effective evacuation plan to take ourselves out of harm's way.

Why Use Risk Assessment for Hurricane Protection?

Much like risk statistics for cars, risk assessment for the hurricane protection system of New Orleans and southeast Louisiana—the *Hurricane and Storm Damage Risk Reduction System*—provides a broad picture of the relative chance of flooding in different areas of southeast Louisiana, and of the losses that could occur as a result of flooding. A risk reduction system, however, only protects people to a degree. The risk remaining is called *residual risk* and is a key factor for planning. Residual risk defines how much risk must be managed by other means.

By estimating residual risk for different locations, we know where the greatest problems are, and why. Risk varies with location due to variations in the chance of high surge and wave conditions, the strength and height of the protective structures, the elevations of the land subject to flooding, the numbers of people and structures exposed to flooding, and different emergency response capabilities.

By understanding the sources of risk, directed action can be brought to bear against specific weaknesses. This helps save lives, minimizes property damage, and rank-orders improvement projects. Options such as evacuation planning and improved evacuation routes can be considered alongside more traditional options such as hardening pumping facilities, increasing first-floor elevations, improving land-use zoning, compartmentalizing drainage basins, armoring levees, and building safe harbors.

What Risk Assessment Is Not

Risk assessment is not forecasting, and risk assessments do not reflect the impact of any single storm. Risk assessment is a long-term look at relative vulnerability from the spectrum of storms that can occur, just as car insurance statistics look at long-term averages from the spectrum of driver experiences. Risk assessments do not predict what will happen in a given year, only what could happen based on long-term averages. Risk assessment forecasts the effects of many individual storms and aggregates the results into patterns.

Risk assessment in the current context is intended to support planning decisions. It is not intended to support engineering decisions. A risk assessment over a large, complex geography like New Orleans requires many generalizations and assumptions, compared to the details of engineering design. Nonetheless, while risk assessment does not generate design information, it does inform design by defining hazards and suggesting alternative approaches to providing protection.

Mission of the IPET Risk Team

The mission of the IPET risk and reliability analysis was to examine risks to life and property posed by hurricanes in New Orleans for two conditions: The HPS in place prior to Katrina (pre-Katrina), and the HPS reconstructed after Katrina and as existing in June 2007. The risk analysis considered the expected performance of the many elements of the system and the consequences associated with that performance. The purpose of the analysis was to identify areas protected by the HPS that are vulnerable to flooding, to identify the causes of that vulnerability, and to provide estimates of the frequency of flooding within each area. The comparison of pre-Katrina and current risks was made to understand the effectiveness of the repairs and improvements.

The risk analysis intends to answer the following specific questions concerning the performance of the HPS:

1. What was the reliability of the pre-Katrina HPS for preventing flooding of protected areas given the range of hurricanes expected to impact New Orleans?

2. What is the reliability of the current, post-Katrina HPS for preventing flooding of protected areas given the range of hurricanes expected to impact New Orleans? Specifically, what is the annual rate of occurrence of system failure due to the range of expected hurricane events?

3. What are the annual rates of occurrence of economic consequences and loss of life resulting from failures of the HPS given the range of hurricanes expected to impact New Orleans?

4. What is the uncertainty in these estimates of annual rates of occurrence?

The risk analysis results are intended to provide decision makers with information concerning the vulnerabilities of the 2007 HPS and how potential investments could reduce those vulnerabilities. However, the analysis is not intended to identify final design configurations, or to set design elevations of proposed levees or floodwalls. The hurricane surge and wave studies on which the risk analysis is based are not of the detail required to establish design elevations. Additional detailed hydrologic and engineering studies will be required to make final decisions concerning the most effective HPS configuration to reduce risks and the height of the HPS necessary for future conditions.

The pre-Katrina risk analysis does not attempt to recreate the design intent or knowledge that the designers used to determine the configuration of the HPS. Instead, the risk analysis used design data, engineering parameters, foundation conditions, and additional information gained by IPET through exploration and testing after the hurricane to evaluate the performance of individual components of the system.

The changed, post-Katrina demographics of the local areas protected by the system were not considered when estimating consequences. In some areas, many homes and much of the infrastructure were destroyed by the hurricane, and some homes and infrastructure may not be rebuilt. Therefore, the pre-Katrina populations and property values were impacted and will have to be considered in future analyses, but to provide a consistent basis for comparison they were not considered here. Were different demographics used in the two cases studied, risk reductions would have been found just from the fewer protected people and lesser protected property inside the HPS.

Evacuation and emergency action planning can have a significant impact on loss of life. The actual evacuation experienced during Katrina was effective and could have been used as a calibration example for the use of evacuation effectiveness in the risk analysis. However, the loss of life estimates presented herein does not consider the specific evacuation effectiveness during Katrina. A mean value of a distribution of evacuation effectiveness was used to determine loss of life estimates; therefore, the loss predictions should be considered to be potential losses and not actual loss predictions. Consequence information used in the risk analysis was provided by the Consequence Team, as reported in *IPET Volume VII* (USACE 2006).

Risk refers to expected losses in lives and dollars, calculated by multiplying the probability of system failure by the consequences associated with that failure. In order to compare the performance of the pre- and post-Katrina systems, frequency of inundation was used as the

primary measure of effectiveness. Risk-based inundation mapping and associated stage–frequency curves are intended for estimating relative risks for the purpose of identifying areas of vulnerability. These estimates should not be compared to inundation mapping conducted under the Federal Emergency Management Agency's (FEMA) National Flood Insurance Program (NFIP); the methods and purposes of the respective analyses are different.

System failure refers to the failure of the HPS to provide protection from flooding in one or more protected areas, and it can be any failure of one or more components, overtopping of walls or levees, or open gates that prevents the HPS from performing its function. The effectiveness of the protection system also depends on how well the operational elements of the system perform. Elements such as road closure structures, gate operations, and pumping plants, which require human operation and proper installation during a flood event, can dramatically impact flood levels. The lessons learned concerning the observed performance of these elements during Katrina were considered in the analysis.

The findings presented herein have been examined to extract principal lessons learned. These lessons learned represent the big picture guidelines that can help shape future policy and practice with regard to understanding and reducing risk for New Orleans as well as other areas impacted by serious natural hazards. They deal with both the risk assessment process itself as well as the information and insights that the risk assessment provides for the New Orleans area.

Risk Assessment Process

The risk assessment process required a rigorous data collection effort. The risk assessment was complicated by lack of data, the large geographical area and many components of the HPS being assessed, and need to adapt existing risk methods to this new application. The availability of up-to-date data from a single source would have greatly facilitated this effort. The data collected in the analyses should be maintained and the risk analysis periodically updated.

The definition of the hurricane hazard for the future was the most demanding and complex technical challenge. While it was clear that the historical record is not sufficient, most alternatives were either simple extrapolations of the historical data or too computationally intensive to be practical tools. The Joint Probability Method-Optimal Sampling (JPM-OS) methods developed in this study exploited the value of historical data in conjunction with modern high resolution, physics-based models and high-performance computing to provide a comprehensive definition of the hurricane-generated surge and wave hazards that face New Orleans. The range of hurricanes that were modeled and sampled were less frequent, higher intensity storms, since the purpose of the risk analysis was to determine the vulnerability of the New Orleans HPS. Consideration of more frequent but less intense storms would not have improved understanding of the HPS performance.

The reliability assessment process proved to be a difficult effort due to the vast amount of geologic, structural design, and facility condition data available on the 350 miles of HPS. This included the task of dividing the HPS into reaches of uniform performance potential, estimating the fragility of each reach, transition, and feature; and of handling the complex issue of overtopping and erosion impact on HPS performance. While difficult, the process was necessary to provide a clear picture of system performance.

Consequences were limited to pre-Katrina population and property conditions, but required extrapolation of loss of life through the *LIFESim* model (IPET 2006, Vol. VII 2006). This was essential due to the lack of fatality information that would allow correlations of geography and demographics leading to fatalities.

The overall process used to estimate vulnerability to flooding and consequent risk to life and property generates reasonable results when compared to losses from historical events. Significant uncertainties, however, can be expected in the application of such methods because of the large data sets, sophisticated models, and many steps required to create the risk products.

Risk Assessment of New Orleans and Vicinity

Having a quantitative estimate of vulnerability and risk is important for understanding both the current situation and the relative value of alternative risk reduction measures for the future. The public at large and public officials at all levels benefit by having a common situational awareness of risk. This common picture provides a focus for communication, for current risk reduction measures, and for risks that should be examined for the future.

The 2007 HPS has provided measurable reductions in loss of life and economic risk that are directly relatable to the differences in the character of the 2007 HPS as compared to the pre-Katrina HPS. However, even with an improvement in performance with the 2007 HPS, the overall residual loss of life and economic risk levels for New Orleans remain high for flooding events beyond the 50-year (2%) frequency of occurrence and is extreme for flood events at the 500-year frequency of occurrence. New Orleans remains a region of high risk, and additional risk reduction measures are critical to its recovery and future vitality.

Pumping capabilities, if operational at or above 50% of ideal capacity, can play an important role in reducing vulnerability to flooding and managing risk; however, it is only an effective measure when the volume of flood waters to be managed is minimized by the performance of the HPS.

Results

The effectiveness of repairs and improvements made to the hurricane protection system can best be measured by contrasting predicted inundation probabilities for the pre-Katrina HPS with those for the 2007 HPS. The risk analysis results show that moderate inundation reductions have been achieved for more frequent events of less than 50-year or 2% frequency of occurrence level, but predicted inundation elevations are mostly unchanged for less frequent storms such as 100-year or 1% frequency levels, and 500-year or 0.2% frequency levels; and thus, there is still significant risk of inundation. It follows, therefore, that the consequences are only impacted during more frequent events and are mostly unchanged for infrequent events. Detailed analysis of the results is presented in Appendix 13. Summary examples of the depth maps and consequence maps are provided later in this portion of the report.

New Orleans is widely vulnerable to some flooding at the 50-year or 2% frequency of occurrence level if significant pumping capacity is not available. There is no significant difference in the flood elevations between the pre-Katrina and 2007 HPS at the 2% frequency of

occurrence. This is likely due to the dominance of rainfall as the source of water at this event frequency. If this is true, hurricanes are not the dominant threat to New Orleans at such return period. Pumps operating at a capacity that is equivalent to or greater than the 50% of the nominal capacity of the sub-basins, can have a dramatic impact in reducing flood elevations at 2% frequency of occurrence in a number of the basins. It must be noted that the storm set considered in the hazard analysis only included infrequent storms and that the more frequent tropical storms can result in significantly more rainfall and, therefore, more flooding than 2% frequency inundation shown.

Without pumping, the majority of the New Orleans area remains vulnerable to moderate to deep flooding (greater than 4 ft) at the 100-year or 1% frequency of occurrence. The area with least vulnerability is Jefferson Parish East (JE) and St. Charles Parish (SC) where flood threats are moderate (less than 4 ft). The improvements in the HPS from pre-Katrina to the 2007 HPS have provided significantly reduced flood levels in a few areas, notably portions of Orleans Main (OM) and moderate reductions in the 1% flood level in St. Bernard (SB) and Plaquemines (PL11). Improvements in Orleans Main are largely due to the presence of the new gates and temporary pumps at the ends of the outfall canals. Continued vulnerability of the areas adjacent to the Inner Harbor Navigation Canal (IHNC) can be attributed to the remaining pre-Katrina elevations and significant fragility of the I-walls along the IHNC. Strengthening of the I-walls with stability berms and relief wells has improved the performance of the structures in the IHNC, but they remain unable to cope with surge conditions created by large storms. Pumping capacity equal to or greater than the 50% ideal capacity can have a significant impact on the 1% flood elevations. Primary areas that benefit the most are OM and JE. The sub-basins adjacent to the IHNC remain vulnerable to flooding even when pumping is considered. The West Bank area remains highly vulnerable to flooding with the 2007 HPS, and pumping will likely have little impact until all of the planned protective structures are completed.

Virtually all of New Orleans region remains highly vulnerable to deep and catastrophic flooding at the 500-year or 0.2% flood frequency. The vast majority of the region would experience flooding of greater than 8 ft. There is essentially no difference in the flooding vulnerability at this frequency of occurrence between the pre-Katrina and 2007 HPS. Pumping has no impact at this level of flooding for either the pre-Katrina or the 2007 HPS because of the large amount of overtopping and the fragility of portions of the HPS.

Risk Team Members

The Risk Team comprised more than 30 members from academe, consulting, federal agencies, ERDC and USACE districts. The following served at various times during the study, with area of responsibility:

Co-Leads

Jerry L. Foster, PE	HQUSACE	Project Manager
Bruce Muller, PE	USBR	Assistant Project Manager

Headquarters Liaison

Donald R. Dressler, PE	HQUSACE	Project Sponsor
Anjana Chudgar	HQUSACE	Project Monitor

Members

Bilal M. Ayyub, PhD, PE	UMD	Lead FoRTE Developer
Gregory B. Baecher, PhD	UMD	Geotechnical Reliability
Brian Blanton	UNC	ADCIRC/STWAVE Modeler
David Bowles, PhD	USU	Consequences
Sheree Castain, PG	USACE-NAB	Geotechnical Data Review
Jennifer Chowning	USACE-LRL	GIS Mapping
David Cole, PE	USACE-NAE	System Definition
Robert Dean, PhD	University of Florida	Coastal Engineering
David Descouteax	PE USACE-NAE	System Definition
David Divoky	Watershed Concepts	Lead Hurricane Modeling
Bruce Ellingwood, PhD	Georgia Tech	Technical Review
Alex Garneau, PE	USACE-NAE	System Definition
Brian Glock, PG	USACE-NAB	Geotechnical Data Review
Richalie Griffith	USACE-NAE	System Definitions
H. Wayne Jones	ERDC-ITL	Program Manager
Mark Kaminskiy	PhD UMD	Risk Methodology
Burton Kemp	MVN (Ret.)	Field Geologist
Fredrick Krimgold, PhD	Virginia Tech	Consequences
Therese McAllister, PhD, PE	NIST	Uncertainty & Review
Marty McCann, PhD	JBA	Uncertainty Analysis
William McGill, PE	UMD	Risk Modeler
Robert C. Patev, PE	USACE-NAE	Lead Geotechnical Reliability
Donald T. Resio, PhD	ERDC-CHL	Senior Scientist

David Schaaf, PE	USACE-LRL	System Definition
James Snyder, PG	USACE-NAB	Geotechnical Data Review
Terry Sullivan, PE	USACE-LRL	Field Surveys
Pat Taylor	ERDC-GSL	Field Surveys
Nancy Towne	ERDC-ITL	GIS Mapping
Thomas Rossbach, PG	USACE-NAB	Geotechnical Data Review
Gregory Walker	ERDC-ITL	Programmer
Mathew Watts	USACE-LRL	Field Surveys
Allyson Windham	ERDC-ITL	GIS Mapping
John Winkleman	USACE-NAE	ADCIRC Interpretation

Scope of the Assessment

For New Orleans and vicinity, the IPET risk and reliability team was assigned the mission to determine estimates of the potential annual loss of life and property value based on the chances of flooding from future hurricanes. The risk analysis methodology developed by the team to accomplish this mission included the following major steps which are described in subsequent sections and summarized in Figure 1.

Step 1: Define the HPS. Characterizing the HPS for the risk analysis began with defining the drainage areas within which flooding might occur. The large drainage basins generally follow parish boundaries and smaller sub-basins were defined within each basin to model the interior drainage characteristics of the basin. The boundaries are defined based on the location and character of the hurricane protection system components, the topography of the area, and (to a limited extent) the internal drainage system. The HPS scenarios for which the flooding vulnerability and risk was assessed include the pre-Katrina and 2007 HPS. The repairs and structural enhancements made following Katrina have been factored into the data used to model the 2007 HPS as shown in Figure 1. The computation of how much water would enter each area required that the structures and features that constitute the HPS be defined so their individual and collective performance could be examined. The HPS was divided into reaches and features. Reaches are lengths of levees or wall sections that have structures of uniform elevation, strength, and foundation conditions. Reaches, typically sections of levees or floodwalls, may be short or long depending on the character of the structures. Features are discrete structures within a reach such as pumping stations, closure gates, and transitions. Transitions are points at which there is a change from one type of structure to another (e.g., where an earth levee meets a concrete floodwall).

Step 2: Determine the Hazard. The hazard is the event or condition with the potential for causing an undesirable consequence. In the present context, the hazard is surge and wave conditions caused by hurricanes; it is not the hurricanes themselves. To assess the hazard, it is first necessary to identify the range, character, and frequency of hurricanes that may strike the southern Louisiana coast. IPET used state-of-the-art methods, including supercomputer models, to compute the surge and wave conditions that a wide variety of hurricanes would produce around New Orleans. This analysis led to estimates of the frequency of extreme surges and waves everywhere around the HPS. These estimates are for current climate conditions, and they do not project climate variations into the future, although continuing work is investigating the effect of potential climate change.

Step 3: Evaluate the System Performance. System Performance is the response of the HPS to the hazard, that is, to surge and wave conditions generated by the hurricanes. The system performance is assessed by modeling the reliability of the HPS under loads generated by surge and wave. This leads to an estimate of the likelihood that the HPS can withstand those loads, and correspondingly to an estimate of the chance of flooding at various places across the city and region. This chance of flooding is sometimes called the vulnerability. The reliability analysis starts with a detailed inventory of the engineering characteristics of every section of the hurricane protection system. Then, the potential for overtopping and breaching is estimated for the spectrum of surge and wave conditions forecast in the hazard assessment. Combining the potential for overtopping and breaching with the frequencies of the corresponding hazards leads to an assessment of vulnerability to flooding from the spectrum of hurricanes that are possible for the region. The calculation also includes the chance of water entering through open gates and the amount of rainfall associated with hurricanes. System performance was evaluated for the pre-Katrina and June 2007 conditions, continuing analysis is being performed of the 2011 system.

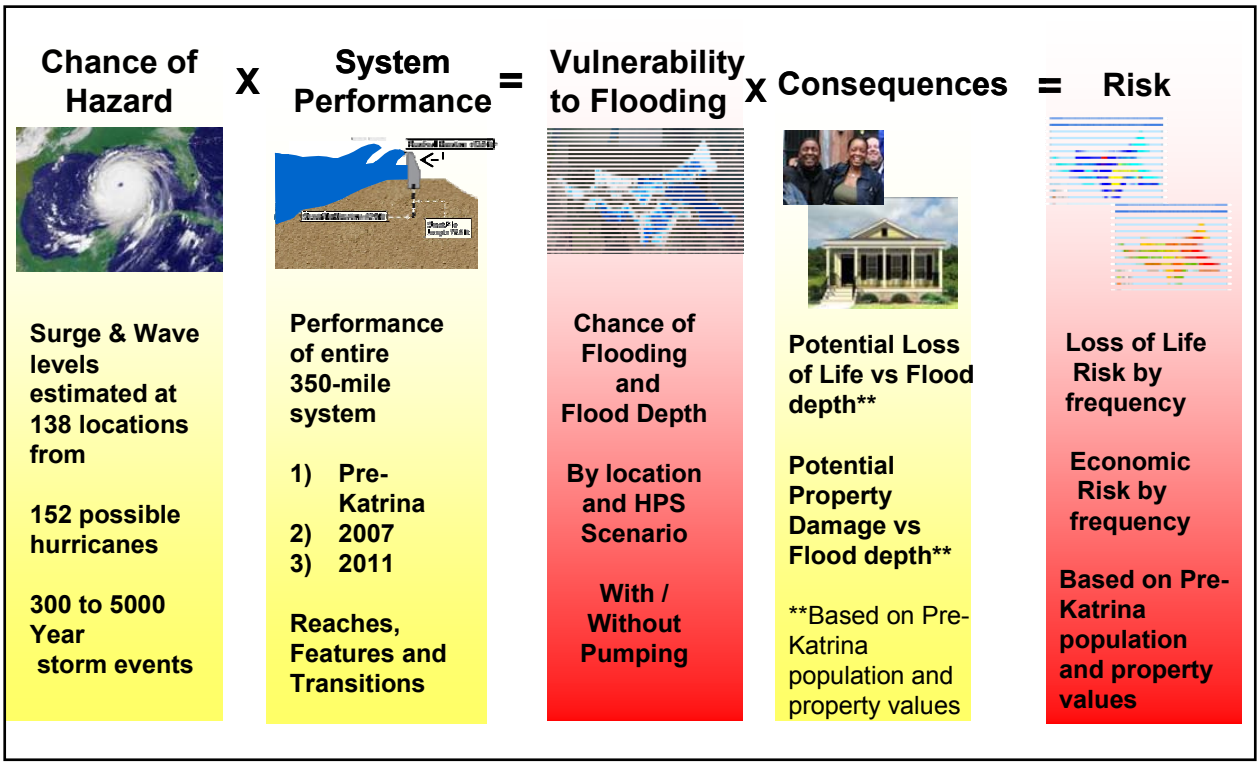

Figure 1. Risk computation for New Orleans.

Step 4: Determine the Consequences. The consequences of flooding, measured by potential loss of life and property damage, are estimated by defining the distribution of people and structures within each sub-basin, the elevations of all structures and the surrounding land, and the value of the properties; and then by applying actuarial information and models to approximate losses. Consequences were estimated for different depths of flooding to determine expected losses across the spectrum of hurricanes. The results are summarized for three chances of occurrence, specifically, the 1/50-, 1/100-, and 1/500-year floods. For loss of life estimation, a sophisticated simulation model was developed using geo-spatial census databases and evacuation

plans. For property damage estimation, historical data from flood control and coastal protection projects across the nation were used to develop flood-depth vs. damage relationships.

Step 5: Determine the Risk. Risk is calculated by combining the chance of flooding consequences occurring with the magnitude of the consequences of that flooding should it occur. This allows an estimate of risk by area, based on the character of the HPS and other measures that may influence who and what is exposed to flooding. Risk is calculated by multiplying the chance of flooding to a certain depth by the losses expected by the flooding. This computation is illustrated in Figure 1. Losses can be expressed as potential loss of life or potential loss of property. Risk was estimated for the HPS as it existed (1) prior to Katrina and (2) for after the repair and rebuilding of the HPS through June 2007. Since a principal purpose of the risk assessment was to determine how risk is changing with respect to the capabilities of the HPS, both the pre-Katrina and post-Katrina risk were estimated using the pre-Katrina distribution of population and property. Using today's population and property conditions would show a dramatic reduction in risk simply because the number of people in some areas is dramatically fewer than before Katrina, not because of changes to the HPS. Maintaining the population and property data as a constant allows changes in the chance of flooding and, therefore, risk to be related to improvements in the HPS.

Overview

The term risk is used in many ways in everyday life to define hazards, losses, and potential outcomes. In the engineering community, risk is generally considered to be the potential for loss resulting from exposure to some uncertain hazard or event. Risk is usually defined for engineering purposes as follows:

$$Risk = Hazard\ probability \times Vulnerability \times Consequences\ of\ failure \quad (1)$$

in which hazard probability is the rate of occurrence (including uncertainty) of the causal event. In the present case, this is the annual probability of hurricane surges and waves of given description. Vulnerability is the reliability with which the constructed system withstands the loads or other demands caused by the hazard. This is the performance of the system during a specific hurricane. Consequences of failure are the costs in lives and dollars accruing in the event of a failure. In the present study, risk was expressed as the annual probability of levels of loss of life or economic consequence being exceeded.

This definition suggests that there are at least two ways to manage risk: by making the system more reliable, or by reducing the potential consequences of failure. Reliability can be influenced by strengthening existing structures, by adding additional components to the protection or by increasing the height of the existing protection. Consequences can be influenced by developing evacuation and emergency response plans or by limiting floodplain development. Nonetheless, no matter how well designed an HPS may be, some level of residual risk always remains: risk is never reduced to zero. Therefore, even with the reconstruction and strengthening of the New Orleans HPS, some residual risk will always remain.

In densely populated areas, increasing system reliability may not be a feasible way to reduce risks to acceptable levels because of limited funding, local opposition to land acquisition, or

environmental issues. Continued floodplain development can increase consequences and thus offset improvements in reliability. A comprehensive approach to determining risks, developing structural and non-structural risk mitigation measures, and evaluating the residual risks that will exist is necessary. The public must be aware of the residual risk that will exist with any engineered system so that they can make informed decisions on how to manage their personnel risk tolerance levels.

Hurricane models can predict winds, waves, and surges only with limited accuracy, and the reliability models used to predict levee performance when subjected to hurricane forces are similarly limited. Hence, the risk profiles of hurricane-induced flooding cannot be established with certainty. Risk analysis must include not just a best estimate of risk but also an estimate of the uncertainty in that best estimate. By identifying the sources of uncertainty in the analysis, measures such as gathering additional data and improving analysis models can be taken to reduce the uncertainty and improve the risk estimates.

The risk model described in this volume was developed to meet the needs of the IPET and a prototype risk analysis that indicates the value of and need to consider risk in the planning of hurricane protection projects. The study also shows that the reliability of all of the components of a hurricane protection project play a role in the performance of the overall project and, therefore, the project must be looked at as a system if the risks are to be fully evaluated. The large uncertainty in this study, and in any analysis of a project of the magnitude of the New Orleans HPS, shows that the system must be continually monitored, maintained, and periodically reevaluated in order to identify potential weaknesses and gain understanding of the factors that affect uncertainty in the performance of the HPS.

Risk Analysis Methodology

Probabilistic risk analysis (PRA) was used to evaluate the HPS (Figure 2). The following sections describe the principal components of this approach.

The first step in the PRA was developing an influence diagram (Figure 3). An influence diagram charts the inter-relationships of key elements of the HPS, and it intends to lead to a basic understanding of risk factors upon which subsequent analyses can be built. The influence diagram is built out of four entities: (1) chance nodes (circular areas) which are uncertain factors that affect how the system performs, (2) decision nodes (square-corner boxes) which are factors where decisions by stakeholders or planners can affect consequences, (3) value nodes (rounded-corner boxes) which are factors or consequences affected by system performance, and (4) arrows which identify relationships and dependencies among the foregoing entities.

The influence diagram of Figure 3 was used to develop the process flow diagram of Figure 4. The process flow diagram is the fundamental guide that the Risk Team used in determining the processes and products required to implement the PRA. The team was subsequently organized to provide disciplinary expertise along the lines of the process flow chart.

Initial Assumptions and Constraints

To implement the PRA it was necessary to identify key assumptions and constraints. The term constraints is used to mean events or situations not modeled explicitly in the analysis. The assumptions and constraints are discussed as they arise in the subsequent sections of this report; however, a summary of the limitations and constraints is the following:

1. The geographic area is limited to elements of the HPS in the basins shown in Figure 2.

2. The risk model does not produce time profiles of inundation and consequences, but it does produce spatial profiles accumulated over the durations of storms.

3. The risk model includes assumptions about the parameters used in various major aspects of the HPS characterization (e.g., hurricane simulation, reliability analysis, inundation analysis, and consequence analysis), but it incorporates uncertainties in the corresponding parameter values.

4. Modeling procedures that existed prior to Katrina and that were used in the original General Design Memoranda (GDM) for structural and geotechnical performance of the levee and

floodwall systems were used to evaluate reliability, although calibrated by current knowledge and understanding, and by information generated in the post-Katrina IPET research.

5. The following hazards and consequences were not considered in the risk analysis: Wind damage to buildings; barge impact; fire; civil unrest; indirect economic consequences; effect of a release of hazardous materials; and environmental consequences.

6. The evacuation plan for New Orleans was not explicitly modeled in the risk analysis. Evacuation effectiveness was, however, considered in the LIFESim consequence model used in IPET (2006) Vol. VII.

Defining the HPS

The HPS scenarios for which risk was assessed included (1) pre-Katrina conditions, and (2) conditions as of June 2007. Repairs and structural enhancements made following Katrina and on-the-ground as of June 2007 (e.g., gates on the drainage canals of Orleans Metro) were factored into the model the 2007 HPS. Separate models of the HPS were required for each scenario in order to determine the effects of repairs and improvements made since Katrina.

Systems definition models for the HPS were developed based on-site surveys by team personnel, engineering design and construction information as documented in USACE GDM for the many projects constituting the HPS, pre- and post-Katrina high resolution aerial photography and LiDAR surveys, and results of post-Katrina field reconnaissance by the Risk Team and studies performed by the IPET Performance Team and the IPET Pump Stations Team (see IPET 2006 Volume IV). Subsequent to the field work, computer models of the components of the HPS were developed for the PRA.

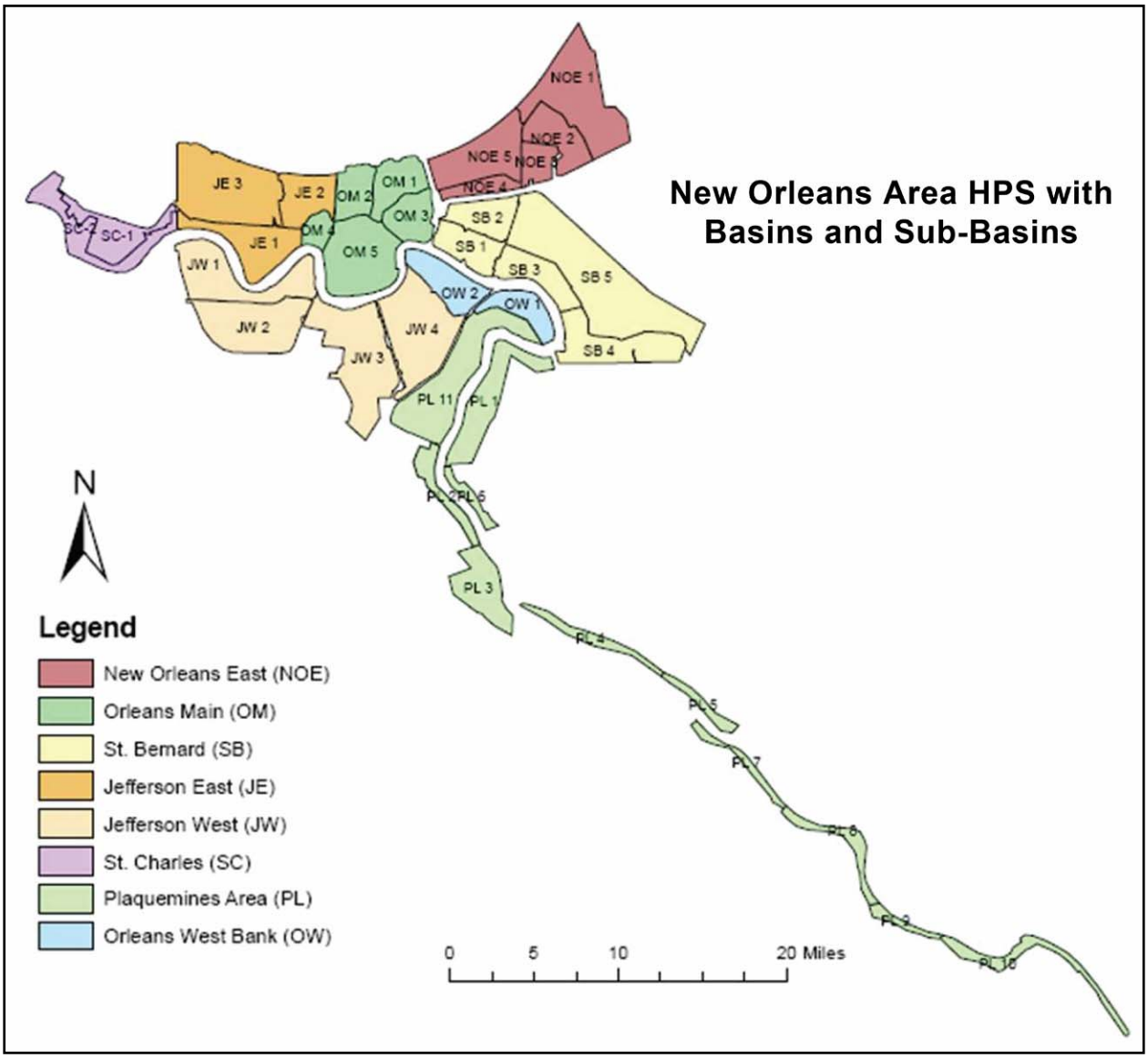

Figure 2. Geographic limits of New Orleans HPS.

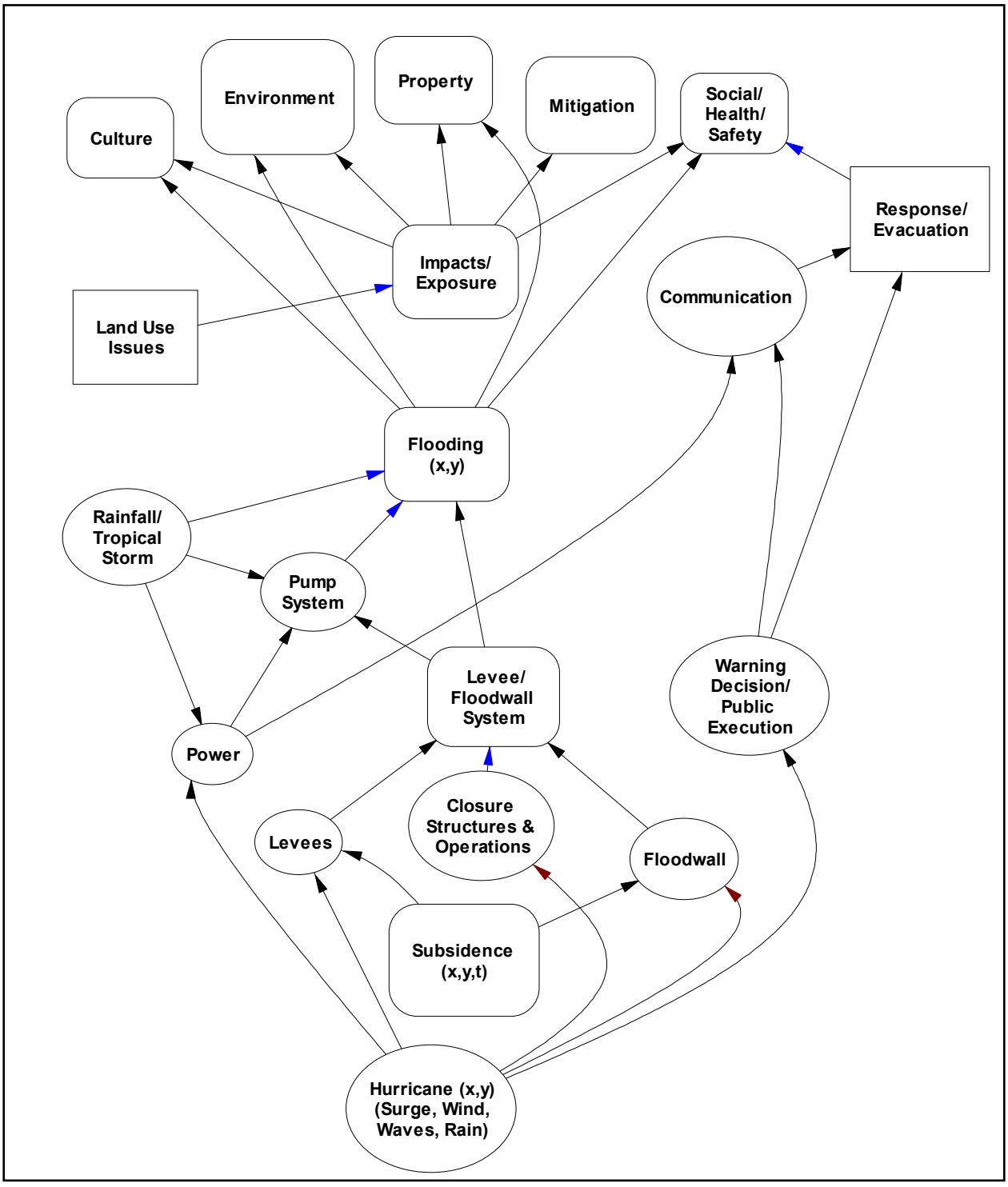

Figure 3. Influence diagram of risk factors and components of the NOLA Hurricane Protection System.

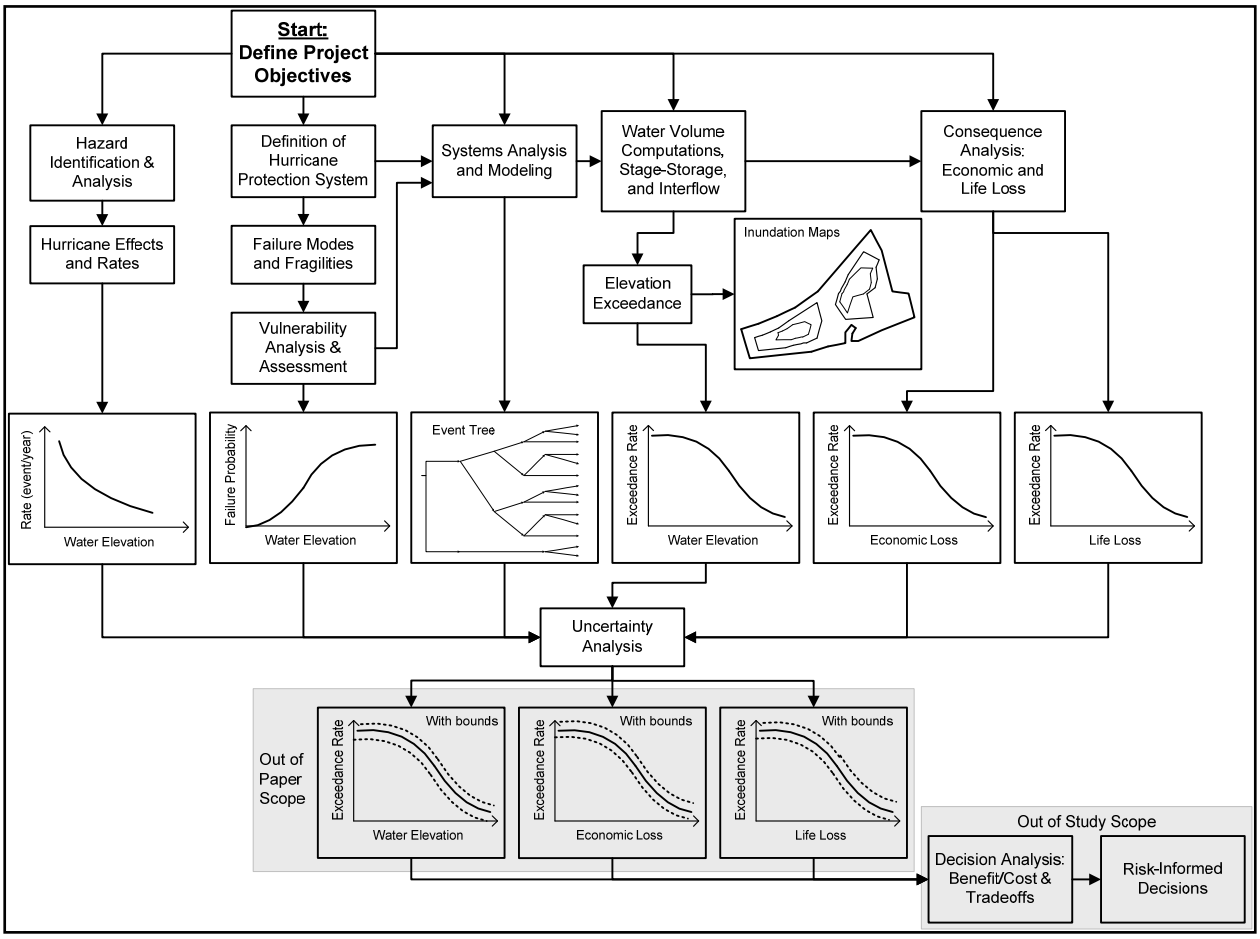

Figure 4. Risk methodology flow chart.

Analysis Boundaries

An initial step in the defining of the HPS was to delineate the bounds of the study and the physical descriptions of the various components of a HPS. These included defining the geographic bounds of the study region and the elements of the HPS, the resolution of information and analysis to be performed, and analysis assumptions and constraints.

Characterizing the HPS for the risk analysis began with defining the drainage areas within which flooding might occur. The large drainage basins in the New Orleans area generally follow parish boundaries, and smaller sub-basins exist within each basin to funnel interior drainage to canals then to pump stations that remove water from the protected areas. This breaks the area up into large drainage basins that generally follow parish boundaries, such as Jefferson Parish, and smaller sub-basins that subdivide each larger basin based on the drainage and pumping characteristics of the parish. These boundaries are also based on the location and character of the hurricane protection system structures, the topography of the area and (to a limited extent) the internal drainage system. The basin and sub-basin boundaries used are shown in Figure 2. The boundary of the HPS considered in the risk assessment consists of six major parishes and 27 sub-basins within those parishes. The parishes and the number of sub-basins within each that are considered in the analysis are as follows:

- Jefferson Parish East Bank (JE) 3 sub-basins
- Jefferson Parish West Bank (JW) 4 sub-basins
- New Orleans East Parish 5 sub-basins
- Orleans Parish East Bank (OM) 5 sub-basins
- Orleans Parish West Bank (OW) 2 sub-basins
- Plaquemines Parish (PL) 11 sub-basins but only upper Plaquemines (PL11) included in the analysis
- St. Bernard Parish (SB) 5 sub-basins
- St. Charles Parish (SC) 2 sub-basins

The risk assessment process was developed to determine the amount of water that would enter and flood these areas for the surge, wave, and rainfall conditions created by each storm.

Physical Description of the HPS

The HPS as described above is a combination of low-lying tracts of land enclosed by levees and floodwalls that form drainage basins, which are independently maintained and operated by the local parishes and levee boards. The computation of how much water would enter each area required that the structures and features that are components of the HPS be identified and defined so that their performance could be examined to determine probabilities of breaching and overtopping.

Detailed physical descriptions for each basin based on pre-Katrina conditions were provided by USACE (2006). Data collected during site inspections were also used to define the current characteristics of the basins and their interdependence. This was a critical and time-consuming step in the development of the risk model that has yielded a comprehensive description of the entire HPS. These descriptions were developed by examining available information gathered by IPET including the following:

- USACE GDM and supporting design documents
- High-resolution aerials photos from pre-Katrina and post-Katrina
- Construction documents and plans
- Inspection reports
- Katrina damage reports
- Reports of repairs made to the system post-Katrina
- Detailed field surveys conducted by the Risk Team to verify the location and configurations of the HPS
- Studies conducted by other IPET teams

During the course of the study, the entire perimeter length of levee and floodwall that form the HPS was inspected by the Risk Team as part of the reconnaissance effort and an inventory of components documented. Geometric and engineering material properties were identified for each reach and photos taken of levees, wall, features and transitions. Structural cross sections were identified by a review of the corresponding GDM, as-built drawings, aerial photographs, and geographic information system (GIS) overlays; and were subsequently confirmed in on-site reconnaissance. Geotechnical cross sections and corresponding soil engineering properties were

derived from the original GDMs for the respective project areas of each drainage basin, supplemented by site characterization data collected post-Katrina at levee and floodwall failure sites (reported in IPET Volume IV, USACE 2006). Detailed data from these inspections are presented in Appendices 2 through 7 of this Volume. The HPS comprises a variety of subsystems, structures, and components, which include earthen levees, floodwalls, transitions between levees and walls, gates, ramps, and pumping stations. Additional interior components of the HPS such as canals, wall closures, power supply systems, and operations personnel were indirectly considered in the analysis. The general inventory of components of the system includes the following:

- Earthen levees
- Earthen levees with I-walls
- Sheet-pile I-walls
- Sheet-pile I-walls capped with concrete
- Concrete T-walls
- Concrete L-walls
- Transitions between levees and the various types of walls or other structures
- Pump stations
- Drainage structures
- Closure gates of various types of design
- Road crossings (ramps), some requiring sandbagging during a hurricane
- Railroad crossings

The information gathered was incorporated into detailed GIS maps of each basin that included locations of all features (walls, levees, pumping stations, and closure gates), geotechnical information (boring logs, geologic profiles), aerial photographs, and photos of each feature.

Classifying the Components of the HPS

The data collected were used to divide the HPS into reaches, transitions and features:

- Reaches were identified as lengths of levee or wall sections that have structures of uniform cross-section, elevation, strength, and foundation conditions.
- Features within the reaches were identified as such things as pumping stations, closure gates, and transitions.
- Transitions between one kind of structure to another (for example, an earth levee to a concrete floodwall) were identified as important because of their poor performance during Katrina.

The information in these GIS databases was again confirmed in the field surveys of the entire system conducted by the Risk Team. Photos, global positioning coordinates, and notes were taken during these surveys to document each reach, feature, and transition used in the risk model, and to confirm information gathered from design information. This undertaking resulted in a comprehensive description of the HPS.

Determining the tops of levee and wall elevations proved to be challenging because of datum inconsistencies, subsidence, and the lack of current survey information. Elevations were initially established using design documents and the New Orleans District surveys which were evaluated based on LIDAR and field surveys provided to the Risk Team by other IPET teams. Final elevations for each reach were confirmed at meetings with the New Orleans District.

Figure 5. Typical New Orleans levee.

The primary components that form the perimeter of the hurricane protection against surges and waves are levees and floodwalls. A typical New Orleans levee, Figure 5, is constructed of available soils and may or may not have slope protection to guard against erosion due to wave action. A typical cross section is shown in Figure 6.

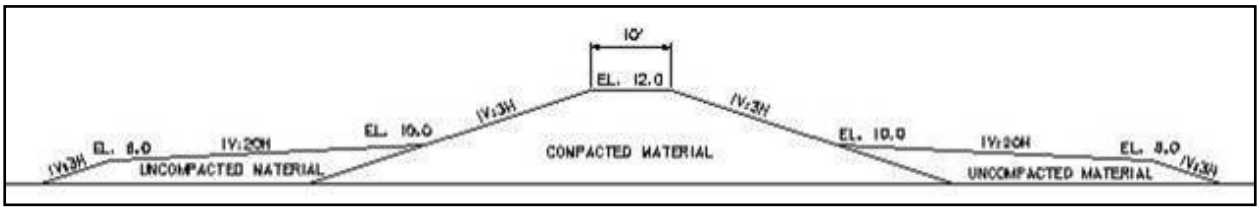

Figure 6. Typical levee cross section.

Floodwalls in the HPS were found to be of several different designs that varied due to constraints of available right-of-way. The most common of these are I-walls. I-walls are constructed by driving steel sheetpiling into the ground with a portion remaining above ground as a water barrier (Figure 7). A typical I-wall cross section is shown in Figure 8.

In some cases, the portion of the piling above ground was capped with concrete as shown in cross section in Figure 9 and the cross section in Figure 10. Several I-walls failed during Katrina, as shown by the collapsed section of uncapped I-wall in Figure 11, and the damaged capped I-wall in Figure 12.

T-walls are generally built upon steel H-piles driven into the ground as shown in Figure 13 and Figure 14. These walls performed well during Katrina. A closely related structure is the L-wall shown in Figure 15.

Key components of the HPS are the many gates and road closures in and around the system. These are intended to close gaps in the perimeter protection caused by road, railroad, and pedestrian crossings. They are treated as features within a reach in the risk model. These gates vary in design from a fully engineered steel gated road closure as shown in Figure 16 to a ramp across a levee which must be sandbagged during a storm. Gates are also used to control interior drainage. Road closures must remain open long enough to allow evacuation, yet must be closed in time to prevent flooding. Several gates and road closures (about 10%) were left open during Katrina and contributed to flooding.

A large part of the New Orleans area is below sea level and requires constant pumping to remove water from rainfall and groundwater seepage. An interior drainage system has evolved over the years into a sophisticated—although aging—system of conduits, culverts, pipes, and ditches (Figure 17) that moves water into drainage canals and then to pump stations (Figure 18). These pumping stations are designed to handle water from tropical storms with about a 10-year return period, and they are not designed to pump the large volumes of water caused by levee breaches or overtopping. Many of the pump stations are 50 or more years old. Many or most did not operate during Katrina because they lost power or were abandoned. Pump stations were treated as features in the risk analysis when they intersect levees or floodwall reaches.

Figure 7. Typical sheet-pile I-wall.

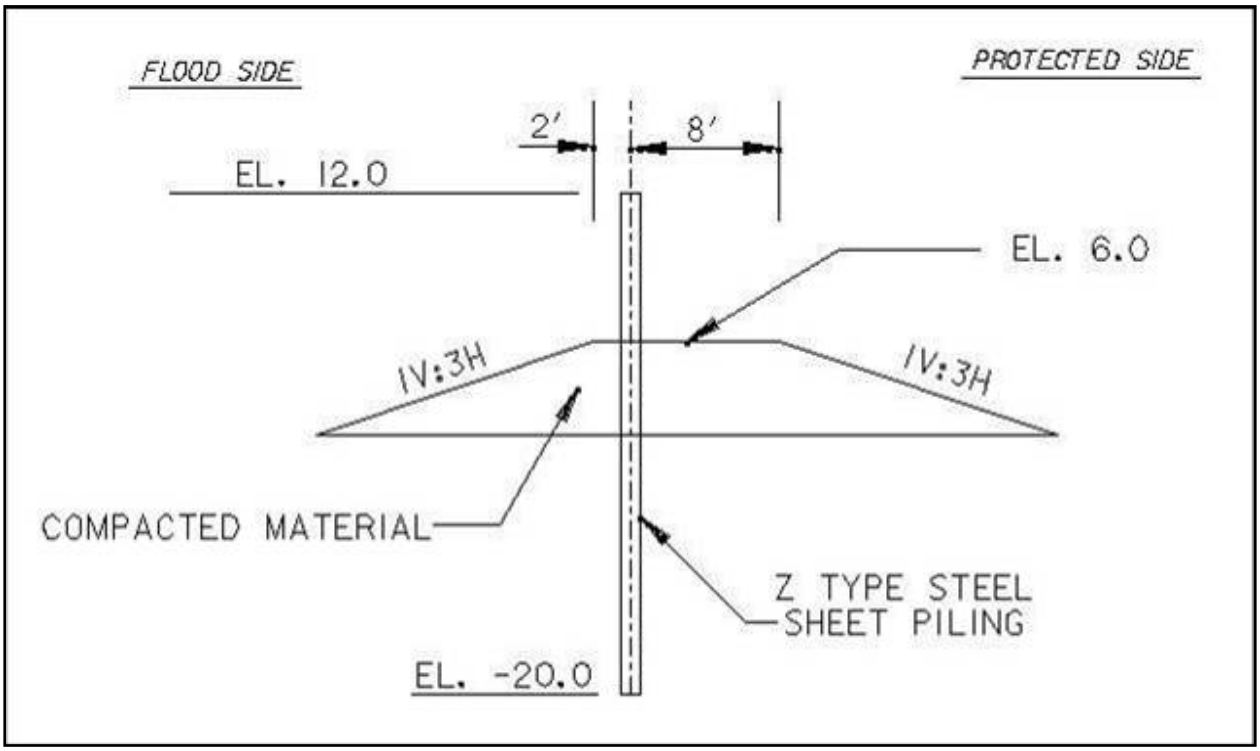

Figure 8. Concrete capped I-wall cross section.

Figure 9. Concrete capped I-wall.

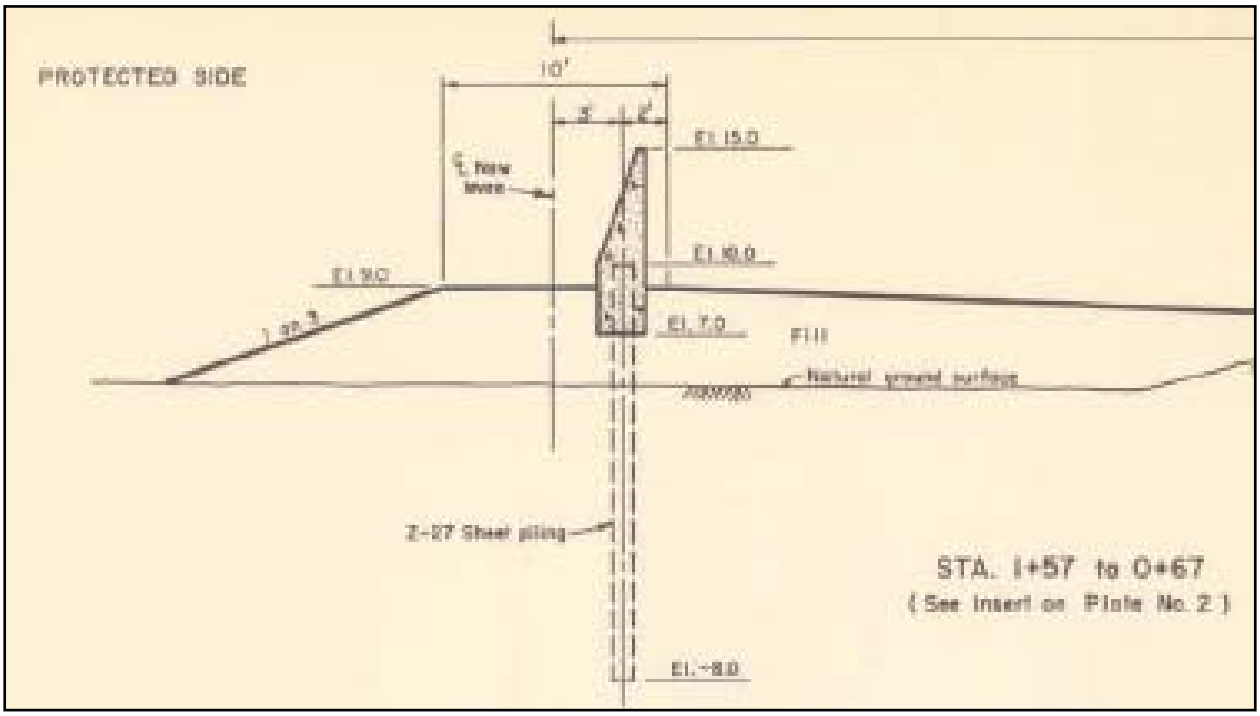

Figure 10. Typical sheet-pile I-wall cross section.

Figure 11. Katrina damaged I-wall.

Figure 12. Katrina damage to concrete capped I-wall.

Figure 13. Typical T-wall.

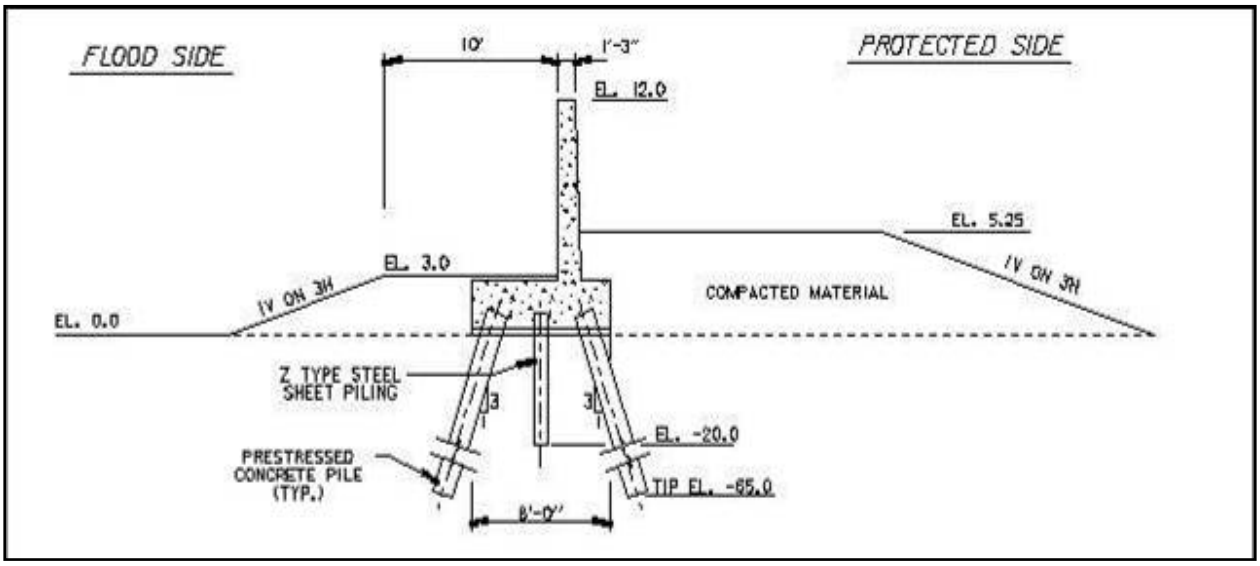

Figure 14. Typical T-wall cross section.

Figure 15. Typical L-wall.

Figure 16. Road crossing.

Figure 17. Local drainage structure.

Figure 18. Local pump station.

Figure 19. I-wall transition to concrete structure and levee.

Figure 20. Katrina erosion at transition.

Figure 21. Katrina erosion at transition from levee to closure structure.

Transitions between types of structures (Figure 19) turned out to be critical features during Katrina, serving as focal points of erosion when the HPS was overtopped (Figure 20). Some of these failures at transitions can be attributed to differences in elevation across the transition, which created eddies during overtopping that eroded the foundation or levee on the protected side.

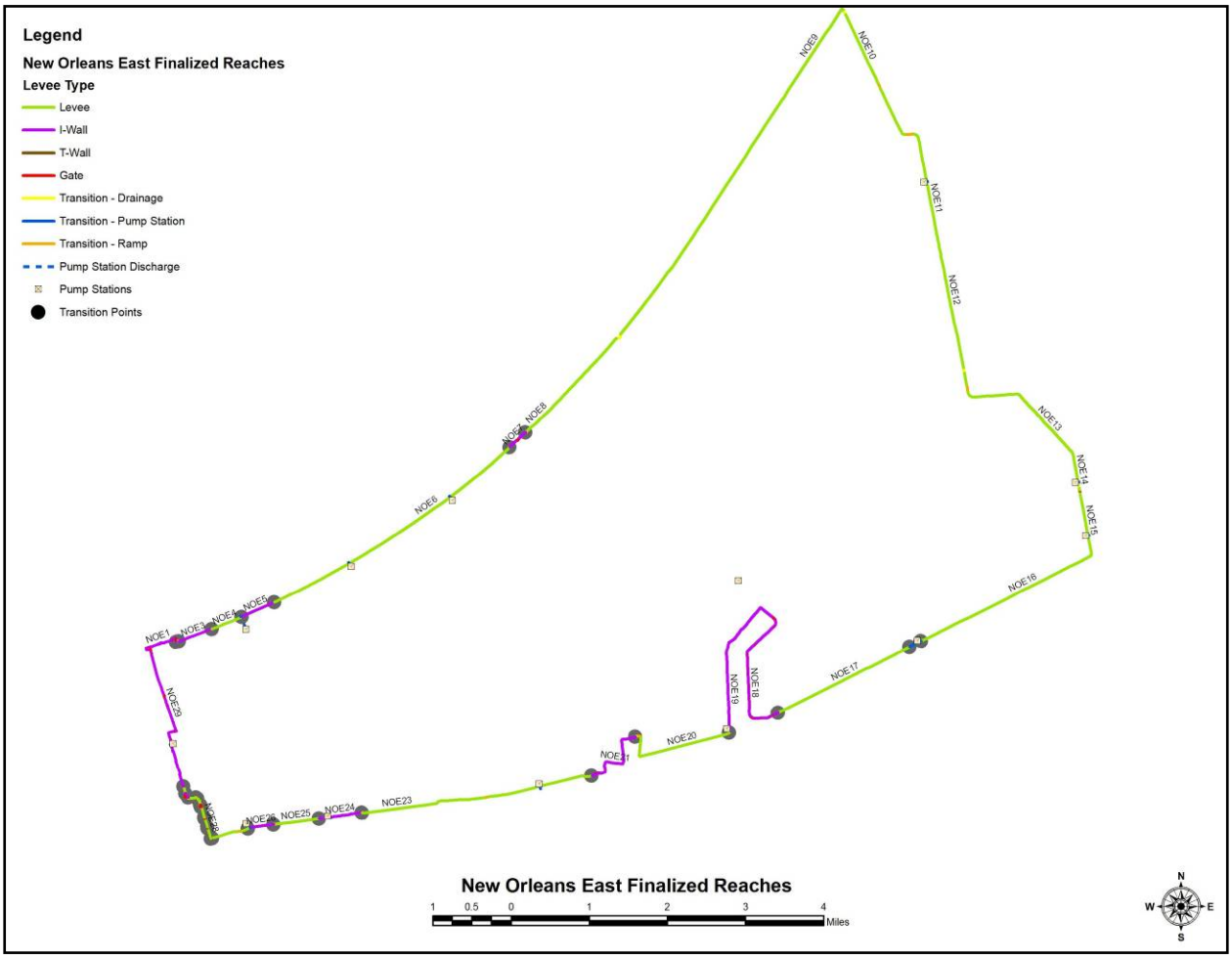

Figure 22. NOE reaches (levees in green, walls in purple)

HPS Model for Risk Analysis

The systems characterization information gathered by the Risk Team served as the basis for a model of the HPS in risk analysis. The perimeter of each parish and sub-basin was divided into reaches that define sections of similar physical and engineering characteristics (Figure 22). Initially, the reaches were defined using the beginning and ending stations shown in the original design memoranda. The stations were adjusted based on examinations of geological and geotechnical information to form reaches that were expected to have similar performance.

For each reach, the following geometric and geographic characterization was developed:

- Reach Number—A unique reach number is assigned
- Length—The length in feet of the selected reach
- Top Elevation—The elevation in feet referenced to NAVD88 (2004.65)
- Design Water Elevation—The water elevation used in the design of the reach.
- Reach Type—The structural configuration of the reach (levee, wall, or transition)
- Reach Weir Coefficient—The applicable weir coefficient if water overtops the reach

- Basin Reference—The basin where the reach is located.
- Sub-basin Reference—The sub-basin where water flows from a breach or overtopping
- Reach Name—The name of the reach.

This information was translated into a flat-file database as suggested by Table 1. All the basins and sub-basins in the HPS were characterized in this manner.

Similar information developed for all features (Table 2). For each feature, the following characterization was developed:

- Feature Number—Unique identification feature number
- Reach Name—The name of the reach
- Basin Reference—The basin where the reach is located
- Sub-basin Reference—The sub-basin where water will flow
- Type—Structural type of the feature
- Correlated Feature—A reference value for correlated features
- Length—Length in feet of the opening
- Bottom Elevation —The invert elevation of the gate
- Probability Open—Probability that the gate will not be closed

For each transition, the following characterization was developed (Table 3):

- Transition Number—A unique transition number
- Reach Name—The name of the reach
- Basin Reference—The basin where the reach is located
- Sub-basin Reference—The sub-basin where water will flow
- Transition Type—The structural configuration of the structure that the transition
- Length—The length in feet selected for the transition
- Elevation(s)—The physical elevation(s) in feet referenced to the NAVD88 (2004.65)
- Design Water Elevation—The water elevation used in the design of the transition

A description of reaches, features, and transitions is presented in Appendix 14. For the pre-Katrina condition, 135 reaches were identified; for the current condition three gates were added, one each at the Lake Pontchartrain ends of the 17th Street, London Avenue, and Orleans drainage canals. In both cases, 197 point features and 178 transitions were identified. Reach elevations and lengths used in risk assessment for New Orleans East in the pre-Katrina and 2007 HPS, referenced to NAVD88 (2004.65) are shown in Table 4.

Table 1. New Orleans East Reach Definitions

Reach	Length (ft)	Top Elevation (ft)	Design Water Elevation (ft)	Reach Type	Reach Weir Coefficient	Basin Reference	Sub-basin Reference	Reach Name
1	2,405	15.5	12.5	W	3.0	NOE	NOE5	NOE1
2	250	15.5	11.5	L	2.6	NOE	NOE5	NOE2
3	2,325	15.5	12.5	W	3.0	NOE	NOE5	NOE3
4	2,330	15.5	11.5	L	2.6	NOE	NOE5	NOE4
5	2,270	15.5	12.5	W	3.0	NOE	NOE5	NOE5
6	19,110	15.5	11.5	L	2.6	NOE	NOE5	NOE6
7	1,475	15.5	12.5	W	3.0	NOE	NOE5	NOE7
8	2,725	15.5	11.5	L	2.6	NOE	NOE5	NOE8
9	32,900	18.5	14.5	L	2.6	NOE	NOE1	NOE9
10	5,830	17.0	13.0	L	2.6	NOE	NOE1	NOE10
11	13,325	17.0	13.0	L	2.6	NOE	NOE1	NOE11
12	8,910	18.0	14.0	L	2.6	NOE	NOE1	NOE12
13	9,185	22.0	18.0	L	2.6	NOE	NOE1	NOE13
14	2,615	22.0	18.0	L	2.6	NOE	NOE1	NOE14
15	4,470	25.0	21.0	L	2.6	NOE	NOE1	NOE15
16	13,045	28.0	24.0	L	2.6	NOE	NOE1	NOE16
17	10,570	32.0	28.0	L	2.6	NOE	NOE2	NOE17
18	10,760	17.9	14.9	W	3.0	NOE	NOE2	NOE18
19	9,320	17.9	14.9	W	3.0	NOE	NOE3	NOE19
20	7,905	16.0	12.0	L	2.6	NOE	NOE3	NOE20
21	5,520	16.0	13.0	W	3.0	NOE	NOE3	NOE21
22	385	16.0	12.0	L	2.6	NOE	NOE3	NOE22
23	15,320	15.0	9.9	L	2.6	NOE	NOE4	NOE23
24	2,910	15.0	10.8	W	3.0	NOE	NOE4	NOE24
25	3,230	15.0	9.8	L	2.6	NOE	NOE4	NOE25
26	1,640	15.0	10.8	W	3.0	NOE	NOE4	NOE26
27	2,750	15.0	9.8	L	2.6	NOE	NOE4	NOE27
28	4,100	13.0	9.0	L	2.6	NOE	NOE4	NOE28
29	11,185	13.5	10.5	W	3.0	NOE	NOE5	NOE29

Table 2. New Orleans East Feature Definitions

Feature Number	Type	Category	Reach	Correlated Features	Length (ft)	Bottom Elevation (ft)	Prob Open	Reach Name
1	G	G	1	1	35.0	1.0	0.010	NOE1
2	G	G	1	2	22.0	1.8	0.010	NOE1
3	G	G	1	3	63.0	-0.5	0.010	NOE1
4	G	G	7	4	32.0	-1.5	0.010	NOE7
5	G	G	11	5	30.0	6.0	0.010	NOE11
6	G	G	12	6	80.0	10.0	0.010	NOE12
7	G	G	15	7	20.0	5.7	0.010	NOE15
8	G	G	18	8	20.0	9.8	0.000	NOE18
9	G	G	18	9	20.0	9.8	0.000	NOE18
10	G	G	18	10	20.0	9.8	0.010	NOE18
11	G	G	18	11	20.0	9.8	0.010	NOE18
12	G	G	18	12	20.0	9.8	0.000	NOE18
13	G	G	18	13	20.0	9.8	0.010	NOE18
14	G	G	18	14	20.0	9.8	0.010	NOE18
15	G	G	18	15	20.0	9.8	0.000	NOE18
16	G	G	18	16	20.0	9.8	0.010	NOE18
17	G	G	18	17	20.0	9.8	0.010	NOE18
18	G	G	18	18	20.0	9.8	0.010	NOE18
19	G	G	18	19	20.0	9.8	0.010	NOE18
20	G	G	18	20	20.0	9.8	0.010	NOE18
21	G	G	18	21	20.0	9.8	0.010	NOE18
22	G	G	18	22	20.0	9.8	0.010	NOE18
23	G	G	18	23	20.0	9.8	0.010	NOE18
24	G	G	18	24	20.0	9.8	0.010	NOE18
25	G	G	18	25	20.0	9.8	0.000	NOE18
26	G	G	19	26	20.0	12.8	0.010	NOE19
27	G	G	21	27	20.0	12.8	0.010	NOE21
28	G	G	21	28	20.5	6.5	0.010	NOE21
29	G	G	27	29	20.0	7.8	0.010	NOE27
30	G	G	28	30	20.0	6.5	0.000	NOE28
31	G	G	28	31	20.0	6.5	0.010	NOE28
32	G	G	28	32	17.0	6.5	0.000	NOE28
33	G	G	28	33	20.0	7.2	0.000	NOE28
34	G	G	28	34	37.0	6.5	0.010	NOE28
35	G	G	29	35	35.0	6.5	0.000	NOE29
36	G	G	29	36	15.0	7.2	0.010	NOE29
37	G	G	29	37	17.0	4.7	0.010	NOE29
38	G	G	29	38	20.0	5.2	0.010	NOE29
39	G	G	29	39	17.0	2.2	0.010	NOE29
40	G	G	29	40	30.0	-0.8	0.010	NOE29
41	G	G	29	41	33.0	9.2	0.010	NOE29
42	G	G	29	42	32.0	5.7	0.010	NOE29

Table 3. New Orleans East Transitions Definition

Transition	Length (ft)	Weighted Elevation (ft)	Design Water Elevation (ft)	Transition Type	Transition Weir Coefficient	Reach Reference	Sub-basin Reference	Reach Reference
1	25	15.5	15.5	R	3.0	NOE1	NOE5	1
2	125	15.5	15.5	T	3.0	NOE3	NOE5	3
3	80	15.5	15.5	T	3.0	NOE3	NOE5	3
4	155	15.5	15.5	T	3.0	NOE5	NOE5	5
5	95	15.5	15.5	T	3.0	NOE5	NOE5	5
6	140	15.5	15.5	T	3.0	NOE7	NOE5	7
7	130	15.5	15.5	T	3.0	NOE7	NOE5	7
8	450	18.5	18.5	D	3.0	NOE9	NOE1	9
9	830	18.5	18.5	D	3.0	NOE9	NOE1	9
10	65	17.0	17.0	D	3.0	NOE10	NOE1	10
11	215	17.0	17.0	R	3.0	NOE10	NOE1	10
12	145	17.0	17.0	R	3.0	NOE11	NOE1	11
13	255	17.0	17.0	G	3.0	NOE11	NOE1	11
14	75	17.0	17.0	D	3.0	NOE11	NOE1	11
15	55	18.0	18.0	D	3.0	NOE12	NOE1	12
16	330	19.0	19.0	G	3.0	NOE12	NOE1	12
17	120	18.0	18.0	D	3.0	NOE14	NOE1	14
18	95	30.0	30.0	G	3.0	NOE15	NOE1	15
19	870	34.0	34.0	P	3.0	NOE17	NOE2	17
20	135	16.0	16.0	T	3.0	NOE18	NOE2	18
21	60	16.0	16.0	T	3.0	NOE19	NOE3	19
22	75	16.0	16.0	R	3.0	NOE20	NOE3	20
23	140	16.0	16.0	T	3.0	NOE21	NOE3	21
24	25	16.0	16.0	T	3.0	NOE21	NOE3	21
25	50	14.0	14.0	P	3.0	NOE23	NOE4	23
26	40	14.0	14.0	R	3.0	NOE23	NOE4	23
27	40	14.0	14.0	R	3.0	NOE23	NOE4	23
28	75	14.0	14.0	T	3.0	NOE24	NOE4	24
29	80	14.0	14.0	T	3.0	NOE24	NOE4	24
30	75	14.0	14.0	T	3.0	NOE26	NOE4	26
31	60	13.0	13.0	T	3.0	NOE26	NOE4	26
32	150	14.0	14.0	P	3.0	NOE26	NOE4	26
33	70	14.0	14.0	R	3.0	NOE27	NOE4	27
34	70	14.0	14.0	R	3.0	NOE27	NOE4	27
35	90	14.0	14.0	G	3.0	NOE27	NOE4	27
36	100	14.0	14.0	G	3.0	NOE28	NOE4	28
37	100	14.0	14.0	G	3.0	NOE28	NOE4	28
38	195	14.0	14.0	G	3.0	NOE28	NOE4	28
39	135	14.0	14.0	G	3.0	NOE28	NOE4	28
40	35	14.0	14.0	R	3.0	NOE28	NOE4	28
41	80	14.0	14.0	G	3.0	NOE28	NOE4	28
42	90	14.0	14.0	G	3.0	NOE28	NOE4	28
43	95	14.0	14.0	T	3.0	NOE29	NOE5	29
44	50	14.0	14.0	R	3.0	NOE29	NOE5	29
45	30	14.0	14.0	G	3.0	NOE29	NOE5	29

A portion of the systems definition for New Orleans East (NOE 5) in the vicinity of the Lakefront Airport is shown in Figure 23.

This figure suggests the resolution of information developed by the risk team from the GDMs. The red targets and light blue station labels show the location of point features and transitions. This figure also includes point features such as gates (red in color) as well as pumping stations (blue lines) and transitions (grey circles). These data were transformed into reaches as shown in Figure 24, in which wall reaches are indicated in purple and levee reaches in green.

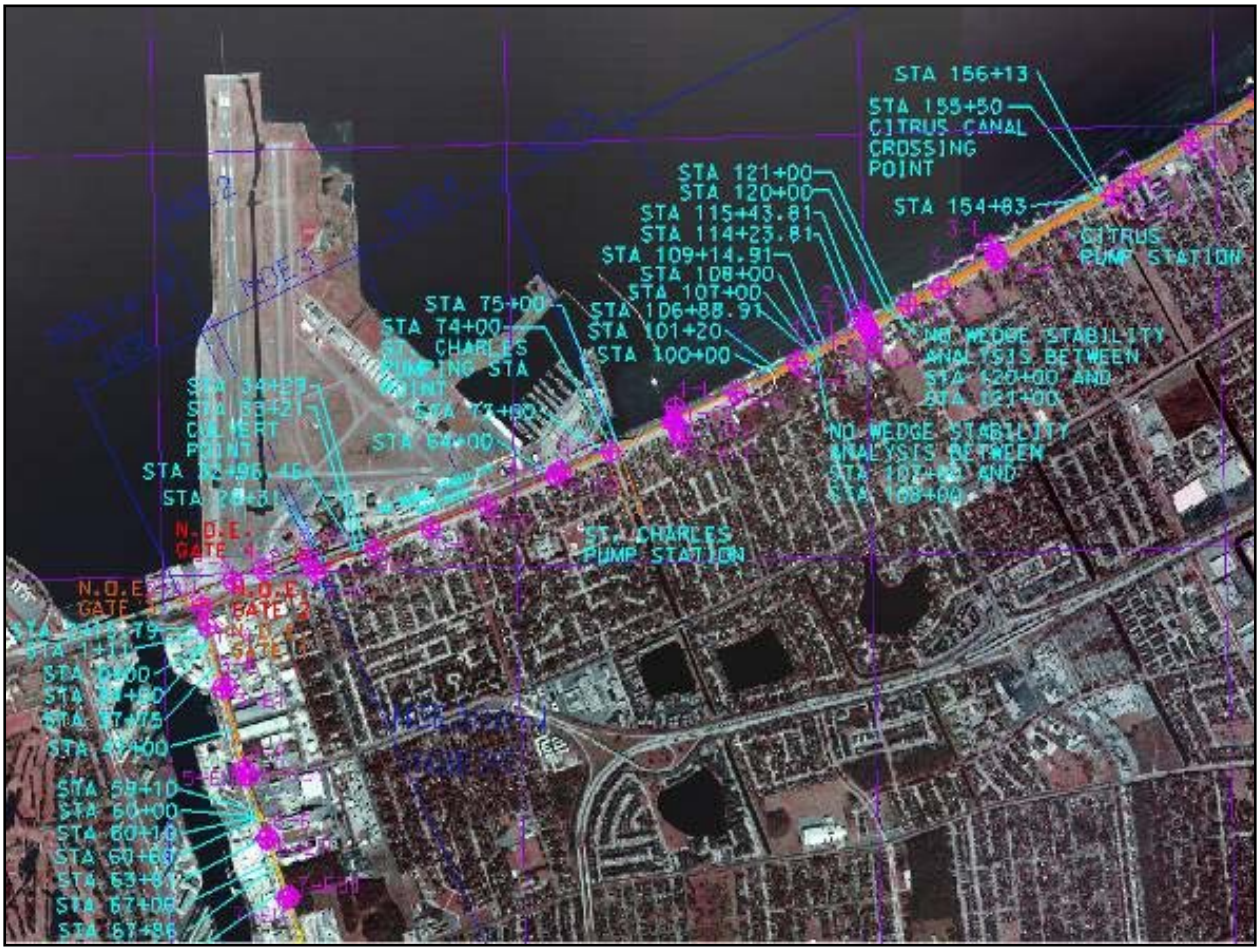

Figure 23. Detail of HPS definition at Lakefront Airport.

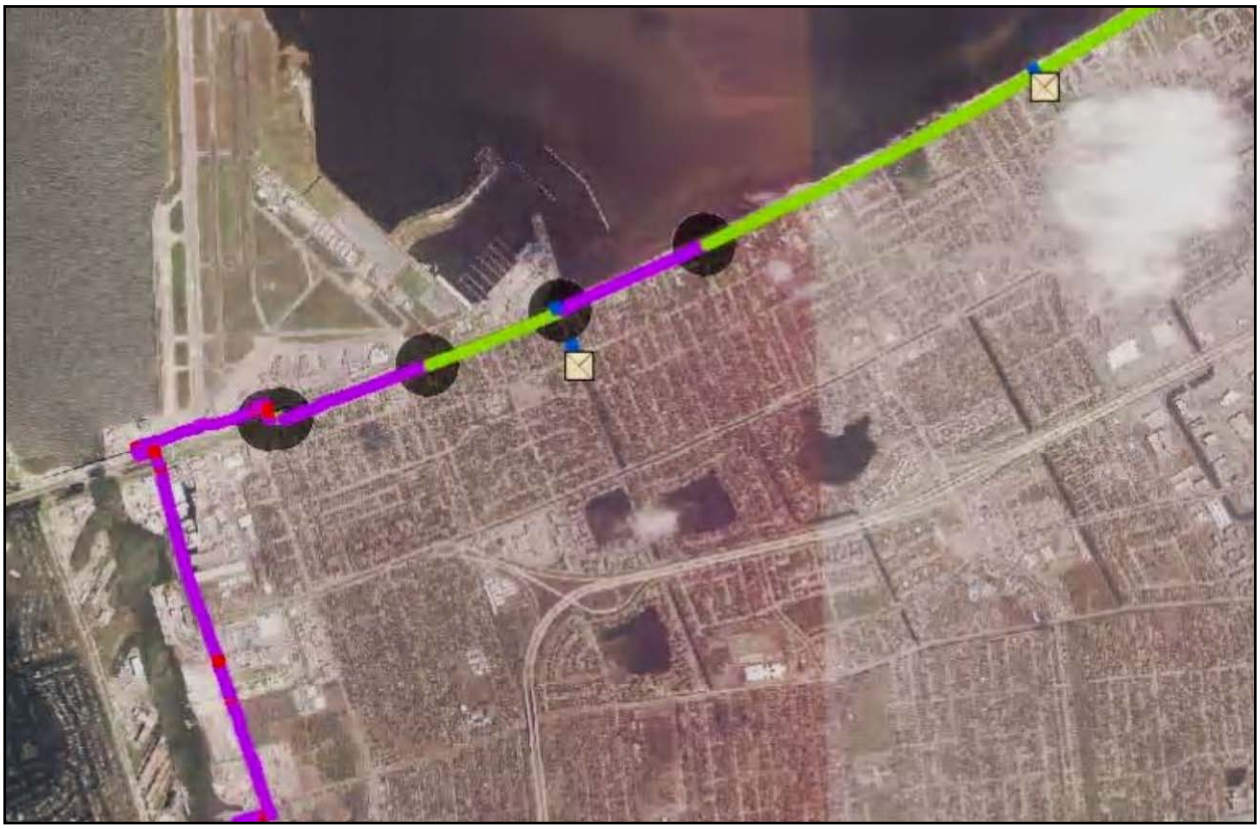

Figure 24. Detail of HPS definition at Lakefront Airport.

Table 4. Reach Elevation for HPS Scenarios

Reach	Length (ft)	Reach Name	Pre-Katrina HPS, ft	2007 HPS, ft
1	2,405	NOE 1	12.0	10.8
2	250	NOE 2	10.0	10.8
3	2,325	NOE 3	12.0	10.8
4	2,330	NOE 4	13.0	10.8
5	2,270	NOE 5	14.0	10.8
6	19,110	NOE 6	13.0	13.0
7	1,475	NOE 7	13.0	13.0
8	2,725	NOE 8	13.0	13.0
9	32,900	NOE 9	18.5	18.2
10	5,830	NOE 10	15.0	13.8
11	13,325	NOE 11	11.0	14.0
12	8,910	NOE 12	15.0	15.0
13	9,185	NOE 13	16.0	15.8
14	2,615	NOE 14	17.0	16.0
15	4,470	NOE 15	18.0	18.0
16	13,045	NOE 16	15.5	18.0
17	10,570	NOE 17	16.8	18.0
18	10,760	NOE 18	18.0	17.9
19	9,320	NOE 19	17.9	17.9
20	7,905	NOE 20	17.0	16.0

Reach	Length (ft)	Reach Name	Pre-Katrina HPS, ft	2007 HPS, ft
21	5,520	NOE 21	17.0	16.0
22	385	NOE 22	14.0	16.0
23	15,320	NOE 23	14.0	13.9
24	2,910	NOE 24	12.5	13.8
25	3,230	NOE 25	13.5	13.8
26	1,640	NOE 26	14.0	13.8
27	2,750	NOE 27	14.0	13.8
28	4,100	NOE 28	12.5	13.0
29	11,185	NOE 29	13.0	13.5
30	6,745	JE1	12.5	12.8
31	5,915	JE2	13.0	13.9
32	4,945	JE3	12.5	13.9
33	36,430	JE4	15.0	16.5
34	19,925	JE5	16.0	16.5
35	12,300	JE6	13.0	15.5
36	4,205	JE7	24.5	25.3
37	53,090	JE8	25.5	25.4
38	2,595	JE9	6.0	9.6
39	17,500	SC1	11.0	11.0
40	11,710	SC2	10.0	13.0
41	23,190	SC3	10.0	10.0
42	70,465	SC4	27.0	27.9
43	9,280	SC5	21.0	20.5
44	3,795	SC6	17.0	20.3
45	12,740	OM1	13.0	15.5
46	9,280	OM2	14.0	14.0
47	3,155	OM3	14.0	14.0
48	9,110	OM4	14.0	14.0
49	3,610	OM5	14.0	14.7
50	12,130	OM6	13.5	13.5
51	3,880	OM7	13.5	13.5
52	12,765	OM8	13.5	13.5
53	3,030	OM9	13.5	13.5
54	2,925	OM10	13.0	12.0
55	6,310	OM11	18.5	18.0
56	9,940	OM12	17.0	17.0
57	2,380	OM13	17.5	16.5
58	3,220	OM14	19.5	16.5
59	7,605	OM15	17.0	16.5
60	1,155	OM16	14.0	14.4
61	9,095	OM17	12.5	13.5
62	9,170	OM18	12.5	13.8
63	1,490	OM19	11.0	15.0
64	8,390	OM20	13.0	13.8
65	875	OM21	21.0	20.1
66	1,980	OM22	21.0	21.5
67	8,915	OM23	21.8	22.5
68	25,450	OM24	22.2	23.6
69	10,780	OM25	22.5	24.3

Reach	Length (ft)	Reach Name	Pre-Katrina HPS, ft	2007 HPS, ft
70	14,180	OM26	24.0	24.8
71	3,350	OM27	25.0	25.8
72	6,570	SB1	13.0	15.0
73	1,115	SB2	13.0	13.3
74	26,995	SB3	13.5	13.6
75	84,195	SB4	17.5	20.0
76	44,650	SB5	15.0	15.7
77	25,545	SB6	20.1	22.0
78	26,950	SB7	20.1	21.2
79	15,885	SB8	20.1	20.5
80	870	SB9	20.9	22.0
81	22,000	PL1	6.0	9.5
82	41,525	PL2	9.0	8.5
83	57,470	PL3	18.0	18.1
84	50,610	PL4	8.0	8.5
85	36,605	PL5	17.0	16.4
86	60,615	PL6	6.0	6.4
87	25,865	PL7	17.0	15.7
88	17,170	PL8	9.5	11.2
89	39,195	PL9	15.5	16.2
90	27,100	PL10	12.5	13.5
91	19,120	PL11	12.2	13.6
92	13,774	PL12	11.8	12.7
93	6,635	PL13	12.2	13.8
94	49,470	PL14	15.5	16.3
95	6,160	PL15	14.0	14.9
96	26,710	PL16	14.0	15.0
97	78,500	PL17	14.0	14.7
98	79,100	PL18	14.5	15.0
99	22,740	PL19	14.5	13.9
100	51,200	PL20	16.5	16.6
101	32,235	PL21	16.5	15.6
102	50,475	PL22	15.0	17.3
103	29,050	PL23	15.0	17.5
104	62,810	PL24	10.5	12.0
105	30,940	PL25	10.5	12.4
106	61,710	PL26	18.5	18.6
107	25,225	PL27	18.5	17.0
108	21,496	CW1	3.0	6.5
109	13,947	CW2	8.0	7.8
110	24,047	CW3	8.0	7.0
111	8,180	CW4	6.0	9.0
112	1,730	CW5	4.0	4.0
113	320	CW6	8.0	8.0
114	1,495	CW7	9.0	9.0
115	85,639	CW8	24.0	26.3
116	3,060	WH1	9.0	9.0
117	11,240	WH2	8.5	8.0
118	16,370	WH3	10.0	9.8

Reach	Length (ft)	Reach Name	Pre-Katrina HPS, ft	2007 HPS, ft
119	22,135	WH4	13.0	12.5
120	6,690	WH5	13.0	12.0
121	16,120	WH6	9.0	9.0
122	26,700	WH7	8.0	8.0
123	9,510	WH8	5.0	5.0
124	1,165	WH9	13.0	24.8
125	20,710	WH10	23.0	24.2
126	40,198	HA1	22.0	22.0
127	14,550	HA2	22.0	23.2
128	28,337	HA3	5.0	5.0
129	44,000	HA4	9.0	8.3
130	920	HA5	20.0	16.0
131	26,040	HA6	22.0	20.1
132	920	HA7	20.0	16.0
133	5,050	HA8	6.0	9.5
134	10,745	HA9	9.0	8.0
135	1,165	HA10	13.0	24.8
136	190	17th St	NA	16.50
137	215	Orleans	NA	18.00
138	160	London Ave	NA	18.00

Hazard Definition

Hazard is the likelihood of water levels created by storm surge and waves at each component of the HPS. The relationship between water levels and how frequently they are expected to occur must be established for many locations around the HPS. It is important to note that the IPET, Corps, FEMA and the National Oceanic and Atmospheric Administration (NOAA) have worked together with top hurricane experts to make sure that the process used is appropriate for this purpose. Collectively, these experts have greatly advanced the understanding of hurricane forces. The method used to define the hazard, Joint Probability Method - Optimal Sampling, is depicted in Figure 25 and in Appendix 8.

What storms might occur? The first step in defining the hazard requires looking at potential hurricanes. In the past, this was typically established by analyzing historical hurricanes and at times extrapolating from these records. In the initial design of the New Orleans HPS, historical data were used to define a "standard project hurricane." The standard project hurricane (HPS) is defined as a hypothetical hurricane intended to represent the most severe combination of hurricane parameters that is reasonably characteristic of a specified region, excluding extremely rare combinations. The surge created by the SPH traveling along a few select tracks was used as the basis of design. More recently, the historical record was used to artificially generate a larger sample of storms, much like those that have occurred, to provide multiple storms for modeling surge conditions that could occur. Experts believe these approaches are no longer adequate, especially with the recognition of trends towards more frequent and more intense storms. Yet the historical storms are important because they allow any process to be checked against what has already happened.

One of the major findings of the Katrina investigations was the importance of considering both the intensity of the storm (central pressure deficit related to the Saffir-Simpson scale) and the physical size (measured as the radius to the maximum wind speed of the storm) to adequately understand the surge generation capability of the storm. It was Katrina's combination of relatively high intensity and relatively large size that allowed it to create the highest surge ever experienced in North America. Figure 26 shows the pressure deficit—size relationship for historical storms. Note that Camille (Category 5 on Saffir-Simpson Scale at landfall) was a more intense storm than Katrina (Category 3 at landfall), but Katrina was considerably larger and had significantly greater surge generation potential.

Estimation of Probabilities of Maximum Surges

The key input driving the risk model is the spectrum of possible surge and wave conditions around the perimeter of the HPS. There are two primary steps in deriving this information:

(1) specification of surge and wave maxima and their corresponding probabilities, and (2) time sequences of surge and wave conditions near the time of peak surge. These are summarized in hydrographs for each reach, respectively, in the HPS model. Details of the methodology used to construct storm tracks and associated wind fields for this effort are included in Appendix 8 of this volume; however, a brief synopsis will be given here.

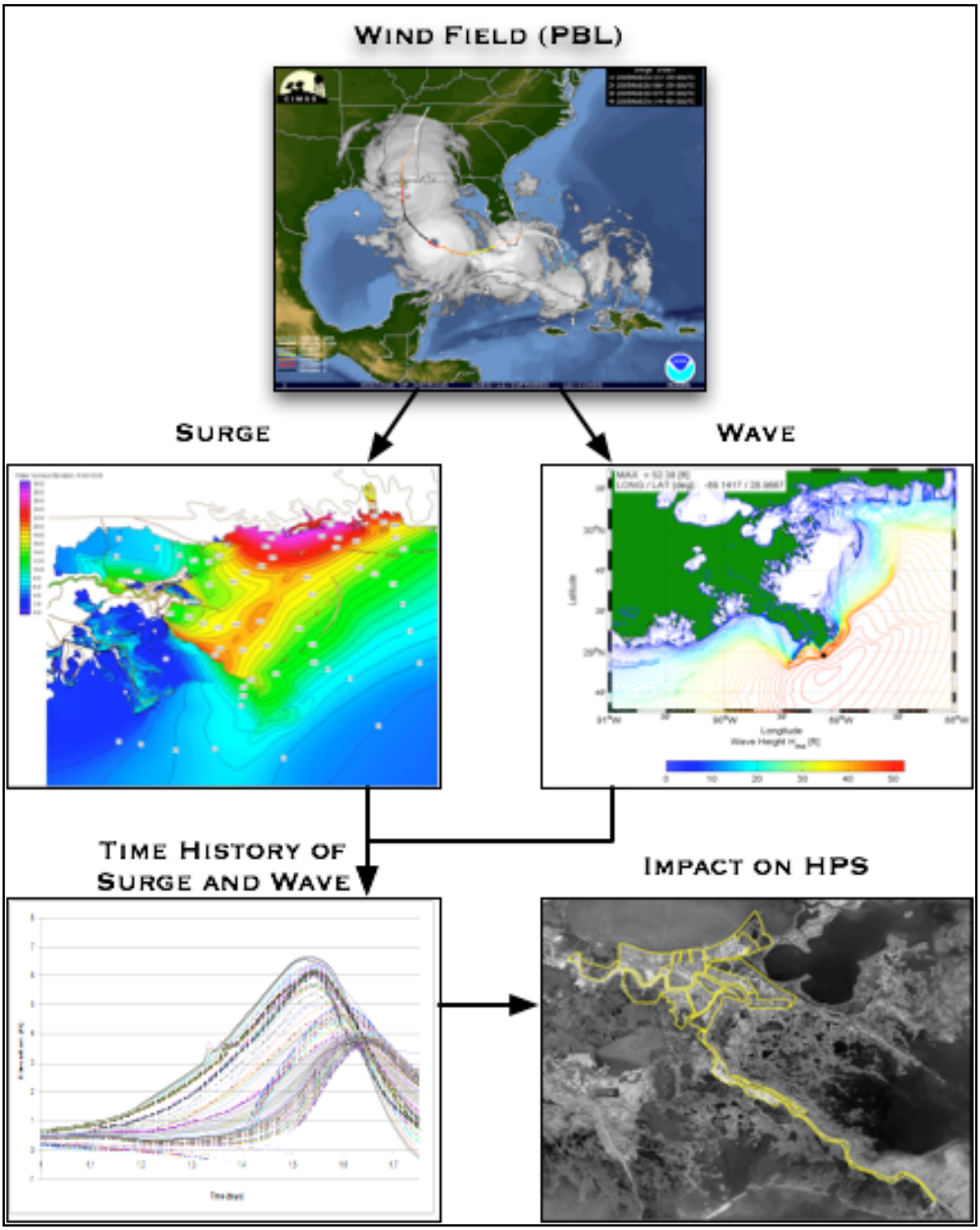

Figure 25. Concept and components of the hazard analysis.

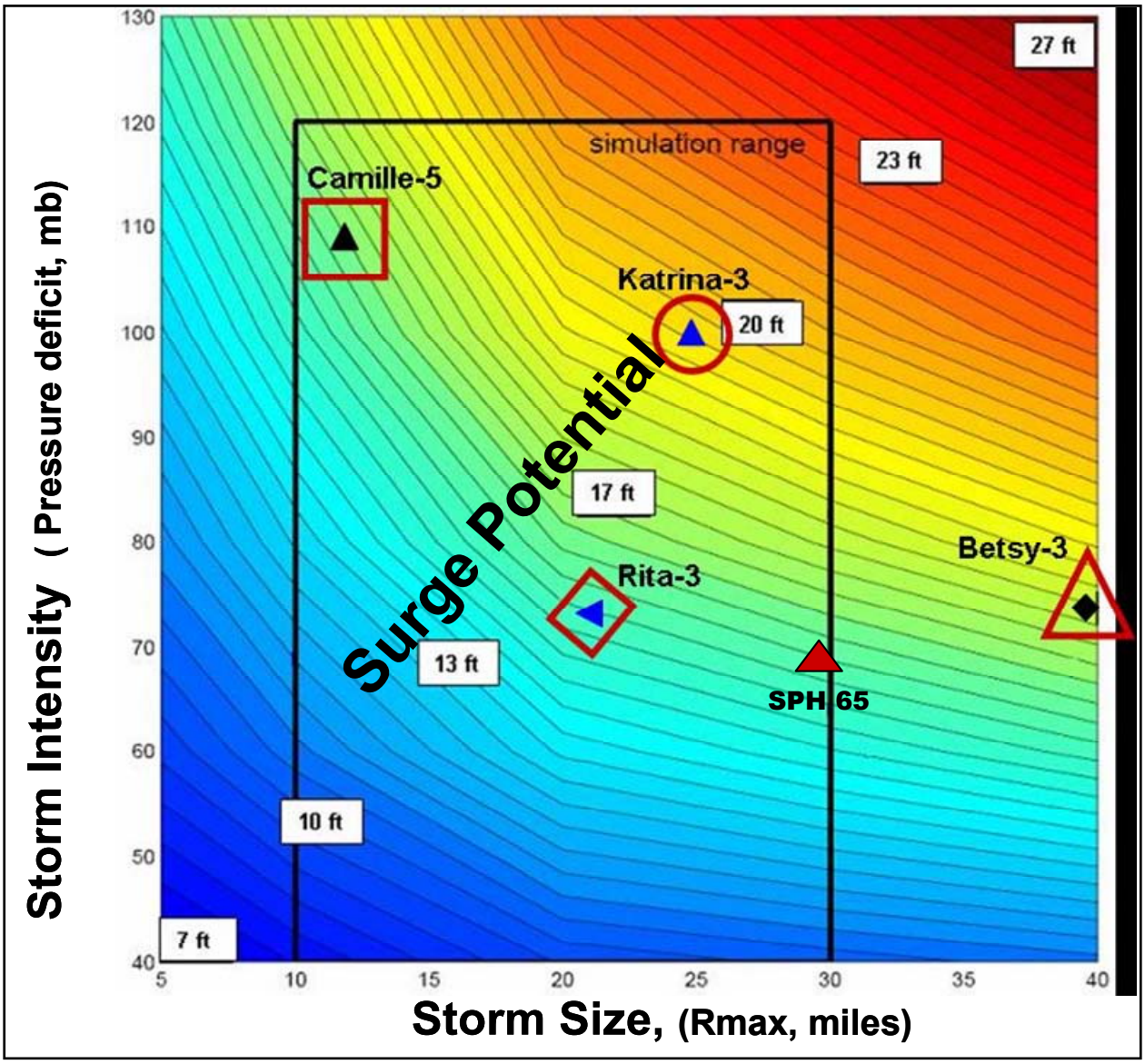

Figure 26. Relationship of storm intensity to size of historic storms.

The Joint Probability Method (JPM) for characterizing the probability of storms was developed in the 1970s (Myers 1975; Ho and Meyers 1975) and extended by a number of investigators (Schwerdt et al. 1979; Ho et al. 1987) to circumvent problems related to limited historical records. In early applications, the JPM assumed that storm characteristics were constant along the entire section of coast from which a sample of storms was drawn.

The JPM used four parameters to characterize storms:

1. Central pressure,
2. Radius of maximum wind speed,
3. Storm forward speed, and
4. The angle of the storm track relative to the coast.

Initial applications of the JPM assumed that the values of these parameters varied only slowly in storms approaching the coast; therefore, the values of the parameters at landfall could be used to estimate the surge at the coast. As shown in Appendix 8, recent data show that this is not a good assumption. Since storms are stronger off the coast, the use of landfall pressures to generate surge and wave fields tends to significantly underestimate storm intensities during the approach to land.

In the JPM, the surge at a point of interest located at $\underline{x}$ at time t can be thought of as being generated by an equation of the form

$$\eta(x,t) = \Phi(\underline{G},\underline{W} \mid c_p, R_{max}, v_f, \theta, S(t), t)$$

where

$\eta(x,t)$ is the storm surge at location x and time t,

Φ is a numerical model used to generate surges over a grid,

$\underline{G}$ is a time invariant grid of bathymetry/topography,

$\underline{W}$ is a wind field over the grid at time t, (2)

c_p is the central pressure,

R_{max} is the radius to maximum wind speed from the center of the storm,

v_f is the forward velocity of the storm,

θ is the geographic angle of the track, and

$S(t)$ is the position of the storm along the track at time t,

For a non-constant grid (levee breaching, variations in coastal landforms, etc.) and non-constant wind field parameters, this becomes,

$$\eta(x,t) = \Phi(\underline{G}(t),\underline{W}(t) \mid c_p(t), R_{max}(t), v_f(t), \theta(t), S(t), t) \quad (3)$$

where the dependence on time is explicitly shown. In either case, for a given storm define a maximum surge value for that storm, $\eta_{max}(x,t)$. With constant parameters, the probability for each event simulated can be associated with the probability of the parameters used to drive the wind model,

$$\Delta p(\eta_{max}) = p(c_p, R_{max}, v_f, \theta_l, x - x_0)\Delta c_p \Delta R_{max} \Delta v_f \Delta \theta_l \delta(x - x_0)$$

where

Δ here denotes the incremental size of the parameter element (4)

θ_l is the angle of the track relative to the coast at landfall and

$x - x_0$ is the distance between the point of interest and the landfall location

In this form of the equation, the size of the discretization can be seen to play a potentially important role in defining surge probabilities. Also in this form, the fifth parameter associated

with the earlier JPM approach, a location parameter relative to the landfall point, x_0, is introduced in order to extend the concept to multiple tracks.

Most JPM studies on even relatively small reaches of coast used 300 to 600 storm simulations to adequately resolve the probability structure, which imposed a computational burden compared to the historical storm approach. A particular deficiency of the JPM as it was initially applied was that little or no attention was paid to the impact of various sources of uncertainty on the results. As discussed in Appendix 8, it is possible to incorporate uncertainty directly into the JPM integral. This is an important step forward, since it allows us to recognize that predictive tools and statistical estimates all contain potential errors.

Recently, it has become clear that it is essential to resolve coastal bathymetry and landforms more precisely than they were resolved in earlier studies. This includes not only the need to resolve various small-scale features (such as roads, ridges, levee crests, etc.) in order to reliably assess impacts to these small-scale features, but also the need to resolve regions where physical processes (such as wave-current interactions) occur on a relatively small scale. As an example, the ADCIRC model domain for the New Orleans area used in recent simulations now contains over 2,000,000 computational nodes.[1] This level of resolution greatly increases the computational burden required to conduct a JPM-based study.

Since the JPM was introduced in the 1970s several issues have arisen which could directly affect the number of parameters which must be considered with an application. In 1980, Holland provided evidence that hurricanes (tropical cyclones/typhoons) exhibit considerably more variability in the peakedness of their velocities along a radial than could be explained by the simple wind models available at that time. Holland introduced a new parameter, now known as the Holland B term, which enhanced the ability of wind models to match observations. This introduces another parameter that should be considered within JPM. Since the assumption of constant parameters during approach to the coast is often violated by major storms, the variability of storm characteristics during this period represents another potential source of variability that might require parameterization and inclusion within the JPM.

Modern surge models have adopted a coupled model approach that combines the contributions of direct wind-driven surge with radiation stresses from wave fields. Since wave fields evolve over time intervals that are longer than those of coastal surges (tens of hours compared to hours), storm tracks cannot be treated as straight line segments over short distances near landfall for wave generation. Instead, physically consistent tracks must be defined over the typical distances which are involved in the development of the wave fields expected to accompany a hurricane, which potentially introduces a third source of variability that should be considered within the JPM.

It is apparent that the computational burden to simulate an individual storm accurately is large. One option would be to simplify the grid and some of the modeling complexity; however, it is hard to estimate the types and magnitudes of errors that result from such simplifications. In

[1] The Advanced Circulation Model (ADCIRC) is a finite element hydrodynamic model for coastal oceans, inlets, rivers and floodplains, and a product of the ADCIRC Development Group, http://www.nd.edu/~adcirc/index.htm.

the New Orleans area, such simplifications lead to serious misestimates for recent major storms. An alternative method is to develop an approach that reduces the number of sample storms that have to been simulated to provide a reasonable statistical characterization of the storm population. The overall approach to accomplish this optimization within the context of the JPM has now been termed JPM-Optimal Sampling, or the JPM-OS.

JPM-Optimal Sampling (JPM-OS)

One method to optimize a storm sample is to select a set of discrete storms via a process that replicates certain properties of the overall probability distribution. If one knows the characteristic scales of variation due to each parameter of the JPM along with their co-variation, it is possible to select the storm set quite efficiently. However, in situations where the probability distribution could change (climatic variability and/or due to additional years of data within the sample), it is advantageous to use a method which does not depend on prior knowledge of the joint distributions of the parameters. Such a method defines the storm set to be simulated to cover the expected range of conditions affecting the return periods of interest and generates a response function that is used to interpolate (and possibly extrapolate) over short parameter distances. This method, termed a response-surface method here, is presented here.

The definition of continuous (rather than discrete) surface probabilities via numerical storm surge models for an arbitrary number of parameters is,

$$p(\eta) = \int ... \int p(x_1, x_2, ..., x_n) \delta[\Psi(x_1, x_2, ..., x_n) - \eta] dx_1 dx_2 ... dx_n \quad (5)$$

where η (= η_{max} for each individual storm at a fixed spatial location) is the storm surge level, is $\delta[.]$ the Dirac delta function and $\Psi(x_1, x_2, ..., x_n)$ is a numerical model or system of models that operate on the set of parameters ($x_1, x_2, ..., x_n$) to provide an estimate of the surge level at a fixed location. This can be integrated to yield the CDF for surge levels

$$F(\eta) = \int ... \int p(x_1, x_2, ..., x_n) H[\eta - \Psi(x_1, x_2, ..., x_n)] dx_1 dx_2 ... dx_n \quad (6)$$

where $H[.]$ is the Heaviside function. If a sufficient number of degrees of freedom are retained to resolve the wind fields exactly, if the numerical codes are also "exact," and if the specification of the joint probability function $p(x_1,x_2,\ldots,x_n)$ is known exactly, this equation is an exact integral for the CDF with no uncertainty in its expected value. The sampling variability can be estimated by re-sampling methods along the lines of the empirical simulation technique (EST).[1]

[1] EST (Empirical Simulation Technique) is a statistical procedure for simulating life-cycle risk analysis of events such as storms and their corresponding environmental impacts. The EST is based on a "bootstrap" re-sampling-with-replacement, interpolation, and subsequent smoothing of observed and/or computed site-specific historical events.

The CDF integral shows that the number of dimensions required for an exact representation of the surge CDF must equal the number of degrees of freedom contained within the system (for practical purposes determined by the number of degrees of freedom contained in the wind fields). Since all wind fields, wave models, and surge models remain inexact, and since the estimates of joint probabilities are hampered by the small sample size, the actual representation of this integral should be written as

$$F(\eta) = \int \cdots \int p(x_1, x_2, \ldots, x_n, \varepsilon) H[\eta - \Psi(x_1, x_2, \ldots, x_n) + \varepsilon] dx_1 dx_2 \ldots dx_n d\varepsilon \quad (7)$$

where ε is an "error" term due to wind field deficiencies, ocean response model deficiencies, unresolved scales, etc. In this form, there is a trade-off between modeling accuracy and the magnitude of the error term, ε. There is also a trade-off between errors and uncertainties in the probability estimates and the overall accuracy in estimates of the surge CDF. These errors increase if the small sample is split (for example the historical hurricane record in the Gulf of Mexico) into information for too many dimensions.

It is advisable to limit the number of parameters considered in the JPM probability integral to those which most impact surge response and to include an approximation for all of the neglected terms within the error term, ε. As noted previously, planetary boundary layer (PBL) models provide a relatively accurate representation of the broad-scale structure within hurricanes. Furthermore, wind fields from PBL models have a long history of providing accurate ocean response estimates in Gulf of Mexico hurricanes (Cardone et al. 1976). Consequently, the logical choice appears to be to limit the number of dimensions in the JPM integral to the number of parameters contained within such PBL models,

$$F(\eta) = \int \cdots \int p(c_p, R_p, v_f, \theta_l, x, B) p(\varepsilon) H[\eta - \Psi(\vec{X}) + \varepsilon] dx_1 dx_2 \ldots dx_n d\varepsilon \quad (8)$$

where the error term has been separated from the rest of the probability distribution and with the vector set of parameters reduced to

$$\Psi(\vec{X}) = \Psi(c_p, R_p, \theta_l, v_f, B) \quad (9)$$

In this form, the "error" term allows the inclusion of additional effects on water levels, such as tides (albeit in an uncoupled, linear fashion). The term $R_{\max}$ is replaced with R_p (a pressure field scaling term rather than a wind speed scaling term), since the latter term is used in the PBL model that is used in the actual wind field construction here (Thompson and Cardone 1996).

Effort has gone into re-analyzing hurricane characteristics and hurricane wind fields for their impacts on coastal surges. One significant finding is that the Holland B parameter in mature storms within the Gulf of Mexico tends to fall into a fairly small range 0.9–1.6. Furthermore, numerical sensitivity tests of both wind fields and coastal surges driven with the PBL winds generated with the Thompson and Cardone (1996) model suggest that the adoption of a constant value of 1.27 for storms centered more than 90 nautical miles from the coast provided a

reasonable first approximation to both the wind fields and the surges. Thus, if the effects of B-variations are added into the "error" term, the CDF equation becomes

$$F(\eta) = \int \cdots \int p(c_p, R_p, v_f, \theta_l, x) p(\varepsilon \mid \eta) H[\eta - \Psi(\vec{X}) + \varepsilon] dx_1 dx_2 \cdots dx_n d\varepsilon \tag{10}$$

with

$$\Psi(\vec{X}) = \Psi(c_p, R_p, \theta_l, v_f, \overline{B})$$
$$\text{where} \tag{11}$$
$$\overline{B} \text{ is the mean value of } \overline{B}$$

Construction of Extended Storm Tracks for Wave Predictions

To obtain realistic wave fields for the wave component of the surge, it is essential to have representative tracks that extend across the entire wave-generation region. Figure 27 gives an example of one class of tracks defined by the working group for storms within the Gulf of Mexico.

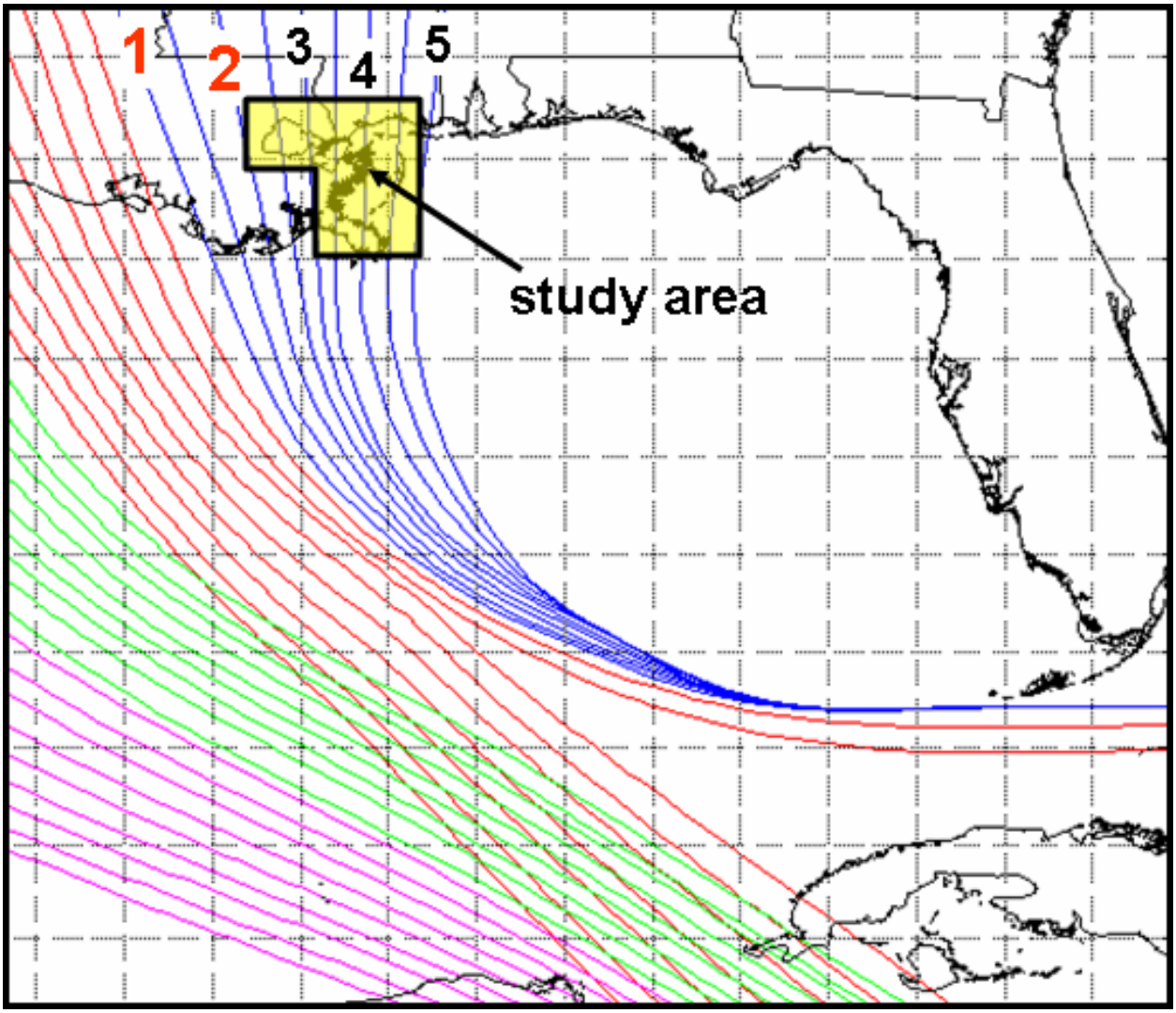

Figure 27. Example of one class of extended storm tracks for Gulf of Mexico.

The Effect of Time Variations in the Parameter Set

Considerable evidence has emerged in recent years that the wind fields in hurricanes vary considerably during the approach to shore. One approach to characterize this in a statistical context is to discretize the rate of change of each of the four wind field parameters and consider this within the scope of the simulations. Unfortunately, this would increase the computational burden at least by a factor of 3. Sensitivity studies have shown that the typical range of variations in storm angle and storm speed during approach to land is small and does not appear to affect estimated surge values significantly. Thus, it is primarily variations in storm intensity and storm size (and to a lesser extent the variation in the mean value of the Holland B term) that are important to capture during approach to land. This would change the form of Equation 5 to

$$\Delta p(\eta_{max}) = p(c_p, R_{max}, v_f, \theta_l, x_0, \Delta c_p, \Delta R_{max}) \Delta c_p \Delta R_{max} \Delta v_f \Delta \theta_l \Delta x_0$$

where

Δc_p is the change in the central pressure during its approach to land and

ΔR_{max} is the change in storm size during its approach to land. (12)

and would reduce the number of additional degrees of freedom in the simulation to two. However, even if only three categories were used to represent variations in both of these parameters, it would still increase the computational burden by a factor of nine. An alternative to this is to use a deterministic function to capture the mean values of Δc_p and ΔR_{max} much in the manner that was used for the Holland B term.

Based on an analysis of all data for hurricanes within the Gulf of Mexico that attained central pressure less than or equal to 955 mb at some time during their passage through the gulf, the following equation provided a reasonable fit to the rate of change over the last 90 nautical miles of approach to the coast

$$< \Delta c_p > = R_{max} - 6$$

where

c_p is in millibars and

R_{max} is in nautical miles. (13)

where the < > brackets denote the averaging over the entire sample.

The mean rate of change appears to be size dependent. The finding of an average storm de-intensification during approach to shore is consistent with the findings of Rappaport (2007). Kimball (2006) has shown that such decay is consistent with the intrusion of dry air into a hurricane during its approach to land. Other mechanisms for decay might include lack of energy production from parts of the hurricane already over land and increased drag in these areas. In any event, the evidence appears rather convincing that major hurricanes begin to decay before they make landfall, rather than only after landfall as previously assumed. Since the empirical basis for this decay is drawn only from data in the northern Gulf of Mexico, these results should be treated as site specific to that area.

During this study it was also found that the mean variation in storm size could be represented by a simple multiplicative factor, independent of storm intensity, with storms increasing their size by about 30% over the last 90 nautical miles of approach to the coast. It was also determined that the Holland B term decreased from its average value of 1.27 off the coast to a value of about 1 at the coast. Thus, the final form for the continuous probability is

$$F(\eta) = \int \cdots \int p(c_p, R_p, v_f, \theta_l, x) p(\varepsilon \mid \eta) H[\eta - \Psi(X) + \varepsilon] dx_1 dx_2 \ldots dx_n d\varepsilon \quad (14)$$

with

$$\Psi(\vec{X}) = \Psi(c_p, R_p, \theta_l, v_f, \overline{B}, <\Delta c_p>, <\Delta R_p>) \quad (15)$$

The error term now must add potential sources of variability due to the parameters represented by "mean" approximations. Numerical sensitivity studies indicate that the overall variations in peak surges due to the "filling" characteristics and longer track variations are actually relatively small compared to the assumption of holding the Holland B term constant. A conservative estimate of this 15% of the total surge for the constant Holland B assumption encompasses the expected variability due to all three of these sources of variation that were suppressed here.

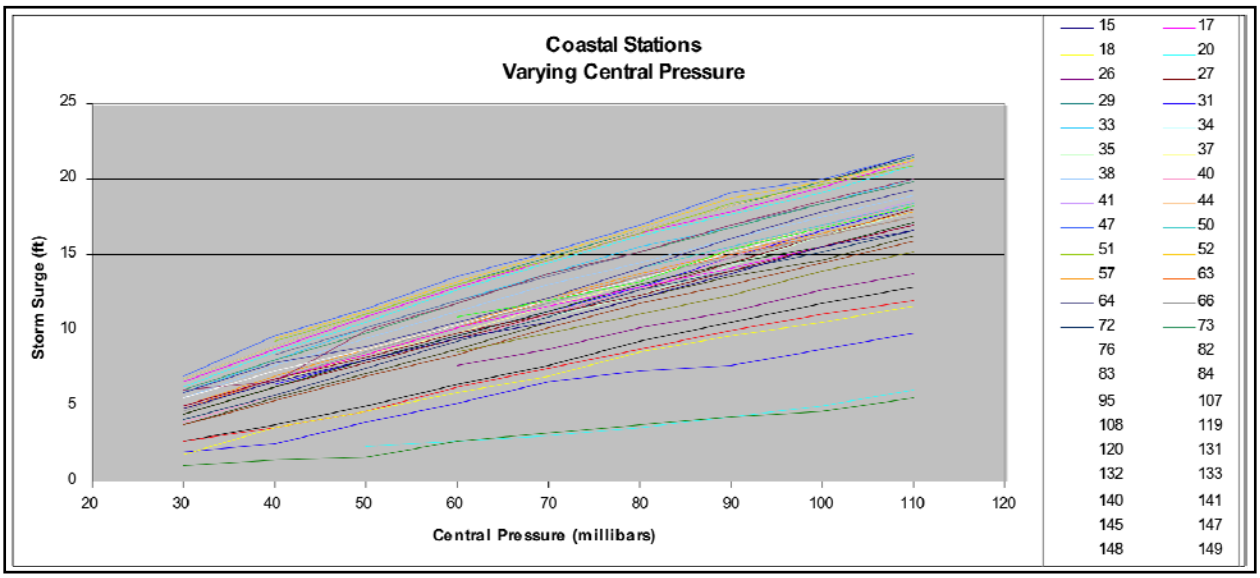

Figure 28. Characteristic variation in coastal surges as a function of central pressure from SLOSH simulations along the Mississippi coast.

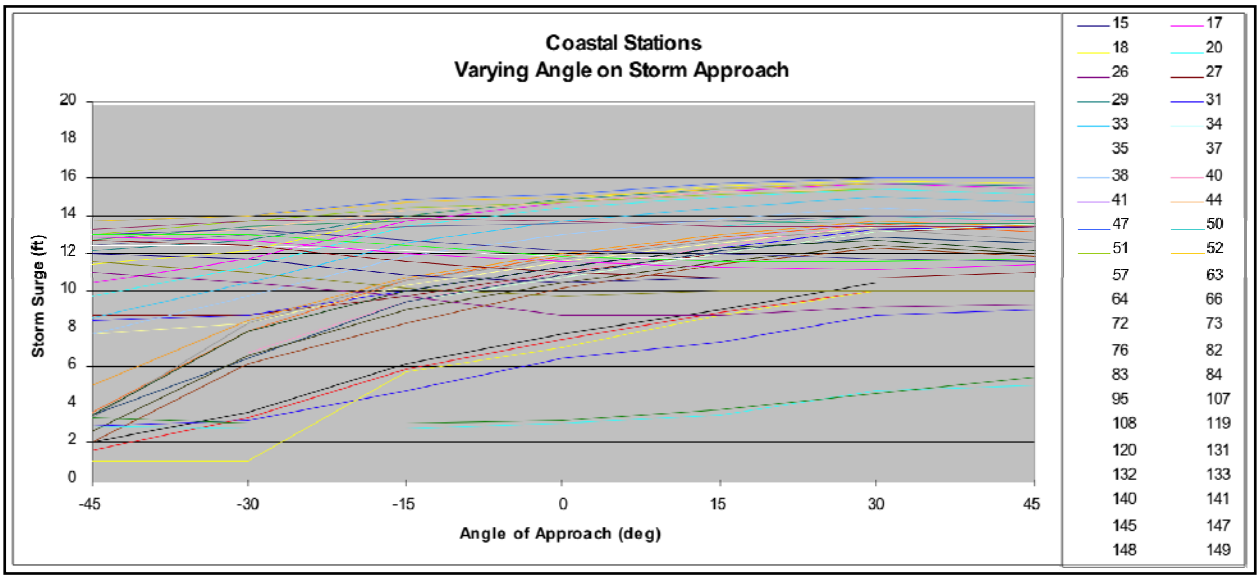

Figure 29. Characteristic variation in coastal surges as a function of angle of storm approach from SLOSH simulations along the Mississippi coast.

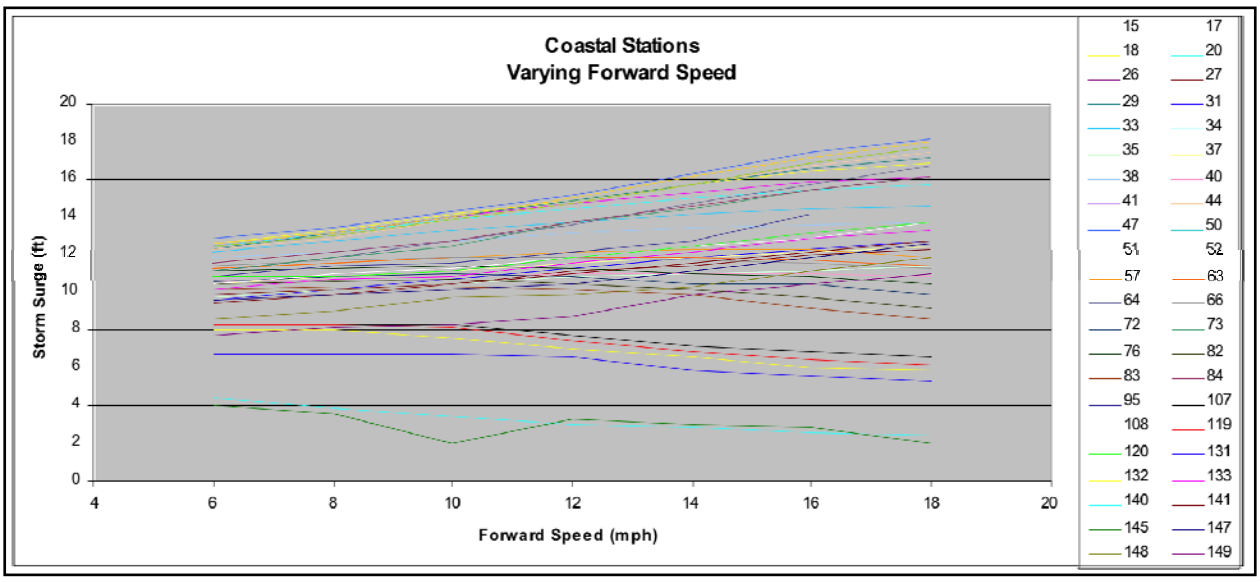

Figure 30. Characteristic variation in coastal surges as a function of forward storm speed from SLOSH simulations along the Mississippi coast.

Numerical studies using ADCIRC and SLOSH have shown that coastal surge levels are dependent on storm intensity, typically categorized by pressure differential defined as the peripheral pressure minus central pressure (i.e., $\Delta p = p_0 - c_p$, where p_0 is the peripheral pressure), storm size ($R_{\max}$ or R_p), and storm location relative to a site. Storm surge is less sensitive to forward storm speed and angle of the storm relative to the coast. Figure 28 shows the characteristic variation of surge elevations at coastal stations as a function of variations in pressure differential ($p_0 - c_p$), based on SLOSH tests along the coast of Mississippi. Figure 29 and Figure 30 show the characteristic variations of coastal surges as a function of storm angle relative to the coast (θ_l) and forward storm speed (v_f), respectively. As can be seen here, surge

variations as a function of these three parameters tend to be smooth with either linear or slightly curved slopes in these figures.

For a given location, a major portion of the surge response to hurricanes has been shown to be captured by the variation of Δp and R_p (Irish et al. 2007). Because of this, the surge response integration method uses $\Delta p - R_p$ planes as the primary variables within the five dimensional parameter space used in the JPM. Thus, for a fixed value of storm landfall location (x), storm track angle at the coast (θ_l), and storm speed (v_f), the response function at location (x,y) is defined as

$$\eta_{\max}(x, y) = \phi_{kmn}(\Delta p, R_p, x, y) \tag{16}$$

where ϕ_{kmn} is the surge response function and the subscripts *k, m,* and *n* denote a specific track angle, storm speed, and landfall location, respectively. This notation reflects the fact that this response function must be defined for each spatial (*x, y*) point in the computations. Figure 31 shows the set of storm size and intensity values that were used to cover the range of storms used in the simulations for New Orleans. Since the variations of surge with storm size and intensity have been relatively well established, extrapolation of these parameter values is accomplished inside the probability integral.

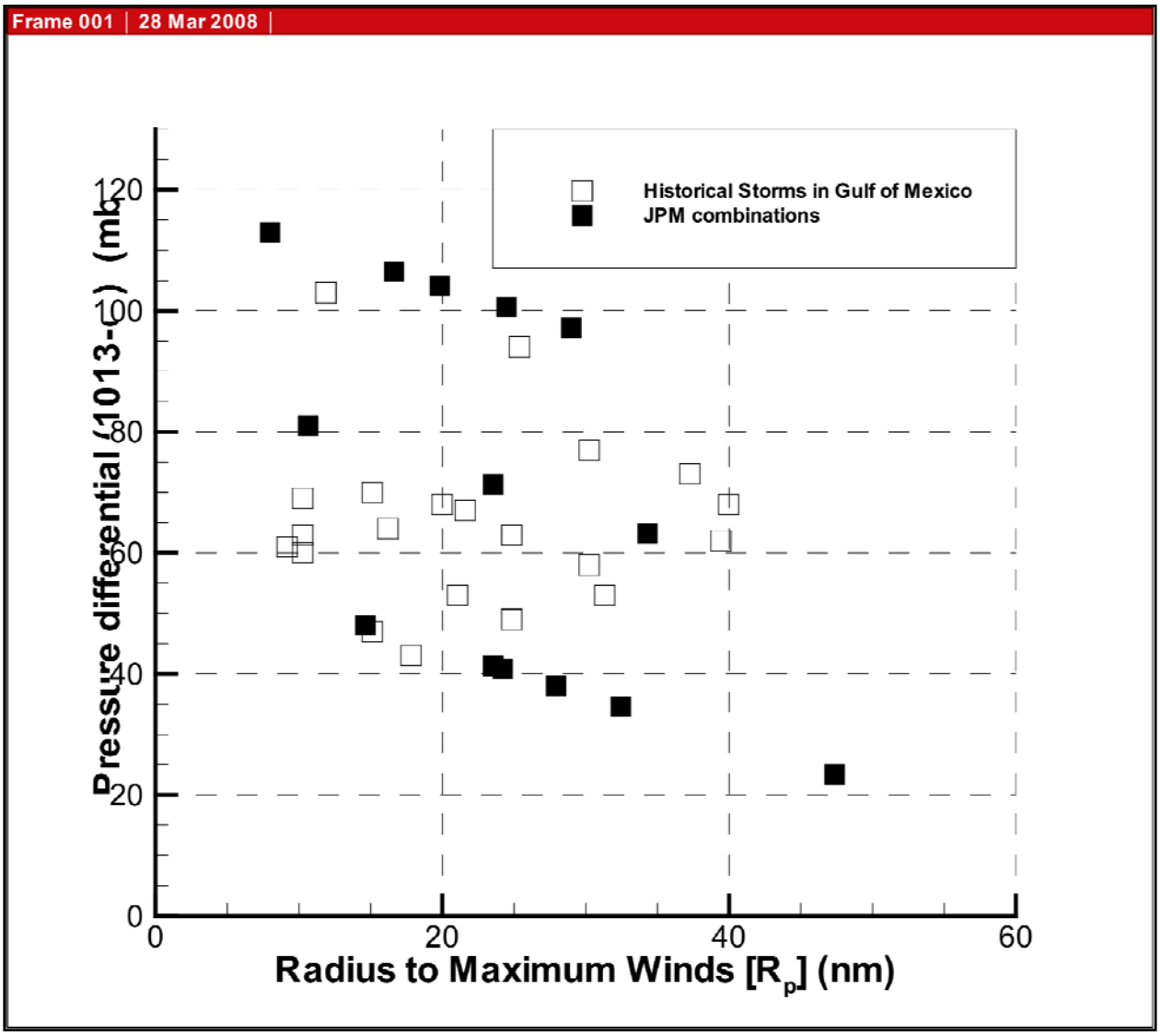

Figure 31. Relationship of central pressures and storm sizes simulated in JPM study to historical storms within the Gulf of Mexico.

The effect of variations in storm speed has been found to be fairly small and tends to have fairly linear slopes that are roughly independent of $R_{\max}$ and Δp; consequently, only a small number of storms is required to represent the variation in surge levels as a function of forward storm speed. This retains the overall structure of the response function for the initial forward speed values used in Equation 12. In general within this approach, the value of $[\phi_{kmn}(\Delta P, R_p, x, y)]$ for different forward speeds is obtained from the relationship

$$\phi_{kmn}(\Delta P, R_p, x, y) = \phi_{k_0 m_0 n}(\Delta P, R_p, x, y) + \Psi_{kmn} \tag{17}$$

where

The subscript "0" refers to the central speed and angle categories for a specific landfall location; and

$$\Psi_{kmn} = \frac{\partial \phi_{kmn}(\Delta P, R_p, x, y)}{\partial v_f} \delta v_f + \frac{\partial \phi_{kmn}(\Delta P, R_p, x, y)}{\partial \theta_l} \delta \theta_l$$

For the cases in which a single storm is used to infer the variation with forward speed Ψ_{kmn} reduces to a constant.

One concern is the sensitivity of probability estimates to storm track spacing. In the study of the New Orleans area, two sets of tracks were investigated: primary tracks with a spacing of about 40 km, and secondary tracks midway between the primary tracks. The sufficiency of the spacing of the primary tracks to represent the surge response in this area can be investigated by comparing results from the secondary tracks to results of interpolations between primary tracks. Figure 32 shows the results of these comparisons. In general little or no bias is introduced into the probability integration by using only results from the primary tracks over the entire range of surges in the 50- to 100-year return interval range.

In recent numerical studies, the use of the surge-response approach that was applied in the New Orleans area continues to be validated. Recently, storm surges along the Texas coastline were computed using the finite-element long-wave numerical model ADCIRC (Westerink et al. 1992, 2007). The ADCIRC model domain included the entire Gulf of Mexico water body and North Atlantic basin, and the domain highly resolved the entire northern Gulf of Mexico nearshore and inland bay system particularly along the Texas coast. These numerical domain and associated calibration inputs were verified for surge simulation demonstrating accuracy within 30 cm for most locations within inland bays and along the open coast throughout the northern Gulf of Mexico (USACE 2006a, 2006b).

Storm surge within ADCIRC for this investigation was forced with meteorological inputs for wind and barometric pressure. Figure 33 shows a typical comparison of estimates based on larger track spacing (using defined surge response characteristics from a similar storm set as used in the New Orleans study) to estimates from intermediate tracks. This figure shows comparisons of the surges estimated from 60-km spacing (red) to those from intermediate tracks (30-km spacing). The resulting estimates are all similar. Similar comparisons have shown that this agreement continues to the 15-km track spacing. This further supports the argument that the scale of track spacing used in the New Orleans area should provide a very good representation for estimating storm surges from intermediate tracks along the coast and suggests that the 152-storm set used is functionally equivalent to a storm set that is at least two to four times larger in terms of numbers of tracks. Since storm intensity, storm size, and storm track are the primary variables affecting storm surge and since these appear to have functions which can be well specified in terms of their surge response characteristics, there is little reason to believe that the 152-storm set used does not produce very similar results to those that would be obtained from a much large set of simulations.

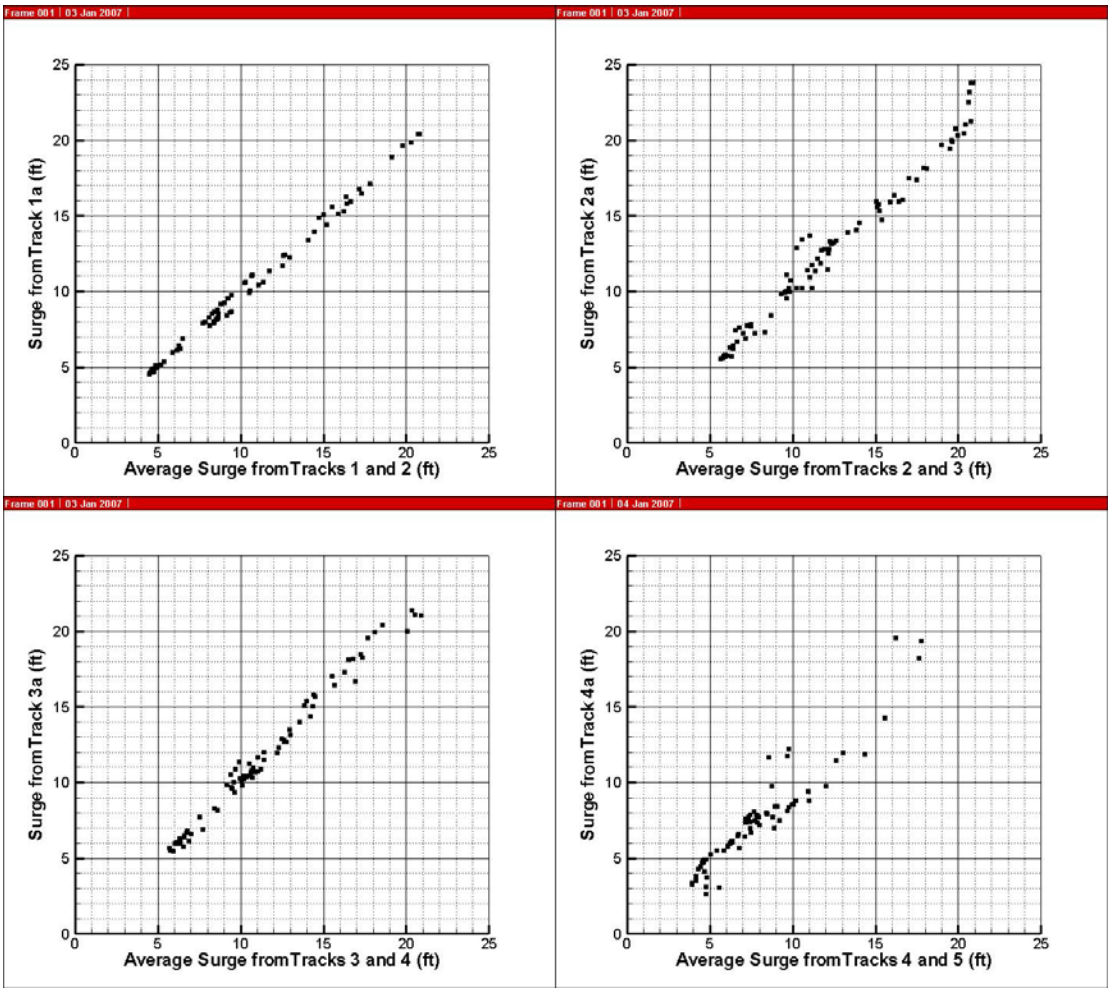

Figure 32. Plots of interpolations from tracks with spacing to results from intermediate tracks for points in the New Orleans area for various track combinations.

Considerable progress has been made and continues to be made in the area of estimation of probabilities of maximum surges in hurricanes. Based on the material shown here, it seems that the overall methodology used here is as good as the state of the art permits. Table 5 and Figure 34 to Figure 36 show the resulting 50-, 100-, and 500-year storm surge levels for Louisiana coastal areas developed via the methodology described here. In Resio et al. (2007) it is shown that the Vickery wind model and the Oceanweather wind model used here give very similar results. Furthermore, it is also shown that the storm intensity (central pressure) distributions are essentially identical for the entire Gulf of Mexico and for selected subsections. Additionally the characteristic Holland B values used are very characteristic of the gulf and size and storm sizes are well documented. Given all these facts, the distribution of wind speeds from the methodology used in this study are expected to be also very similar to those used in other accepted methods for wind specification for hazards within this region.

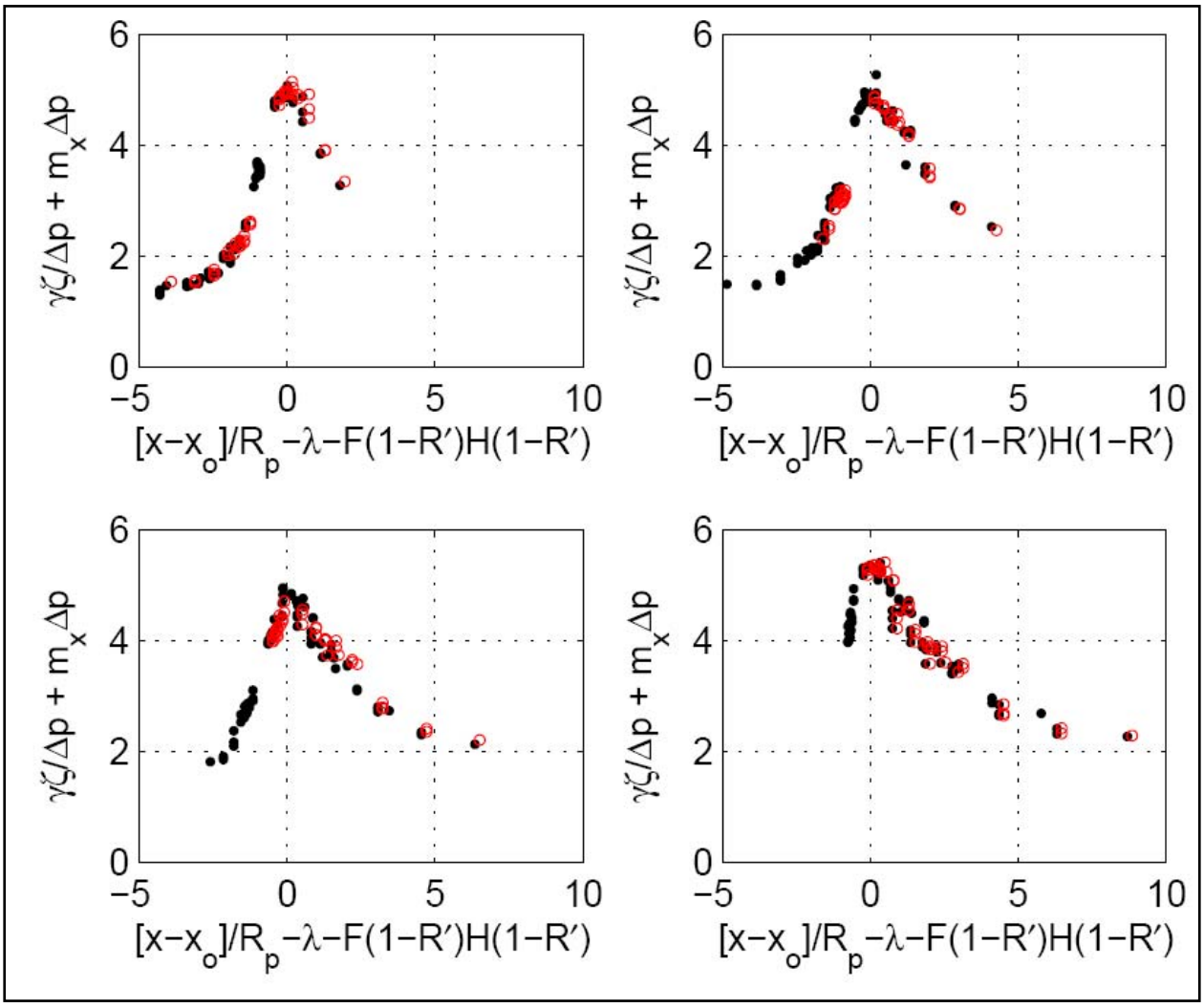

Figure 33. Comparison of interpolated surges from 60-km spaced tracks (red points) to actual computed surges on intermediate tracks (black points) for several track combinations along the Texas coast.

Table 5. Surge height in feet by reach and return period.

Reach ID	50-year	100-year	500-year	1000-year
1	8.3	9.4	12.3	12.9
2	8.4	9.5	12.3	12.9
3	8.4	9.5	11.9	12.9
4	1.2	9.4	11.8	12.9
5	8.3	9.3	11.2	12.1
6	8.3	9.4	11.0	11.9
7	8.3	9.3	11.0	11.7
8	8.3	9.3	11.0	11.7
9	8.4	9.6	11.3	11.8
10	8.6	9.7	11.9	12.7
11	8.8	10.3	13.1	13.9
12	9.8	11.5	13.6	14.2

Reach ID	50-year	100-year	500-year	1000-year
13	10.7	12.0	14.1	15.2
14	12.9	15.1	17.3	18.4
15	14.3	16.7	19.1	20.2
16	15.2	17.5	20.1	21.2
17	15.8	18.2	21.1	22.0
18	16.5	18.9	21.1	21.9
19	16.7	19.2	21.1	21.9
20	16.6	19.1	21.1	21.9
21	16.6	18.6	21.1	21.9
22	16.3	17.6	19.7	20.0
23	15.5	16.5	17.7	18.0
24	15.0	15.8	16.8	17.0
25	14.9	15.7	16.8	17.0
26	14.8	15.6	16.8	17.0
27	14.8	15.6	16.7	17.0
28	14.0	14.7	15.8	16.0
29	11.5	12.3	13.7	14.0
30	10.0	11.9	15.8	16.6
31	9.5	11.4	15.0	15.7
32	9.2	10.8	14.0	14.7
33	8.9	10.3	13.0	13.7
34	8.7	10.1	12.5	12.8
35	8.9	10.5	13.4	13.8
36	12.4	14.3	16.0	16.7
37	12.5	14.3	16.0	16.7
38	10.1	11.7	15.8	16.6
39	10.1	12.6	15.7	16.6
40	10.5	12.5	15.8	16.9
41	10.1	12.4	15.3	15.9
42	12.5	14.3	16.0	16.9
43	9.8	12.5	15.6	16.1
44	10.1	12.3	15.5	15.9
45	8.9	10.5	13.4	13.7
46	8.8	10.3	13.4	13.8
47	8.5	9.6	12.4	12.8
48	8.8	10.3	13.4	13.8
49	8.5	9.6	12.3	12.7
50	8.7	9.9	13.3	13.9
51	8.4	9.4	12.3	12.9
52	8.6	9.9	13.3	13.9
53	8.4	9.4	12.3	12.9
54	8.6	9.8	12.4	12.7
55	8.4	9.6	12.1	12.6
56	8.4	9.5	12.2	12.8
57	8.3	9.4	12.2	12.8
58	8.3	9.3	12.2	12.8
59	8.2	9.2	11.9	12.9
60	8.2	9.2	12.3	12.9
61	11.1	11.9	13.6	13.9

Reach ID	50-year	100-year	500-year	1000-year
62	14.3	15.0	16.0	16.9
63	14.8	15.6	16.8	17.0
64	14.7	15.6	16.8	17.0
65	14.7	15.6	17.0	17.9
66	14.8	15.7	17.5	18.0
67	13.1	14.5	16.3	17.3
68	13.1	14.6	16.3	17.3
69	12.7	14.5	16.5	17.3
70	12.6	14.3	16.0	16.8
71	12.4	14.2	16.0	16.7
72	14.7	15.6	16.8	17.0
73	14.6	15.5	16.8	17.0
74	15.0	15.8	16.9	17.5
75	14.9	17.1	20.2	20.9
76	16.0	18.4	20.9	21.6
77	13.1	14.5	16.2	17.4
78	13.1	14.5	16.2	17.3
79	13.1	14.5	16.4	17.4
80	14.7	15.7	17.0	17.9
81	5.7	7.2	7.9	8.0
82	5.6	7.6	9.0	9.7
83	14.1	15.5	17.7	18.6
84	5.9	8.6	12.2	13.4
85	14.6	16.0	19.3	20.2
86	7.3	9.3	14.1	14.7
87	14.8	16.6	19.4	20.3
88	8.7	12.5	16.0	16.9
89	14.8	18.0	21.2	21.7
90	10.2	13.3	17.3	18.2
91	11.8	13.7	18.0	18.9
92	11.4	13.8	18.8	19.7
93	15.1	18.6	21.8	23.4
94	10.2	12.7	18.0	18.7
95	10.5	13.0	17.9	18.8
96	10.5	12.9	18.4	19.9
97	10.4	12.6	20.2	21.0
98	14.2	16.1	20.5	21.3
99	15.5	18.2	22.7	23.9
100	14.7	16.9	19.6	20.4
101	14.7	17.3	20.0	21.1
102	14.9	17.1	20.3	20.8
103	16.6	19.2	21.9	22.9
104	15.4	18.8	21.8	22.5
105	15.8	17.6	20.2	20.9
106	14.1	15.5	17.8	18.6
107	14.6	16.3	19.2	19.9
108	5.4	6.4	8.2	8.8
109	5.4	7.2	8.2	8.8
110	5.4	7.2	8.3	8.8

Reach ID	50-year	100-year	500-year	1000-year
111	5.3	7.2	8.2	8.7
112	5.3	7.2	8.2	8.7
113	5.3	7.2	8.2	8.7
114	5.3	7.2	8.2	8.7
115	12.5	14.3	16.0	16.7
116	5.3	7.2	8.2	8.7
117	5.3	7.2	8.2	8.7
118	4.8	6.7	8.0	8.5
119	4.7	7.1	8.3	8.8
120	1.1	7.1	9.0	9.7
121	1.1	6.6	9.9	10.7
122	5.6	7.6	9.0	9.6
123	5.7	7.6	9.1	9.7
124	2.8	2.9	3.0	3.0
125	12.6	14.5	16.5	17.3
126	13.1	14.5	16.3	17.4
127	13.1	14.5	16.0	16.8
128	5.6	7.6	9.1	9.7
129	5.6	7.2	7.9	8.0
130	5.7	7.2	7.9	8.0
131	13.1	14.5	16.2	17.3
132	5.7	7.2	7.9	8.0
133	5.7	7.2	7.9	8.0
134	5.7	7.2	7.9	8.0
135	2.8	2.9	3.0	3.0
136	8.6	9.8	12.2	12.7
137	8.4	9.5	11.9	12.5
138	8.4	9.4	12.2	12.6

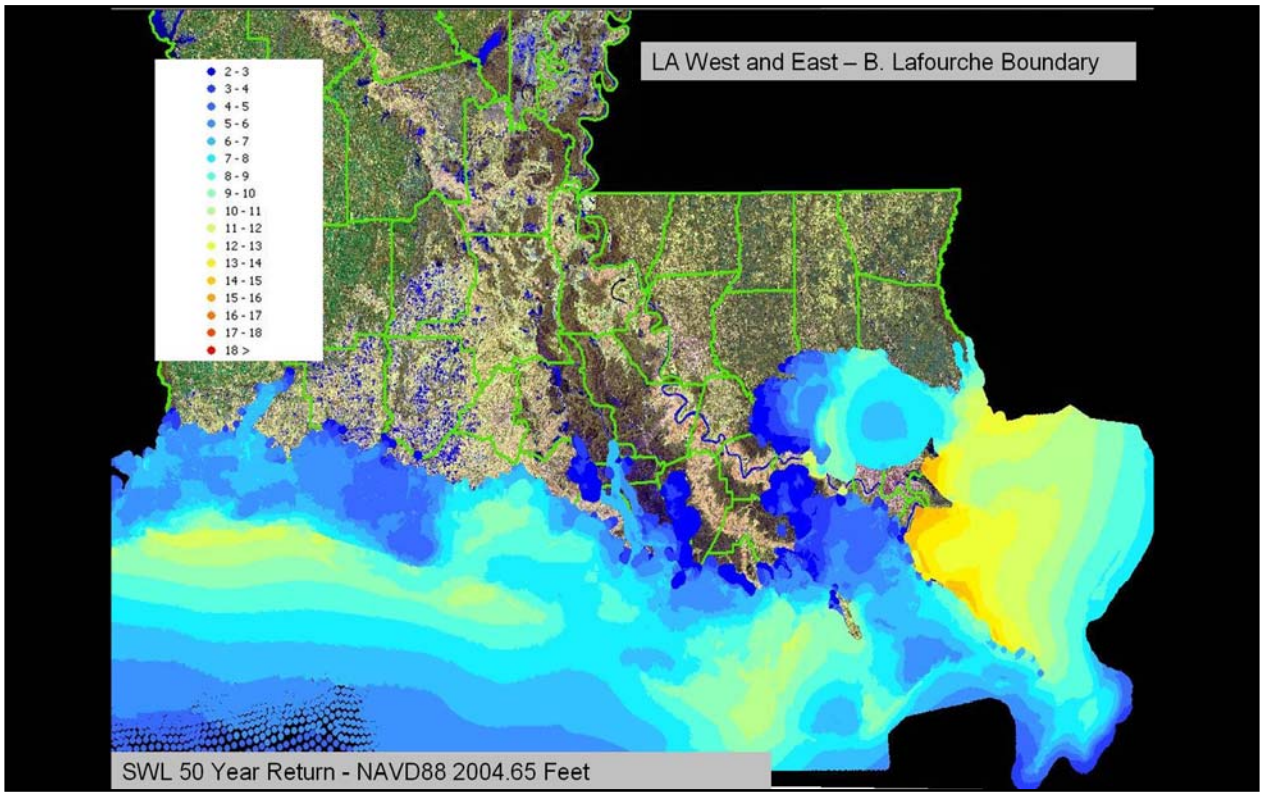

Figure 34. 50-year surge levels estimated from JPM.

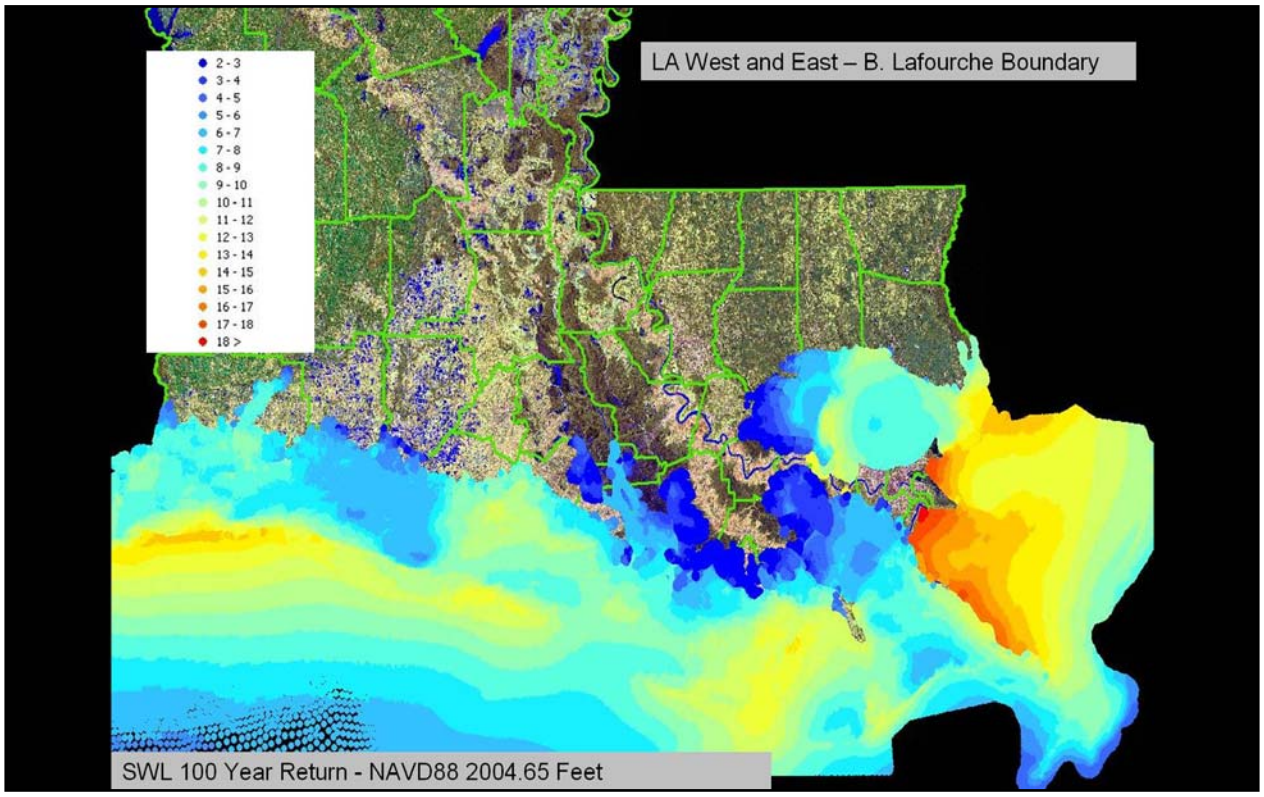

Figure 35. 100-year surge levels estimated from JPM.

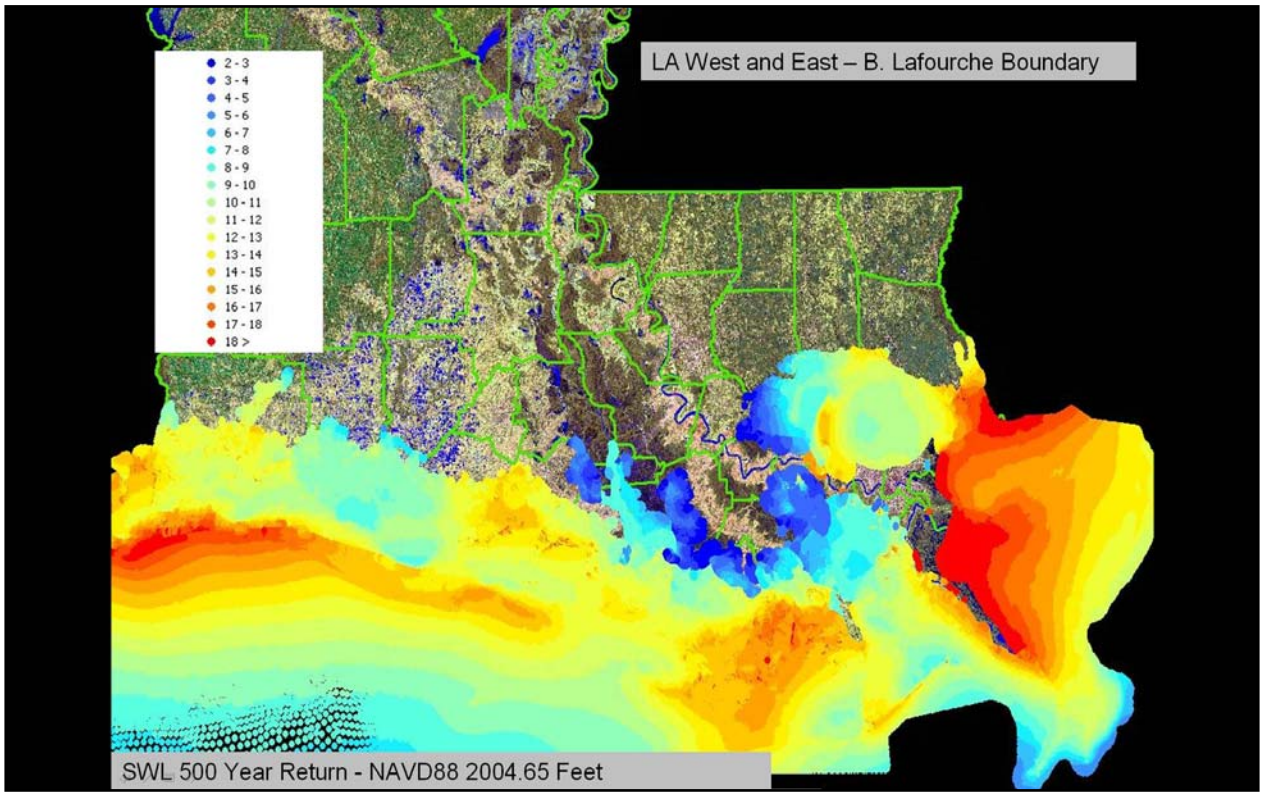

Figure 36. 500-year surge levels estimated from JPM.

Estimation of Maximum Wave Conditions

An important question that remains is what are the wave conditions that affect levees and floodwalls during high surge conditions? The precise co-variation in waves and surges has not been totally resolved at this time; consequently, some level of conservatism is warranted. On flat slopes, current wave models and data sets support a limiting value for the significant wave height as being 0.43 times the depth. For simplicity in subsequent analyses in this report, wave heights along levees exposed to open-coast wave attack are assumed to be represented by this relationship to the surge.

Construction of Surge Hydrographs

Two different approaches to the generation of storm hydrographs centered on the peak surges from the previous section have been investigated, a method based on parametric hydrograph shapes and a method based on non-dimensional empirically based functions. A duration parameter for storm hydrographs should effectively convey the length of time one can expect the surge from a storm with given characteristics to stay above a threshold, taken here as 70% of the peak surge η_{max}. Due to considerable spatial variability caused by bathymetric and topographic features, the duration parameters and trends (versus storm parameters) are very location-specific. Figure 11 shows three storm hydrographs for a location at the northern end of the Mississippi River Gulf Outlet (MRGO), with the time above $0.7\eta_{max}$ shown by the red lines.

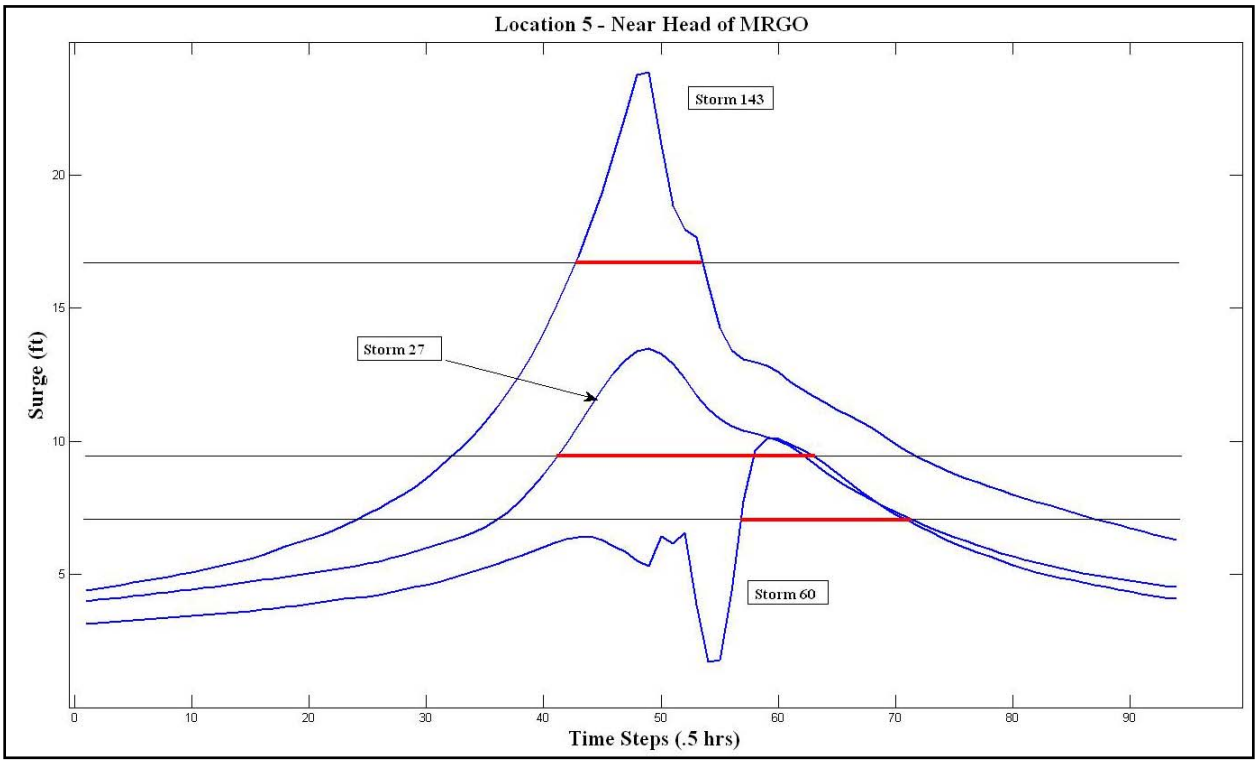

Figure 37. Storm hydrographs from three different storms at a selected location at the northern end of the MRGO.

The storm-to-storm variation in both peak surge and surge variation through time is considerable, as is the total duration above the $0.7\eta_{max}$ threshold. An analysis of the variations in durations with storm characteristics (as well as a shape parameter σ discussed below) is conducted to identify any meaningful trends.

Filtering of Hydrographs

Only hydrographs with η_{max} values of >5.0 ft were considered for further analysis. Additionally, hydrographs where η_{max} was within 10 time-steps of the beginning or end of the curve were dropped from further analysis. One final check was used to filter out hydrographs with significant "dry" periods. Such periods make it difficult to extract duration parameter information from the hydrograph and would likely lead to spurious data points in subsequent trend analysis. Figure 38 to Figure 40 show three examples of hydrographs that are screened from further duration analysis.

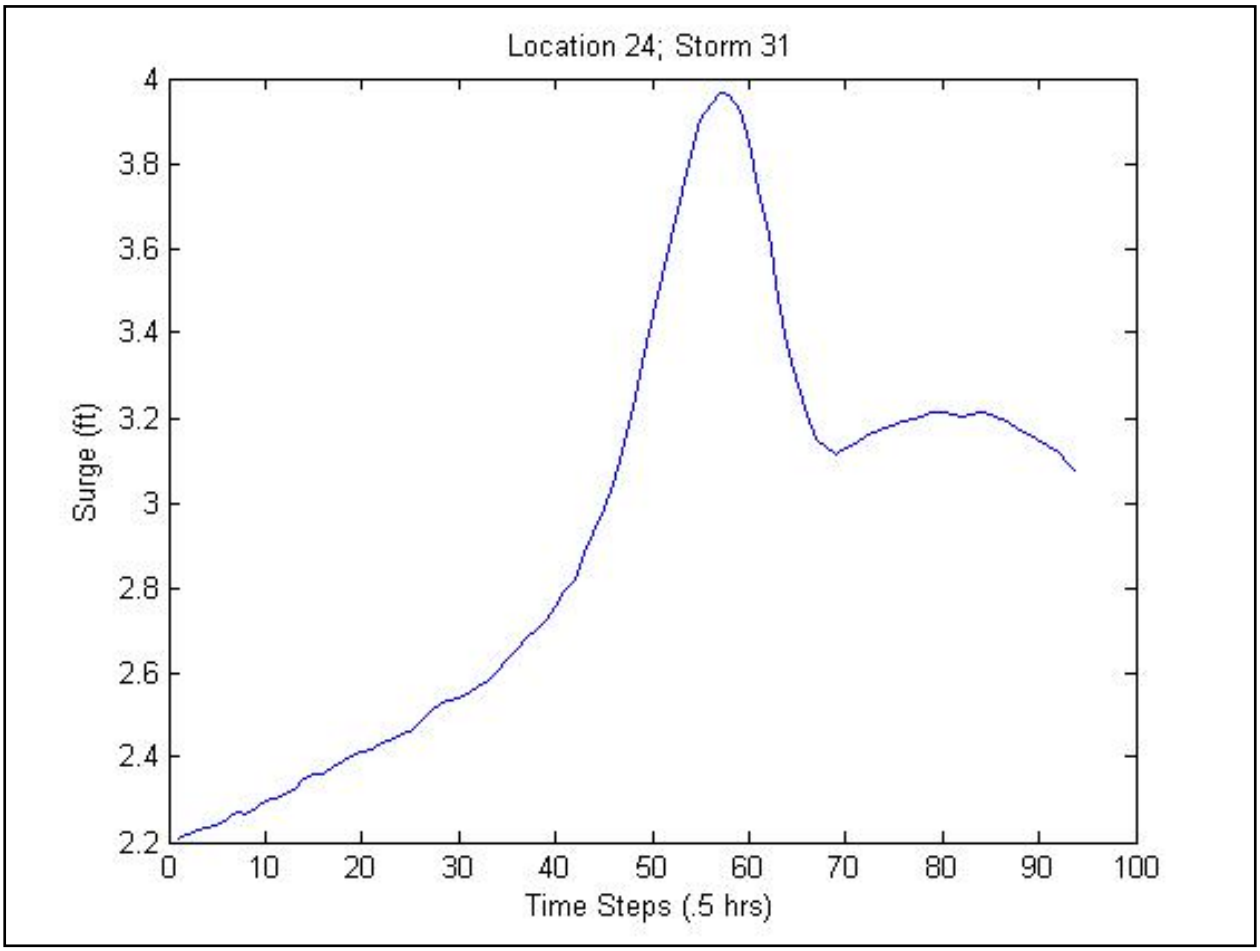

Figure 38. Hydrograph of η_{max} < 5 ft.

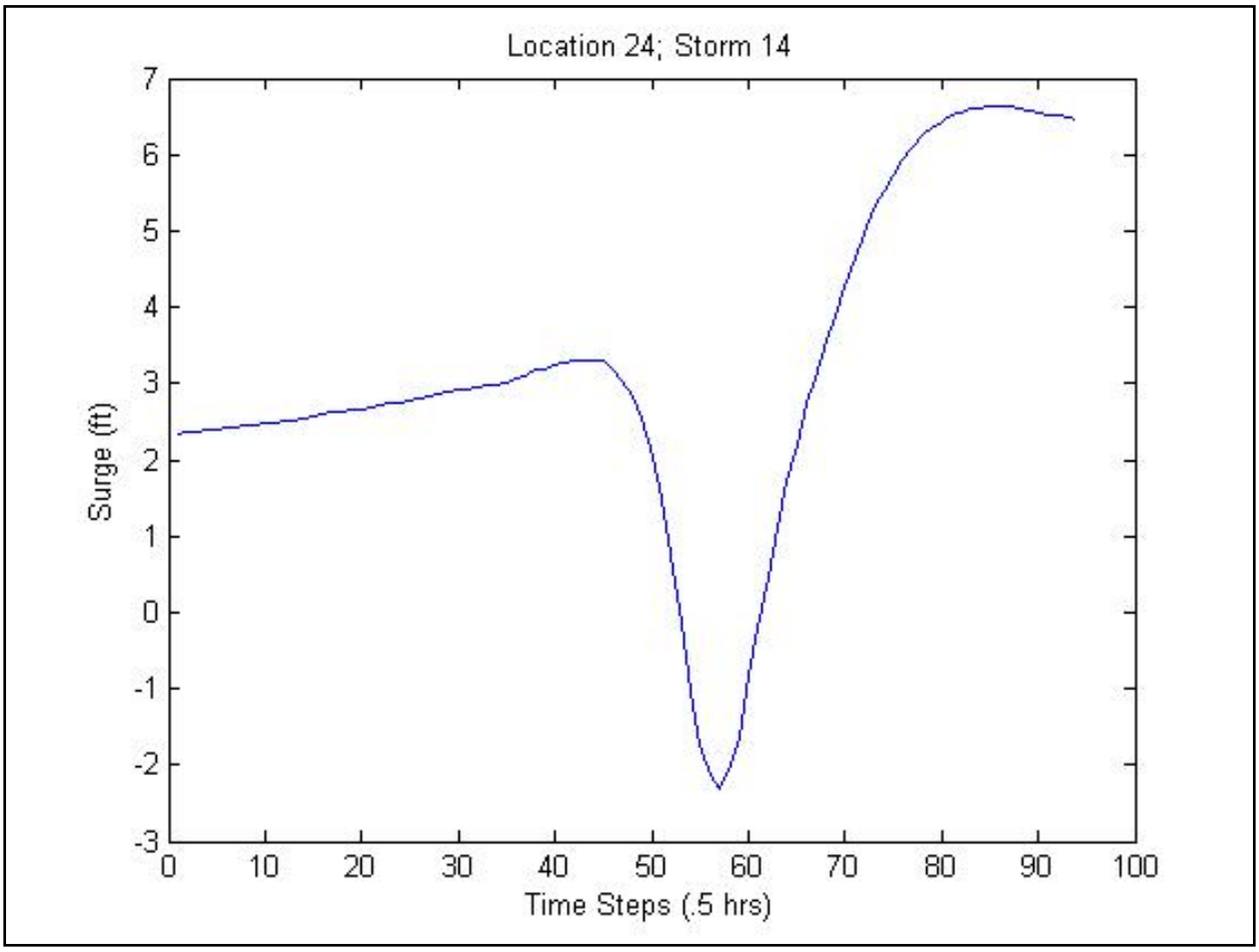

Figure 39. Hydrograph with η_{max} occurring within 10 time-steps of end of curve.

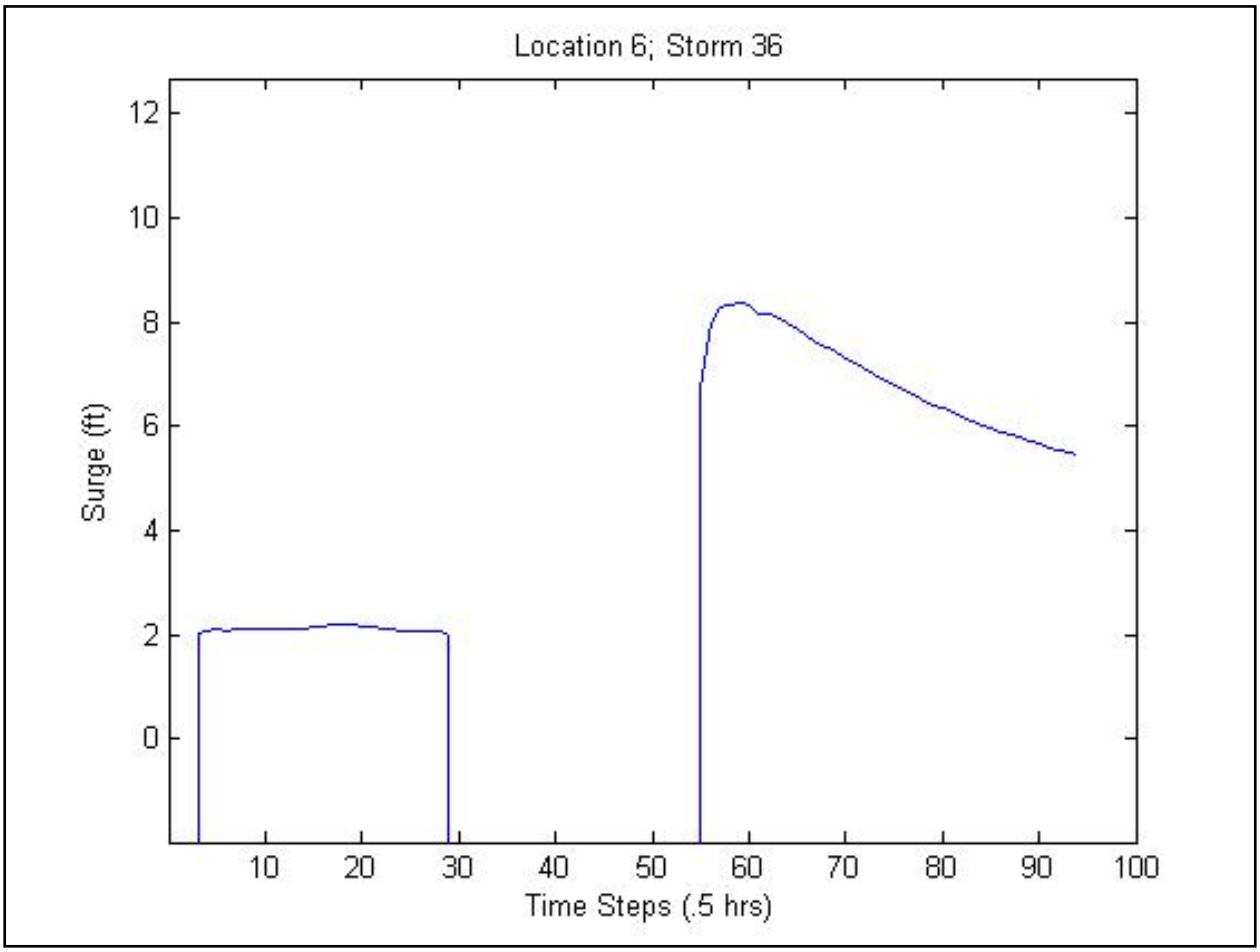

Figure 40. Hydrograph of significant dry period.

Calculating Duration Parameters

For storm hydrographs that satisfied all filtering criteria, a duration parameter σ was calculated for (a) the pre-peak and (b) post-peak portions of the curve. For the purposes of this analysis, the duration parameters are equivalent to the first moments about the peak time $t_{\eta max}$. Prior to η_{max}, σ_a is taken to be

$$\sigma_a = \frac{\sum_{i=1}^{j} \eta_{\max -i}(t_{\eta_{\max}} - t_{\eta_{\max -i}})\Delta t}{Area_a} \tag{18}$$

where j is the number of time-steps between $t_{\eta max}$ and the first time-step for which $\eta_{max\text{-}i} >= 0.7\eta_{max}$, Δt is the time-step size, and $Area_a$ is the area under the curve between $t_{\eta max}$ and $t_{\eta max\text{-}j}$.

The duration parameter σ_b is taken to be

$$\sigma_b = \frac{\sum_{i=1}^{j} \eta_{\max+i}(t_{\eta_{\max+i}} - t_{\eta_{\max}})\Delta t}{Area_b} \tag{19}$$

where j is the number of time-steps between $t_{\eta max}$ and the last time-step for which $\eta_{max+i} >= 0.7\eta_{max}$, and $Area_b$ is the area under the curve between $t_{\eta max}$ and $t_{\eta max+j}$. The moment calculation was used, as opposed to simply the duration ($t_{\eta_{\max+j}} - t_{\eta_{\max}}$), in order to provide additional insight into the shape of the hydrograph, and eventually anticipated overtopping rates. Figure 41 shows a graphical representation of the manner in which the duration parameter σ_b was calculated.

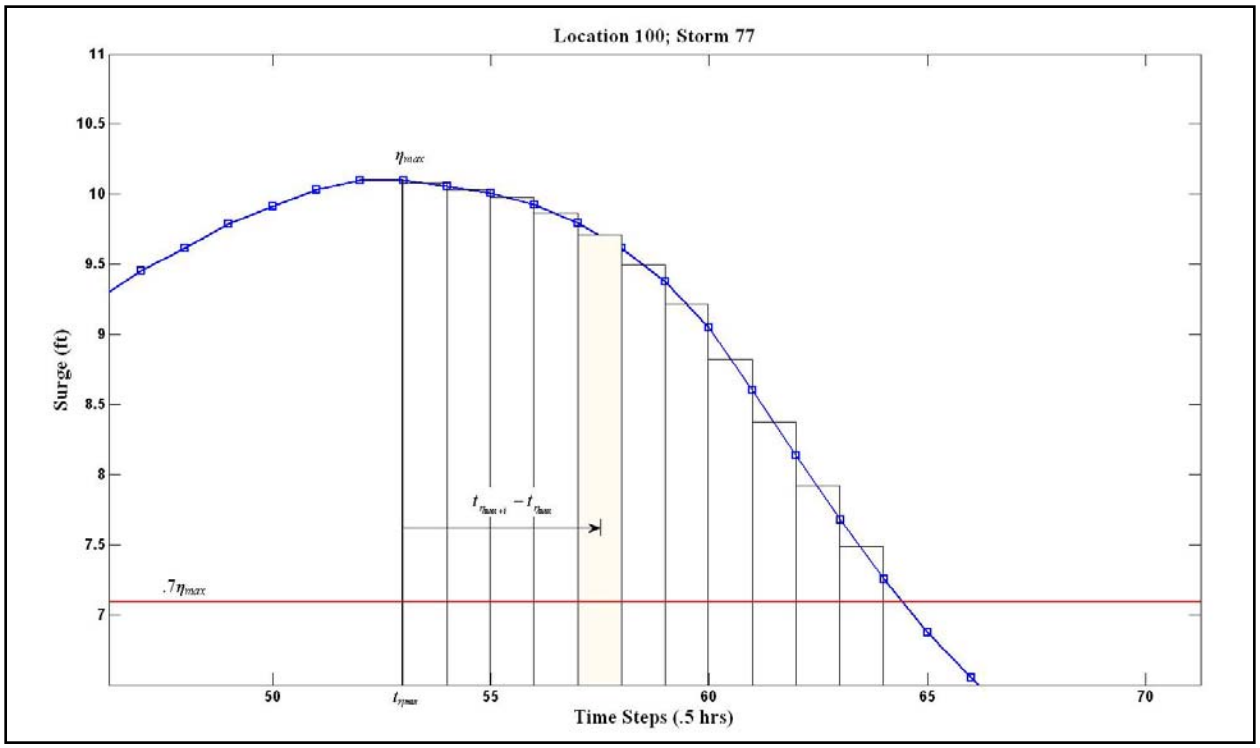

Figure 41. Calculation of duration parameter σ_b.

An adjustment of $0.5\Delta t$ was subtracted from the distance ($t_{\eta_{\max+i}} - t_{\eta_{\max}}$) so as not to bias the resulting moment calculation. For the hydrograph shown in Figure 41, the duration parameter σ_b was found to be 5.21 time-steps (equivalent to 2.6 hr), while the actual duration above $0.7\eta_{max}$ is 11 time-steps (6.5 hr).

In work undertaken for the investigation of levee overtopping, van Ledden (2007) has shown that a relatively good fit to the overall hydrographic shape can be obtained by representing the time series as

$$\eta(t) = \eta_{\max} e^{\left[\frac{-(t-t_0)^2}{2\sigma_i^2}\right]}$$

where

$\eta(t)$ is the water level at time t

t_0 is the time of the peak surge (20)

σ_i is the rms parameter of the Gaussian distribution with

i = 1 designating the interval up to the storm peak and

i = 2 designating the interval following the storm peak.

Figure 42 shows a typical result for a point in the New Orleans area. At first glance this figure seems to imply that storm duration decreases with increasing values of maximum surge; but this is not actually true. As an example, if Δt for the best-fit lines over the range of maximum surge values from 15 to 25 ft for this point is computed, duration curves can be estimated as a function of maximum surge value.

Figure 42. The rms parameter for hydrographs of individual storms plotted against the maximum surge level for those storms (from the work of van Ledden (2007)). Crosses indicate estimates of the rms duration parameter for different storms, with the color denoted whether the parameter is for the interval up to the storm peak (blue) or for the interval following the storm peak (red). The dashed lines represent the best overall fit to the data for all of the storms, again color-coded to indicate the relevant portion of the storm being fit.

Figure 43 shows the behavior of Δt as a function of surge level and a set of maximum surge levels from 15 ft to 25 ft for the interval preceding the storm peak. Figure 44 provides similar information for the interval following the storm peak. As can be seen here, even though σ_1 and σ_2 both decrease as the maximum surge increases, the duration increases. This behavior can be understood by rearranging Equation 20,

$$\Delta t = t - t_0 = \sigma_i \sqrt{2 \ln\left(\frac{\eta_{\max}}{\eta}\right)} \tag{21}$$

where

Δt is the duration of water levels above η.

The change in the expected duration as a function of maximum surge is given by

$$\frac{\partial \Delta t}{\partial \eta_{\max}} = \frac{\partial \sigma_i}{\partial \eta_{\max}} \sqrt{2 \ln\left(\frac{\eta_{\max}}{\eta}\right)} + \sigma_i \frac{\partial \sqrt{2 \ln\left(\frac{\eta_{\max}}{\eta}\right)}}{\partial \eta_{\max}} \tag{22}$$

From Equation 22, two terms contribute to the rate of change of Δt, not just the variation in σ_i as a function of $\eta_{\max}$. In this case and in a number of other cases analyzed independently, the overall duration of surge levels is seen to be an increasing function of maximum surge.

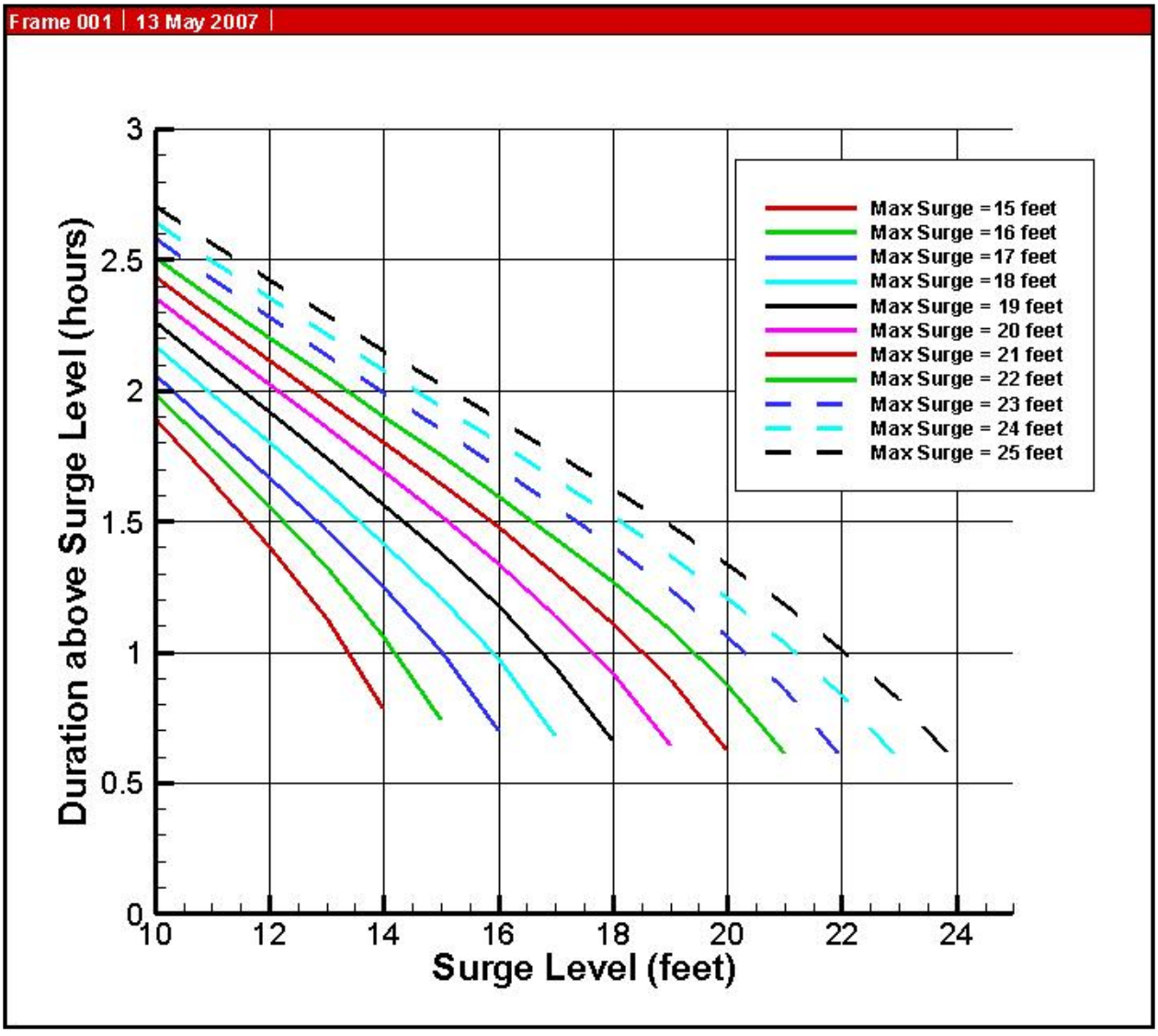

Figure 43. The best-fit line for the storm interval up to the storm peak from Figure 46 converted to absolute duration of water levels.

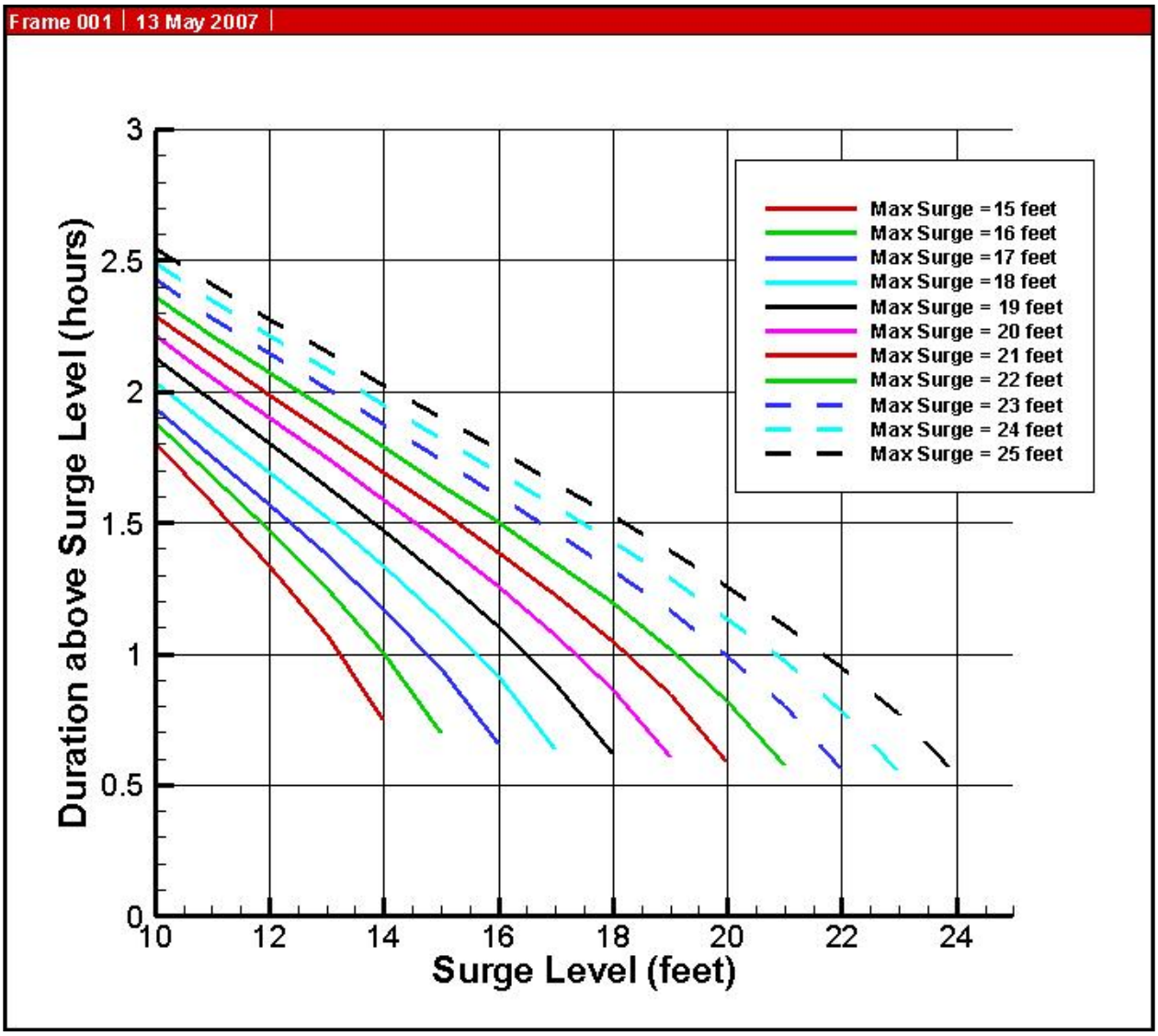

Figure 44. The best-fit line for the storm interval following the storm peak from Figure 46 converted to absolute duration of water levels.

From these figures and equations, one can construct synthetic storm hydrographs associated with each of the storm peaks estimated in the previous sections; however, upon close scrutiny of the comparisons between these synthetic storm hydrographs and actual hydrographs, it was observed that certain storm approach angles (primarily storms out of the southeast) produce hydrographs with shapes that were not well fit by this approach. Thus, although the information generated from this method is valuable for understanding the time scale of hurricane surges, a second method of hydrograph generation was undertaken for estimating hydrographs for input to the risk model.

This second approach defined the characteristic variation around the peak as a simple ratio of the value at time t to the value at the peak, i.e.,

$$\eta(x,t) = \eta_{max}(c_p, R_{max}, v_f, \theta, x - x_0)\Psi(t) \quad (23)$$

which returns to the form of Equation 3, with the function Ψ defined as the ratio of the surge at time t to the peak surge. This function is defined for all of the combinations of parameters and in conjunction with definition of the peak surge probabilities can be used to generate a very large number of storm sequences and their probabilities.

Initially, the risk model was driven with information from 76 actual storms for all points along the basin reaches. To examine the adequacy of this number of storms, this number was tripled to 231 storms for all points along the basin reaches; and this information was provided to the rest of the team. The initial set of storms covered the entire range of storm intensities, sizes, and angles of approach for each storm track, but it held the storm forward speed constant (11 knots). Storm speed does not strongly influence peak surges in this area, with sites along the basins typically seeing differences of less than ±10% in peak surge for the 6-knot and 17-knot cases. However, as might be expected, the speed of the storm does change the duration of the storm.

Although final comparisons of the agreement between overtopping produced by the 76 storms versus the 231 storms should be based on results from the risk model, we can examine the agreement between water levels estimated by the 76 and 231 storms directly. Figure 45 shows a plot of the estimated 100-year surge levels based on the 76 storms and the 231 storms. As can be seen here, the differences are quite small.

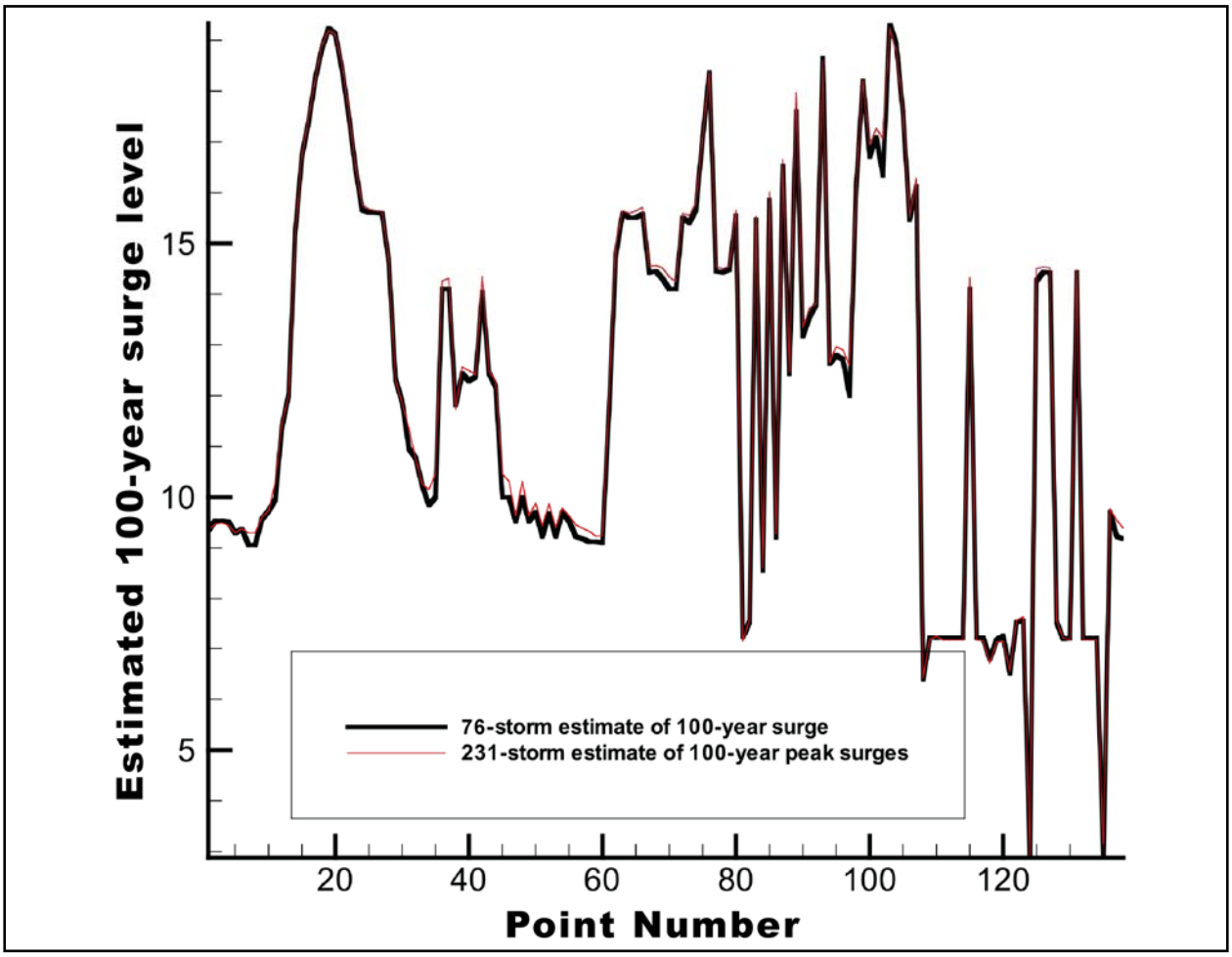

Figure 45. Comparison of 76-storm and 231-storm estimates of 100-year surge values along all 138 points used in the risk simulations.

Estimating Wave Hydrographs

There was insufficient wave information available to specify an independent set of wave hydrographs. Thus, wave heights should be taken as the limiting value for shallow-sloping bottoms, about 0.43 times the depth. This factor can be applied to the surge hydrographs to generate associated wave hydrographs.

Investigating the Effects of Climate Variability on Surge Levels

Two aspects of the sensitivity of estimated surge levels to climate variability will be addressed here: The situation with an increase in storm frequency while holding the conditional distribution of storm intensities constant, and a situation in which both the storm frequencies and conditional distribution are allowed to vary.

The probability method used here treats storm probabilities and the development of the response surface separately. Approximating to the smoothed curve for Atlantic tropical cyclones from Holland and Webster (2007) as one estimate of what might happen if hurricane frequencies

were allowed to increase in proportion to the increase according to a shift from a Tropical Cyclone Regime 2 to a Tropical Cyclone Regime 3, approximately a 60% increase in the overall hurricane frequencies.

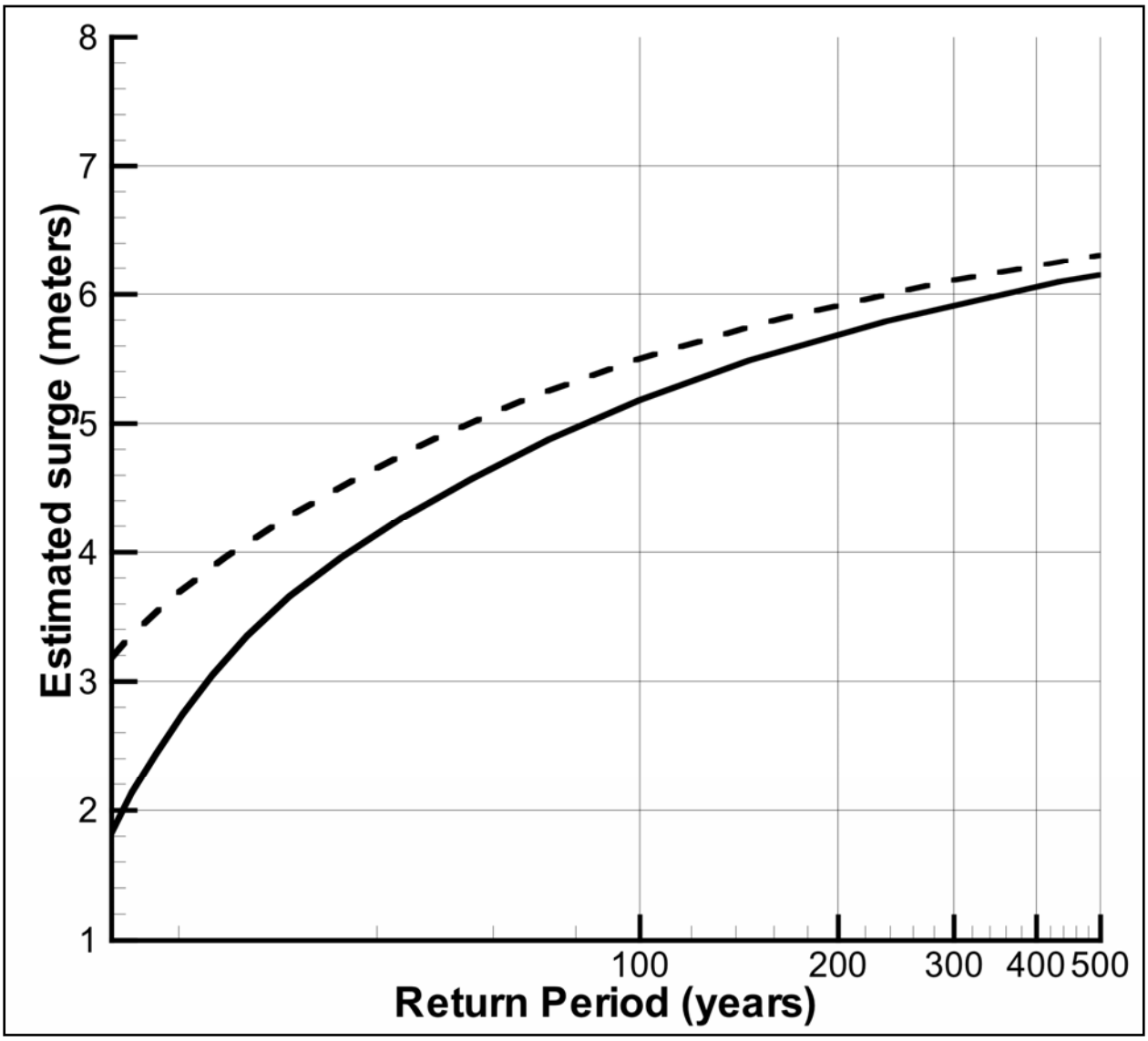

Figure 46. Comparison of JPM results from the base sample (solid line) to a situation with a 60% increase in hurricane frequency.

Figure 46 shows the CDF (solid line) obtained from the method used here for a point along the St. Bernard Parish levee. The dashed line is based on the assumption that future hurricane frequencies increase by 60%. The entire line shifts toward the left and the old 160-year surge becomes the new 100-year surge. Since the surge response in this region tends to be of the Fisher-Tippet III (Weibull) form, the effect of this shift is diminished at longer return periods. For a return period of 100 years, the existing 100-year value would only be increased by about 7%.

For the second scenario, a shift was made in which all future years have both the frequency characteristics and the condition distributions of storm intensities to double the number of "high-activity/high-intensity" storms in the New Orleans area. This is simply a sensitivity study and no studies have suggested that this is a likely future climate pattern. Using the different frequency and intensity distribution bases within the JPM, it was found that the expected impact on the surges is approximately 12% at the 100-year return period. Similar to the previous scenario, the reason for the relatively small increase is the characteristic Weibull shape of the surge distribution.

Risk Modeling

The performance of the HPS is evaluated based its ability to prevent flooding within the protected areas. This requires the determination of probabilities of failure of the components of the system and an estimate of the amount of water expected to reach protected areas for a particular hurricane if a component fails or the HPS is overtopped by surges and waves. The water volume entering the protected areas was determined to be the result of one or more of the following cases:

- Non-breach events including overtopping, closures (i.e., gates) that are left open, and backflow from pumping stations
- Breach events due to failure of walls, transitions or levees (with and without overtopping)
- Rainfall during hurricane events

The pumping system can move water out of the HPS; it can reduce flooding by reducing the net water volume in a basin. The risk quantification framework was, therefore, based on obtaining estimates of net water volumes entering the HPS due to these events and calculating associated flooding elevations.

Event Tree Development

The event tree of Figure 47 was developed from the influence and flow diagrams shown in Figures 3 and 4 and was based on the team's understanding of the factors that lead to interior flooding. It shows the progression of the calculations required to determine net water volumes and the resulting flood elevations. Figure 47 shows a total of twelve branches that are constructed per hurricane for every reach and transition and Table 6 provides a summary of the branches. A spreadsheet program was developed to perform the many required computations, and the sections that follow provide a discussion of the events that make up the tree and the associated water volume computations.

The determination of the frequency of flooding elevations from these net water volumes required that all storms be evaluated for all possible combinations of events (all event tree branches) for all the sub-basins. The number of combinations per storm for eight basins and 12 branches of the event tree was 1,073,741,824. Dependency among the basins was not examined in order to reduce the number of possible combinations. The risk results obtained by examining the individual basins were considered adequate for evaluating the relative risks and vulnerabilities of the HPS.

The arrival of surges and waves at a reach from a hurricane is the initiating event in the tree that triggers the subsequent events in the tree. Each event in the branch is conditional on the previous event. For example, a calculated volume of water will enter the HPS if a breach occurs in a reach, when that reach is overtopped and the gates are open, and when a specific surge and wave condition exists at that reach.

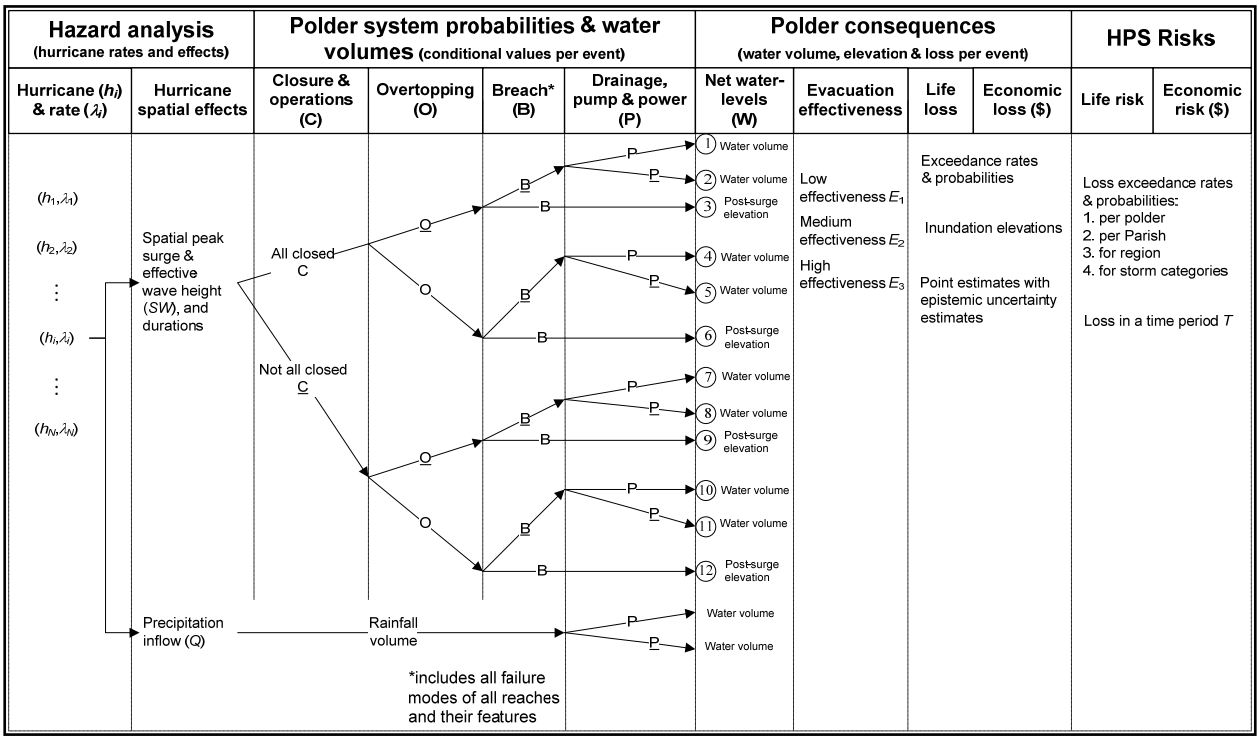

Figure 47. Event tree for quantifying risk in a basin (polder).

Initiating Event

The water elevations generated by hurricane surges and waves place loads on the components of the HPS that must be resisted if the system is to perform its intended function of preventing interior flooding. Therefore, these loads are the initiating events in the event tree. The hydrographs that were developed in the hazard analysis provide the water elevations required to determine the loads as a function of time for each hurricane at each reach in the system. Figure 31 shows a sample of the hydrographs for all the reaches in one basin. A total of 10,336 hydrographs were required for the reaches in the pre-Katrina HPS and another 10,564 for the reaches in the June 2007 HPS for the hurricanes studied. Elevations from the hydrographs were sampled at 30 minute time-steps and the effect on the subsequent events in the tree was evaluated for each elevation. The frequency of each hurricane and, therefore, of the elevation being evaluated are also applied to the tree branch under consideration. Appendix 8 provides a complete discussion of the methods used to develop the hydrographs.

Gates and Closures Events

The second event to be evaluated in the event tree is the performance of gates and closure structures. Each gate or closure is treated as a separate feature and is assigned a probability of being open. This probability is used to determine the amount of water that might enter protected areas when water levels created by the initiating event exceed the base elevation of the gate or closure structure. Anecdotal evidence suggested that approximately 10% of the gates or closures in the system were left open during Katrina. This value was used in the analysis. The event tree therefore branches again at the closure event where the probability of a gate being open is 10% and the probability of it being closed is 90%. For open gates, the 10% open rate is applied to the volume of water that could flow through the gate and that volume is assumed to enter the protected area for that storm time increment. This is repeated for each time increment (30 minutes) of the hydrograph and each closure or gate structure to estimate the entire volume of water that would enter by this event for each sub-basin for the entire HPS.

Table 6. Definition of the major branches of the event tree.

Branch	Branch Water Volume
1. Non-Breach	Use precipitation volume, with pumping
2. Non-Breach	Use precipitation volume no pumping
3. Breach	Use post-surge breach water elevation, no pumping
4. Non-Breach	Use overtopping and precipitation volume, with pumping
5. Non-Breach	Use overtopping and precipitation volume no pumping
6. Breach	Use post-surge breach water elevation, no pumping
7. Non-Breach	Use precipitation and not-all-closed-closure volume, with pumping
8. Non-Breach	Use precipitation and not-all-closed-closure volume no pumping
9. Breach	Use post-surge breach water elevation, no pumping
10. Non-Breach	Use overtopping, precipitation and not-all-closed-closure volume, with pumping
11. Non-Breach	Use overtopping, precipitation and not-all-closed-closure volume no pumping
12. Breach	Use post-surge breach water elevation, no pumping

Overtopping Events

The next event to evaluate is whether on not a reach is overtopped by the initiating event and, if it is overtopped, to determine the volume of water that will flow over the reach. The determination of the probability of overtopping is a simple comparison of the water elevation from the time-step of the hydrograph to the crest elevation of the reach. If the crest elevation is exceeded, the probability of overtopping is equal to 1.0 — 0.0 if it is not exceeded. The overtopping rate was computed assuming that the crest of the reach acts as a rectangular weir. If the overtopping water flow has the elevation H and width L and is assumed to be a ideal liquid, the energy conservation law can be used to show that the flow rate Q (L^3/T) is given by

$$Q = \frac{2}{3}(2g)^{1/2} LH^{3/2} \tag{24}$$

where g is the acceleration of gravity. The actual flow over the weir is known to be less than ideal because the effective flow area is smaller than the product LH. The overtopping flow model can be enhanced further for engineering applications by replacing the term $\frac{2}{3}(2g)^{1/2}$ with an empirical coefficient, known as the weir coefficient C_w; thus

$$Q = C_W L H^{3/2} \tag{25}$$

where

$$C_W = \begin{cases} 3.33 & \text{if } L \text{ and } H \text{ are given in English units} \\ 1.84 & \text{if } L \text{ and } H \text{ are given in SI units} \end{cases} \tag{26}$$

Note that the C_w for the ideal fluid case is $\frac{2}{3}(2g)^{1/2}$ which is 2.95 m/s^2. This coefficient takes a value of 3.0, 2.6, and 2.0 for floodwalls, levees, and gates, respectively, with a coefficient of variation of 0.2 in inch-pound units (L and H in feet).

The mean volume of the overtopping water for a given reach can be calculated by integrating

$$\mu_V = C_w L \int_{\text{over } t \text{ where } h_s > H_r} \left(X_s h_s(t) - H_r\right)^{3/2} dt \tag{27}$$

where the surge hydrograph is represented by $h_s(t)$; H_r is the reach height; L is the reach length; C_w is the weir coefficient with a coefficient of variation of 0.2, and a mean $\mu(C_w)$ of 3.0, 2.6, and 2.0 for floodwalls, levees, and gates, respectively; X_s is an aleatory uncertainty random factor with a lognormal distribution (0.20 log standard deviation and a median of 1.0).

These equations are the basis for the overtopping analyses conducted for each hurricane and each reach. A complete presentation of the mathematics used to determine overtopping rates and volumes is presented in Appendix 9 of this volume.

Breaching Events

The next event to evaluate is whether or not a breach failure occurs within a reach and the water level produced by the initiating event, given the preceding events. If the reach does fail, the volume of water that flows through the breach must be determined. Three cases of breach failure were examined that corresponded to the breaching branches presented in the event tree. The three cases are as follows:

- Breach given no overtopping
- Breach given overtopping

- Breach due to feature (closure gate, pump house, etc.) or transition failures

Breach-given-overtopping is primarily driven by erosion, resulting from overtopping water flow. The probability of reach failure was determined using reliability methods of analysis to develop fragility curves for each reach. The development of the fragility curves is provided in Appendix 10 and a summary is provided later in this section.

Breach Parameters

The breaching scenarios require knowledge of the average breach length and depth to determine basin inflows. The HPS condition after Katrina was reviewed to identify basic characteristics of the major breaches. The identified characteristics were used to develop general rules for estimating breach dimensions in the risk model. One critical characteristic for determining the volume of water flowing through a breach is the duration of time that the breach is open. During Katrina, the breaches could not be repaired in time to have an effect on the level of water achieved inside the basins. Therefore, the time that the breach is open was assumed to have no effect on inflow volumes and water elevations.

Breach without Overtopping

IPET studies indicated that the London Ave. and 17th St. Canal breaches occurred during Katrina before the water level in the canals reached the top of the floodwall; the breaches appeared to have been the result of a foundation and/or design failure. Therefore, these breaches were modeled in the risk analysis as having occurred without overtopping. The high-water marks (HWM) identified inside the Orleans Basin (where the canal breaches occurred) and the length of time that surge elevations exceeded lake levels in the canals were examined. The HWM during Katrina in the Orleans Basin was within about 1 ft of the peak surge in the canals. For example, it appears that the London Ave. South breach occurred when the canal water level was at about 7 to 8 ft, or about 3 ft below the top of wall. The peak surge in the canal was about 10 to 11 ft, and the HWM in the Orleans Basin was about 10 ft.

There was a time lag of several hours between the surge elevation that failed the floodwall and the peak surge elevation. This was a sufficient time period for the water elevation inside the Orleans Basin to reach the peak surge elevation in the canal. The inverts of the canal breaches were well below the normal lake level, so water flowed back into the lake after the surge passed. Based on these observations, it seemed appropriate to use the peak surge level as the water elevation achieved inside the basin when a catastrophic breach (full levee height) occurred during a non-overtopping event. Therefore, for breaching without overtopping, the following assumptions were used in the breaching model:

- All breaches were considered to be a result of a structural or foundation failure and the breach depth was set to lowest elevation of the levee or floodwall.

- The breach depth was extended below the adjacent lake or river level.

- The maximum basin water elevations caused by the breach were set to the maximum surge elevation experienced adjacent to the breach.

Breach During an Overtopping Event

For levees subject to overtopping and erosion, general rules were developed that determined breach invert elevation based on the depth of overtopping relative to the top of levee and the type of soil in the levee. In the case where the breach invert elevation was higher than adjacent lake or river levels, the depth and length of the breach, the duration of time that the surge level exceeded the breach invert, and the weir coefficient were required to calculate inflow water volumes for the breach. The breach lengths for the levees were assumed to be similar to that experienced during Katrina. Breach lengths at the major canal breaches varied (450 to 1000+ ft), but were all on the order of several hundred feet. At the IHNC where overtopping did occur, the two Lower Ninth Ward breaches were similar in length to breaches at canals where overtopping did not occur. The depth of the breaches at canals where overtopping did not occur were below the normal canal water levels; water flowed out through these breaches when the surge passed. Based on these observations, it was assumed that using the peak surge level as the maximum water elevation achieved inside the basin was appropriate when a full-depth breach occurred during an overtopping event.

For the case of a less than full-depth breach given overtopping, breach parameters for width and height were not available for determining inflows. The risk model did not consider breaches that were less than full-depth.

The following assumptions were made in the breaching events given overtopping:

- Breaches occurred as a result of an erosion failure due to surge and/or waves.

- Breach depths were assumed to be variable; however, the depth of overtopping required to cause a breach was dependent upon soil properties. Assumed values are shown in Table 7.

- Durations of overtopping were calculated from the hydrographs.

- The maximum basin water elevations caused by the breach were set to the maximum surge elevation experienced adjacent to the breach.

Rainfall and Pumping Events

Rainfall during hurricanes is another event that affects the inundation of the basins. While rainfall is not of primary concern for the HPS, it is a contributor to the frequency of low-level flood losses. Hence, it was decided that a relatively coarse model of hurricane-induced rainfall would suffice.

The model adopted relates the rainfall intensity to storm strength and position within the storm. The model first assumes a uniform rainfall rate within the radius to maximum winds and an exponentially declining rate at greater distances. The rainfall is taken to be asymmetric, with the more intense rains occurring to the east of the storm, when facing the direction of storm travel. Two calculations were done using this model. First, the total rainfall accumulation into each sub basin for each storm was determined. Second, time dependent intensities for each sub-basin were also calculated. The rainfall volumes that would be associated with each of the

hurricanes defining the hazard were estimated based on this model using NASA data that correlate rainfall intensity and volume with hurricane characteristics. The total rainfall volume entering each sub-basin was computed for each hurricane and is documented in Appendix 15. By adding the additional water volumes from rainfall, a total influx volume of water, for each storm, was determined for each sub-basin.

Uncertainty in the rainfall estimates is large owing to the paucity of data, and it is expressed by a lognormal random variable with mean value 1 and log standard deviation 0.69. This random factor is applied to the entire mean rainfall time-history. In reality, rainfall intensity inside a basin would display significant fluctuations in time and space, which locally could far exceed a factor of 2. However, the above random factor is considered adequate to reflect uncertainty on the total precipitation in a basin during the passage of a hurricane.

Table 7. Breaching Model

Breaching Model						
Reaches						
Levee/Floodwall Breach Model Given Overtopping (erosion breach)						
		0 to 1ft		**1ft to 3ft**		
Material	**Symbol**	**Depth (ft)**	**Breach Width (w), Reach Length <1000ft**	**Depth (ft)**	**Breach Width (w) (ft), Reach Length <1000ft**	**Depth (ft)**
Hydraulic Fill	H	0	0	9	0.50*L to max 400	18
Clay	C	0	0	3	0.50*L to max 135	13
Unknown (Average)	U	0	0	6	0.50*L to max 290	17
Wall	W	0	0	0	0	17
		Length Modifiers Reach L>1000 ft				
		Overtopping Depth (ft)				
Material	**Symbol**	**0 to 1ft**		**1ft to 3ft**		**>3 ft**
Hydraulic Fill	H	0.0		400 < w < 0.40*L		430 < w < 0.40*L
Clay	C	0.0		135 < w < 0.10*L		135 < w < 0.10*L
Unknown (Average)	U	0.0		290 < w < 0.30*L		315 < w < 0.30*L
Wall	W	0.0		0.0		315 < w < 0.10*L
Levee/Floodwall Breach Model Given No Overtopping						
			Breach Width (w), (ft)			
Material	**Symbol**	**Depth (ft)**	**L ≤ 1000 ft**	**1000 < L≤ 10,000 ft**	**L>10,000 ft**	**Notes**
Hydraulic Fill	H	18	0.50*L to max 500	500 < w ≤ 0.15*L	0.15*L	3 Breaches / 10,000 reach
Clay	C	13	0.50*L to max 500	500 < w ≤ 0.10*L	0.10*L	2 Breaches / 10,000 reach
Unknown (Average)	U	17	0.50*L to max 500	500 < w ≤ 0.125*L	0.125*L	2.5 Breaches / 10,000 reach
Wall	W	17	0.50*L to max 500	500 < w ≤ 0.075*L	0.075*L	1.5 Breaches / 10,000 reach
Transitions						
Transitions Breach Model Given Overtopping						
		Breach size (ft)				
Transition Type	**Symbol**	**Width**		**Depth**		
Ramps	R	25		3		
Floodwall-Levee	T	50		3		
Drainage Structures	D	65		5.5		
Pump Stations	P	100		5		
Gates	G	25		5		
Unprotected sections	U	N/A		N/A		
Transitions Breach Model Given No Overtopping						
		Breach size (ft)				
Transition Type	**Symbol**	**width**	**Depth**			
Ramps	R	-	-	Treated as opened or closed (sand bagged)		
Floodwall-Levee	T	-	-	No breaching until OT		
Drainage Structures	D	-	-	No breaching until OT		
Pump Stations	P	-	-	No breaching until OT		
Gates	G	-	-	Treat as opened or closed		
Unprotected sections	U	N/A	N/A			

The effect of operational pumping stations was studied by subtracting a volume of water that the stations could remove in a sub-basin for four scenarios. A simplified pumping model was used to determine the relative impact of having the stations operating at 25%, 50%, 75%, and 100% of the total available capacity. It is noted that the stations could not be expected to operate at 100% of capacity, but information was not available on pump station reliability. Therefore, a range of operating capacity was studied to show the relative effect of pumping on flooding in the HPS. The model assumed that the pumps would be operational to remove rainfall water and would be most effective during the most intense period of the rainfall. The pumps were not expected to be operational during a catastrophic flooding event. The available pumping capacity within a sub-basin was totaled and used as the pumping capacity of the sub-basin as a single pump. The sub-basin pumping capacities are shown in Table 8.

Table 8. Sub-basin pumping capacity

Sub-basin Pumping Capacity	
Sub-basin	**Pump Capacity (cfs)**
OW1	0.00
OW2	0.00
NOE1	0.00
NOE2	2.49E+07
NOE3	1.69E+06
NOE4	2.19E+07
NOE5	1.23E+08
OM1	1.18E+08
OM2	4.23E+08
OM3	2.63E+08
OM4	0.00E+00
OM5	4.12E+08
SB1	1.61E+08
SB2	0.00E+00
SB3	9.10E+07
SB4	5.76E+07
SB5	0.00E+00
JE1	5.88E+06
JE2	2.97E+08
JE3	2.50E+08
JW1	0.00
JW2	1.33E+08
JW3	4.23E+08
JW4	4.09E+08
PL11	1.33E+08
SC1	-9.64E+07
SC2	0.00E+00

The following steps were used in the pumping analysis:

- Determine total sub-basin design pumping capacity.
- Determine volume of rain and runoff appropriate for each sub-basin per storm.
- Determine the duration of pumping per storm from rainfall intensity curves (generally 8 to 12 hr).
- Assumed that pumps will operate at a range of percentages of the total sub-basin capacity (0%, 25%, 50%, 75%, or 100%).
- Determine volume of water that pumps could evacuate per storm at the selected capacity.
- Subtract pump volume from rainfall to determine net volume.
- If net volume is a positive value, replace rainfall with net volume.
- If net volume is a negative value, replace rainfall with net volume = zero.

This process resulted in a net rainfall that was used in the risk model. The net rainfall volume calculations are summarized in Table 8 for NOE4. Only the 0%, 50%, and 100% pumping scenarios were used in the risk model in order to reduce the number of computer runs and inundation mapping required. The resulting analyses provide a picture of how pumping can reduce flood levels if catastrophic breaching or overtopping does not occur.

Table 9. Sample Pumping Calculations

NOE4									
Storm Number	Rainfall Mean (cf)	Runoff Volume from Rain (cf)	Pump Station Capacity (cfs)	Rainfall Duration (hr)	Net Volume (cf) w/100% Pump Reliability	Net Volume (cf) w/75% Pump Reliability	Net Volume (cf) w/50% Pump Reliability	Net Volume (cf) w/25% Pump Reliability	Net Volume (cf) w/0% Pump Reliability
1	8.321E+06	6.823E+06	7.820E+02	6.00	0.00E+00	0.00E+00	0.00E+00	2.60E+06	6.82E+06
2	3.007E+07	2.465E+07	7.820E+02	8.00	2.13E+06	7.76E+06	1.34E+07	1.90E+07	2.47E+07
3	5.104E+07	4.186E+07	7.820E+02	8.00	1.93E+07	2.50E+07	3.06E+07	3.62E+07	4.19E+07
4	5.209E+06	4.271E+06	7.820E+02	6.00	0.00E+00	0.00E+00	0.00E+00	4.84E+04	4.27E+06
5	3.827E+07	3.138E+07	7.820E+02	8.00	8.86E+06	1.45E+07	2.01E+07	2.57E+07	3.14E+07
6	5.705E+07	4.678E+07	7.820E+02	8.00	2.43E+07	2.99E+07	3.55E+07	4.12E+07	4.68E+07
7	2.670E+06	2.189E+06	7.820E+02	6.00	0.00E+00	0.00E+00	0.00E+00	0.00E+00	2.19E+06
8	4.012E+07	3.290E+07	7.820E+02	8.00	1.04E+07	1.60E+07	2.16E+07	2.73E+07	3.29E+07
9	6.361E+07	5.216E+07	7.820E+02	8.00	2.96E+07	3.53E+07	4.09E+07	4.65E+07	5.22E+07
10	1.935E+07	1.586E+07	7.820E+02	8.00	0.00E+00	0.00E+00	4.60E+06	1.02E+07	1.59E+07
11	4.018E+07	3.295E+07	7.820E+02	8.00	1.04E+07	1.61E+07	2.17E+07	2.73E+07	3.29E+07
12	5.835E+07	4.785E+07	7.820E+02	8.00	2.53E+07	3.10E+07	3.66E+07	4.22E+07	4.78E+07
13	1.701E+07	1.395E+07	7.820E+02	8.00	0.00E+00	0.00E+00	2.69E+06	8.32E+06	1.40E+07
14	5.506E+07	4.515E+07	7.820E+02	8.00	2.26E+07	2.83E+07	3.39E+07	3.95E+07	4.52E+07
15	7.111E+07	5.831E+07	7.820E+02	8.00	3.58E+07	4.14E+07	4.71E+07	5.27E+07	5.83E+07
16	1.313E+07	1.077E+07	7.820E+02	8.00	0.00E+00	0.00E+00	0.00E+00	5.14E+06	1.08E+07
17	6.251E+07	5.125E+07	7.820E+02	8.00	2.87E+07	3.44E+07	4.00E+07	4.56E+07	5.13E+07
18	8.366E+07	6.860E+07	7.820E+02	8.00	4.61E+07	5.17E+07	5.73E+07	6.30E+07	6.86E+07
19	1.967E+07	1.613E+07	7.820E+02	8.00	0.00E+00	0.00E+00	4.87E+06	1.05E+07	1.61E+07
20	3.164E+07	2.594E+07	7.820E+02	8.00	3.42E+06	9.05E+06	1.47E+07	2.03E+07	2.59E+07
21	4.604E+07	3.775E+07	7.820E+02	8.00	1.52E+07	2.09E+07	2.65E+07	3.21E+07	3.78E+07
22	2.103E+07	1.725E+07	7.820E+02	8.00	0.00E+00	3.54E+05	5.98E+06	1.16E+07	1.72E+07

NOE4									
Storm Number	Rainfall Mean (cf)	Runoff Volume from Rain (cf)	Pump Station Capacity (cfs)	Rainfall Duration (hr)	Net Volume (cf) w/100% Pump Reliability	Net Volume (cf) w/75% Pump Reliability	Net Volume (cf) w/50% Pump Reliability	Net Volume (cf) w/25% Pump Reliability	Net Volume (cf) w/0% Pump Reliability
23	4.418E+07	3.622E+07	7.820E+02	8.00	1.37E+07	1.93E+07	2.50E+07	3.06E+07	3.62E+07
24	5.570E+07	4.567E+07	7.820E+02	8.00	2.32E+07	2.88E+07	3.44E+07	4.00E+07	4.57E+07
25	2.086E+07	1.711E+07	7.820E+02	8.00	0.00E+00	2.17E+05	5.85E+06	1.15E+07	1.71E+07
26	5.187E+07	4.253E+07	7.820E+02	8.00	2.00E+07	2.56E+07	3.13E+07	3.69E+07	4.25E+07
27	6.627E+07	5.434E+07	7.820E+02	8.00	3.18E+07	3.75E+07	4.31E+07	4.87E+07	5.43E+07
28	1.105E+07	9.062E+06	7.820E+02	8.00	0.00E+00	0.00E+00	0.00E+00	3.43E+06	9.06E+06
29	2.581E+07	2.116E+07	7.820E+02	8.00	0.00E+00	4.27E+06	9.90E+06	1.55E+07	2.12E+07
30	3.986E+07	3.268E+07	7.820E+02	8.00	1.02E+07	1.58E+07	2.14E+07	2.71E+07	3.27E+07
31	9.053E+06	7.423E+06	7.820E+02	6.00	0.00E+00	0.00E+00	0.00E+00	3.20E+06	7.42E+06
32	3.456E+07	2.834E+07	7.820E+02	8.00	5.82E+06	1.15E+07	1.71E+07	2.27E+07	2.83E+07
33	4.649E+07	3.812E+07	7.820E+02	8.00	1.56E+07	2.12E+07	2.69E+07	3.25E+07	3.81E+07
34	6.442E+06	5.283E+06	7.820E+02	6.00	0.00E+00	0.00E+00	0.00E+00	1.06E+06	5.28E+06
35	3.835E+07	3.145E+07	7.820E+02	8.00	8.92E+06	1.46E+07	2.02E+07	2.58E+07	3.14E+07
36	5.351E+07	4.388E+07	7.820E+02	8.00	2.14E+07	2.70E+07	3.26E+07	3.82E+07	4.39E+07
37	5.577E+06	4.573E+06	7.820E+02	6.00	0.00E+00	0.00E+00	0.00E+00	3.50E+05	4.57E+06
38	2.063E+07	1.691E+07	7.820E+02	8.00	0.00E+00	2.36E+04	5.65E+06	1.13E+07	1.69E+07
39	3.688E+07	3.024E+07	7.820E+02	8.00	7.72E+06	1.34E+07	1.90E+07	2.46E+07	3.02E+07
40	3.527E+06	2.892E+06	7.820E+02	6.00	0.00E+00	0.00E+00	0.00E+00	0.00E+00	2.89E+06
41	2.558E+07	2.097E+07	7.820E+02	8.00	0.00E+00	4.08E+06	9.71E+06	1.53E+07	2.10E+07
42	4.011E+07	3.289E+07	7.820E+02	8.00	1.04E+07	1.60E+07	2.16E+07	2.73E+07	3.29E+07
43	1.813E+06	1.487E+06	7.820E+02	6.00	0.00E+00	0.00E+00	0.00E+00	0.00E+00	1.49E+06
44	2.644E+07	2.168E+07	7.820E+02	8.00	0.00E+00	4.79E+06	1.04E+07	1.60E+07	2.17E+07
45	4.422E+07	3.626E+07	7.820E+02	8.00	1.37E+07	1.94E+07	2.50E+07	3.06E+07	3.63E+07
46	2.677E+07	2.195E+07	7.820E+02	8.00	0.00E+00	5.06E+06	1.07E+07	1.63E+07	2.20E+07
47	3.720E+07	3.050E+07	7.820E+02	8.00	7.98E+06	1.36E+07	1.92E+07	2.49E+07	3.05E+07
48	2.068E+07	1.696E+07	7.820E+02	8.00	0.00E+00	6.66E+04	5.70E+06	1.13E+07	1.70E+07
49	5.251E+07	4.306E+07	7.820E+02	8.00	2.05E+07	2.62E+07	3.18E+07	3.74E+07	4.31E+07
50	3.335E+07	2.734E+07	7.820E+02	8.00	4.82E+06	1.05E+07	1.61E+07	2.17E+07	2.73E+07
51	4.235E+07	3.472E+07	7.820E+02	8.00	1.22E+07	1.78E+07	2.35E+07	2.91E+07	3.47E+07
52	3.055E+07	2.505E+07	7.820E+02	8.00	2.53E+06	8.16E+06	1.38E+07	1.94E+07	2.51E+07
53	6.417E+07	5.262E+07	7.820E+02	8.00	3.01E+07	3.57E+07	4.14E+07	4.70E+07	5.26E+07
54	4.190E+07	3.436E+07	7.820E+02	8.00	1.18E+07	1.75E+07	2.31E+07	2.87E+07	3.44E+07
55	4.887E+07	4.008E+07	7.820E+02	8.00	1.76E+07	2.32E+07	2.88E+07	3.44E+07	4.01E+07
56	4.934E+07	4.046E+07	7.820E+02	8.00	1.79E+07	2.36E+07	2.92E+07	3.48E+07	4.05E+07
57	8.032E+07	6.586E+07	7.820E+02	8.00	4.33E+07	4.90E+07	5.46E+07	6.02E+07	6.59E+07
58	2.877E+07	2.359E+07	7.820E+02	8.00	1.07E+06	6.70E+06	1.23E+07	1.80E+07	2.36E+07
59	3.397E+07	2.785E+07	7.820E+02	8.00	5.33E+06	1.10E+07	1.66E+07	2.22E+07	2.79E+07
60	3.445E+07	2.825E+07	7.820E+02	8.00	5.73E+06	1.14E+07	1.70E+07	2.26E+07	2.82E+07
61	5.421E+07	4.446E+07	7.820E+02	8.00	2.19E+07	2.76E+07	3.32E+07	3.88E+07	4.45E+07
63	4.121E+07	3.379E+07	7.820E+02	8.00	1.13E+07	1.69E+07	2.25E+07	2.82E+07	3.38E+07
64	3.057E+07	2.507E+07	7.820E+02	8.00	2.54E+06	8.17E+06	1.38E+07	1.94E+07	2.51E+07
65	6.221E+07	5.101E+07	7.820E+02	8.00	2.85E+07	3.41E+07	3.97E+07	4.54E+07	5.10E+07
66	2.887E+07	2.367E+07	7.820E+02	8.00	1.15E+06	6.78E+06	1.24E+07	1.80E+07	2.37E+07
67	3.330E+07	2.731E+07	7.820E+02	8.00	4.79E+06	1.04E+07	1.60E+07	2.17E+07	2.73E+07

NOE4									
Storm Number	Rainfall Mean (cf)	Runoff Volume from Rain (cf)	Pump Station Capacity (cfs)	Rainfall Duration (hr)	Net Volume (cf) w/100% Pump Reliability	Net Volume (cf) w/75% Pump Reliability	Net Volume (cf) w/50% Pump Reliability	Net Volume (cf) w/25% Pump Reliability	Net Volume (cf) w/0% Pump Reliability
68	3.591E+07	2.945E+07	7.820E+02	8.00	6.93E+06	1.26E+07	1.82E+07	2.38E+07	2.94E+07
69	5.406E+07	4.433E+07	7.820E+02	8.00	2.18E+07	2.74E+07	3.31E+07	3.87E+07	4.43E+07
70	2.626E+07	2.153E+07	7.820E+02	8.00	0.00E+00	4.64E+06	1.03E+07	1.59E+07	2.15E+07
71	3.190E+07	2.616E+07	7.820E+02	8.00	3.64E+06	9.27E+06	1.49E+07	2.05E+07	2.62E+07
72	2.782E+07	2.281E+07	7.820E+02	8.00	2.90E+05	5.92E+06	1.16E+07	1.72E+07	2.28E+07
73	5.020E+07	4.117E+07	7.820E+02	8.00	1.86E+07	2.43E+07	2.99E+07	3.55E+07	4.12E+07
74	2.153E+07	1.766E+07	7.820E+02	8.00	0.00E+00	7.66E+05	6.40E+06	1.20E+07	1.77E+07
75	2.825E+07	2.316E+07	7.820E+02	8.00	6.42E+05	6.27E+06	1.19E+07	1.75E+07	2.32E+07
76	1.893E+07	1.552E+07	7.820E+02	8.00	0.00E+00	0.00E+00	4.26E+06	9.89E+06	1.55E+07
77	4.179E+07	3.427E+07	7.820E+02	8.00	1.18E+07	1.74E+07	2.30E+07	2.86E+07	3.43E+07

Branch and Sub-Basin Water Volumes

The resulting volume from each branch of the event tree, shown in Figures 32 and 33, also has have a rate of occurrence associated with it, based on the storm frequency and the probability of the individual events in the branch. The volumes and their rates are accumulated for the sub-basin they are associated with to determine the exceedance rate for that total water volume for a given storm. The stage-storage curves are used to convert the volumes to elevations to develop elevation-exceedance curves for the sub-basin.

Figure 48. Typical stage storage curve.

Table 10. Interflow Elevation Matrix

NOE Basin (elev in ft.)					
Sub-basin	**NOE1**	**NOE2**	**NOE3**	**NOE4**	**NOE5**
NOE1		-0.560			3.674
NOE2	-0.560		0.595		0.592
NOE3		0.595		0.507	-3.568
NOE4			0.507		1.468
NOE5	3.674	0.592	-3.568	1.468	
Sub-basin	**JW1**	**JW2**	**JW3**	**JW4**	**PL11**
JW1		2.271	5.027		
JW2	2.271		1.687		
JW3	5.027	1.687		4.000	
JW4			4.000		5
PL11	4.000			5	
Sub-basin	**OM1**	**OM2**	**OM3**	**OM4**	**OM5**
OM1		2.677	0.603		2.313
OM2	2.677				0.796
OM3	0.603				3.153
OM4					-0.816
OM5	2.313	0.796	3.153	-0.816	
Sub-basin	**SB1**	**SB2**	**SB3**	**SB4**	**SB5**
SB1		10.000	6.494		6.429
SB2	10.000				0.000
SB3	6.494			5.988	10.000
SB4			5.988		10.000
SB5	6.429	10.000	10.000	10.000	
Sub-basin	**JE1**	**JE2**	**JE3**		
JE1		5.422	2.885		
JE2	5.422		-3.682		
JE3	2.885	-3.682			
Sub-basin	**SC1**	**SC2**			
SC1		2.810			
SC2	2.810				

Sub-basin Interflow

The risk model includes specific elevations for common borders between the sub-basins, as illustrated in Table 9. These elevations represent the water levels where interflow begins between respective sub-basins. For example, NOE1 and NOE2 start interflow at elevation -0.560 ft. NOE1 is also connected to NOE5 at elevation 3.674 ft. For each storm, the water levels are adjusted between sub-basins, based on the interflow elevations. The mathematics required to implement the interflow model is presented in Appendix 9 and the algorithm is depicted in Figure 49.

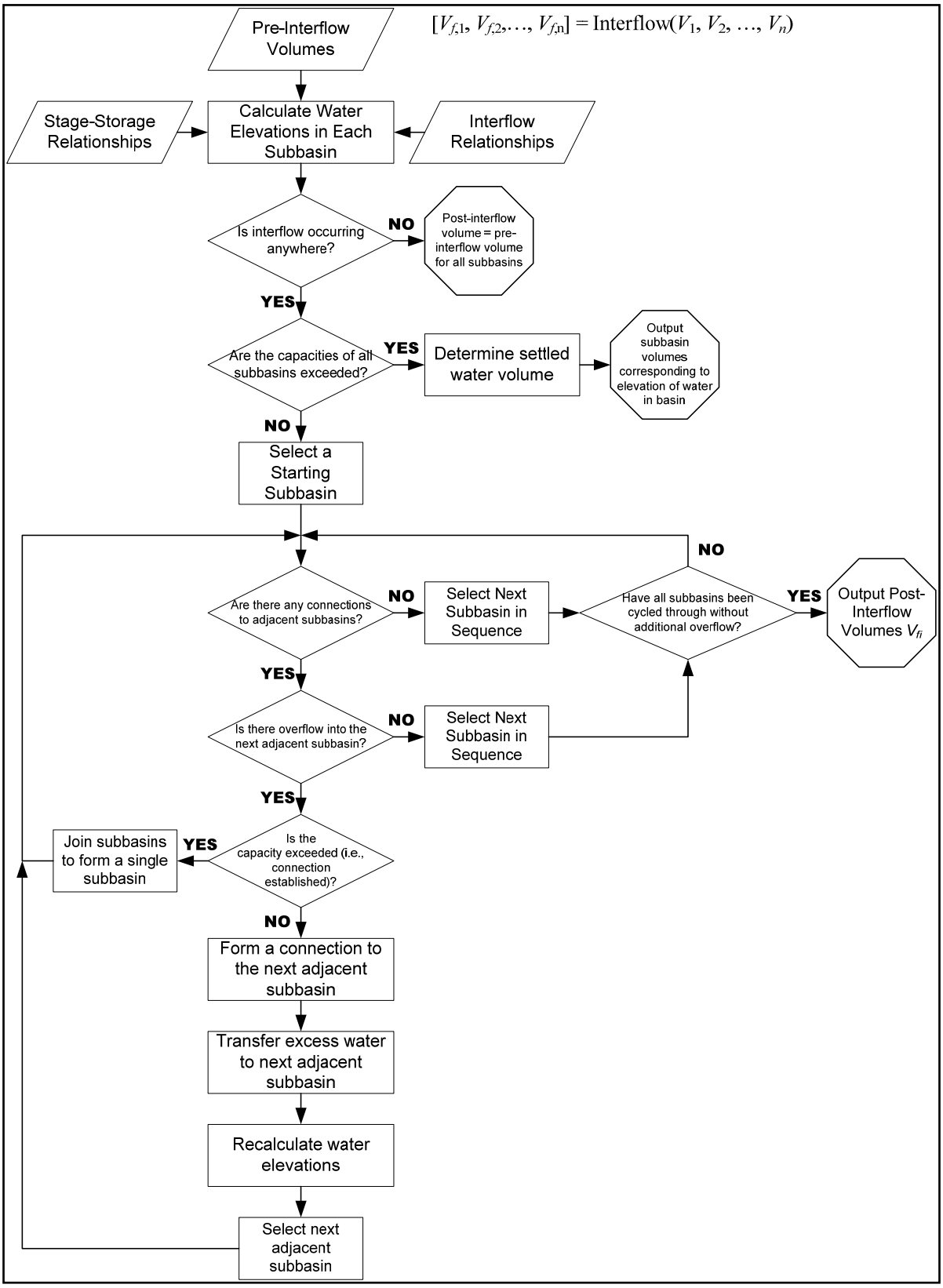

Figure 49. Interflow algorithm.

Reliability Analysis

System reliability can be simply defined as one minus the probability of failure, where the one indicates a completely reliable system with no failures. Therefore, the reliability analysis of the HPS performance determined the conditional probability of failure (i.e., fragility) of structures, systems, and components when they are exposed to the loads of a hurricane.

The reliability analysis had three steps: (1) define and characterize the structures, components, and features constituting the HPS for each drainage basin; (2) define failure and identify failure modes and limit states for each structure, system, component, and feature; and (3) assign conditional probabilities to HPS failure states for given water elevations caused by hurricane conditions.

The reliability of the HPS under potential water elevations due to surge and waves was quantified using structural and geotechnical reliability models integrated within a larger systems description of each drainage basin. Further details are presented in Appendix 10 of this volume.

The reliability models for the HPS components were developed based on design and construction information as reported in the GDM for the specific projects, and on the results of the Performance Team and the Pump Stations Team on-site surveys of existing conditions. No new soil borings, in situ testing, or laboratory testing was undertaken for the risk analysis effort.

Failure and Failure Modes

The HPS for each drainage basin has four components: (1) levees, (2) I-walls (which may be atop levees) and T-walls (which may be atop levees), (3) transitions and closures, and (4) pumping and drainage systems. The reliability analysis examined the performance of the each component, separately and in combination.

Failures that lead to breach of the drainage basin perimeters were associated with four principal failure modes: (1) levee or levee foundation failure, (2) floodwall or floodwall foundation failure, (3) levee or floodwall erosion caused by overtopping and wave runup, and (4) failure modes associated with point features such as transitions, junctions, and closures. The Performance Team found no failures in the HPS which originated in structural failure of the I-wall or T-wall components. All documented failures at I-wall and T-wall locations were geotechnical in nature, with structural damage resulting from the geotechnical failures.

The following failure modes or contributing factors were not considered in the reliability analysis: (1) Internal erosion (piping) of levees due to seepage over times longer than critical hurricane surge loadings; note, this is in contrast to high pore pressures in sand strata, which was considered, as in the vicinity of the London Avenue Canal or the northern end of the IHNC. (2) The effects of maintenance on the HPS capacity over time. Improper maintenance or neglect can lead to reduced capacity of the levees in particular; gates and other moving components also

require maintenance. Trees, landscaping, and pools were observed on protected embankments after Hurricane Katrina, indicating a lack of code enforcement and maintenance of the levees. However, there was insufficient information to include maintenance considerations. (3) Impact by a barge, floating debris, or other large object on the floodwalls or levees. (4) Failure of 3-bulb water stops between I-wall sections.

For each component, a performance level was defined such that its occurrence corresponded to a failure to perform an intended function. The components can fail in a variety of modes. For each mode of failure a limit state was defined, which, if it were to occur would result in a failure to keep water out of the drainage basin.

Engineering models of the mechanics of component performance are limited in their ability to explicitly model a failure state. As a result, an analysis is usually carried out for incipient failure by examining the limits of stability. If this state is equaled or exceeded, the structure or component is expected to fail to perform as intended. Incipient failure models were usually similar to design calculations, and in many cases were adapted from the GDM.

For the purpose of evaluating the performance of the levees and floodwalls, failure was defined as breaching, which allowed water to enter the drainage basin. This failure occurred in two ways: (1) loss of levee or wall stability when the strength of the levee or wall and its foundation was insufficient to withstand the forces placed upon the structure for a given water elevation below the top of the wall or levee (no overtopping); or (2) overtopping caused the protected side of the levee or wall to erode substantially and result in a wall or levee breach, which allowed water to flow freely into the drainage basin.

The HPS was assumed to fail if flooding occurred in a protected area, beyond that expected from rainfall and runoff which can be handled by pumping. Given this definition, a failure of the HPS occurred even if the components making up the system did not fail, for example, if levees or walls were overtopped but not breached.

HPS Systems Definition

The HPS comprises levees, flood walls, levees with floodwalls on top, and various points of transition or localized features such as pumping stations, drainage works, pipes penetrating the barrier, and gates. Each drainage basin perimeter was divided into reaches, which were deemed to be homogeneous in four respects: (1) structural cross section, (2) elevations in the cross section, (3) geotechnical cross section, and (4) hurricane surge.

Geometric and engineering material properties were identified for each reach and summarized in systems definition tables. Structural cross sections were initially identified by review of as-built drawings, aerial photographs, and GIS overlays; and were subsequently confirmed in on-site reconnaissance. Elevations were assessed in the same reconnaissance, supplemented by LIDAR and field surveys provided to the Risk Team. Geotechnical cross sections and corresponding soil engineering properties were derived from original USACE GDM for the respective project areas of each drainage basin, supplemented by site characterization data collected post-Katrina at levee and flood wall failure sites (cone penetrometer and laboratory

measurements on undisturbed samples). GDM are available in PDF format at the IPET Project web site.

Engineering performance models and calculations were adapted from the GDM. Engineering parameter and model uncertainties were propagated through those calculations to obtain approximate fragility curves as a function of water height for components of the HPS. These results were calibrated against the analyses of the Performance Team, which applied more sophisticated analysis techniques to similar structural and geotechnical profiles in the vicinity of failures. Failure modes identified by the Performance Team were incorporated into the reliability analyses as those results became available.

Reaches

The HPS was divided into reaches. A reach is defined for the purpose of the reliability analysis as a continuous length of levee or wall exhibiting homogeneity of construction, geotechnical conditions, hydrologic and hydraulic loading conditions, consequences of failure, and possibly other features relevant to performance and risk.

Thus, reaches are homogeneous lengths of levee or wall that differ from neighboring reaches in at least one of the above properties and which are considered internally homogeneous for the purposes of reliability modeling and risk analysis.

All two-dimensional sections within a reach are considered to be the same with respect to those properties relevant to risk and reliability; thus, the fragility of the levee (i.e., probability of failure as a function of load) is modeled as the same everywhere within an individual reach.

Reach information was summarized in a systems definition file, which is a flat-file database summarizing physical characteristics of each reach. An example for the first 33 defined reaches is shown as Table 11.

Fragility Curves

Reliability assessments were performed for individual components of the HPS for given water elevations. This resulted in fragility curves by mode of failure. A fragility curve gives the probability of failure, conditional upon an event (water elevation in this study), at which a limiting failure state is exceeded (Figure 50).

In actuality, the fragility is a step function at a deterministic loading condition at which failure of the component initiates. Presumably, there is such a loading condition, which if it occurs will cause failure; in reality, that loading condition varies along the length of the reach and is not precisely known before a failure occurs. The S-shaped fragility curve reflects uncertainty about the unique loading condition that causes failure at a particular location. Part of the uncertainty is due to systematic uncertainties, such as the average soil strength or average permeability along the reach, or the simplifications introduced in the performance models; but another part of the uncertainty is due to spatial variability within the reach.

The two types of uncertainty in fragility curves for a single reach introduce a length effect (discussed below). Systematic uncertainties, which cause a bias in the modeling, affect every section within the reach in the same way: if the mean soil permeability is underestimated at one spot it is similarly underestimated everywhere. The spatial variability, on the other hand, does not affect every section in the same way: some spots are weaker and some are stronger. Therefore, the longer the reach, the higher the probability of encountering a particularly weak variation.

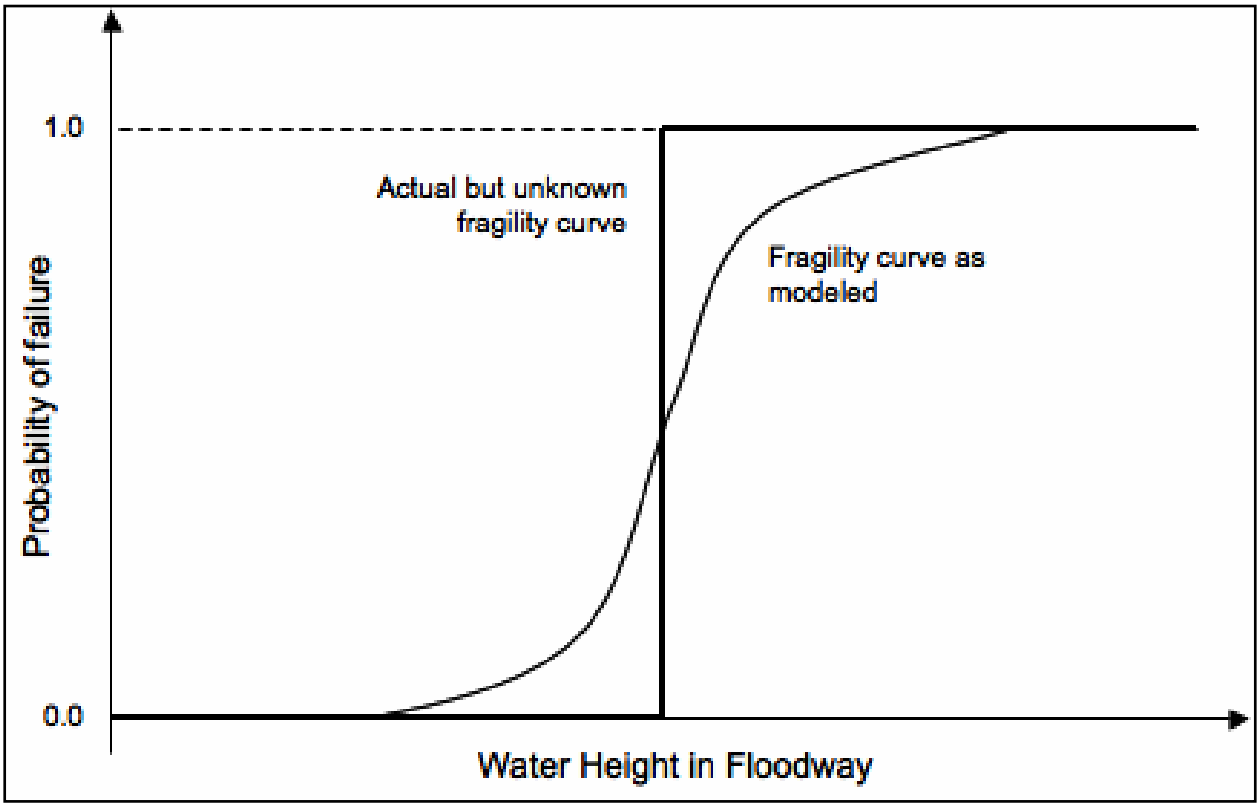

Figure 50. Fragility curve for a section of a step function.

The actual but unknown fragility curve for a component is a step function at the loading conditions that causes failure; this is approximated by an S-shaped probability curve reflecting what is known about the levee and loads.

Uncertainties

The Corps of Engineers Technical Letter ETL 1110-2-556, "Risk-Based Analysis in Geotechnical Engineering for Support of Planning Studies," (USACE 1999) suggests that the principal sources of uncertainty in predictions of levee performance are the following:

- Uncertainty in loadings
- Uncertainty in parameter values
- Uncertainty in analytical models
- Uncertainty in performance

- Performance modes without defined limit states
- Frequency and magnitude of physical changes or failure events
- Condition of unseen features

ETL 1110-2-556 and Appendix 11 go on to observe that geotechnical problems have a number of unique aspects that also require consideration in reliability analyses. These are discussed in detail in Appendix 10 of this report. The reliability analysis undertaken as part of IPET attempts to incorporate all of these uncertainties and considerations.

In modern practice, engineering risk analysis usually incorporates uncertainties of two distinct types: aleatory and epistemic. Aleatory uncertainty is attributed to inherent randomness, natural variation, or chance outcomes in the physical world; in principle, this uncertainty is irreducible because it is assumed to be a property of nature. Epistemic uncertainty is attributed to lack of knowledge about events and processes; in principle, this uncertainty is reducible because it is a function of information. Separating uncertainty into aleatory and epistemic parts is a modeling decision.

Table 11. Reach systems definition (see Table 1) for New Orleans East (partial section, schematic only); showing geometric, material, and design properties to the left; and fragility estimates to the right as a function of still-water level with respect to design elevations.

Reach	Length (ft)	Weighted Elevation (ft) (1) (NAVD88 2004.65)	Fragility Water Elevation (ft) (2) (NAVD88 2004.65)	Reach Type	Foundation Material Type (H, C, S)	Polder Reference	Erosion Modifier for W/L	Pf Fragility Curve (Breach|No Overtopping)			Pf Fragility Curve (Breach|Overtopping)			
								Minimum Elevation for Pf=0	Design Elev. (L) 6ft from TOW (W)	Top of Levee/Top of Wall	1/2 ft Over-topping	1 ft Over-topping	2 ft Over-topping	3 ft Over-topping
1	2,290	11.5	9.52	W	H	2	1	0.0000	0.0023	0.0034	0.0000	0.0569	0.7464	0.8787
2	97	13.3	10.27	L	H	2	1	0.0000	0.0000	0.0000	0.0002	0.0134	0.0565	0.0658
3	2,325	13.5	11.50	W	H	2	1	0.0000	0.0023	0.0035	0.0000	0.0094	0.5269	0.8825
4	2,330	13.3	10.25	L	H	2	1	0.0000	0.0002	0.0003	0.0047	0.2760	0.7524	0.8049
5	2,270	13.7	11.72	W	H	2	1	0.0000	0.0023	0.0034	0.0000	0.0184	0.6484	0.8764
6	19,112	12.9	9.93	L	H	2	1	0.0000	0.0019	0.0029	0.0377	0.9293	1.0000	1.0000
7	1,474	12.1	10.12	W	H	2	1	0.0000	0.0015	0.0022	0.0000	0.0370	0.5865	0.7427
8	2,724	12.6	9.64	L	H	2	1	0.0000	0.0003	0.0004	0.0055	0.3145	0.8045	0.8520
9	33032	18.6	15.64	L	H	2	1	0.0000	0.0033	0.0049	0.0642	0.9897	1.0000	1.0000
10	133	18.6	15.64	L	H	2	1	0.0000	0.0000	0.0000	0.0003	0.0183	0.0766	0.0891
11	27,665	15.1	12.13	L	H	2	1	0.0000	0.0028	0.0041	0.0541	0.9784	1.0000	1.0000
12	8,942	16.7	13.72	L	H	2	1.05	0.0000	0.0009	0.0013	0.0187	0.7359	1.0000	1.0000
13	7,190	17.7	14.65	L	H	2	1.1	0.0000	0.0007	0.0011	0.0158	0.6828	1.0000	1.0000
14	22,257	15.5	12.50	L	H	2	1.1	0.0000	0.0022	0.0033	0.0480	0.9714	1.0000	1.0000
15	111	17.5	15.50	W	H	2	1.05	0.0000	0.0001	0.0002	0.0000	0.0010	0.0624	1.0000
16	382	20.7	18.70	W	H	2	1.05	0.0000	0.0004	0.0006	0.0000	0.0033	0.1988	1.0000
17	10,210	16.8	13.80	L	H	2	1.1	0.0000	0.0010	0.0015	0.0223	0.8042	1.0000	1.0000
18	10,757	17.9	14.92	L	H	2	1.1	0.0000	0.0011	0.0016	0.0000	0.0923	1.0000	1.0000
19	9,318	20.8	18.75	W	H	2	1.05	0.0000	0.0093	0.0139	0.0000	0.2220	1.0000	1.0000
20	7,905	17.2	14.19	L	H	2	1.1	0.0000	0.0008	0.0012	0.0173	0.7170	1.0000	1.0000
21	539	16.7	14.72	W	H	2	1.05	0.0000	0.0005	0.0008	0.0000	0.0144	0.4758	1.0000
22	5616	16.7	14.72	W	H	2	1.05	0.0000	0.0056	0.0084	0.0000	0.1404	0.9988	1.0000
23	15,940	14.0	11.02	L	H	2	1.1	0.0000	0.0016	0.0024	0.0346	0.9216	1.0000	1.0000
24	1,820	12.1	10.14	W	H	2	1.05	0.0000	0.0018	0.0027	0.0000	0.0077	0.4868	1.0000
25	3,453	13.4	10.35	L	H	2	1.1	0.0000	0.0003	0.0005	0.0076	0.4239	1.0000	1.0000
26	1,587	14.5	12.50	W	H	2	1.05	0.0000	0.0016	0.0024	0.0000	0.0067	0.4410	1.0000
27	2,348	13.8	10.77	L	H	2	1.1	0.0000	0.0002	0.0004	0.0052	0.3127	1.0000	1.0000
28	3,803	12.2	9.22	L	H	2	1.05	0.0000	0.0004	0.0006	0.0080	0.4323	0.9895	1.0000
29	537	12.4	6.37	W	H	2	1.05	0.0000	0.0550	0.1129	0.0000	0.0023	0.1787	1.0000
30	526	12.6	9.60	L	H	2	1.05	0.0000	0.0001	0.0001	0.0011	0.0753	0.4676	1.0000

Aleatory and epistemic uncertainties affect the outcomes of a reliability analysis in different ways. Aleatory uncertainty manifests as variations, or frequencies of occurrence, over space or time. Epistemic uncertainties manifest as statistical error and systematic biases in probability estimates, and may introduce correlations among aleatory frequencies.

Four categories of engineering uncertainty were included in the reliability analysis:

1. Geological and geotechnical uncertainties, involving the spatial distribution of soils and soil properties within and beneath the HPS.

2. Structural uncertainties, involving the performance of man-made systems such as levees, floodwalls, and point features such as drainage pipes; and the engineering modeling of that performance, including geotechnical performance modeling.

3. Erosion uncertainties, involving the performance of levees and fills around floodwalls during overtopping, and at points of transition between levees and floodwall, in some cases leading to loss of grade or loss of structural support, and consequently to breaching.

4. Mechanical equipment uncertainties, including gates, pumps, and other operating systems, and human operator factors affecting the performance of mechanical equipment.

The reliability analysis takes water elevations and wave characteristics from the hurricane loading conditions as given, and calculates conditional probabilities of failure for specifically stated water elevations. In follow-on risk and reliability studies, for example, those addressing the 100-year system, an allowance is made for 2 ft of combined sea-level rise and subsidence. In the IPET risk and reliability studies of the pre-Katrina conditions and current conditions as of June 2006, no allowance is made for future sea-level risk and subsidence.

Geological Profile and Soil Conditions

The engineering geology of the New Orleans area is discussed in IPET Volume V, *The Performance of Levees and Floodwalls*, Appendix 2, "Description of New Orleans Area Geology, Environments of Deposition."

A typical profile for much of the New Orleans HPS shows a layer of fill at the top, underlain by organic clays (marsh), in turn underlain by lacustrine (distributary) plastic clays, in turn underlain by stiffer Pleistocene clays. Figure 51 shows the profile under the New Orleans East (NOE) Lakefront Levee, which is typical of this profile.

Equally important to the performance of levees in Orleans East Bank (OEB) and NOE is the Pine Island Beach deposit, a buried, barrier island or beach dating to ca. 5,000 years before present (Figure 52). This feature extends northeast along the southern shore of Lake Pontchartrain, adjacent to and north of the Metairie and Gentilly ridges, former natural levees of the Mississippi River. Foundation soils beneath OEB and NOE are affected by this buried sand which provides a high permeability channel for pore pressures.

The spatial variability of this typical section has to do with variations in thickness of the various strata, inter-bedding of sand or silt lenses, and other local conditions. In some places, for example, the marsh can be thicker than average, as for example in the vicinity of the 17th Street Canal failures.

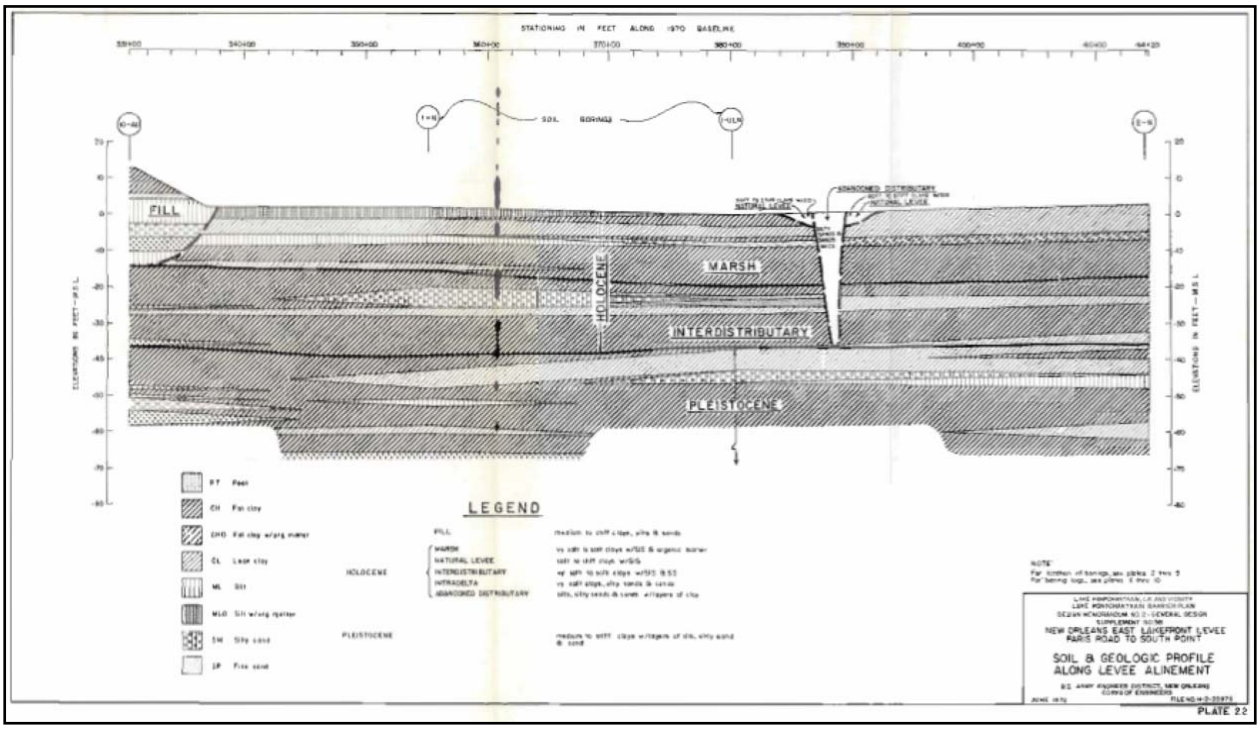

Figure 51. Typical geological profile, NOE lakefront section (USACE 1972).

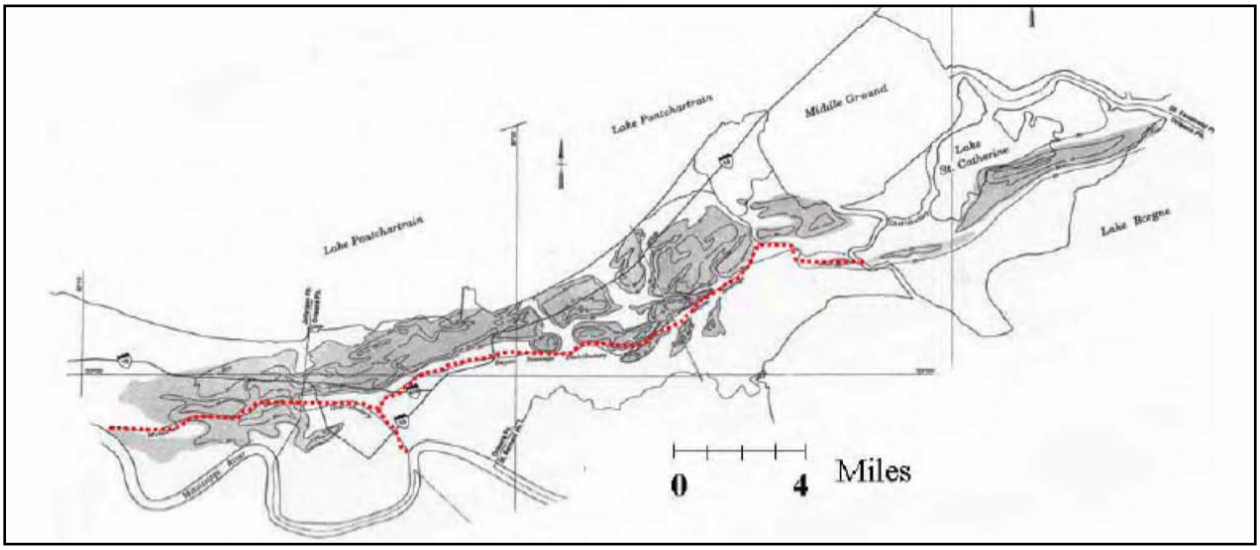

Figure 52. Pine Island (buried) beach ridge, and locations of the canal breaches (after Saucier 1994). The 17th Street breach is located behind the axis of the beach ridge while the London Canal breaches are located on the axis of the ridge. Bayou Metairie is identified in red and forms the Bayou Sauvage distributary course.

Soil Engineering Properties

The Risk Team engaged in no new soil sampling, site characterization programs, or laboratory testing. All the geotechnical information available to the team came from existing sources, principally the GDM and site investigation data taken during design and construction.

Data collected post-Katrina at the site of the drainage canal failures were used to supplement the pre-Katrina data sources.

Soil engineering properties are the principal uncertainties contributing to probability of failure of the levee and I-wall sections in the reliability analysis. The uncertainties in these soil engineering properties are presumed to have two main components: (1) data scatter caused by actual variation of soil properties in space and by random measurement errors, and (2) systematic errors caused by limited numbers of measurements (i.e., statistical estimation error), and by measurement bias in the use of Q-test (UU) data (Figure 53).

Uncertainty Model

The variance in soil properties was assumed to be a composition of four terms,

$$Var(Su) = Var(x) + Var(e) + Var(m) + Var(b) \tag{28}$$

in which $Var(\cdot)$ is variance, Su is the soil property as input to the analysis (in this case, undrained strength), x is the soil property in situ, e is measurement error (noise), m is the spatial mean of the soil property (which has some error due to the statistical fluctuations of small sample sizes), and b is a model bias or calibration term caused by systematic errors in measuring soil engineering properties.

The NOE drainage basin is used here to describe the reliability analysis approach. Analyses of the other drainage basins are similar. The soil profile underlying NOE consists typically of clayey fill overlying marsh (OH, CH), in turn overlying distributary clays (CH), as shown in Figure 51. Critical sections in the GDM and failures observed during Katrina occur in these uppermost strata. The engineering properties of deeper, stronger strata of the Pleistocene formations were not statistically characterized.

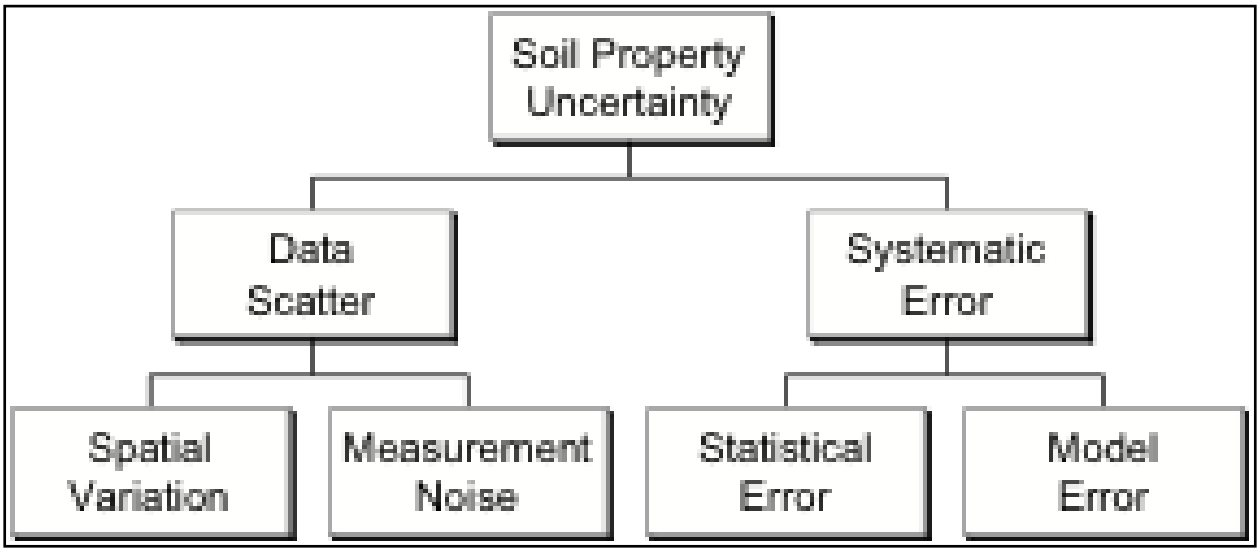

Figure 53. Sources of soil property uncertainty in geotechnical reliability model.

Measured Q-test results reported in the GDM of NOE are shown in Figure 54. Second-moment statistical properties of these data are shown in Table 12. Test values larger than 750 pcf were assumed to be local effects and removed from the statistics to the right in the table. Moments of this sort were used in subsequent calculations. A comparison of undrained soil strengths across the various parishes is shown in Figure 55.

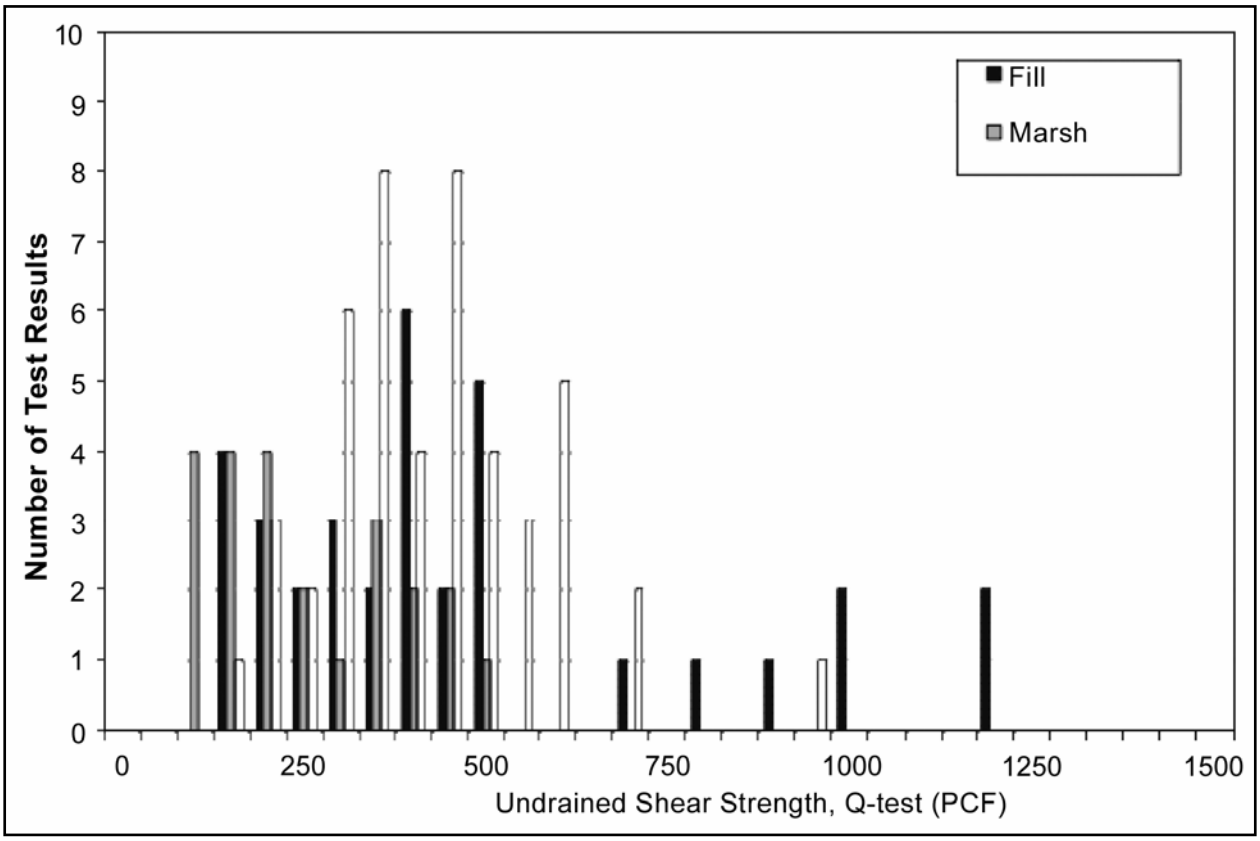

Figure 54. Histograms of undrained strength data (Q-tests), by soil type, NOE GDM: (black) fill, (gray) marsh, (white) distributary clay.

These strength data were compared to post-Katrina sampling and testing performed by Team 7 at the sites of failures along the drainage canals of metro-Orleans Parish (IPET 2006 Vol. V). Those results, based on cone-penetration (CPTU) and laboratory results led to the IPET Strength Model as a basis for the forensic analysis.

Table 12. Statistics of undrained strength data (Q-tests), NOE General Design Memoranda. COV is the coefficient of variation, or standard deviation divided by the mean.

Parameter	All data			Data less than 750 pcf		
	Fill	Marsh	D.Clay	Fill	Marsh	D.Clay
Mean (pcf)	452	405	238	333	392	238
Std Dev (pcf)	297	154	124	142	132	124
COV (data scatter)	0.66	0.38	0.52	0.43	0.34	0.52

The measured shear strengths of the levee fill vary widely, from about 120 psf to more than 5,000 psf, and cannot be interpreted without applying judgment. The values used are based on the combined judgment of the IPET team to make the most reasonable interpretation of the data. Placing the greatest emphasis on data from UU tests on 5-in.-diameter samples, which appear to be the best-quality data available, s_u = 900 psf is a reasonable value to represent the levee fill. This strength can be compared to a value of 500 psf for the levee fill used in the design analyses. The marsh (or peat) deposit is stronger beneath the levee crest where it was consolidated under the weight of the levee, and weaker at the toe of the levee and beyond, where it was less compressed. The measured shear strengths of the marsh also vary widely, from about 50 psf to about 920 psf. Values of s_u = 400 psf beneath the levee crest and s_u = 300 psf beneath the levee toe appear to be representative of the measured values. These strengths can be compared to a value of 280 psf at all locations that was used in the design analyses.

The clay (which has been found to be the most important material with respect to stability of the I-wall and levee) is normally consolidated. Its undrained shear strength increases with depth at a rate of 11 psf per foot of depth. This rate of increase of strength with depth corresponds to a value of s_u /p' = 0.24. There is very little scatter in the results of the CPTU tests, and these values provide a good basis for establishing undrained strength profiles in the clay. The undrained strength at the top of the clay is equal to 0.24 times the effective overburden pressure at the top of the clay. With this model, the undrained shear strength of the clay varies with lateral position, being greatest beneath the levee crest where the effective overburden pressure is greatest and least at the levee toe and beyond where the pressure is lowest, and varying with depth, increasing at a rate of 11 psf per foot at all locations.

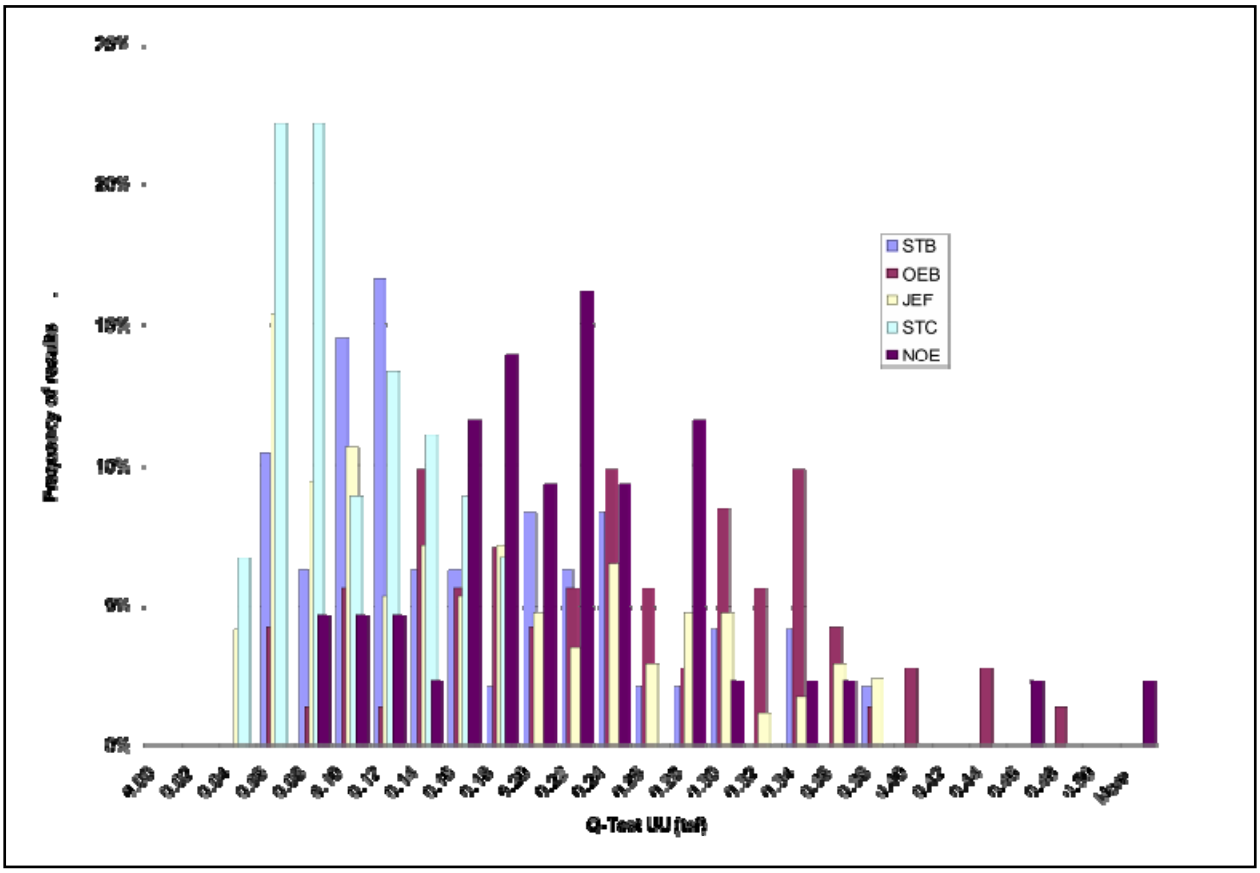

Figure 55. Histograms of undrained strength data (Q-tests), by parish, from USACE GDM of various projects.

Spatial Variation

The spatial pattern of soil variability is characterized by auto-covariance functions. These describe the covariance of soil properties as a function of separation distance. Soils whose properties vary erratically from spot to spot display little spatial covariance, while soils whose properties vary with more waviness display more spatial covariance.

The auto-covariance function of a soil property z is defined as, $C_z(\delta) = E[z(i), z(i+\delta)]$, in which E[·] is expectation, *z(i)* is the soil property at some location *i*, and *z(i+δ)* is the property at another location at distance δ from the first. The autocorrelation function is found by normalizing the auto-covariance by the variance, $R_z(\delta) = E[z(i), z(i+\delta)]Var^{-1}(z)$. The auto-covariance distance is indexed as that separation distance at which $R_z(\delta) = e^{-1}$. This is a representative or characteristic length of the spatial correlation.

The auto-covariance function can only be estimated for distances at least as great as the minimum spacing among observations, that is, the minimum boring spacing in the present case. The minimum boring spacings in NOE are on the order of many hundred feet, with some spacings between adjacent borings as much as several thousand feet. To supplement the information in the GDM, post-Katrina borings made in the vicinity of the 17th Street and London

Avenue breaches were used to estimate auto-covariance functions, and correspondingly the magnitude of measurement noise and the autocorrelation distance.

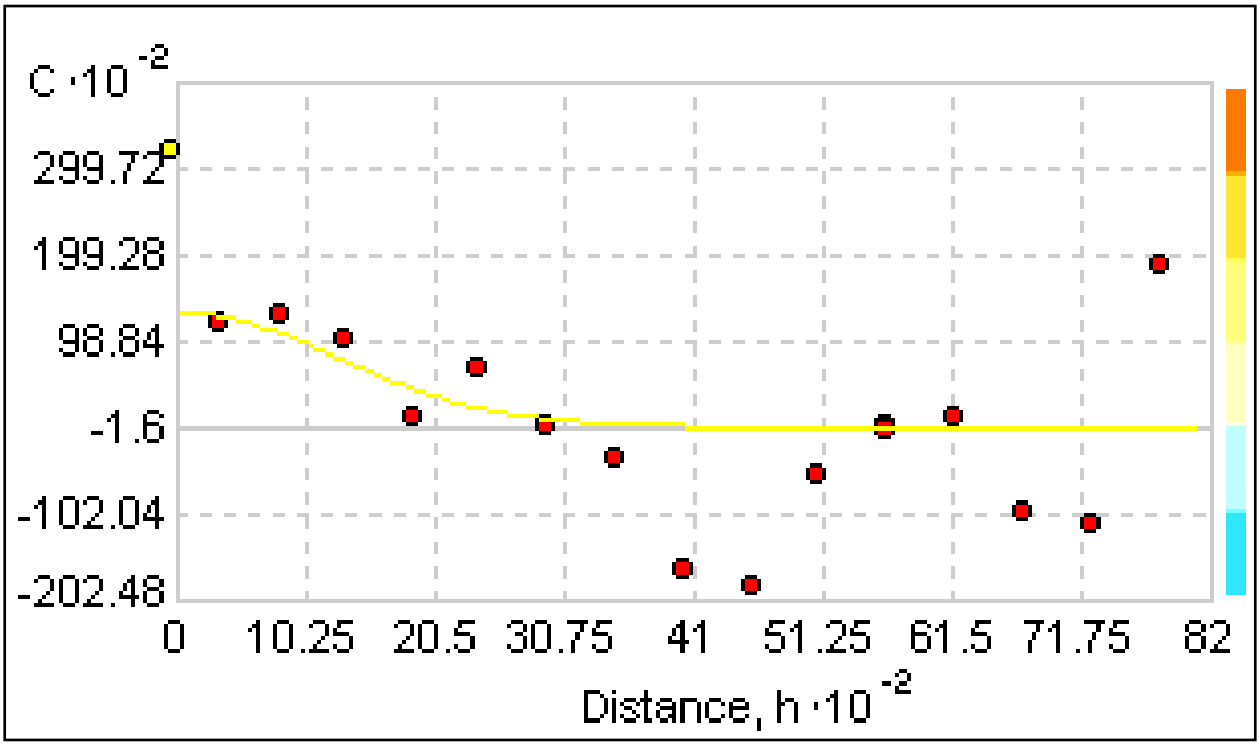

Figure 56. Typical auto-covariance function for CH soils in 17th Street Canal area post-Katrina borings, undrained strength (pcf) from Q-tests at uniform depth below grade.

Statistical estimates of the auto-covariance were made using the ESRI Geostatistical Analyst®, an application running in ArcMap®. Results for the undrained strength (Q-tests) of London Avenue the distributary clays are shown in Figure 56. Analyses for marsh and fill show similar patterns.

Measurement Noise

Soil strength is measured destructively; therefore replicate measurements cannot be used to estimate the magnitude of random measurement error. However, the spatial covariance structure provides an indirect way to make the estimate (DeGroot 2006). Assuming that the measurement z of soil property x is corrupted by a zero-mean error e that is independent from one measurement to the another and independent of the value x, the measurement can be expressed as $z=x+e$. The auto-covariance function of z is the summation of the auto-covariance functions of x and of e: $C(z)=C(x)+C(e)$. But, the auto-covariance function of e is a spike at the origin and zero otherwise. Thus, the difference between the intersection of the observed auto-covariance function of z extrapolated back to the origin, and the total variance Var(z), provides an estimate of the variance of the error, Var(e).

The conclusions drawn from these auto-covariance analyses were (1) the measurement noise (or fine-scale variation) in the Q-test data is roughly ½ to 3/4 the total variance of the data

(suggesting the COVs in the top row of Table 13); (2) the representative auto-covariance distance in the horizontal direction is on the order of 1,000 ft; (3) the representative auto-covariance distance in the vertical direction is assumed to be on the order of 1/100 of the horizontal distance, or about 10 ft, although there are too few Q-test data in individual borings to statistically estimate this value.

Statistical Error

Statistical estimation error in the mean soil property is caused by limited numbers of data within a reach; it is approximated from the standard error of sampling. The variance of the error is approximated as $Var(m) \approx Var(x)/n$, in which m is the mean soil property, x is the spatial variation component of data scatter, and n is the number of measurements (Table 13).

Table 13. Estimates of component uncertainties to soil engineering property mode for NOE.

Component	Fill	Marsh	D.Clay
Spatial COV	0.20	0.17	0.25
Number of measurements	48	21	23
Statistical error in mean	0.06	0.07	0.11
Measurement model bias	0.1	0.1	0.1

Measurement Model Bias (systematic error)

The correction factor, b, is a model bias term introduced to correct for systematic errors in measuring soil engineering properties, in this case by the use of Q-tests rather than more modern test procedures. The predominant soil property test data available in the GDM were unconsolidated–undrained tests. However, in the post-Katrina investigations of floodwall failures along the metropolitan New Orleans drainage canals, IPET Performance Team performed a large number of in situ cone-penetration, and laboratory tri-axial and direct simple shear tests on fill, marsh, and distributary clays (IPET 2006 Vol. V). These test results were compared with Q-test data collected at the same sites and reported in the respective GDM (IPET 2006 Vol. V). The subsequent calibration factors were used to adjust the Q-test data per the measurement bias term, b, in the above equation.

Fragility Curves

Fragility curves summarize the probability of components reaching their respective limit states (i.e., failure), conditioned on levels of water elevation. For example, the fragility curve for a reach of levee might show the probability of failure by deep-sliding instability of a levee reach as a function of water height.

Fragility curves for levees and floodwalls were calculated for two conditions (Table 14.): (1) global stability without overtopping, for which reliability was calculated at two water elevations, design elevation and top of levee, and a smooth curve approximated to water at sea level; and (2) overtopping with subsequent erosion, for which reliability was estimated from empirical experience during Katrina at four water elevations of overtopping: ½, 1, 2, and 3 ft

above the top of levee or floodwall. Fragility curves for all 138 reaches are given in Appendix 10 of this volume.

Table 14. Summary of engineering models used in calculating fragility curves.

Failure Mode	Hazard	Models and Parameters	Source of Inputs	Principal Uncertainty
Static instability	Still-water surge; weak foundation soils	Limiting equilibrium stability	IPET Vol. IV, V; Soil test data; Design Memoranda; In situ surveys	Soil properties; Still-water levels; Existing elevations; Geotechnical model
Under seepage	Still-water surge; high permeability soils	Flow net calculations; Limiting equilibrium stability	IPET Vol. IV, V; Soil test data; Design Memoranda; In situ surveys	Soil properties; Still water levels; Existing elevations; Geological profile geometry
Still water overtopping and scour	Still-water surge; erodible fill	Empirical correlations from post Katrina data	IPET Vol. IV, V	Still water levels Soil fill properties Existing elevations Scour model
Transition point feature erosion	Still-water surge; erodible fill	Empirical observations during Katrina	IPET Vol. V	Still water levels Soil fill properties Existing elevations Scour model
Wave run-up	Wave heights and periods; erodible fill	Empirical (Dutch) correlations and model test results	IPET Vol. IV	Wave height and period; Still water levels; Existing elevations

No Overtopping

Engineering performance models were adapted from the GDM for the respective reaches of levee (Figure 57). Engineering parameter and model uncertainties were propagated through those calculations using a first-order second-moment approximation to obtain approximate fragility curves as a function of water height.

The reliability analysis was based on limiting equilibrium calculations of factor of safety against instability. For levees, the analysis was based on GDM calculations of factor of safety against wedge instability. The calculations were based on undrained failure conditions.

Model bias was calculated based on a comparison of the detailed modeling results of the Performance Team compared to the more simple general method of planes used in the GDM. On average, the GDM calculated factors of safety that were approximately 10% lower than more precise model analysis using the computer programs SLIDE[1] and UTEXAS4[2], varying from about 7% to about 18% (IPET 2006, Vol. V). These model comparisons were summarized in a study conducted by IPET Performance Team for Task Force Guardian.

[1] Available from Rocscience Inc., 31 Balsam Avenue, Toronto, Ontario, Canada M4E 3B5
[2] Available from Shinoak Software, 3406 Shinoak Drive, Austin, TX 78731

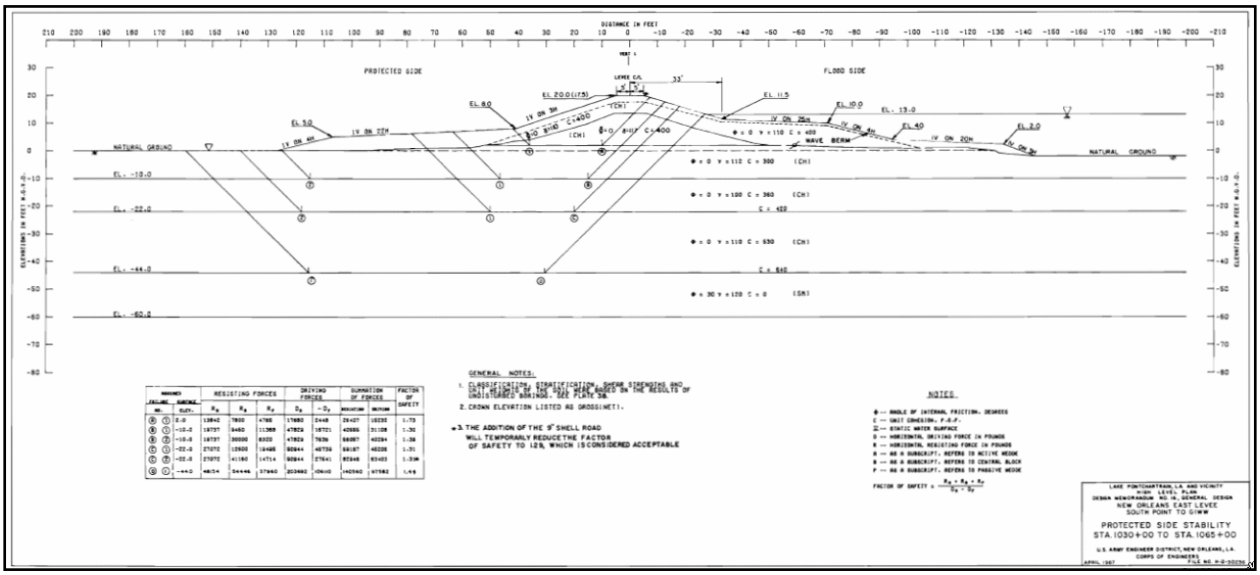

Figure 57. Typical method-of-planes wedge stability analysis of levee section from GDM (USACE 1972).

Best Estimate Calculations

Best estimate calculations were based on mean soil properties, adjusted from calculations in the GDM, which used factored average soil properties (Table 15). That is, the calculation of factor of safety in the GDM was not based on mean observed undrained strengths, but factored strengths, using a reduction factor of 1.2 to 1.3. These were corrected for the reliability analysis to yield a mean factor of safety.

Table 15. Soil property uncertainty by parish.

Parish	Mean Su (TSF)	Point COV	Point COV less noise	Spatial reduction	COV Averaged	N	Depth of data	Bound for outliers	Std Dev in mean
OEB	0.24	0.43	0.22	0.70	0.15	71	0 to -40	0.4	0.05
STB	0.16	0.53	0.27	0.70	0.19	64	0 to -40	0.4	0.07
NOE	0.22	0.58	0.29	0.70	0.20	43	0 to -40	0.4	0.09
STC	0.09	0.41	0.21	0.70	0.14	45	0 to -40	0.4	0.06
JEF	0.16	0.62	0.31	0.70	0.22	169	0 to -40	0.4	0.05

Uncertainties in undrained shear strength were propagated through the GDM calculations to estimate a coefficient of variation in the calculated factor of safety. The factor of safety was assumed to be normally distributed, and a fragility curve was approximated through three calculation points.

Soil property uncertainty in the form of coefficients of variation for undrained soil strengths underlying the levees and walls was propagated through the limiting equilibrium wedge stability calculations to obtain coefficients of variation on factors of safety. In most cases, the stability analyses were linear functions of undrained soil strength so that the coefficient of variation of the factor of safety was the same as the coefficient of variation of the input soil strengths. The mean factor of safety was taken as that calculated in the GDM, adjusted for factored strengths.

Uncertainty in Realized Factor of Safety

For a given water elevation, uncertainty in the realized factor of safety against sliding depends principally on the average soil strength, *Su*, across the area of the failure surface. This average strength varies from cross section to cross section because the soil properties themselves vary from spot to spot (Figure 58). The variability in the average soil strength is less than the variability in the point-to-point properties because, to some extent, the highs and lows of the soil strength balance against each other over the failure surface.

The larger the failure surface relative to the autocorrelation of the soil properties, the greater the variance reduction from the local averages. Vanmarcke (1977) has shown that the variance of the spatial average for a unit-width plain strain cross section decreases approximately in proportion to (L/r_L), for $L>r_L$, in which L is the cross-sectional length of the failure surface, and r_L is an equivalent auto-covariance distance of the soil properties across the failure surface weighted for the relative proportion of horizontal and vertical segments of the surface. The variance across the full failure surface of width w along the axis of the levee is further reduced by averaging in the horizontal direction by an additional factor (w/r_H), for $w>r_H$, in which r_H is the horizontal auto-covariance distance. At the same time that the variance of the average strength on the failure surface is reduced by the averaging process, so, too, the auto-covariance function of this averaged process stretches out from that of the point-to-point variation.

Table 16. Uncertainty analysis for example levee reach in NOE.

Water Level	Design Basis	¾ Design Basis	Top of Levee
Mean FS	1.3	2	1.2
Spatial COV	0.17	0.17	0.17
Spatial average reduction factor	0.8	0.8	0.8
Systematic COV	0.07	0.07	0.07
Total COV	0.15	0.15	0. 15
Reliability Index, b	2.2	6	1.7
Pf for specific 1,000-ft reach	0.014	0	0.045
Increase in Pf per 1,000-ft reach	2%	0.0	5%

For a failure length of approximately 1,000 ft along the levee axis and 30 ft deep, with horizontal and vertical auto-covariance distances of 1,000 ft and 10 ft, respectively, the corresponding variance reduction factors are approximately 0.75 for averaging over the cross-sectional length *L,* and between 0.73 and 0.85 for averaging over the failure length *b*, assuming either an exponential or squared-exponential (Gaussian) auto-covariance. The corresponding reduction to the COV of soil strength based on averaging over the failure plane is the root of the product of these two factors, or between 0.74 and 0.8.

The Reliability Index for the specific levee reach of length w is the number of standard deviations separating the mean condition from the limiting state,

$$\beta_6 = \frac{E[FS]-1}{Var(FS)} = \frac{E[FS]-1}{\Omega_{FS} E[FS]} \tag{29}$$

in which *E[FS]* is the mean factor of safety, *Var(FS)* is the variance, and Ω_{FS} is the COV.

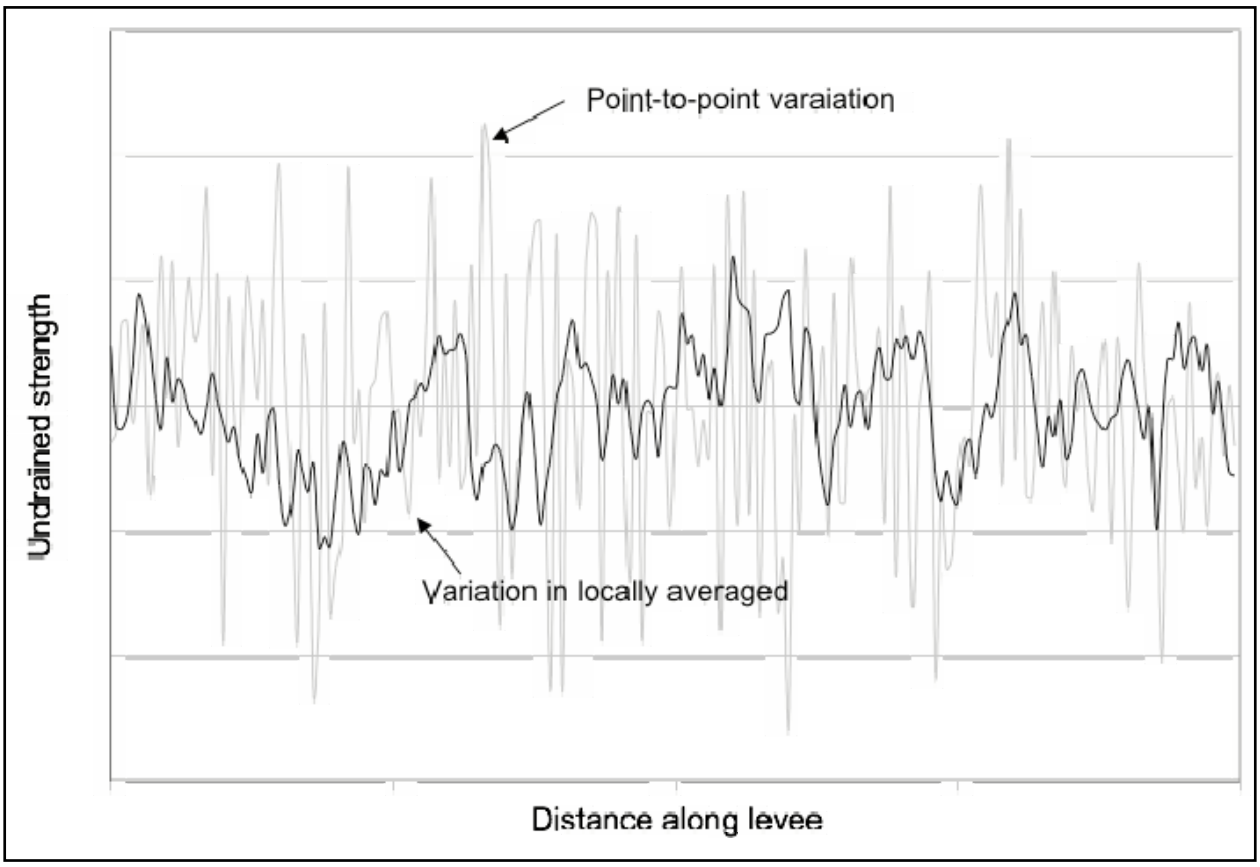

Figure 58. Point variation in undrained strength and variation among locally averaged strength.

Seepage

A number of seepage failure modes were considered for specific reaches of the HPS. Failures due to seepage pressures or erosion were observed during Katrina at the London Avenue Canal site and also present hazards at northern reaches of the IHNC. In this area, the buried Pine Island Beach deposit rises close to the present ground surface.

The fragility curves for any reach in which sands rise to within the critical failure zone under a levee or wall were adjusted for seepage pressure effects. These affected reaches included not only those in the vicinity of the Pine Island Sand, but also those suspected of crossing untreated buried stream channels in other sections of the HPS. The adjustment of the fragility curves was accomplished by estimating potential pore pressure rise in the affected reaches, and reducing effective strengths in the sand layers accordingly. This lowers the predicted mean factor of safety, and correspondingly increases the probability of failure at given still-water levels.

Length Effect

The HPS of New Orleans includes long lengths of embankment or wall extending many miles across ground that is poorly characterized from an engineering perspective. Levees fail at

locations where loads are high and strengths are low. If these critical locations are identified ahead of time, traditional methods can be used to analyze stability and calculate factors of safety. In such situations, the overall length of levee is immaterial, because the weakest spots have been identified and dealt with. The probability that the levee fails is that of these weakest spots.

The more common situation is that the levee system is not characterized with enough detail to know unambiguously where the weakest spots are. In this case, any reach of levee has some probability of experiencing higher than average loads or lower than average strengths, and as a result, of being a "weak spot." Since this critical combination cannot be uniquely identified before a failure occurs, the longer the levee, the greater the chance that a critical combination exists somewhere, and thus the higher the probability of a failure somewhere.

For a long levee, the chance of at least one failure is equivalent to the chance that the variations of the mean soil strength across the failure surface shown schematically in Figure 58 drop below that required for stability at least once along the length. VanMarcke (1977a,b) has shown that this can be determined by considering the first crossings of a random process. The approximation to the probability of at least one failure as provided by VanMarcke was used in the calculations (Appendix 10 of this volume).

The primary level of analysis of levee reliability is the two-dimensional levee section. The presumption is that this 2D section applies over a unit length of levee, defined approximately as the horizontal autocorrelation distance, and treated as a probabilistically independent characteristic length. As the total length of levee increases, the probability of systems failure rises in proportion to length and soon displays a classic exponental saturation shape trending asymptotically toward 1.0, according to the fomula

$$P_f = 1 - (1 - p)^n \tag{30}$$

in which, $P_f = 1 - (1 - p)^n$ is the probability of system failure, p is the 2D probability of failure, and n is the number of characteristic lengths within the reach.

Wave Runup[1]

Wave runup for each reach was calculated by the approach summarized in TAW (2002). Apart from specific cases, a grass-covered levee without floodwalls on top and perpendicular wave attack is assumed. Hence, there is no reduction of the overtopping rate due to friction, wave attack, and vertical walls.

For both levees and floodwalls, the average wave overtopping can be computed using the still-water level from ADCIRC and the wave information from STWAVE. The mean wave period $T_{m-1,0}$ was derived directly from the STWAVE results at 600 ft in front of the

[1] This section draws heavily on the internal USACE memorandum, van Ledden (2007), "Wave overtopping IPET," dated 21 June.

levees/floodwalls[1]. The significant wave height at the toe of the structure (H_{m0}) was also derived from the STWAVE results, but it was adapted because of depth-limited breaking in front of the structure.

The standard deviation for the significant wave height was assumed to be 10% of the value based on STWAVE (or after reduction due to depth-limited breaking according to Equation 5. The error in the wave period was set at 20% of the STWAVE result. The error was assumed to be normally distributed. Both errors are based on expert judgment due to lack of field data.

I-Wall Fragility, No Overtopping

The reliability analysis for I-walls was similarly based on limiting equilibrium calculations of factor of safety against instability. For I-walls, the analysis is based on the Performance Team's mechanism of cracks developing in the soil immediately behind the wall and sheet pile, allowing hydrostatic pressure on the sheet pile. The equilibrium of a soil wedge to the protected side of the wall was calculated for this condition. The calculations were based on undrained failure conditions. Undrained strengths of soils underlying the levees and walls were based on Q-test results. The design consideration of balancing forces and moments on the sheet pile to determine depth of penetration was considered immaterial to the reliability analysis of the wall sections.

Based on the results of the Performance Team's analyses, it was assumed that cracking initiated at 5 ft of water elevation on an I-wall (Figure 59). Thus, for water elevations lower than 5 ft, the factor of safety was that calculated in the GDM. But at 5 ft, when a crack formed in the soil, the factor of safety underwent a step change to a forward (protected side) wedge failure.

[1] Note that only the peak period T_p is available for the 152-storm suite of the 2007 situation. The peak period T_p can be converted easily into the mean period $T_{m-1,0}$ using $T_{m-1,0} = T_p/1.1$.

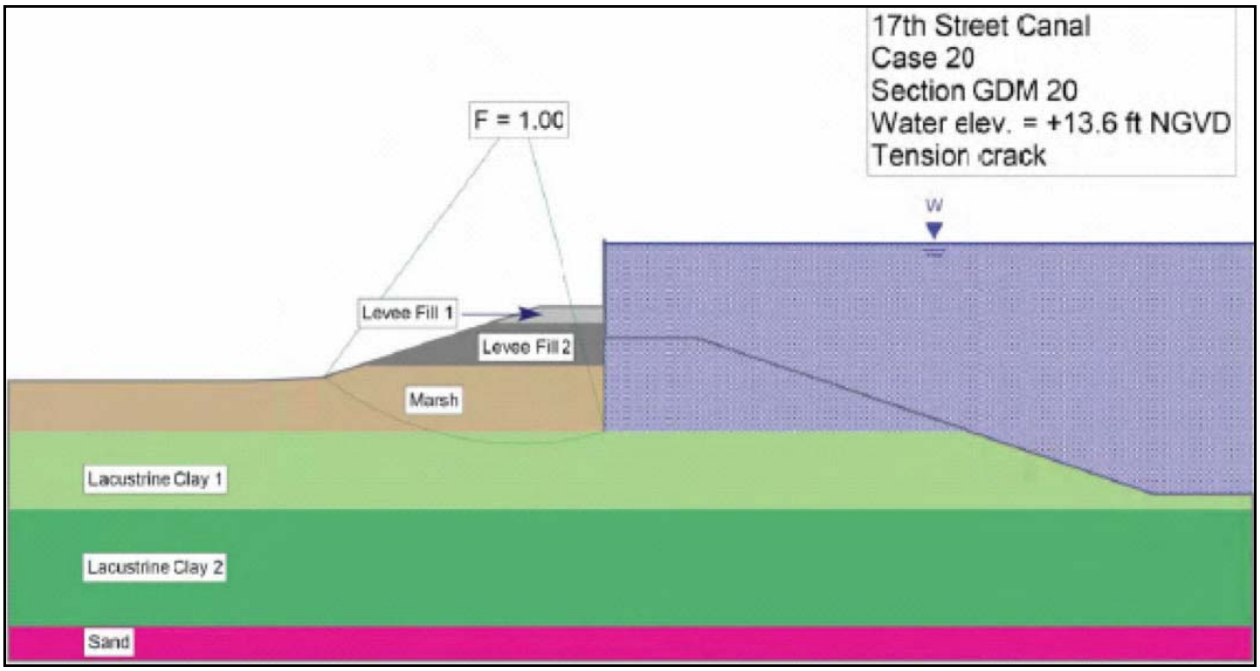

Figure 59. Failure by rotation of I-wall, reducing I-wall elevation (IPET 2006 Vol. V).

Levee and I-Wall Fragility, With Overtopping

Reliability calculations were based on the probability of overtopping causing erosion of the protected side of a levee that led to a breach. Two approaches were considered: The first approach considered flow velocities over the levee or wall. The second approach considered water elevation, which is estimated by the storm surge modeling, as an indirect indicator of flow velocity.

The probability of overtopping of levees or floodwalls leading to scour and consequent failure was directly estimated based on empirically observed rates of failure during Katrina and documented in IPET Vol. V (2006) and as shown in Table 17. These probability values are consistent with later analyses by Briaud et al. (2006).

Table 17. Empirical frequency of overtopping scour failure of levees and walls as observed in Katrina, as a function of the velocity of overtopping flow (correlated to depth of overtopping) and soil type.

Levees	≤0.5 foot	≤1.0 foot	≤2.0 feet	3 feet
Hydraulic Fill	0	0	1	1
Clay	0	0	0.25	0.5
Protected	0	0	0	0.1
Walls	**≤0.5 foot**	**≤1.0 foot**	**≤2.0 feet**	**3 feet**
Hydraulic Fill	0	0	0.5	1
Clay	0	0	0.25	0.5
Protected	0	0	0	0.1

Transitions and Point Structures

A number of breaches were observed at transitions between components. These breaches were typically at levee to I-wall, levee to T-wall, or I-wall to T-wall transitions. Many of the HPS breaches were at point structures such as gates (road and railroad), pump stations, or around drainage control structures. These transitions indicate a weak link due to the differing stiffness of the components which permit them to become areas of significant erosion during a hurricane event.

The failure modes use the qualitative erosion parameters developed by the Performance Team as the basis for change in the stability of components at the transition zones. That is, the fragility of the transitions was taken to be similar to that of overtopped levee sections and to depend on the combination of height of overtopping water and the presence of hydraulic fill enlargement to the levee section. Reliability for point structures (gates, control structures, pump stations) was taken as a point probability of failure for design loading.

Pumping Stations

The adverse performance of mechanical, electrical, and human elements of the HPS, such as pumps, the availability of power, and the closure of gates, was treated as random point (i.e., aleatory) events with discrete probabilities of failure based on the statistical record during Katrina and on information provided by other IPET teams.

The pumping stations are critical HPS system components because they maintain the flood levels on the protected side. Unfortunately, many of the pumping stations during Katrina reached and exceeded their pumping capacity shortly into the storm. Their reliability during Katrina was not exceedingly high as the stations primarily failed due to rising waters at the plants, a lack of external or backup power source, or were shut down due to inefficient pumping. These systems are designed to handle a specific level of rainfall and are easily overwhelmed when the levees are overtopped by a hurricane event. The following failure modes were possible for the pumping stations: no commercial power, backup generator failed, mechanical fuel unavailable, pumps not functioning at time of incident, mechanical failure of components, operator unavailability, debris blocking intakes, or reversed or backflow through outfall pipes.

The reliability of the pumping stations was included in the risk model as point sources. The reliability is based on data collected by the Pumping Team, performance data maintained by Task Force Hope, and information from the dewatering plan for New Orleans developed by the New Orleans District. The fragility curves for each pumping station will be limited to a specific elevation or volume of water within the drainage basin. These fragility curves will vary for each pumping station and will reflect the interior drainage areas and backflow potential as determined by the Interior Drainage Team.

Consequences

All of the consequence data used in the risk analysis was provided by the IPET Consequence Team whose work is reported in Volume VII of the IPET report. The following general discussion is a summary of their work as it applies to the risk analysis. For additional details concerning the procedures used to develop both the stage-damage and stage-fatality relationships used in the risk analysis, the reader is referred to Volume VII, *The Consequences*.

As has been discussed earlier, the risk model was run for 76 hypothetical hurricanes that represent a wide range of hurricane events with different severities, directions, points of landfall, etc. For each of these hurricanes, the risk model represented the performance of the HPS and estimated the probability that inundation would result from insufficient internal drainage, overtopping of the levees, open road closures, and levee breaching. The resulting estimates of inundation depths were used as a basis for interpolation of life loss and property loss estimates using the relationships provided by the Consequence Team. Estimates were made for the pre-Katrina and June 2007 scenarios for each of the 27 sub-basins. Thus, it was necessary for the life loss and property loss estimates to cover a range of elevations associated with a range of expected flooding that could impact New Orleans from minor inundation to an elevation 36 ft above sea level.

In order to best determine the reduction in pre-Katrina risks gained by improvements made to the 2007 HPS, pre-Katrina consequences were used in the June 2007 analysis. The primary reason is that risks in New Orleans have been reduced due to a combination of changes in demographics of the population, reduced property values, and improvements to the HPS. In addition, population is returning to the area and redevelopment has been occurring as recovery continues, so any prediction of post-Katrina consequences would be based on constantly changing factors. Therefore, risk reductions gained solely due to HPS improvements would be difficult to identify if post-Katrina population and property values were used in the risk analysis. While the use of pre-Katrina property values and population levels in the risk analysis results in life and property risks that are overstated for present conditions in New Orleans, it does illustrate how risks have been impacted by improvements to the HPS.

The Consequence Team conducted extensive studies to predict the repopulation and redevelopment after Katrina and that work may be used in future risk studies in New Orleans. Their work also included fatality estimates that included a range of effectiveness of evacuation prior to the arrival of a hurricane. A specific value for evacuation effectiveness was not considered, however, in the fatality estimates used by the Risk Team. A mean value of effectiveness was used based on a distribution of possible evacuation rates. Use of the mean value for evacuation effectiveness results in higher risk estimates of life loss than actually occurred during Katrina. This indicates that the Katrina evacuation was highly successful and the effectiveness value is really several standard deviations above the mean.

Life Loss Estimation

The estimates of life loss were developed as probability distributions and the estimates of property loss were developed as best estimates with an associated 90% confidence interval rather than single-value or point estimates. The probability distributions for life loss and confidence intervals for property losses represent various types of uncertainties in the estimates, which are described below. A sample of the stage-fatality curves used in the risk analysis are presented in Table 18 for NOE4. More detailed presentation of the consequences used in the risk analysis is contained in Appendix 12 of this volume. Life loss was estimated by the Consequence Team using two computer models as follows:

- The *LIFESim* Modeling System[1] was developed (a) to estimate how the population in the flooded sub-basins would redistribute vertically in relation to the depth of inundation; and (b) to classify population into one of three flood lethality zones, which are defined in the *LIFESim* model and by McClelland and Bowles (2002), and an additional sub-zone for people who would be expected to be able to walk away from the inundation area following inundation. Thus, *LIFESim* was run without evacuation.

- A Monte Carlo Uncertainty Model, which was developed to take the vertically redistributed estimates of population in the three flood lethality zones from LIFESim, estimated (a) the immediate loss of life using fatality rate probability distributions from LIFESim and McClelland (2000) accounting for evacuation effectiveness as a random variable that varied according to a triangular probability distribution (65%, 80%, 95%); and (b) delayed fatalities amongst those who survived the initial inundation but were not rescued, where the rescue effectiveness was accounted for a random variable that varied according to a uniform probability distribution between 99.5% and 100% in the Safe Flood Lethality Zone and between 95% and 100% in the Compromised and Chance Flood Lethality Zones.

Direct Property Loss Estimation

The objective of the direct economic damage analysis was to develop stage-damage curves that represent the flood damage potential before Katrina devastated New Orleans on 29 August 2005. This required accounting for the severity of the Katrina. In some areas flooded by Katrina, where water depths were low, damage was minor. In other areas, where water depths were high, damage was extensive and in some areas total. The June 2007 stage-damage tables and curves were estimated using the same sub-basin definitions and damage tables as for the pre-Katrina analysis. The Katrina flooding depths were used to estimate the depth of flooding for each census block. For instance, within the Orleans Metro 5 sub-basin, 1,535 census blocks had flooding of 1 ft or less while a total of 4,400 census blocks were flooded. Table 12-2 shows the complete estimate of the number of the census blocks flooded by Katrina by depth category. From these selected census blocks, damages at each stage were aggregated to the sub-basin level for each recovery category. This calculation determined the amount of the Katrina damage

[1] Institute for Dam Safety Risk Management at Utah State University (Aboelata and Bowles 2005) LIFESim includes a simulation module for warning and evacuation, which was not used in this study.

within each depth category. This was repeated for each of the Katrina flood depth categories. A sample of the stage-damage curves used in the risk analysis is presented in Table 19 for NOE4.

Table 18. NOE 4 Stage-fatality matrix

Elevation (ft)	NOE4		
	5%	95%	Mean
-1.200E+01	0.000E+00	0.000E+00	0.000E+00
-1.100E+01	0.000E+00	0.000E+00	0.000E+00
-1.000E+01	0.000E+00	0.000E+00	0.000E+00
-9.000E+00	0.000E+00	0.000E+00	0.000E+00
-8.000E+00	0.000E+00	0.000E+00	0.000E+00
-7.000E+00	0.000E+00	0.000E+00	0.000E+00
-6.000E+00	0.000E+00	0.000E+00	0.000E+00
-5.000E+00	1.412E-04	3.621E-03	1.636E-03
-4.000E+00	1.412E-04	3.621E-03	1.636E-03
-3.000E+00	1.412E-04	3.621E-03	1.636E-03
-2.000E+00	1.412E-04	3.621E-03	1.636E-03
-1.000E+00	1.421E-03	3.645E-02	1.647E-02
0.000E+00	1.826E-03	4.604E-02	2.081E-02
1.000E+00	2.230E-03	5.562E-02	2.515E-02
2.000E+00	4.176E-03	9.278E-02	4.220E-02
3.000E+00	6.122E-03	1.299E-01	5.925E-02
4.000E+00	1.084E-02	1.533E-01	7.060E-02
5.000E+00	1.556E-02	1.766E-01	8.194E-02
6.000E+00	4.666E-02	3.673E-01	1.663E-01
7.000E+00	7.775E-02	5.580E-01	2.506E-01
8.000E+00	2.179E-01	1.157E+00	5.718E-01
9.000E+00	3.580E-01	1.755E+00	8.929E-01
1.000E+01	6.284E-01	2.425E+00	1.429E+00
1.100E+01	8.987E-01	3.094E+00	1.964E+00
1.200E+01	9.438E-01	3.251E+00	2.064E+00
1.300E+01	9.888E-01	3.408E+00	2.163E+00
1.400E+01	1.081E+00	4.033E+00	2.428E+00
1.500E+01	1.174E+00	4.657E+00	2.694E+00
1.600E+01	1.714E+00	7.458E+00	4.077E+00
1.700E+01	2.255E+00	1.026E+01	5.459E+00
1.800E+01	3.858E+00	1.467E+01	8.754E+00
1.900E+01	5.460E+00	1.908E+01	1.205E+01
2.000E+01	6.148E+00	2.143E+01	1.356E+01
2.100E+01	6.835E+00	2.377E+01	1.507E+01
2.200E+01	6.912E+00	2.403E+01	1.524E+01
2.300E+01	6.988E+00	2.430E+01	1.540E+01
2.400E+01	7.096E+00	2.466E+01	1.564E+01

Table 19. Pre-Katrina – Stage-Damage NOE4.

Water Elevation	Basin Name	5%	Mean	95%
-3	NOE4	0	0	0
-2	NOE4	0	0	0
-1	NOE4	0	0	0
0	NOE4	0	0	28
1	NOE4	0	0	36
2	NOE4	0	25	39
3	NOE4	0	33	54
4	NOE4	22	35	59
5	NOE4	29	49	61
6	NOE4	31	54	62
7	NOE4	44	56	63
8	NOE4	49	57	63
9	NOE4	51	57	65
10	NOE4	52	58	66
11	NOE4	52	59	66
12	NOE4	53	60	67
13	NOE4	54	61	69
14	NOE4	55	62	69
15	NOE4	55	63	71
16	NOE4	56	64	72
17	NOE4	57	65	72
18	NOE4	58	66	72
19	NOE4	59	66	72
20	NOE4	60	66	72
21	NOE4	60	66	72
22	NOE4	60	66	72
23	NOE4	60	66	72
24	NOE4	60	66	72
25	NOE4	60	66	72

Uncertainty Analysis

One of the principal questions to be addressed in the risk and reliability analysis for the HPS concerns the level of uncertainty associated with estimated levels of flooding that may occur in New Orleans. The uncertainty in the risk and reliability analysis results manifests itself in the estimate of the 100-year area (and depth) of inundation. The assessment of uncertainty takes into account the uncertainties associated with the analysis of hurricane occurrences (how frequently they occur as well as their size), the estimated surge and wave elevations, and the performance of the HPS (its reliability). A complete description of the uncertainty analysis is presented in Appendix 11 of this volume.

Uncertainty Taxonomy

For the purpose of evaluating uncertainty it is useful to establish a taxonomy or framework within which different types of uncertainty can be identified and evaluated in the analysis. Two types of uncertainty are defined: aleatory and epistemic. The first is attributed to the inherent randomness of events, manifesting as variability over time for phenomena that take place at a single location (temporal variability), or variability over space for phenomena that take place at different locations but at a single time (spatial variability), or as variability over both time and space. These events are predicted in their frequency of occurrence (for example, per annum in the case of hurricanes, or per trial in the case of a levee reach that is impacted by a given surge event). Aleatory uncertainty is, in principle, irreducible because it is considered a property of nature.

Epistemic or knowledge-based uncertainty is attributed to our lack of knowledge or information (data) about events, or lack of understanding of physical processes that limits our ability to model the natural phenomena (hurricane surges) or events of interest (levee performance). For example, limitations in available data sets (length of record, data quality) impact the assessment of model parameters (shear strength of soils) or the likelihood of an event such as the annual rate of hurricane occurrences. When limited data are available, parameter estimates may be quite uncertain (i.e., statistical confidence intervals on parameter estimates can be large). A second type of knowledge uncertainty is attributed to a lack of understanding or knowledge about physical processes that must be modeled (e.g., the meteorological processes that generate hurricane events, hydrodynamic modeling of storm surges). In these instances model comparisons to measured events or expert evaluations are often required to assess the current state-of-knowledge and to quantitatively evaluate the level of uncertainty. In principle, epistemic uncertainties are reducible with the collection of additional data or the use of improved models.

Uncertainties impact the assessment of each element of the HPS risk and reliability analysis: the hurricane and surge analysis, reliability analysis of the HPS, the assessment of flooding and inundation, and the analysis of consequences. To assess or model uncertainties, a characterization of aleatory and epistemic uncertainties is made by partitioning models and estimates of model parameters. Modeling uncertainty represents differences between the actual physical process (hurricane, embankment failure) and prediction models. Modeling uncertainty can be estimated by comparing model predictions to actual, observed events/performance. Parameter uncertainty is the uncertainty in the estimates of model parameters. Parametric uncertainty is quantified by observing the variation in parameters inferred (either in a direct or indirect manner). This taxonomy is summarized in Table 20.

Table 20. Taxonomy of Uncertainties.

	Overall uncertainty	
	Epistemic	**Aleatory**
Modeling	Uncertainty about a model and the degree to which it can predict events (i.e., to what extent a model has a tendency to over- or under-predict observations).	Aleatory variability cannot be explained by a model. For instance, variability between model predictions and observations may be due to elements of a physical process that is not modeled and, therefore, represent an unexplainable variability (random differences).
Parametric	Parametric epistemic uncertainty is associated with the estimates of model parameters given available data, indirect measurements, etc.	This uncertainty is similar to aleatory modeling uncertainty. This is variability that may be due to systematic, but random variations associated with parameters of a model. For instance, there may be storm-to-storm variation in hurricanes with the same parameters, but which differ due to details of the storms that are not modeled, but have a systematic effect. This is an aleatory, inter-event, variability that may be considered independent from event to event.

The distinction between aleatory and epistemic uncertainty can be difficult to identify, and is model dependent. For example, a simple model of an event (levee performance) or a system may have higher model aleatory variability than a more complex model that models more details of a physical process. At the same time, the more complex model may have larger parametric epistemic uncertainty. Nonetheless, making a distinction between the sources of uncertainty in a logical manner helps insure that all uncertainties are quantified and identified.

Approach

The risk analysis of the HPS performance was evaluated using best estimate (mean) models and parameters. The analysis quantifies the aleatory component of uncertainty (see the Risk Analysis Methodology section) and is the basis for the inundation maps that are developed and presented in this volume. The 50-year inundation levels were primarily due to rainfall whereas the 100-year and 500-year inundation levels were primarily due to surge and wave effects. The uncertainty in the 50-year inundation levels due to rainfall was considerably less than that of the 100-year and 500-year inundation levels due to surge and wave effects. In this context, an analysis was performed to assess the epistemic uncertainties in the primary elements of the risk analysis and to propagate these uncertainties through the analysis to assess their impact on the estimate of the 100- and 500-year inundation area and depth. The focus is a set of normalized probability density functions that quantify the epistemic uncertainty in the 100-year and 500-year depth of inundation for each basin. This result is schematically illustrated in Figure 60.

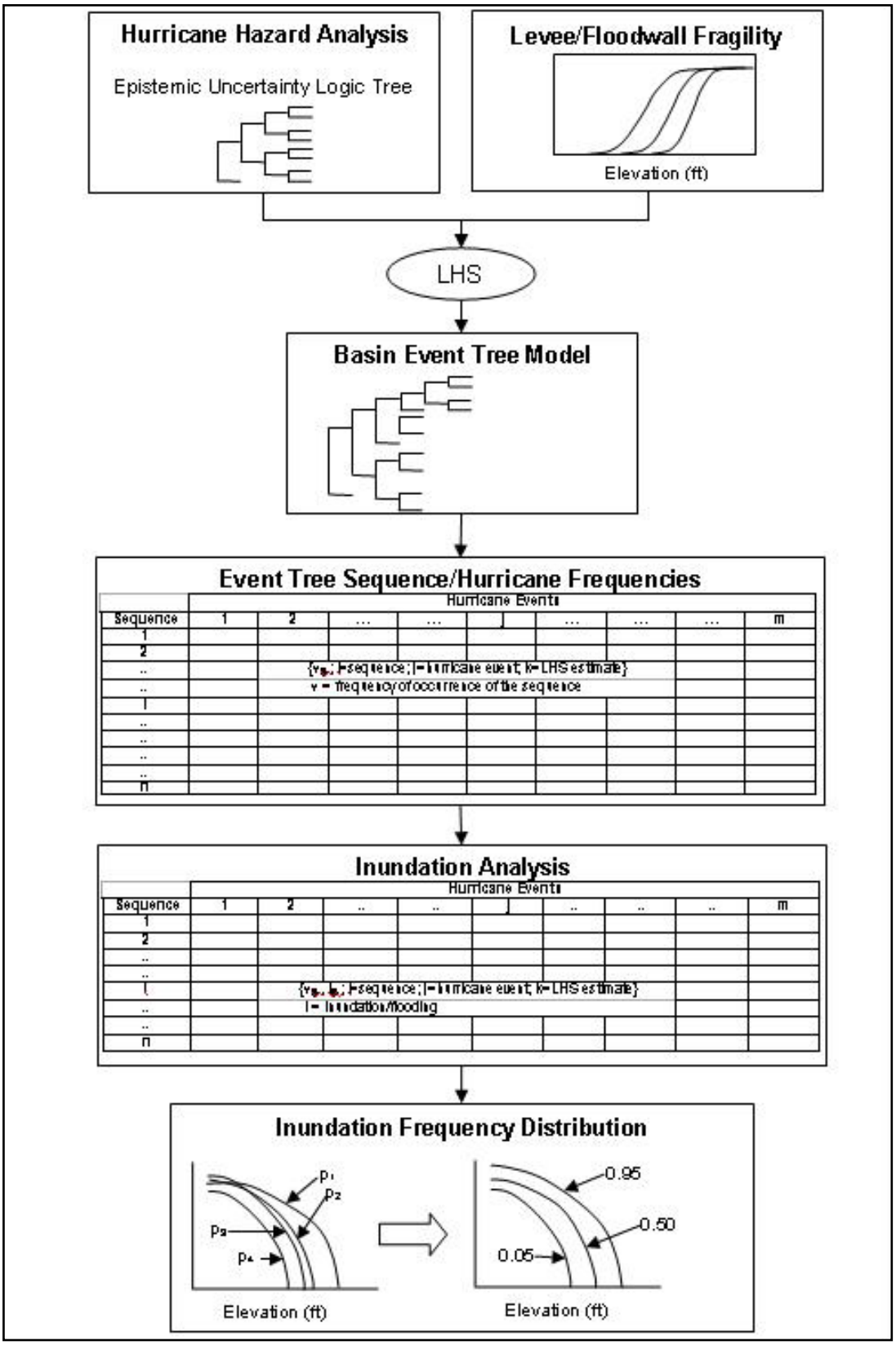

Figure 60. Steps in the uncertainty analysis for the New Orleans Hurricane Protection System.

The Risk Analysis Methodology section describes the main elements of the risk analysis and associated random variables. Only aleatory uncertainty is modeled in the main risk analysis. To evaluate epistemic uncertainty, model and parameter uncertainties in hurricane occurrence, wave and surge models, and levee and floodwall performance were explicitly considered.

Considering that the protected basins are well-defined areas, it was judged that epistemic uncertainty in volume–stage relationships is low, and thus uncertainty in the 100- and 500-year inundations is principally due to uncertainty in the hurricane, surge, and reliability analyses. Further, the contribution of rainfall to the 100- and 500-year inundations is comparatively small, and consequently its contribution to epistemic uncertainty is also. Other models or parameters whose epistemic uncertainties were not addressed in this analysis include the weir coefficient and the reliability of gate operations. The epistemic uncertainty in these parts of the analysis was judged to have limited contribution to the total uncertainty at the 100- and 500-year flooding levels.

Hurricane Analysis Uncertainty

The following sections summarize the uncertainty in each element of the analysis and the quantification process. Appendix 11 to this volume presents a complete description of the uncertainty analysis methodology and results. The hazard is specified as,

$$\{\lambda_i, h_i\} \tag{31}$$

where,

λ_i = frequency of occurrence of hurricane event i
h_i = hurricane event i

A hurricane, h_i, is modeled by the following six parameters:

ΔP = central pressure deficit at landfall (mb)
R_p = radius to maximum winds at landfall (km)
X = longitudinal landfall location relative to downtown New Orleans (km)
θ = direction of storm motion at landfall (degrees)
v_f = storm translation speed at landfall (m/s)
B = Holland's radial pressure profile parameter at landfall (Holland 1980)

A hurricane event, H_i, can be generally written in terms of the parameters that define it as

$$h_i = h_i(\Delta P_j, R_{p,k}, \theta_l, v_{f,m}, B) \tag{32}$$

Similarly, the frequency of a hurricane can be expressed in terms of the frequency of occurrence of the parameters that define it as

$$\nu_i = \nu_i(\Delta P, R_P, v_f, \theta_l, x) \tag{33}$$

The hurricane joint probability model (as described in the Hazard Analysis section) estimates the frequency of occurrence of hurricanes with a combination of properties. This is denoted

$$\nu_i(\Delta P, R_P, v_f, \theta_l, x) = \Lambda_1\Lambda_2\Lambda_3\Lambda_4\Lambda_5 \tag{34}$$

where,

Λ_1 = probability of hurricane central pressure deficit, ΔP
Λ_2 = probability of storm radius, R_p
Λ_3 = probability of forward velocity, v_f
Λ_4 = probability on azimuthally approach/ track direction at landfall, θ
Λ_5 = frequency of storms per year per location along the coast, λ

In the IPET hurricane analysis, the Holland B parameter was set to a fixed value (Appendix 8) and thus not considered a random variable in modeling the occurrence of hurricane events.

Equation 34 defines the frequency of occurrence of the hurricane event. In addition to the variable used to model the hurricane, other factors contribute to the randomness of water-surface elevations that are realized. These factors include Holland's B and astronomic tide, among others.

The water-surface elevations that occur can be expressed by

$$s(\underline{x}) = S(h_i, \underline{x}) + \varepsilon \tag{35}$$

where,

$S(h_i, \underline{x})$ = surge and waves estimate at locations, $\underline{x}$, for hurricane i
ε = random term with zero mean and variance, σ^2 (this is an aleatory variability term)

The random term captures the variability due to Holland's B, astronomical tides, and other factors associated with the hurricane event or the hydrodynamic model (grids, bathymetry, hydraulic parameters, etc., that are not explicitly modeled and thus contribute to random deviations between model estimates and observations. As part of the HPS risk analysis methodology, the aleatory variability in water-surface elevations is taken into account in the best estimate of New Orleans flooding.

Table 21 describes sources of aleatory and epistemic uncertainty in the hurricane hazards analysis in terms of the model and parametric parts of the analysis. Appendix 8 describes the estimates of the difference sources of uncertainty in the hurricane analysis.

To model the epistemic uncertainty in the hurricane hazard analysis, a logic tree was constructed. The logic tree illustrates the models/parameters that are considered in the uncertainty analysis. In this analysis, exclusive branches on the logic tree are not a priori defined. The uncertainty values of parameters are selected in a Latin Hypercube Simulation (LHS) and

combined using the structure in the logic tree. The logic tree in Figure 61 illustrates the elements of the epistemic uncertainty in the hurricane analysis.

Table 21. Summary of Hurricane Analysis Aleatory and Epistemic Uncertainties.

Element	Epistemic	Aleatory
Model	Surge/Wave Modeling – 1) Uncertainty in the estimate of peak water elevations in New Orleans due to hurricane events. This uncertainty corresponds to the systematic error that may exist in predicted, mean peak surge/wave elevations at New Orleans HPS levee/floodwall reach locations.	Surge/Wave Modeling – Unexplained variability between model predictions and the estimate of peak surge/wave elevations observed for Hurricanes Katrina and Rita. Frequency Model – Randomness of hurricane occurrences and hurricane events with specific properties (i.e., Cp, Rp, etc.)
Parametric	Frequency Model – 1) Uncertain estimates in the mean rate of hurricane occurrences; 2) Uncertainty in the estimate of the parameters of models used in the joint probability analysis (e.g., GEV model parameters, Rp-Cp relationship).	Surge/Wave Modeling – Factors considered in this category include the effects of astronomical tides and Holland's B. Frequency Model – No aleatory parametric sources of variability were identified.

Hurricane Surge/Wave Model Uncertainty

Causes of epistemic uncertainty in wave and surge levels are primarily sourced in hurricane model errors; for example, the wind field idealization, the coefficient of friction with the water surface, the effects of waves on water level, etc., are estimated by hindcasting historical events or by comparing results from different modeling assumptions. For New Orleans, efforts were made to calibrate the ADCIRC and wave modeling to the observations from Hurricanes Katrina and Rita. Based on these hindcast assessments, an estimate of the storm surge modeling epistemic uncertainty can be made.

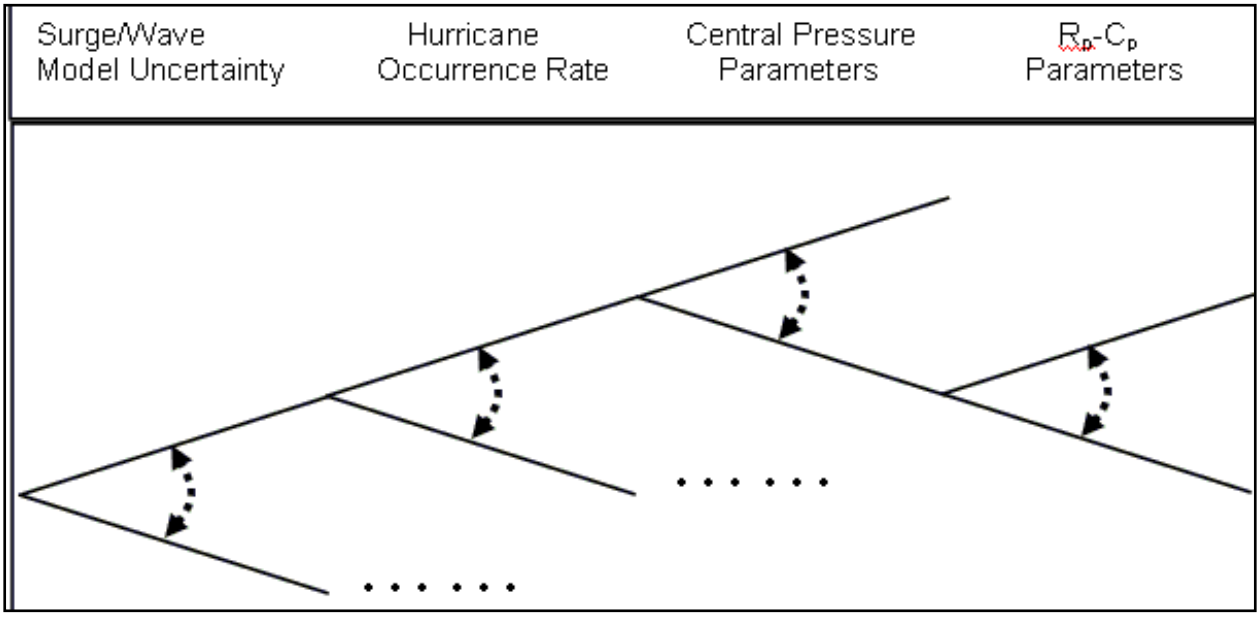

Figure 61. Hurricane analysis epistemic uncertainty logic tree.

Hurricane frequency rates are uncertain due to the limited historical sample size and possible errors in the assumed form of marginal and conditional distributions (especially in the tail regions).

For storms sizes considered in the IPET hurricane analysis, relatively few data are available to estimate the parameters of the Gumbel Extreme Value (GEV) distribution used in the modeling. As part of the uncertainty analysis, the uncertainty due to the limited numbers of data for the estimate of the GEV model parameters was considered.

There is considerable uncertainty in the estimate of the radius to maximum winds. As discussed in Appendix 8, a correlation between radius to maximum winds and the central pressure deficit was used in the hurricane modeling and analysis. There is, however, considerable scatter in the radius to maximum winds model and uncertainty in the best estimate relationship. As part of the uncertainty analysis, the uncertainty in the estimate of the parameters of R_p-C_p relationship and scatters was evaluated. Appendix 8 describes the estimate of the hurricane analysis uncertainties for each element of the logic tree.

Reliability Analysis Uncertainty

Fragility curves for individual levee and floodwall reaches were developed in two parts: first, for low water levels on a section up to the top of the levee or wall, and second, for water at the top of levee or wall to 6 ft above the top. The fragility calculation involved the following:

- The first part was based on a limiting-equilibrium stability analysis using the method of planes of the New Orleans District (MVN), and

- The second part was based on observations of levee and floodwall performance during Hurricane Katrina that were used to relate the fraction of overtopped levee or wall sections that breached due to overtopping erosion.

The approach to evaluate the reliability of levees and floodwalls and the epistemic uncertainty in these two parts of the fragility is presented in the Reliability Analysis section and in detail in Appendix 10. A summary of the approach and typical results is presented here.

The epistemic uncertainty in the fragility analysis for the water levels up to the top of levee or top of wall evaluated the uncertainties in the estimated mean of the factor of safety (FS) and in the variance of FS. Factors considered in the analysis included the following:

- Bias in the method of planes calculation of FS compared to more accurate methods. The mean bias was taken to be about +20% based on comparative calculations by Team 7.

- Statistical estimate of the error in the mean soil property due to the limited number of measurements.

- Conservative bias associated with using the undrained strength at the 1/3-point of the test results (i.e., the practice of defining a “best estimate” as 1/3 of the data below it).

- Epistemic (bias) uncertainties in the variance of the FS occur as a random measurement noise in the soil properties that should be removed before calculating the variance above. Soil property data, especially as measured in traditional USACE practice by the unconsolidated undrained (UU) test, is notoriously noisy. The fraction of the total variance attributable to measurement noise is estimated using statistical filtering techniques based on the autocorrelation function.

Another source of uncertainty is the length effect. The characteristic length of a failure section was taken to be 1,000 ft. Each characteristic length was assumed to behave independently of its adjacent lengths, and the probability of at least one failure in a reach of *n* lengths was approximated as *P=[1-(1-p)^n],* in which *p* is the probability of failure of the characteristic length. The characteristic length was estimated from the autocorrelation structure of the soil properties and from observations of failure lengths during Katrina. It is thought that the length could range from 500 to 2,000 ft, although there is much uncertainty about these numbers in the way they influence probability of system failure.

For failures that occur as a result of overtopping and levee erosion, the fragility is based on the observation experience during Hurricane Katrina. The epistemic uncertainty in these estimates is attributed to the limited number of observations available to estimate the fraction of levee or floodwall failures that occur as a function of water level.

Table 22 describes sources of aleatory and epistemic uncertainty in the reliability analysis in terms of the model and parametric parts of the analysis. Appendix 8 describes the estimates of the difference sources of uncertainty in the hurricane analysis.

Table 22. Summary of Reliability Analysis Uncertainties.

Element	Epistemic	Aleatory
Model	Levee Instability – Model uncertainty associated with the method of planes. Levee Overtopping – No model uncertainties were identified.	Levee Instability – Spatial variability of soil properties within a levee reach. Levee Overtopping – Variability in the performance of levee and floodwalls that were overtopped during Hurricane Katrina.
Parametric	Levee Instability – 1) Uncertainty in the estimate of mean soil properties due to limited data; 2) Uncertainty in the selection of soil properties used in the slope stability analysis. Levee Overtopping – Uncertainty in the estimate of the fraction of levee failures that occur due to depths of overtopping.	No sources of parametric aleatory variability were identified and modeled.

The epistemic uncertainty in the levee and floodwall fragility is quantified as a coefficient of variation in the estimate of the mean and variance of the FS or standard deviation in the probability of failure (see the Reliability Analysis section and Appendix 10) for a given water level in the case of overtopping.

For purposes of the uncertainty quantification, the epistemic uncertainty in the levee and floodwall fragility for each reach in the HPS model is discretized. In the analysis, a three-point distribution is used. These points correspond to the 0.05, 0.50, and 0.95 levels of the uncertainty distribution. Probability mass values of 0.185, 0.63, and 0.185 are assigned to each curve. These discrete values and associated weights are an appropriate representation of the complete

distribution that preserves the mean and variance of the complete distribution (Pearson and Tukey 1965). Figure 63 shows an example of the epistemic uncertainty in levee fragility.

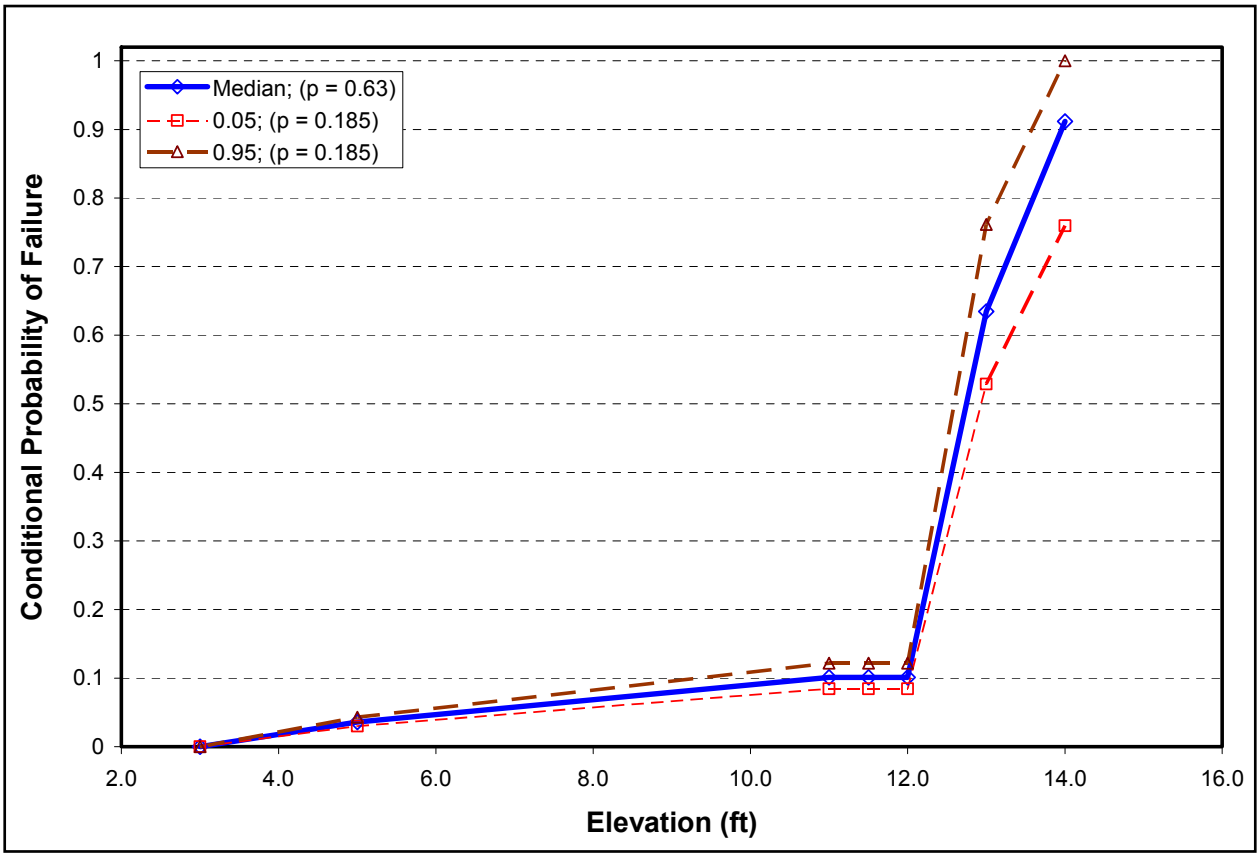

Figure 62. Illustration of the uncertainty in levee fragility – St. Charles, Reach 1.

Uncertainty Quantification

The epistemic uncertainty in the hurricane hazard and levee/floodwall fragility parts of the risk analysis are combined to estimate the uncertainty in the analysis products such as the frequency of levee failure in a basin and the frequency of inundation of New Orleans basins and parishes.

As part of the uncertainty analysis, an event tree model was developed for each basin in the HPS. The event tree was set up to capture the sequences of events that could lead to sub-basin and basin flooding due to levee failure (as a result of levee and floodwall instability or overtopping) and levee and floodwall overtopping. The set of sequences in an event tree considers the combinations of levee reach performance failures and non-failures associated with instability or overtopping, and flooding due to levee overtopping. Each sequence in the event tree corresponds to a combination of levee failures and non-failures and overtopping events. For a hurricane event, the conditional probability of a sequence occurring (given the event and the surge and wave elevations produced at each levee reach location) is determined from the levee and floodwall fragility curves. The sequences in the event tree define an exhaustive set of the possible combinations of levee and floodwall reach performance states.

In the quantification, the uncertainty in the hurricane hazard and the levee fragility for a basin was sampled by LHS. Each LHS sample from the hurricane hazard and levee fragility was combined to estimate the frequency of occurrence of each sequence in the event tree. This process was repeated until all combinations of the LHS fragility and the hurricane hazard were exhausted. The result for each sequence in the system event tree is a discrete probability distribution on the frequency of occurrence for each hurricane event and for all events combined in a basin.

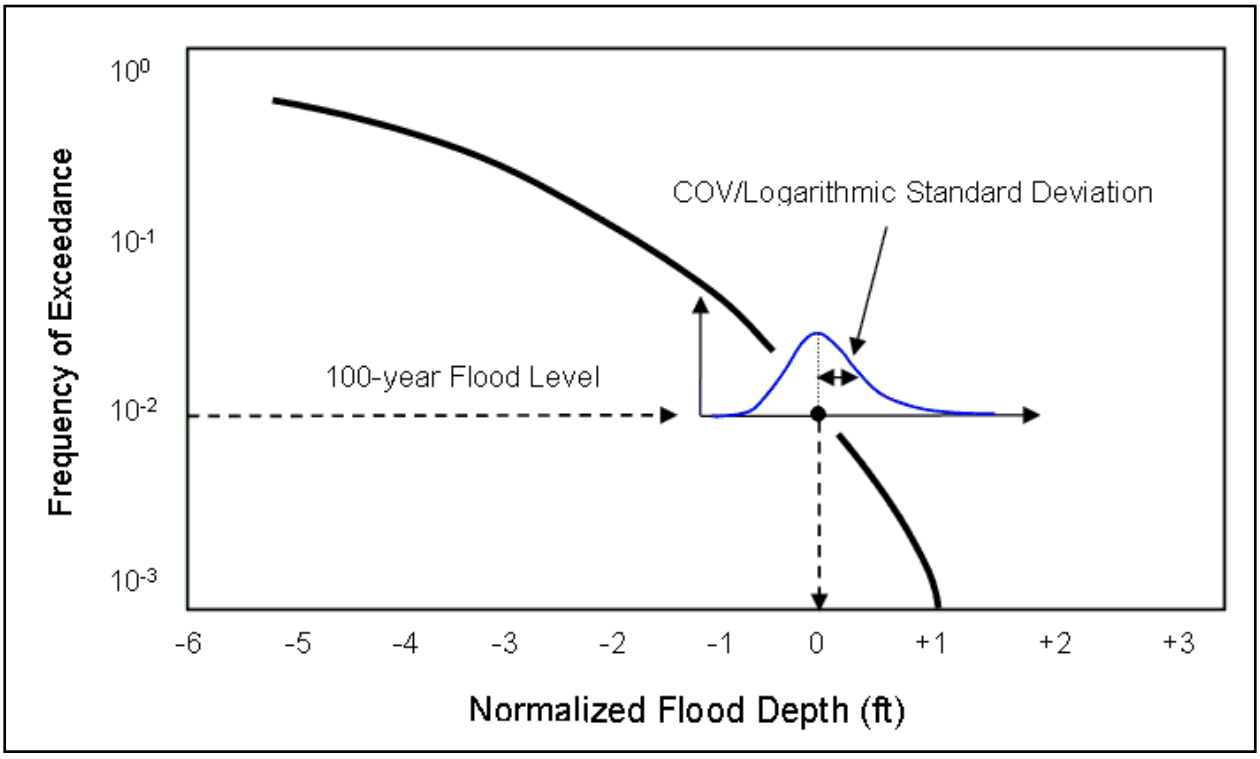

Figure 63. Schematic illustration of the epistemic uncertainty in the 100-year depth of flooding.

For each event tree sequence and hurricane event pair, the volume and flood elevation in a basin or sub-basin was determined. The estimates of flood inundation are combined with the sequence frequency of occurrence for each hurricane event. The basin inundation frequency estimates are combined over all sequences and all hurricanes to determine the frequency distribution of basin flooding. Propagating the uncertainty in the hurricane hazard and the levee fragility produces a probability distribution on the frequency of flooding as illustrated in Figure 63 and Figure 64.

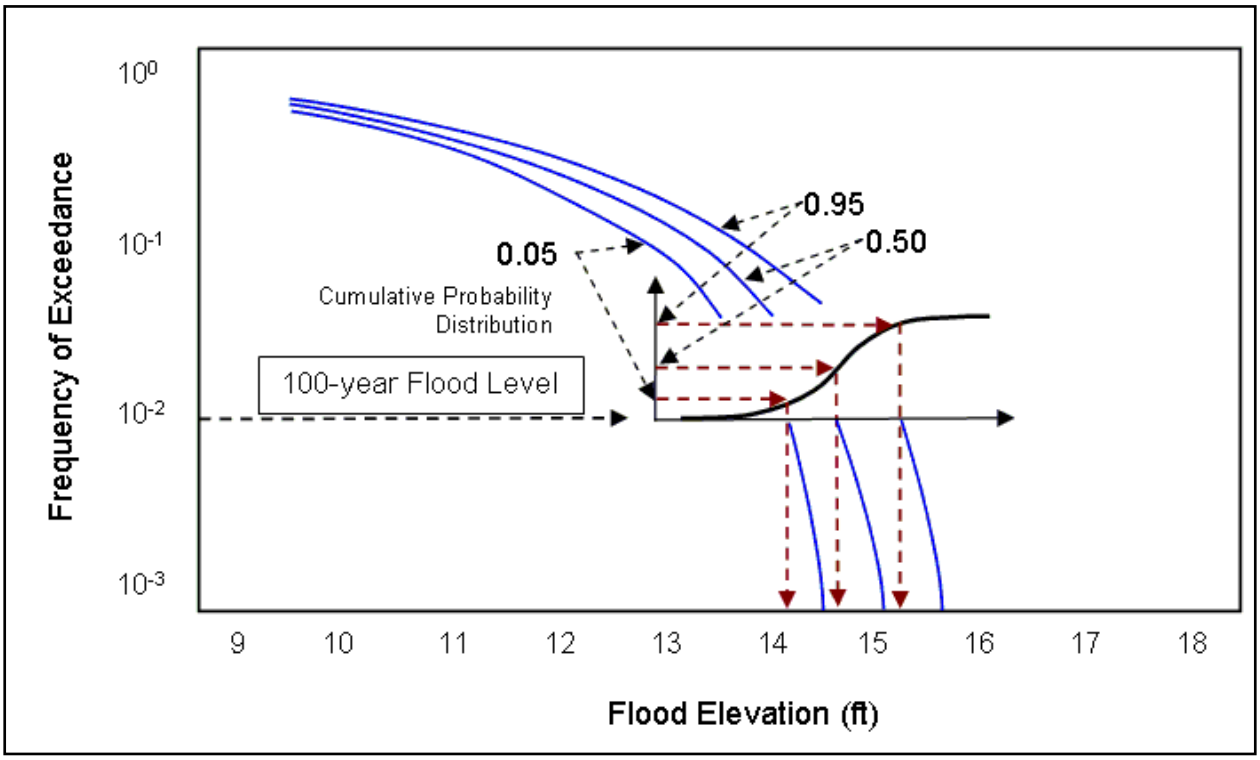

Figure 64. Illustration of the uncertainty in basin flooding.

Conclusion of the Uncertainty Analysis

The epistemic uncertainty in the hurricane hazard and levee and floodwall fragility parts of the risk analysis were combined to estimate the uncertainty in the frequency and level of flooding in New Orleans. Together, these parts of the analysis can contribute an order of magnitude or more variation between the 0.05 fractile and the 0.95 fractile of the annual non-exceedance curves of inundation volumes in individual basins. Put another way, as a first approximation, the 0.05 or "lower bound" on epistemic uncertainty may be a factor of 3 lower than the best estimate, while the 0.95 or "upper bound" is typically about three times the best estimate. Thus, the spread between the 0.05 and the 0.95 fractile estimates of the frequency of flooding is about an order of magnitude or more. Thus, given the epistemic uncertainties, the best estimate of the 100-yr flooding may have a range in its occurrence rate that varies from being an estimated 30-yr to 300-yr event. Looking at the epistemic uncertainty in the 100-year flood elevations, analyses indicate the one-standard deviation on the estimated flood elevations varies from 0.5 ft to as much as 2.0 ft about the best estimate, depending on the basin.

This spread of epistemic uncertainty in inundation volumes would appear large, but it is consistent with other recent studies of epistemic uncertainty in technological risk analyses involving seismic risk (Jack R. Benjamin & Associates, Inc. 2005), nuclear safety (Knudsen and Smith 2000), transportation systems (Kurowicka and Cooke 2006; Bedford and Cooke 2001), environmental impacts (Linkov and Ramadan 2005), and other technological systems (Paté-Cornell 2002).

Risk Analysis Results

The following is a summary of the major findings of the risk analysis. These findings summarize the more detailed findings presented in Appendix 13 and represent a big picture perspective. To facilitate understanding of the risk results, color coded categories have been established to portray the results. Five categories of flooding depth, ranging from 0-8 ft, were established as shown in Table 23. The depths shown are relative to the ground level topography of the sub-basin and are not related to structure floor elevations. The depths are based on the elevations determined from the stage–storage curve for the basin using the expected volume of water entering the basin. The volume is distributed within the basin by gravity and does not consider the interior drainage characteristics of the basin. The flood depth maps provide an overall perspective of the flooding vulnerability of the entire area of Greater New Orleans for which the risk assessment was performed. Results are shown for three different flood frequencies (0.02, 0.01, and 0.002), and for the two HPS and the three pumping scenarios modeled. Detailed maps for each of the individual major basins are also provided in Appendix 13. Mapping of property losses is based on the percentage of total value lost. This measure was chosen to show the relative impact of the loss of property in an area of varied demographics. Six categories of property losses were established ranging from less than 10% to more than 90% of total value. Four categories of loss of life were established to portray relative risk within the sub-basins ranging from less than 10 to more than 1,000. Total economic and life loss estimates can be found in tables for each sub-basin in Appendix 13.

Table 23. Categories of flood depth, property loss, and fatalities for consequence analysis

Flooding Depth Categories	Property Loss Categories (percentage of Total Value Lost)	Fatalities Categories
> 8 ft	Less than 10%	Less Than 10
6 - 8 ft	10%-30%	10 to 100
4 - 6 ft	30&-50%	100 to 1000
2 - 4 ft	50%-70%	More than 1000
0-2ft	70%-90%	
	Greater than 90%	

The results are provided in three major forms. First the vulnerability to flooding is presented as inundation frequency depth estimates displayed as maps (Figures 65 thru 82). The inundation depth maps show the mean depth of flooding that could occur or be exceeded at three specific exceedance frequencies (2%, 1%, and 0.2%) or return periods (50-, 100-, and 500-year). The flood depth information is provided at the highest level of resolution available with respect to the local topography. Risk is provided in terms of both mean values of expected loss of life and property losses at the specific exceedance frequencies (2%, 1%, and 0.2%) or return periods (50-, 100-, and 500-year). The loss of life and property loss risk maps (Figures 83 through 117) show relative risk levels at the sub-basin level. In addition to being available within the IPET report and IPET web site, the risk maps have been made available in a limited interactive mode through

Google Earth and in a more complete interactive mode through Microsoft Virtual Earth. The initial versions of the inundation depth maps (East Bank only) were first provided to the public in June 2007. Maps including the West Bank areas were published in July 2007 and maps showing the impact of pumping were published in March 2008.

50-Year Flood Event

Flood Risk

New Orleans is widely vulnerable to some flooding at the 50-year or 2% frequency of occurrence level if significant pumping capacity is not available.

There is no significant difference in the flood elevations between the pre-Katrina and 2007 HPS at the 50-Year (2%) frequency of occurrence. This is likely due to the dominance of rainfall as the source of water at this level of event. At this return period, the dominant threat to New Orleans is tropical rainfall and not hurricanes.

The impact of pumping is directly related to the total volume of water that must be managed; therefore, pumping is most effective when flooding is not extensive or deep.

Pumping operating at a capacity that is equivalent to or greater than 50% of the ideal or nameplate capacity of the sub-basins modeled can have a dramatic impact in reducing the flood elevations at the 50-Year or 2% frequency of occurrence in a number of the basins modeled. There is a small benefit in NOE and a significant benefit in OM, portions of JE, JW, and PL.

Life Loss Risk

Pre-Katrina potential for loss of life risk was extreme in OM2 sub-basin and very high in portions of JE, JW, PL, and OW.

The 2007 HPS (without pumping) reduced loss of life risk in the majority of OM and JE and portions of QW, JW, NOE, and PL north. Loss of life risk remains high in OM2 due primarily to the IHNC vulnerability.

Pumping at an operational capacity equal to or greater than the 50% ideal capacity modeled reduces loss of life risk to the lowest category at the 50-year (2%) flood frequency. This demonstrates the importance of maintaining and improving the reliability of the pumping system.

Property Loss Risk

Property loss is relatively low for the 50-year (2%) flood frequency, being below 10% of total value in most areas and from 10 to 20% in areas of Orleans Main near the canals and Orleans West.

Property loss maps for pre-Katrina and 2007 HPS are essentially the same at this return period.

Pumping at operational capacities equal to or greater than the 50% ideal value modeled would reduce the entire region to the lowest category with the exception of OW which remains the same.

100-Year Flood Event

Flood Risk

Without pumping, the majority of the New Orleans area remains vulnerable to moderate to deep flooding (greater than 4 ft) at the 100-year or 1% frequency of occurrence. The area with least vulnerability is Jefferson Parish East and St. Charles Parish where flood threats are moderate.

The improvements in the HPS from pre-Katrina to the 2007 HPS have provided significantly reduced flood levels in a few areas, notably portions of Orleans Main (OM2 and OM4) and moderate reductions in the 1% flood level in St. Bernard (SB) and Plaquemines (PL11).

Improvements in Orleans Main are largely due to the presence of the new gates and temporary pumps at the ends of the outfall canals. Continued vulnerability of the areas of OM and NOE adjacent to the IHNC can be attributed to the significant fragility of the I-walls along the IHNC and the top of wall elevations which are unchanged from pre-Katrina elevations. Strengthening of the I-walls with stability berms and relief wells has improved the performance of the structures in the IHNC, but they remain unable to cope with surge conditions created by large storms.

Pumping capacity equal to or greater than the 50% ideal capacity modeled can have a significant impact on the 100-year or 1% flood elevations. Primary areas that benefit the most are OM and JE. The sub-basins adjacent to the IHNC remain vulnerable to flooding even when pumping is considered.

The West Bank area remains highly vulnerable to flooding in 2007, and pumping will likely have little impact on this conclusion until all of the area is protected by portions of the HPS yet to be completed.

Life Loss Risk

At the 100-year flood frequency, pre-Katrina potential for loss of life risk was extreme for OM2 and very high for SB and portions of OW and JW.

The 2007 HPS, without pumping, reduces loss of life risk for OM2 but has little impact elsewhere.

Pumping at an operational capacity equal or greater than the 50% ideal capacity modeled would reduce loss of life risk in portions of OW, JE, and PL north but has little impact elsewhere.

Property Loss Risk

Prior to Katrina, with the exception of a portion of Jefferson East, Jefferson West and northern Plaquemines, property loss was very high across New Orleans at the 100-year or 1% flood frequency. In most cases, property would experience damages greater than half of its total value in this type of flood event.

The 2007 HPS provides a risk reduction in 3 of the 5 sub-basins of Orleans Main, those nearest the IHNC remaining at higher risk levels. There is also some reduction in St. Bernard but none on the West Bank or in New Orleans East.

Without pumping, in 2007, moderate to high risk exists in most of New Orleans East, St. Bernard and the West Bank.

Pumping at an operational capacity equal to or greater than the ideal 50% capacity modeled would provide significant property loss reduction in all of Jefferson East and Orleans Main, and in portions of New Orleans East. Property loss remains high elsewhere with the exception of the northern part of Plaquemines.

500-Year Flood Event

Flood Risk

Virtually the entire New Orleans region remains highly vulnerable to deep and catastrophic flooding at the 500-year or 0.2% flood frequency. The vast majority of the region would experience catastrophic flooding depths. As shown by the Katrina experience, the depth of flooding and area affected for an event of this magnitude would be dependent upon the actual path of the storm.

Note that the property loss and fatality estimates cannot be compared to losses actually inflicted by any particular storm such as Katrina. This is due to the fact that the risk analysis is a probabilistic estimate of potential flooding elevations and losses in each subbasin in the entire region for the suite of storms studied. For example: The 1% chance property value loss maps are based on the 1% flooding elevation occurring everywhere in the subbasin and the entire HPS. A single event with a 1% return period, and particular characteristics such as storm track, may produce elevations within other subbasins that have higher or lower return periods. This happened during Katrina where portions of the HPS experienced conditions that have a low return period (0.003 to 0.002 per year) while other portions experienced conditions with a much higher return period (0.02).

There is essentially no difference in the flooding vulnerability at this frequency of occurrence between the pre-Katrina and 2007 HPS.

Pumping has no impact at this level of flooding for either the pre-Katrina or the 2007 HPS because of the large volume of water entering the system from overtopping and breaching of fragility of portions of the HPS.

Life Loss Risk

The 500-year (0.2%) flood frequency presents an extremely high potential for high loss of life risk for all of OM, most of JE and a large portion of NOE, SB, OW, and JW for both pre-Katrina HPS and the 2007 HPS.

Areas with lower loss of life risk are primarily areas with lower populations exposed to flooding such as portions of NOE, SB, and SC.

Pumping makes no difference in loss of life risk at the 500-year flood frequency for either HPS.

Property Loss Risk

The property loss for the 500-year (0.2%) flood frequency is extremely high in all areas.

There is essentially no change in property loss at this level between the pre-Katrina HPS and 2007 HPS.

Pumping capacity has little impact on the property loss at this level of flooding.

Summary of Results

Based on the above summary of the results, following are brief answers to the specific questions concerning the performance of the HPS:

What was the reliability of the pre-Katrina HPS for preventing flooding of protected areas given the range of hurricanes expected to impact New Orleans?

While the Katrina experience provided the real answer to this question, the results of the risk analysis confirm that the reliability of structures in portions of the pre-Katrina HPS was very low. The drainage canal walls are the most vivid example of very low reliability, while the levees proved to be of high reliability. The reliability of the entire HPS in preventing flooding was also low, as demonstrated by the high rate of overtopping of the perimeter walls and levees by the storms studied. The return periods of the range of expected storms that were studied by the Risk Team were between 300 and 5,000 years. These storms produced almost 3,200 incidents of overtopping at the reaches that form the hurricane barriers. This represents 16% of the 20,520 possible incidents. Some of this is attributed to unfinished portions of the HPS on the West Bank and is also due the tops of levees and walls at lower than their authorized level due to subsidence or use of incorrect datums.

What is the reliability of the current post-Katrina HPS for preventing flooding of protected areas given the range of hurricanes expected to impact New Orleans? Specifically, what is the annual rate of occurrence of system failure due to the range of expected hurricane events?

The reliability of the post-Katrina (June 2007) HPS has been significantly increased in many portions of the system that did not perform well during Katrina and ongoing improvements are steadily making the system more reliable. Reasons for this are as follows: the gates at the ends of the drainage canals reduce the chance of I-wall failure along the canals; adding overtopping protection at many transitions throughout the system makes them less likely to erode and fail; replacing less reliable I-walls with more reliable T-walls or L-walls reduces probability of failure in those areas; adding erosion protection to levees reduces their susceptibility to damage from waves overtopping them; and the raising of some levees reduces the chance of overtopping erosion. There are, however, areas of the HPS where the project is unfinished, such as on the West Bank, and areas where the structures still have low reliability, such as along the IHNC and GIWW in New Orleans East and St. Bernard. These areas act as weak points in the HPS perimeter chain that lowers the overall reliability of the system. Because these weak points provide possible HPS failure points, the reliability of the June 2007 HPS was found to remain low.

Annual rates of system failure are best judged by examining the elevation–exceedance results. Failure of the HPS is defined as the amount of interior flooding of the basins due to combinations of overtopping, breaching, or open gates. For annual rates up to 0.02 per year (1/50), the system flooding appears to be primarily due to rainfall and, therefore, failure of HPS components would not be expected. At lower rates of occurrence, such as 0.01 per year (1/100), HPS components would experience failures and/or overtopping that would lead to significant

flooding. For extremely low rates, such the 0.002 per year (1/500), complete failure of the HPS would be expected, leading to deep inundation at all locations in the system.

What are the annual rates of occurrence of economic consequences and loss of life resulting from failures of the HPS given the range of hurricanes expected to impact New Orleans?

Annual rates of occurrence of economic consequences and loss of life system failure are directly related to the elevation–exceedance results discussed above. For annual rates of 0.02 per year (1/50), $1.2 billion of economic damages could be expected and about 400 potential fatalities could occur. The loss of life estimates are not based on a specific value for evacuation effectiveness; however, the consequences used in the analysis considered a mean value for evacuation effectiveness. This basis results in fatalities which are considered to be much higher than would actually occur, based on the high evacuation effectiveness experienced during Katrina. At a lower annual rate of occurrence of 0.01 per year (1/100), $31 billion of economic damages could be expected and as many as 3,700 potential fatalities could occur. For extremely low rates, such the 0.002 per year (1/500), complete failure of the HPS could lead to $72 billion of economic damages and as many as 42,000 potential fatalities with a less than a very effective evacuation.

Conclusions

The experience of Katrina proved that the risk to life and property in the New Orleans area before Katrina was high. The results of the risk analysis quantifies the extent of that risk to the pre-Katrina economy and population. The actual direct damages incurred due to the hurricane exceeded $28 billion and the loss of life was more than 1,200. These values correspond to potential damages and life loss values obtained by the risk analysis for less than a 100-year event if no pumping is available. While this conflicts somewhat with the estimated 300- to 400-year frequency of Katrina, it points to the severity of the risk in New Orleans and attests to the effectiveness of the evacuation prior to the hurricane in reducing the loss of life.

Examination of the three pumping scenarios shows the importance of the pumping system in reducing damages during the more frequent events, but also shows that the system was not capable of handling large inflow water volumes from overtopping or breaching during extreme events.

While the HPS has been repaired and improved dramatically over the pre-Katrina HPS, the risk associated with the June 2007 HPS to the area is still considered to be high for extreme events if the pre-Katrina potential consequences are used in the analysis. There are still areas of vulnerability along the IHNC and GIWW that amount to weak points in the system and limit the risk reduction in parts of Orleans Metro, New Orleans East, and St. Bernard. In addition, the unfinished West Bank HPS makes that area as vulnerable in the June 2007 analysis as it was before Katrina.

The risks to life and property would be expected to be reduced if existing demographics and redevelopment values were used; however, the reduction would be due entirely to the reduced consequences of system failure and not due to the improvements to the system. In any case, the human and property losses to New Orleans are still considered to be high during extreme events similar to Katrina, and the most effective risk reduction measure remains to be implementation of an effective evacuation plan.

The analysis presented herein in Volume VIII was a prototype risk analysis that indicates the value of and need to consider risk in the planning of hurricane protection projects. The study also shows that all of the reliability of all of the components of a hurricane protection project play a role in the performance of the overall project and, therefore, the project must be looked at as a system if the risks are to be fully evaluated. The large uncertainty in this study, and in any analysis of a project of the magnitude of the New Orleans HPS, shows that the system must be continually monitored, maintained, and periodically reevaluated in order to identify potential weaknesses and gain understanding of the factors that affect uncertainty in the performance of

the HPS. Part of the uncertainty associated with this study is due to the prototypical nature of the computational processes used and to the lack of a more sophisticated analysis tool. This uncertainty and the accuracy of future analyses can be improved by research and development of better tools.

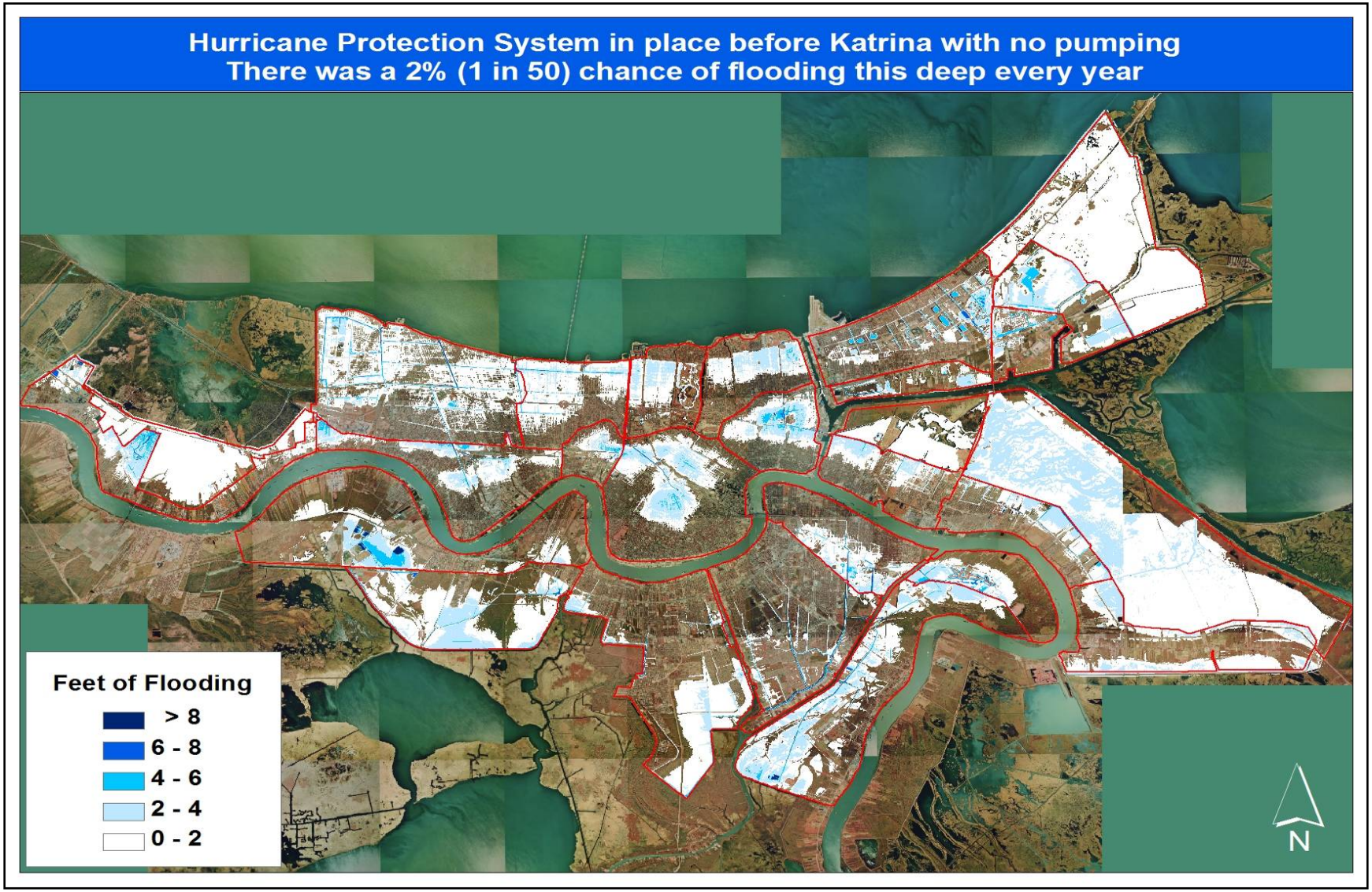

Figure 65. Pre-Katrina depth map (2% chance, no pumping).

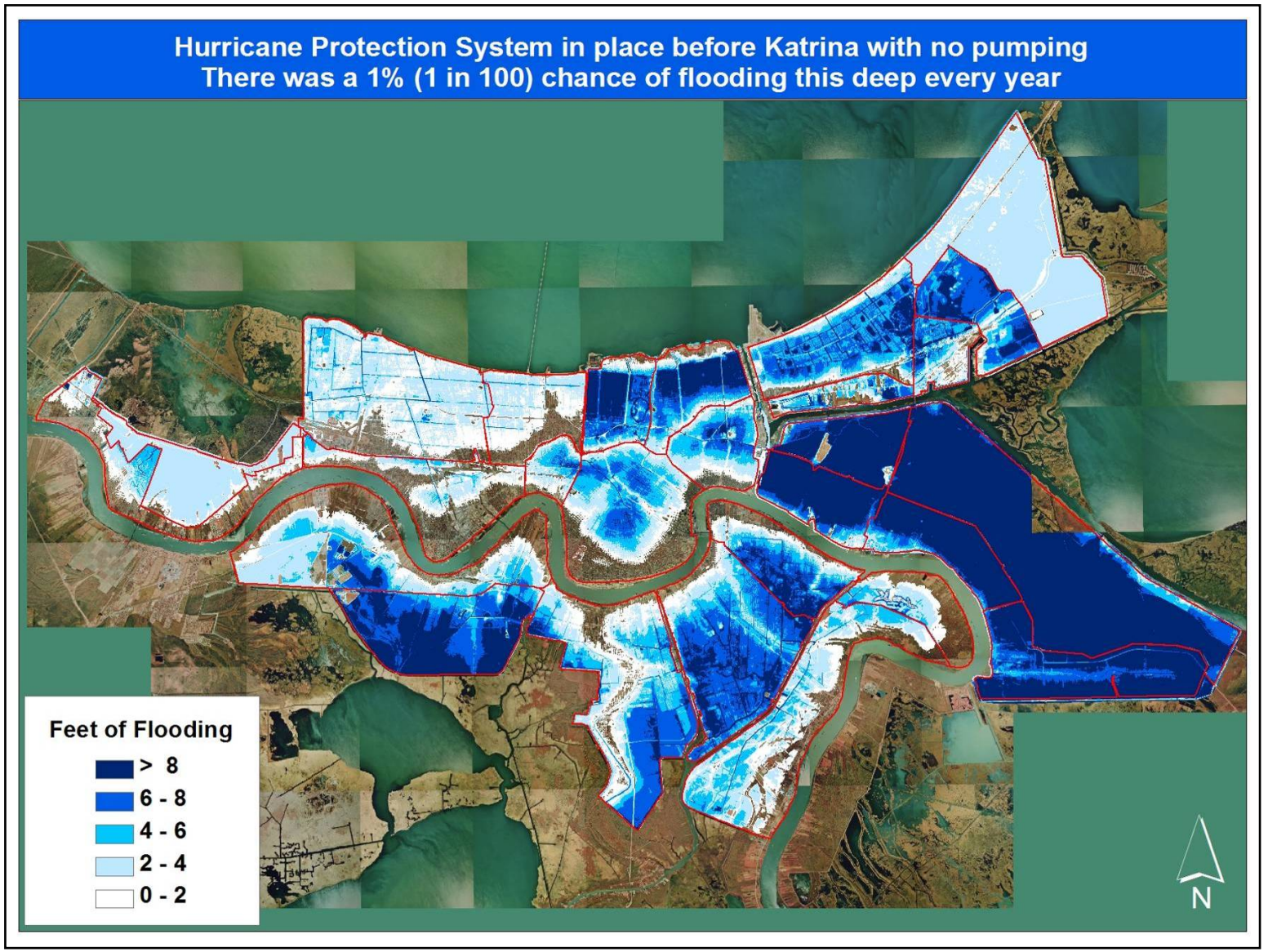

Figure 66. Pre-Katrina depth map (1% chance, no pumping).

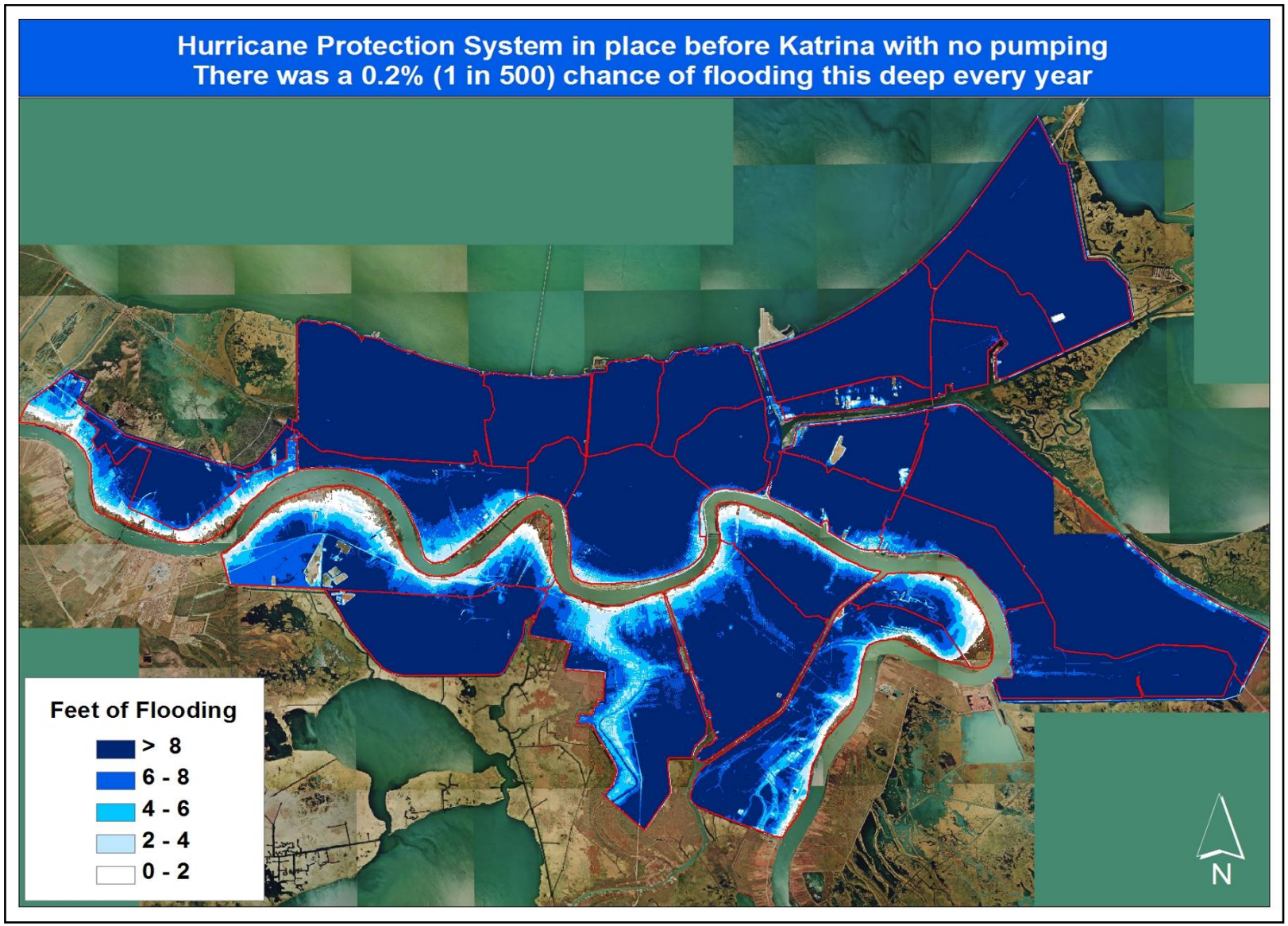

Figure 67. Pre-Katrina depth map (0.2% chance, no pumping).

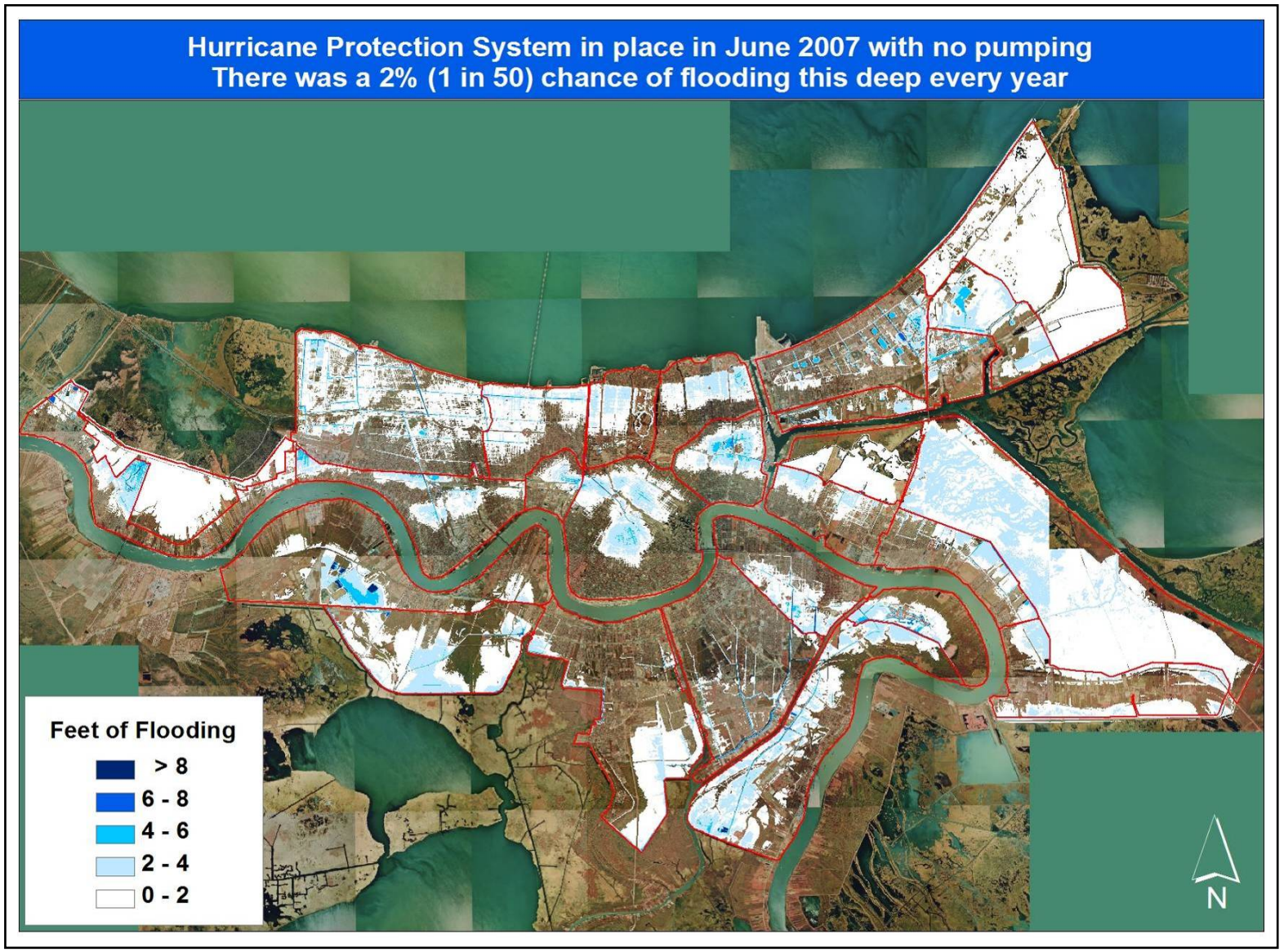

Figure 68. June 2007 depth map (2% chance, no pumping).

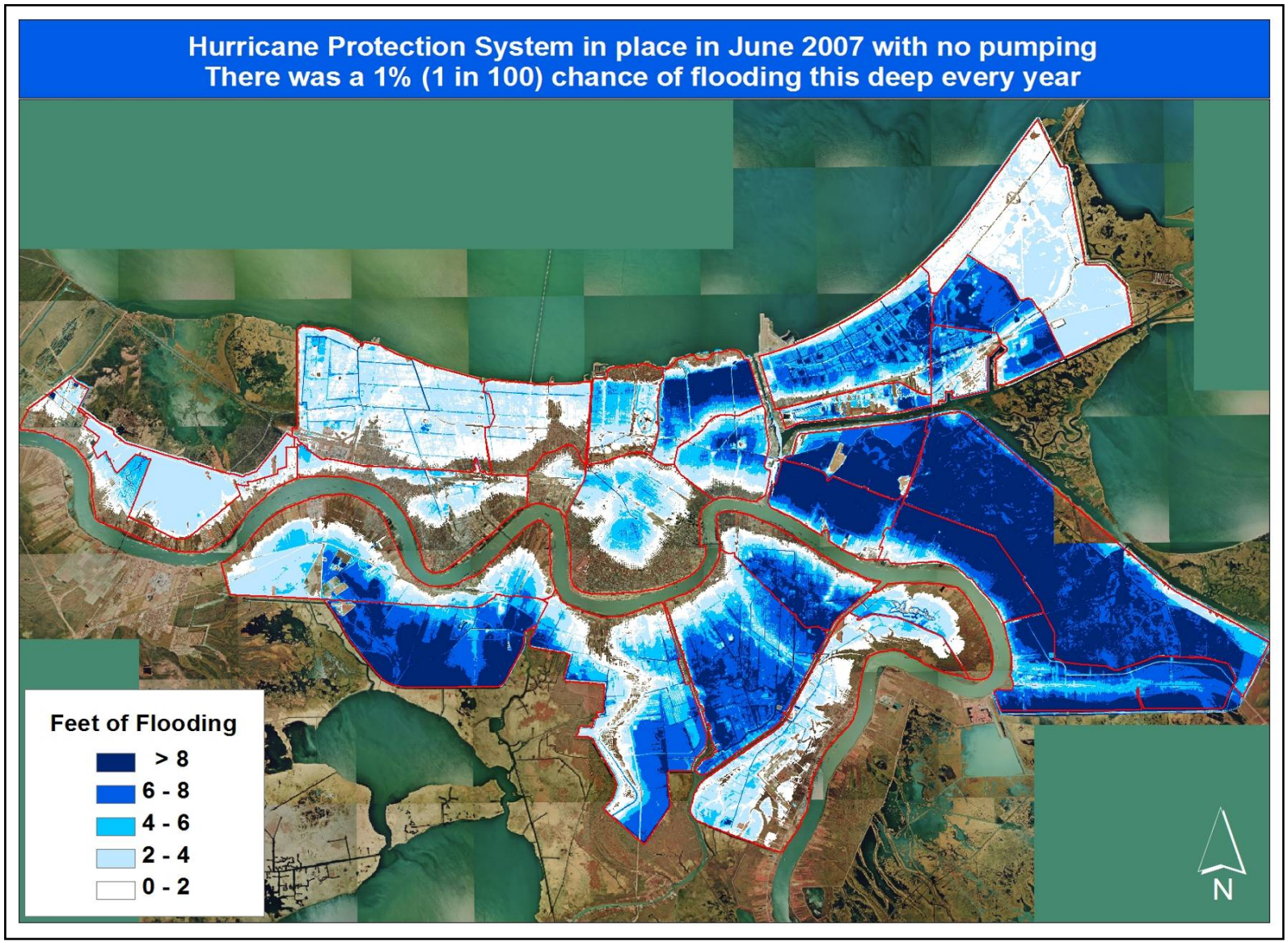

Figure 69. June 2007 depth map (1% chance, no pumping).

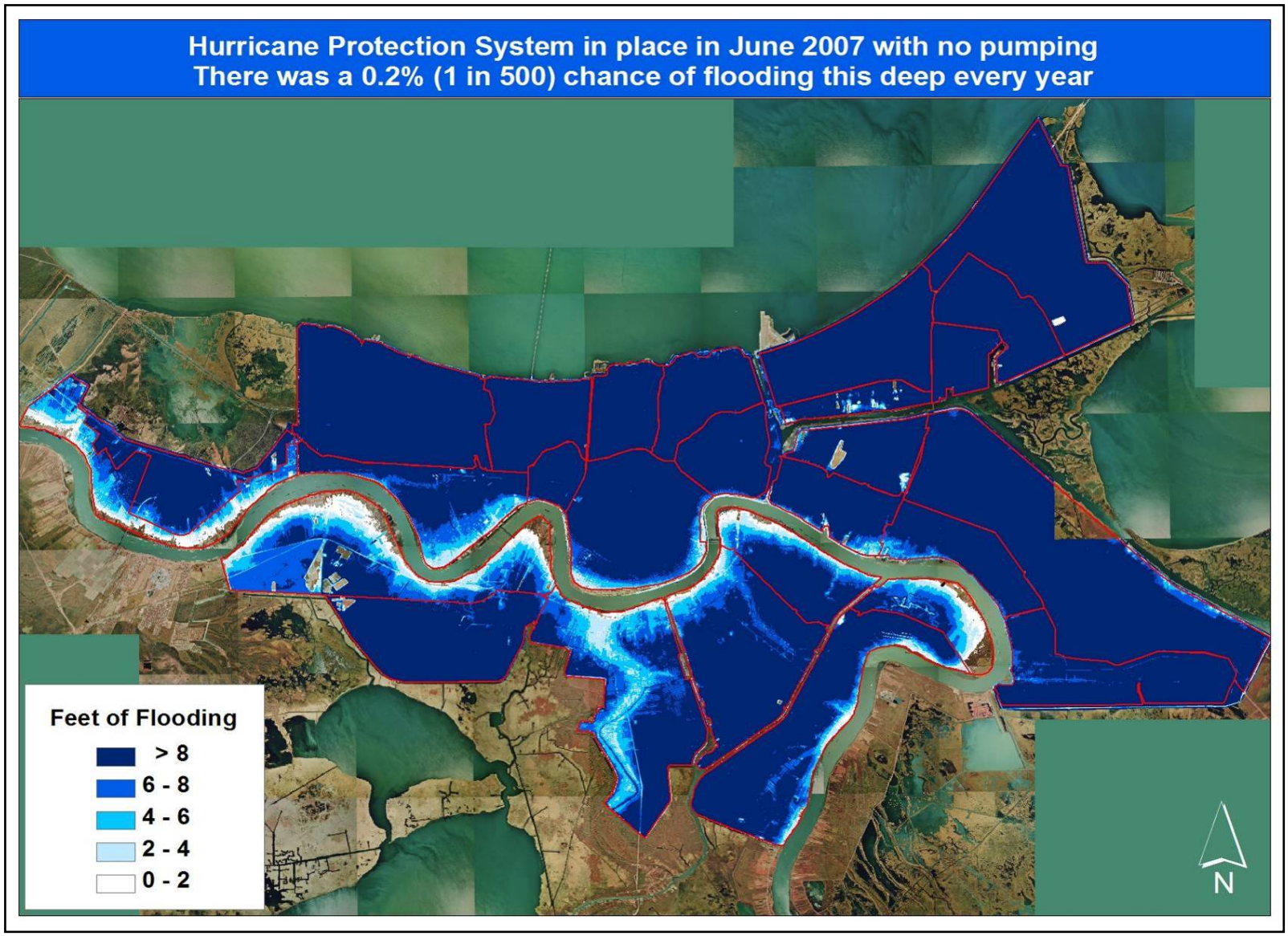

Figure 70. June 2007 depth map (0.2% chance, no pumping).

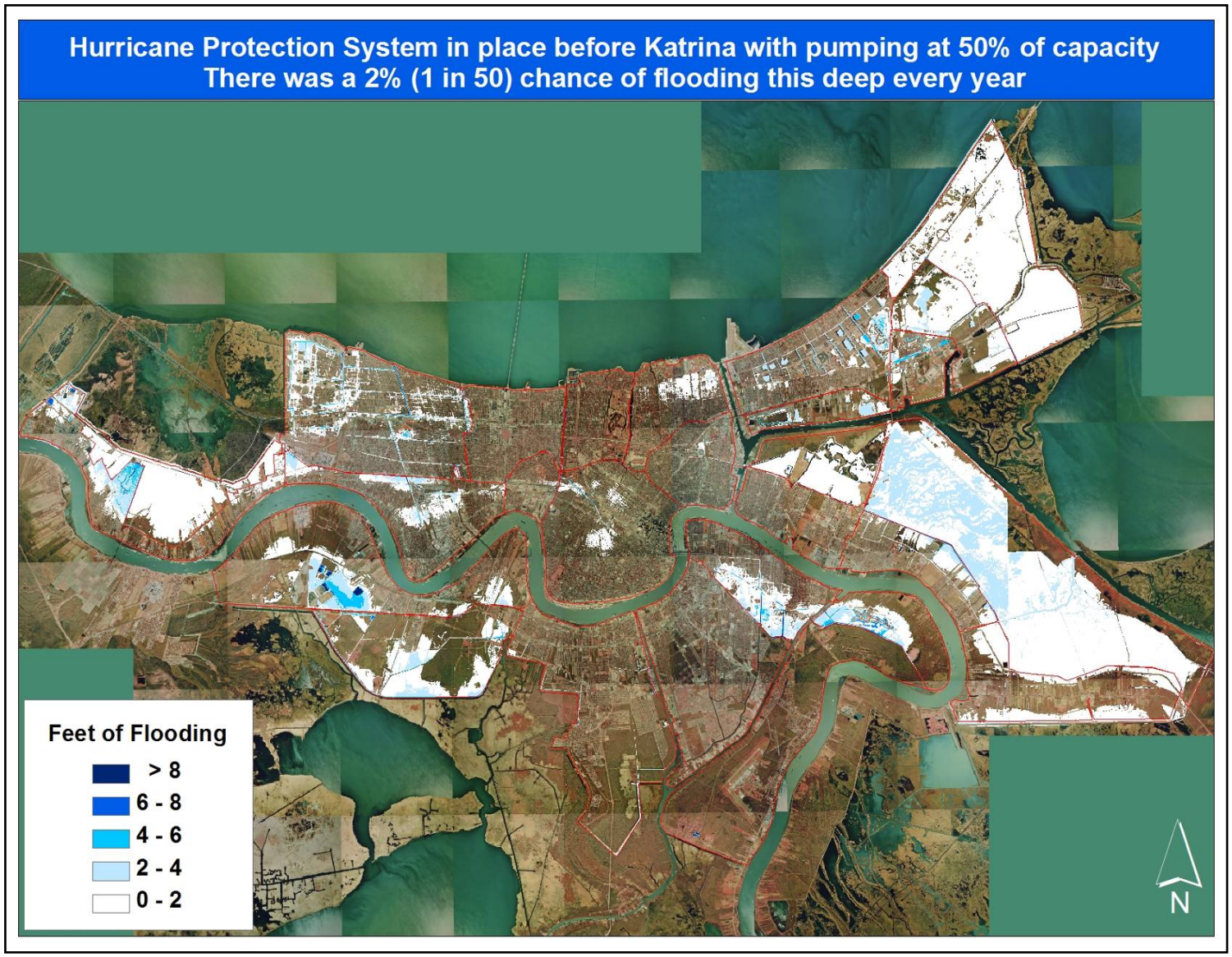

Figure 71. Pre-Katrina depth map (2% chance, 50% pumping).

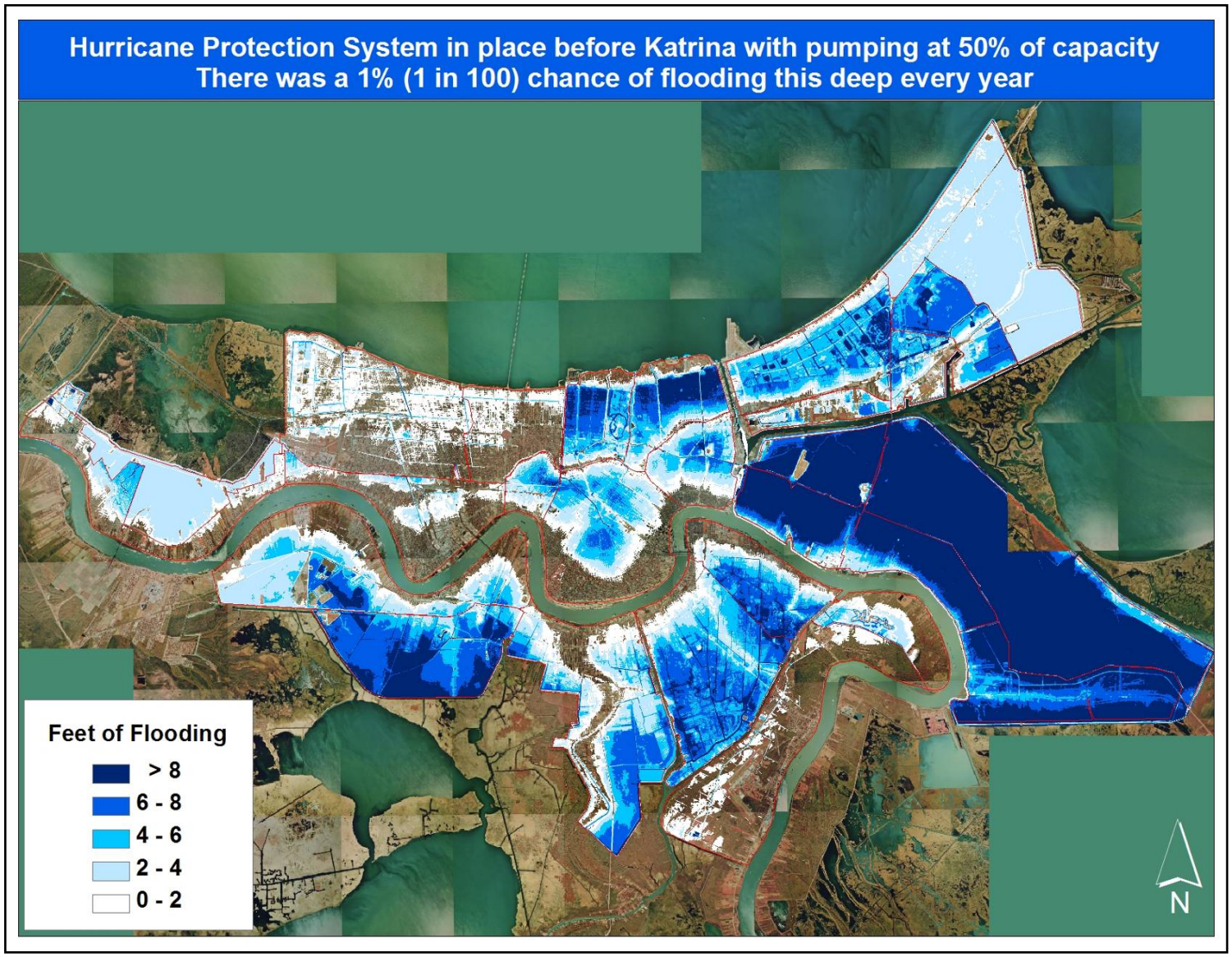

Figure 72. Pre-Katrina depth map (1% chance, 50% pumping).

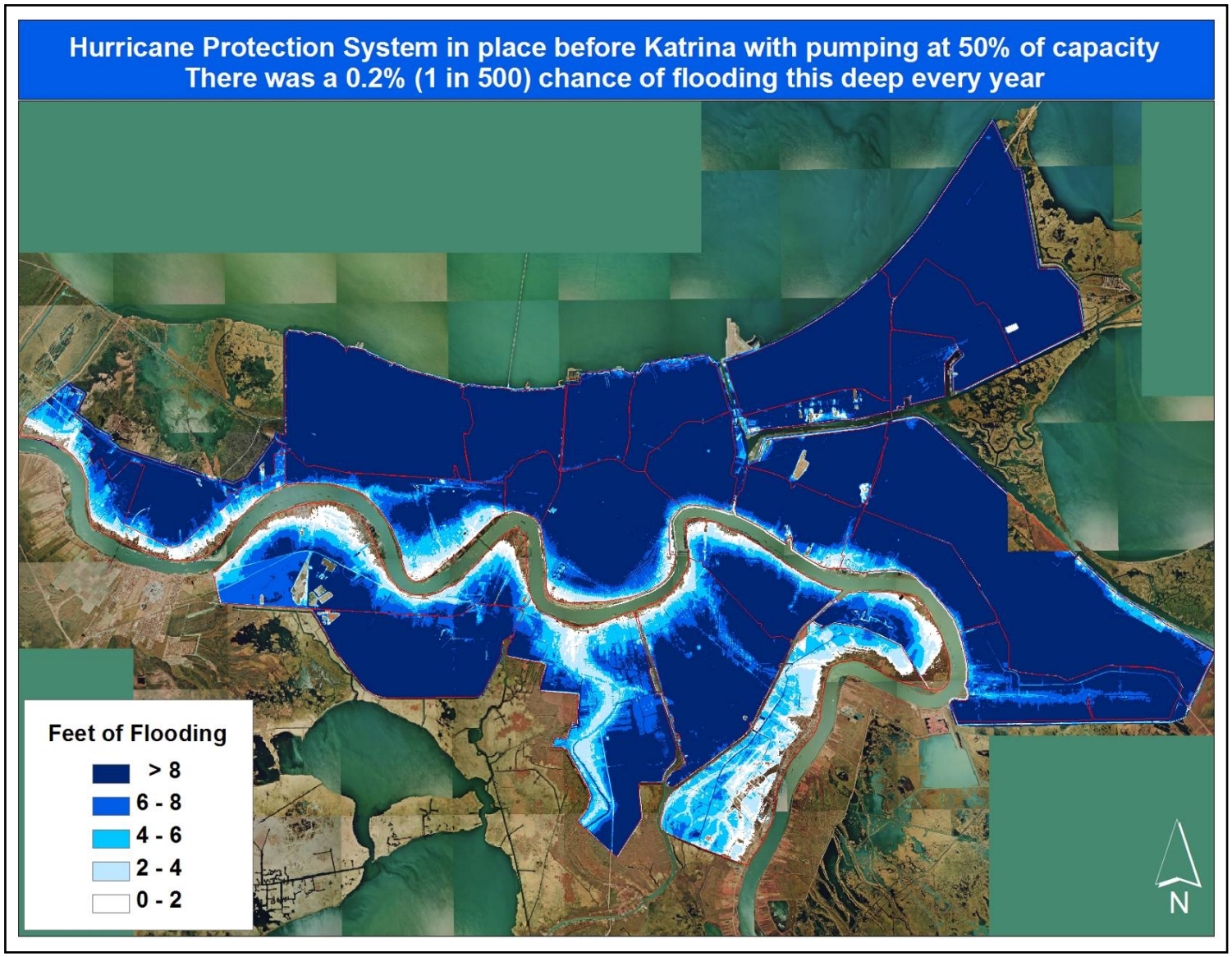

Figure 73. Pre-Katrina depth map (0.2% chance, 50% pumping).

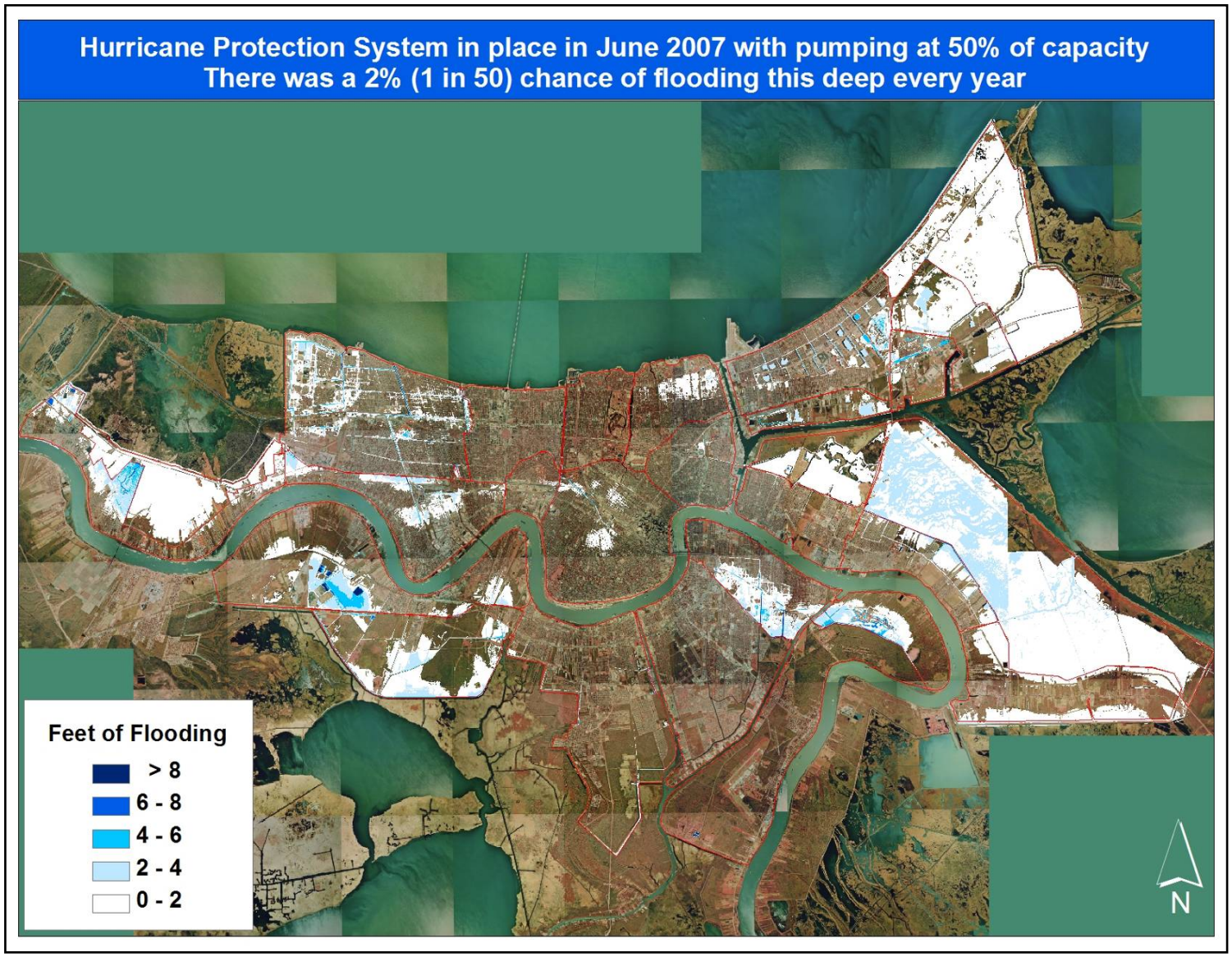

Figure 74. June 2007 depth map (2% chance, 50% pumping).

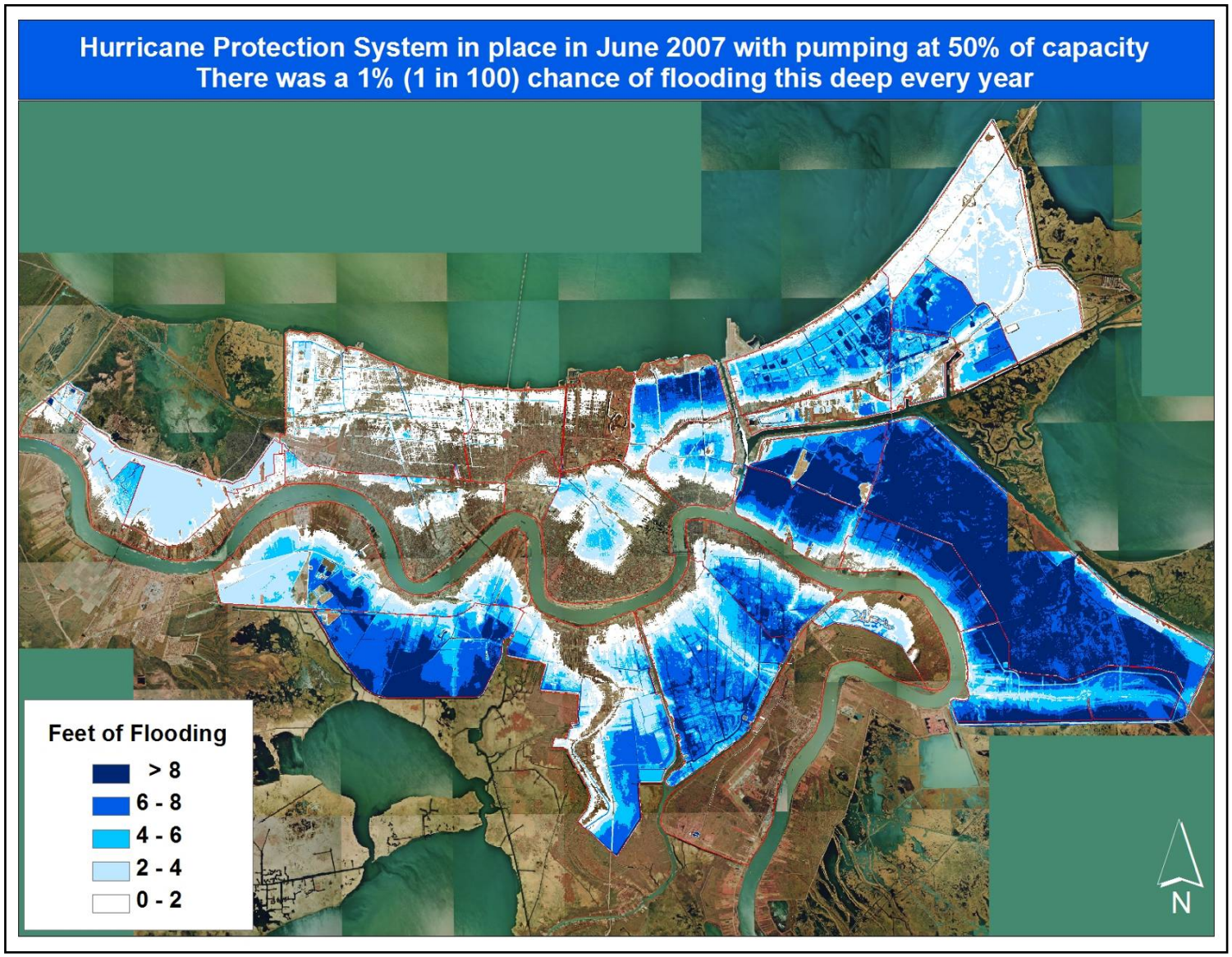

Figure 75. June 2007 depth map (1% chance, 50% pumping).

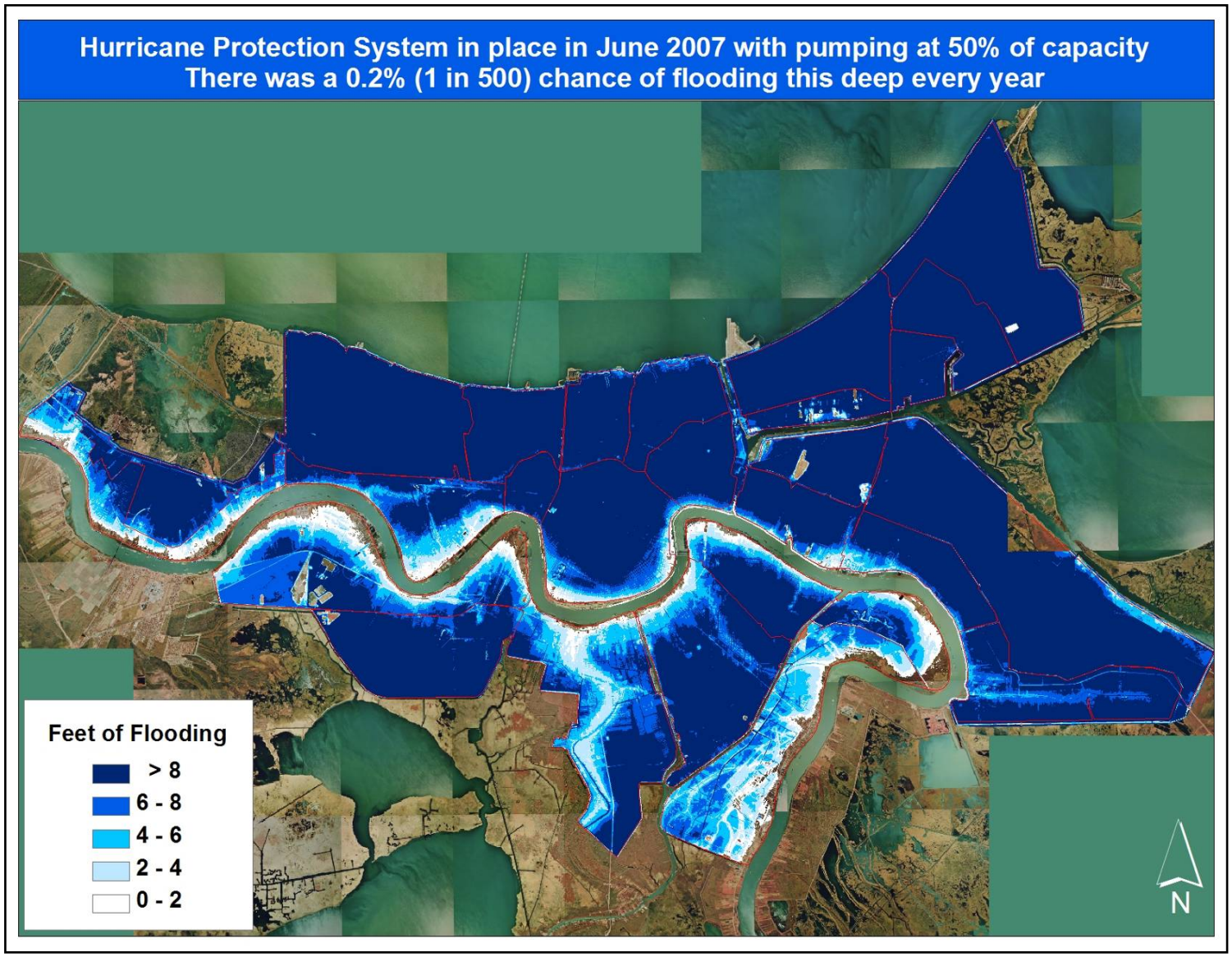

Figure 76. June 2007 depth map (0.2% chance, 50% pumping).

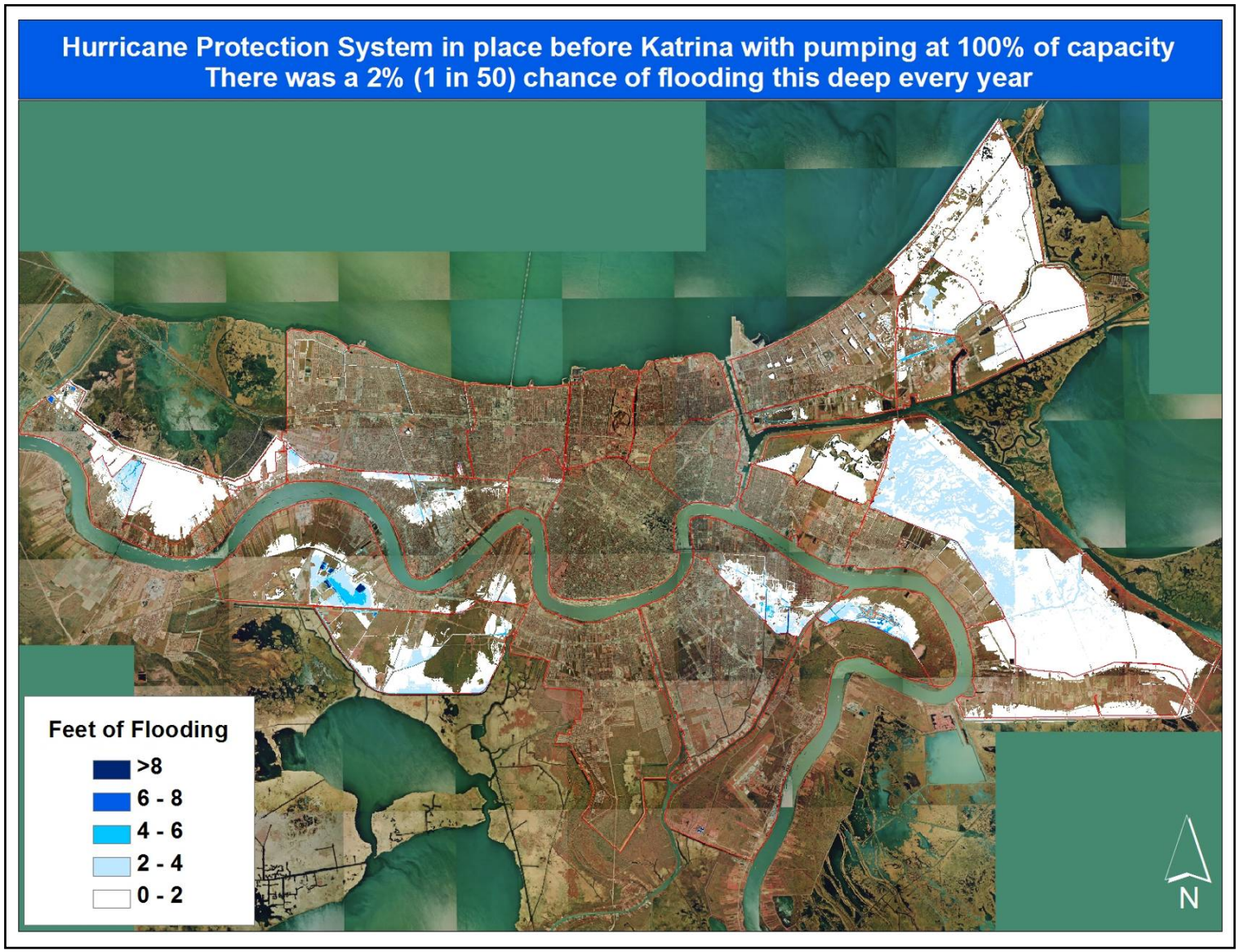

Figure 77. Pre-Katrina depth map (2% chance, 100% pumping).

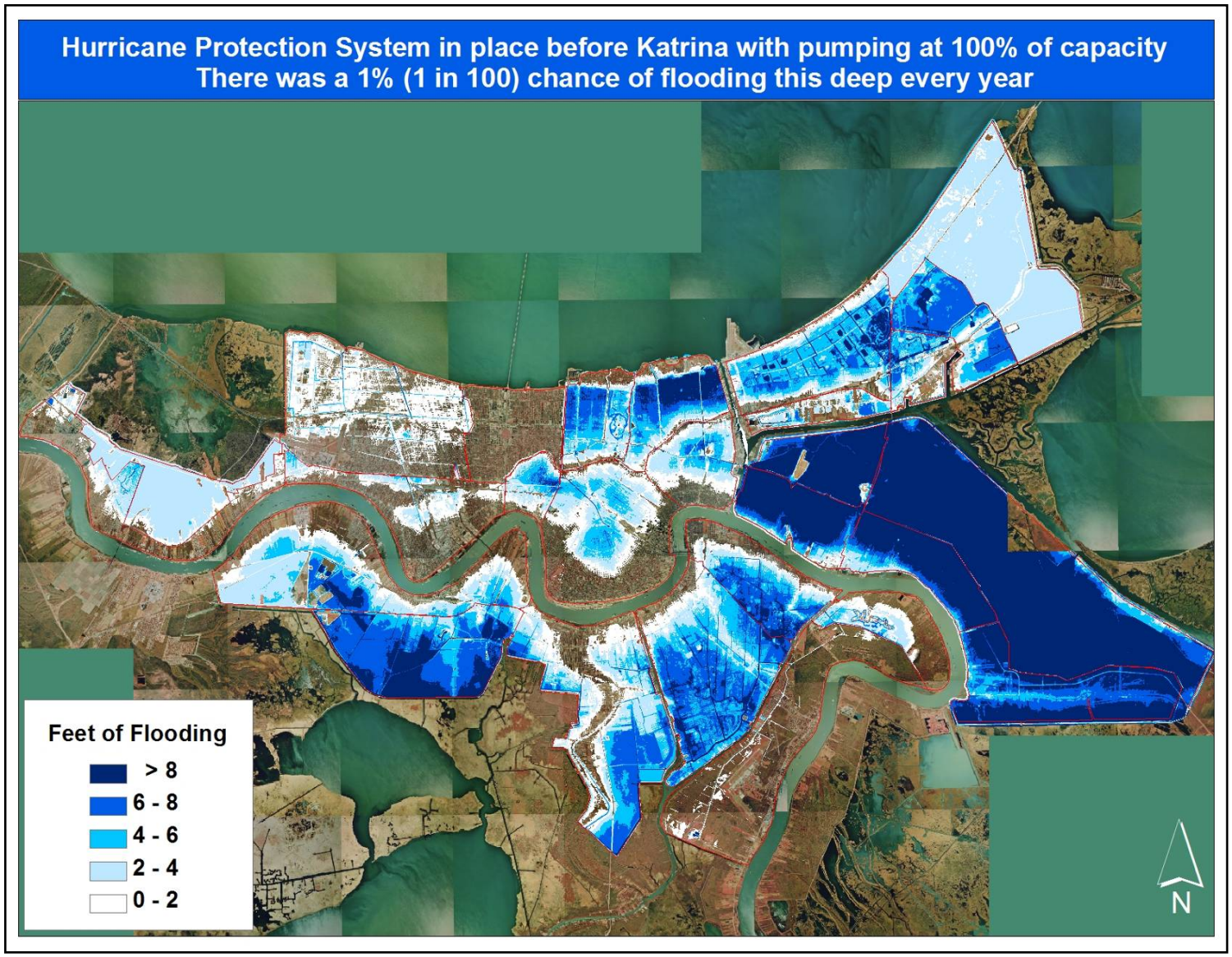

Figure 78. Pre-Katrina depth map (1% chance, 100% pumping).

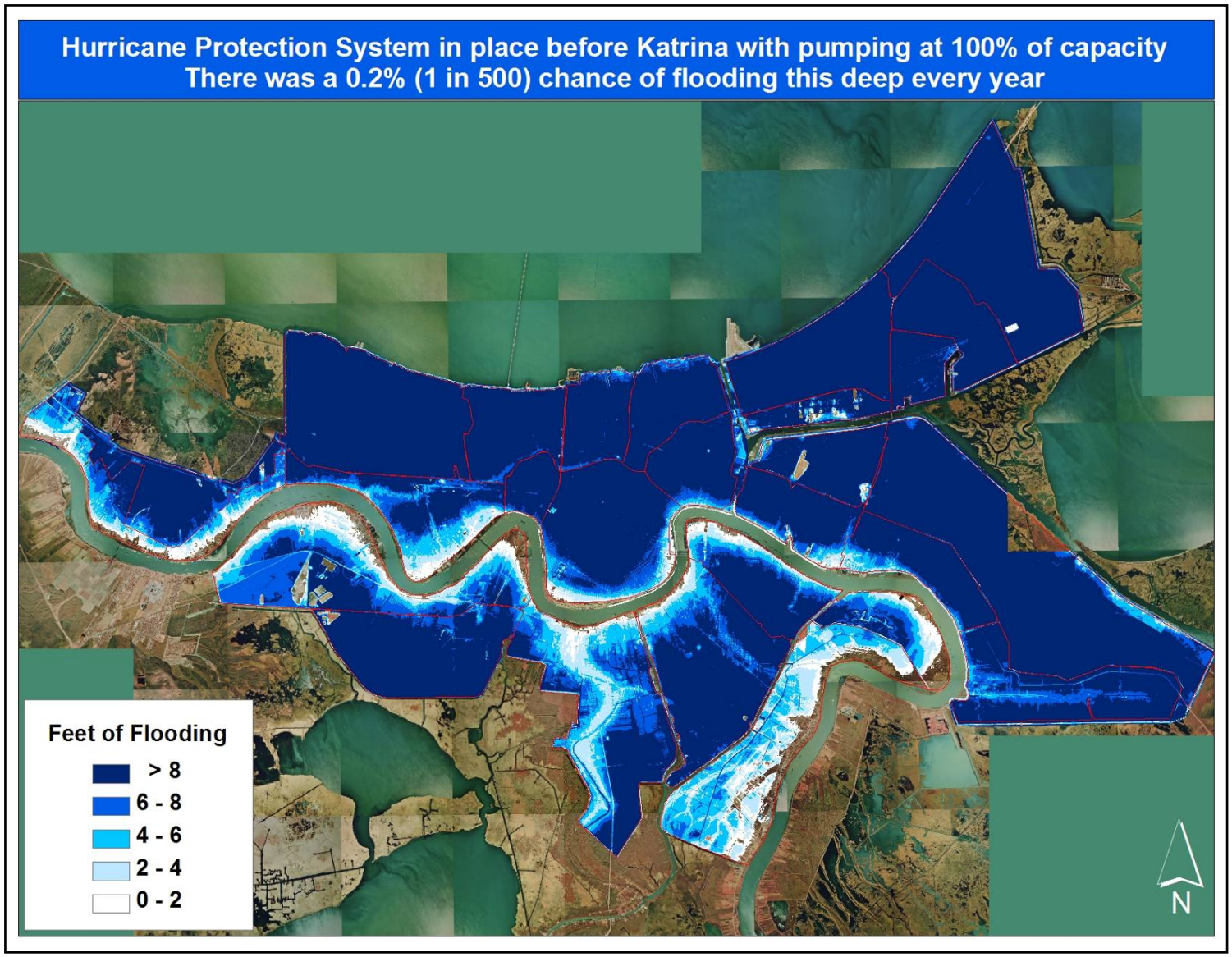

Figure 79. Pre-Katrina depth map (0.2% chance, 100% pumping).

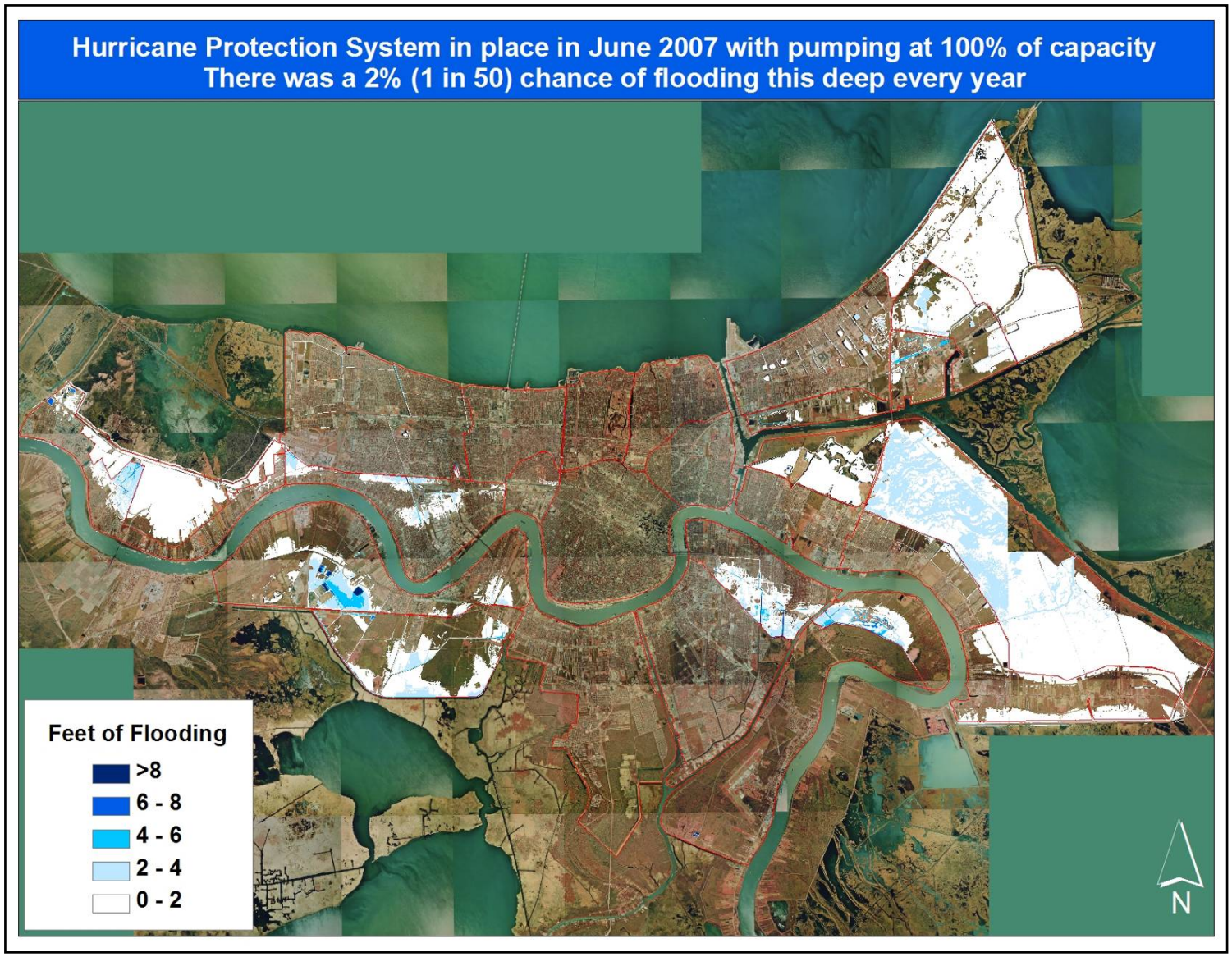

Figure 80. June 2007 depth map (2% chance, 100% pumping).

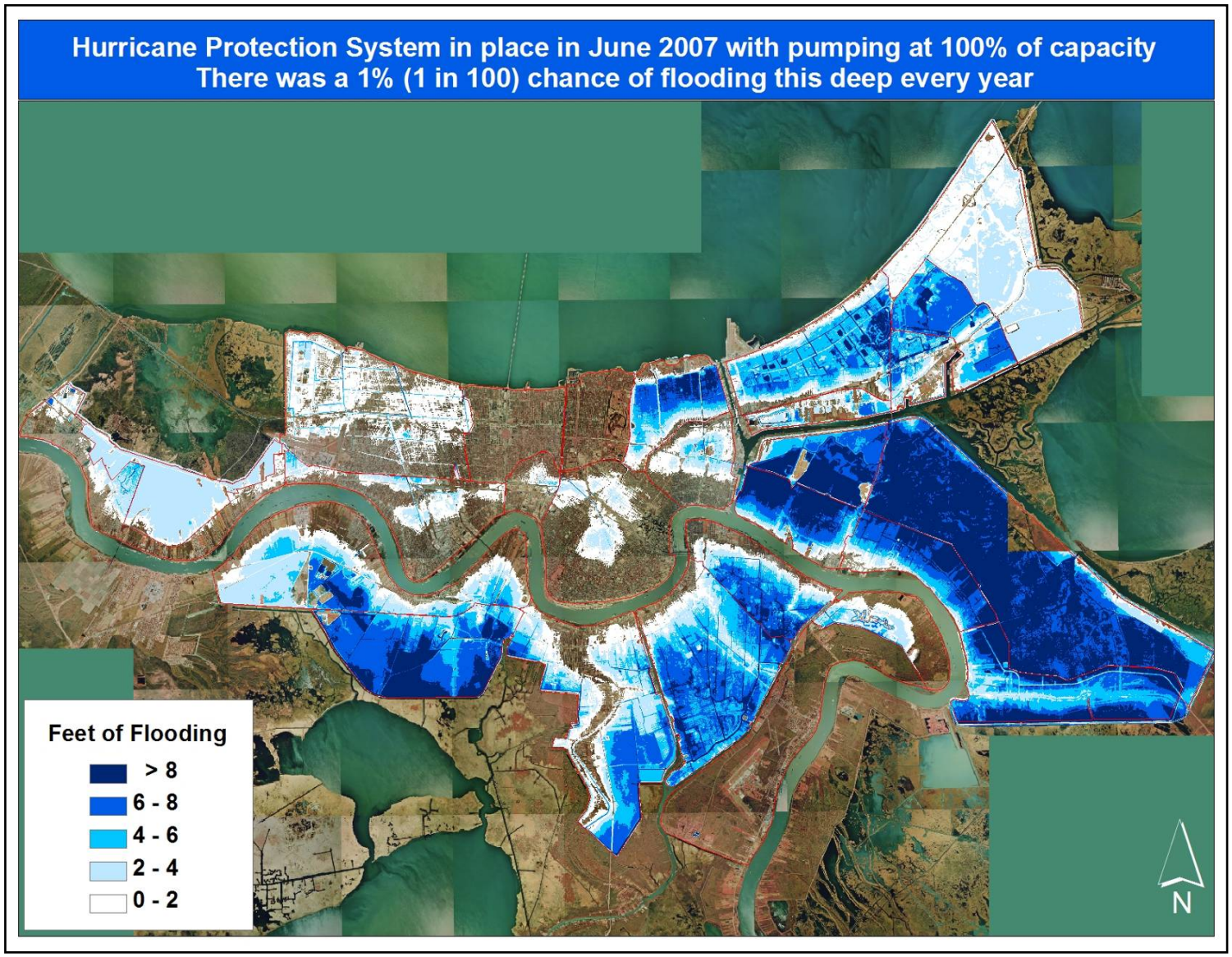

Figure 81. June 2007 depth map (1% chance, 100% pumping).

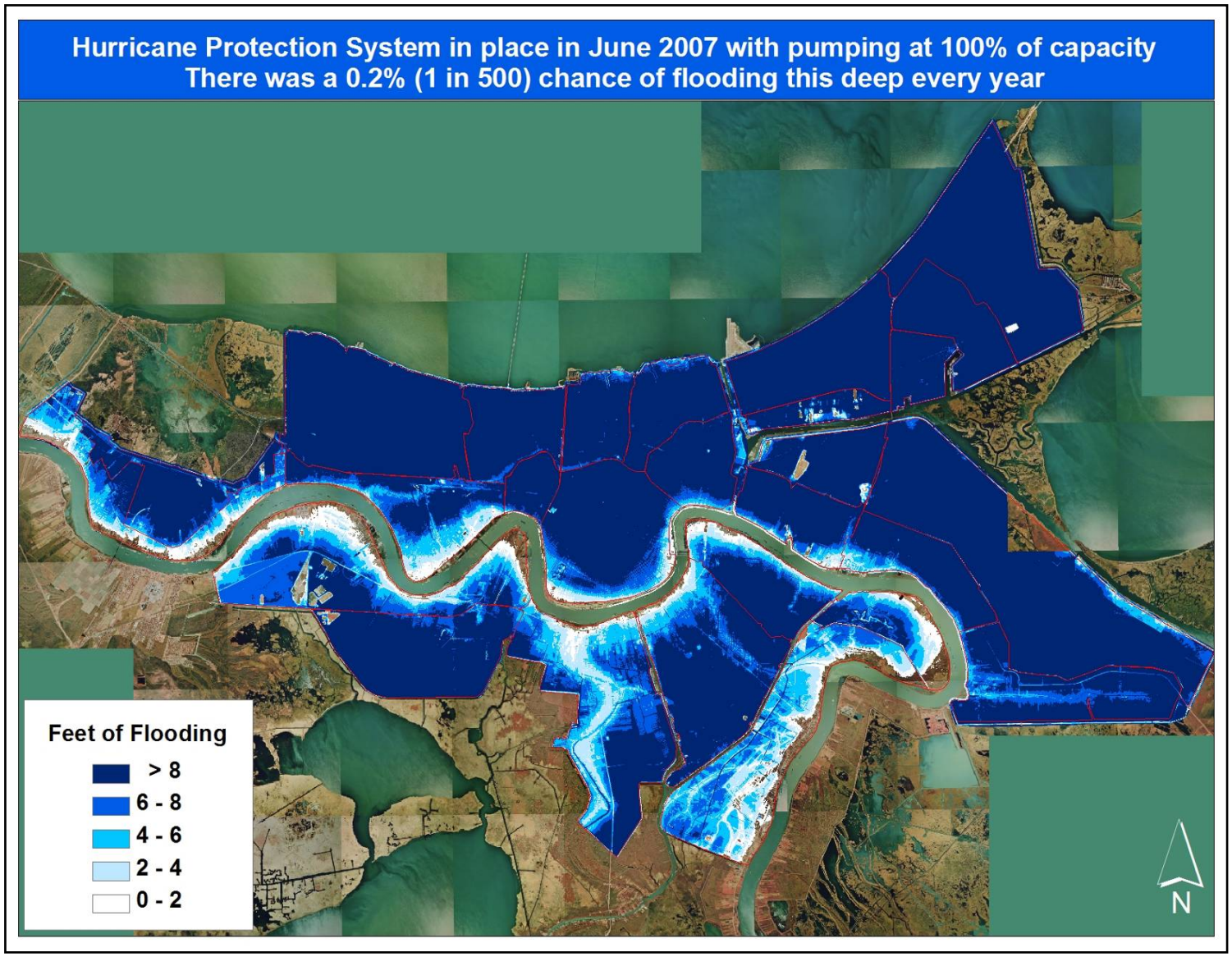

Figure 82. June 2007 depth map (0.2% chance, 100% pumping).

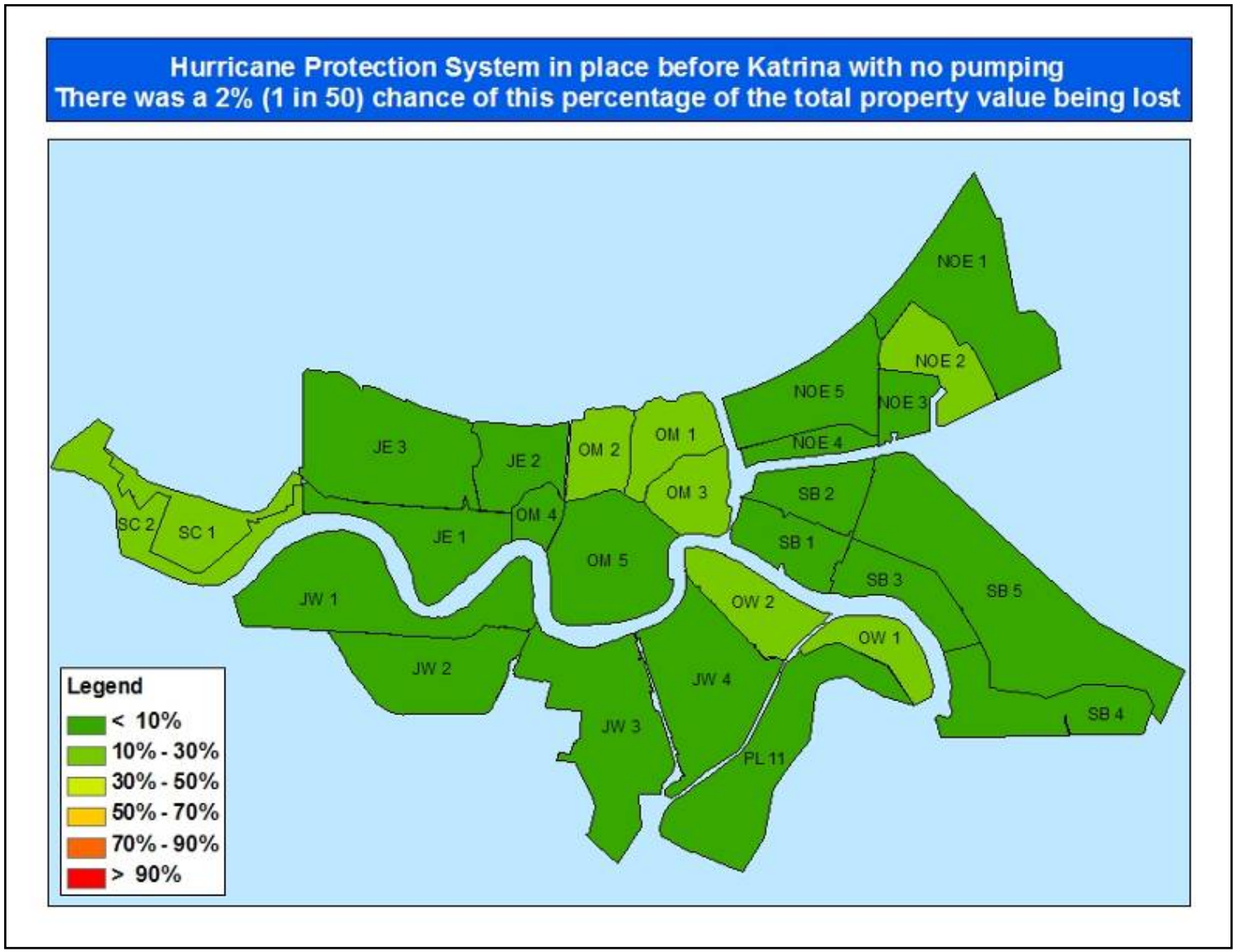

Figure 83. Pre-Katrina % of total value lost (2% chance, no pumping).

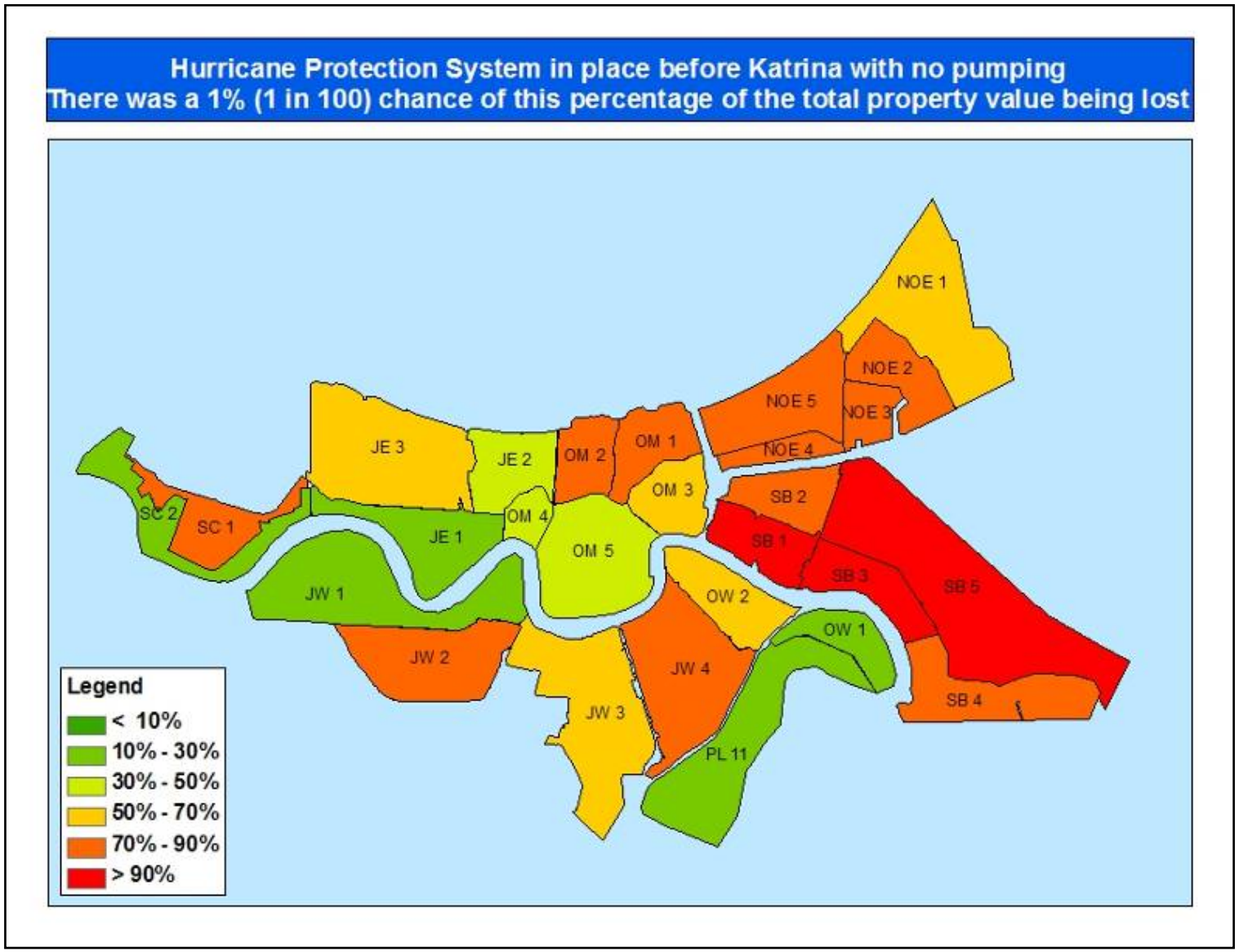

Figure 84. Pre-Katrina % of total value lost (1% chance, no pumping).

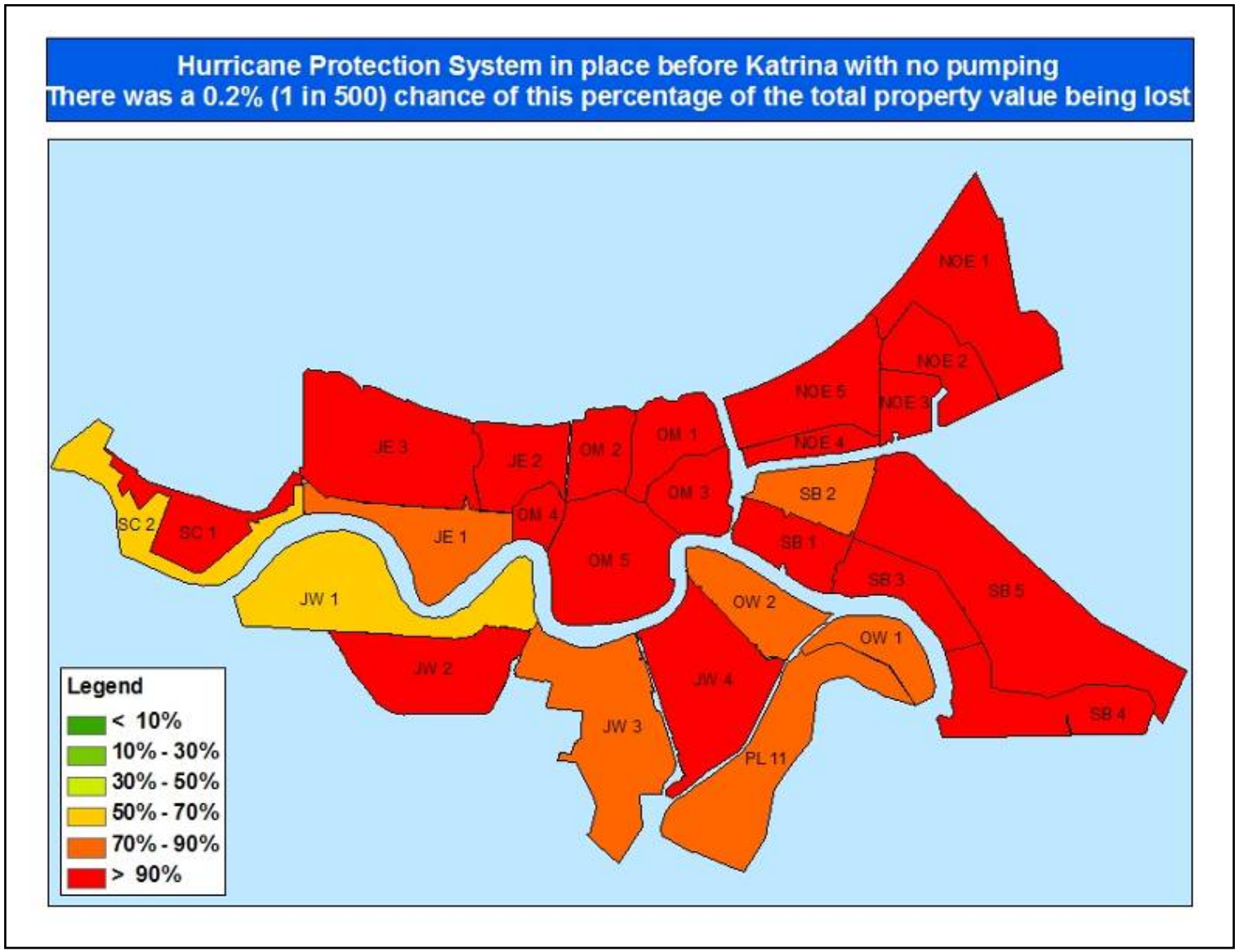

Figure 85. Pre-Katrina % of total value lost (0.2% chance, no pumping.

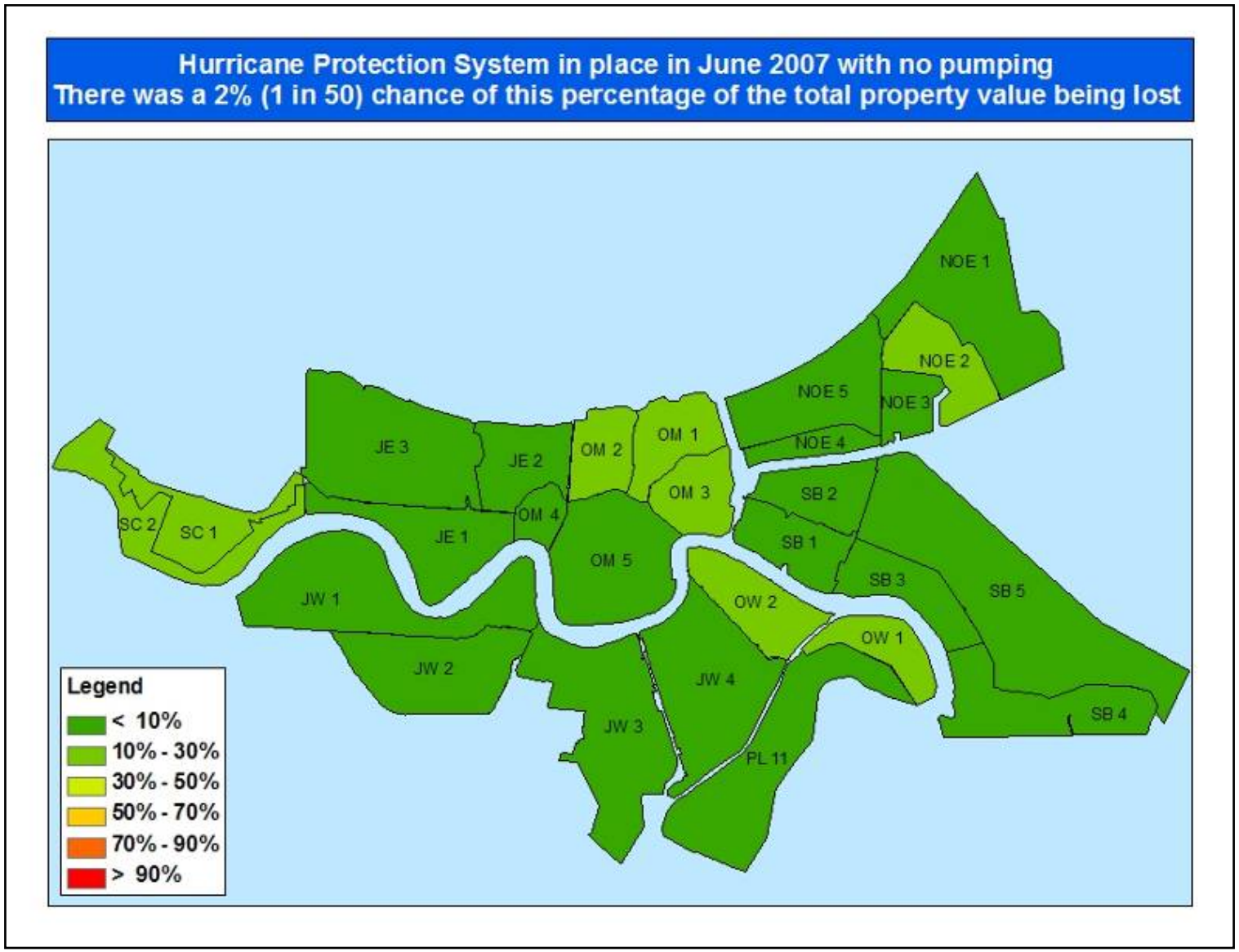

Figure 86. June 2007 % of total value lost (2% chance, no pumping).

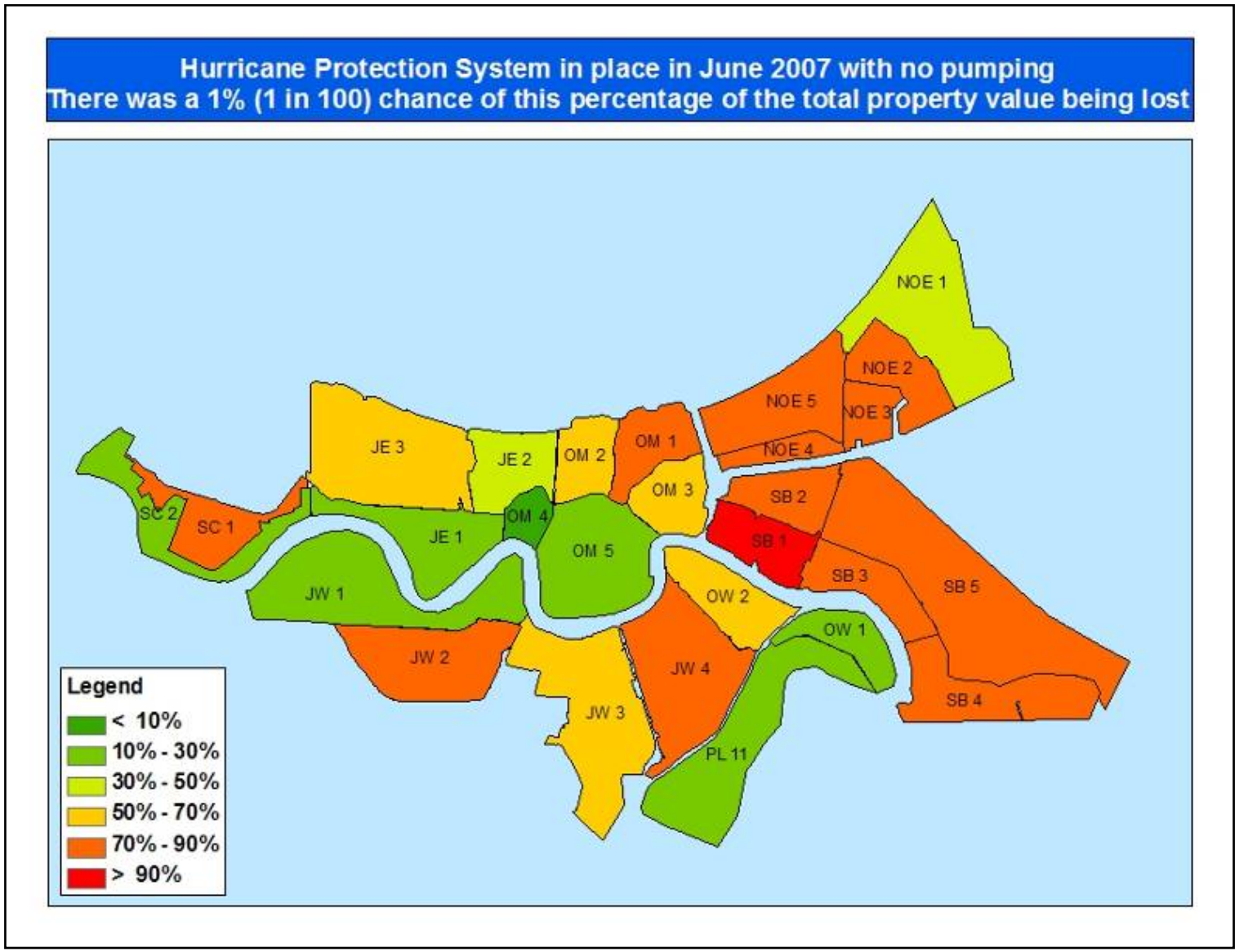

Figure 87. June 2007 % of total value lost (1% chance, no pumping).

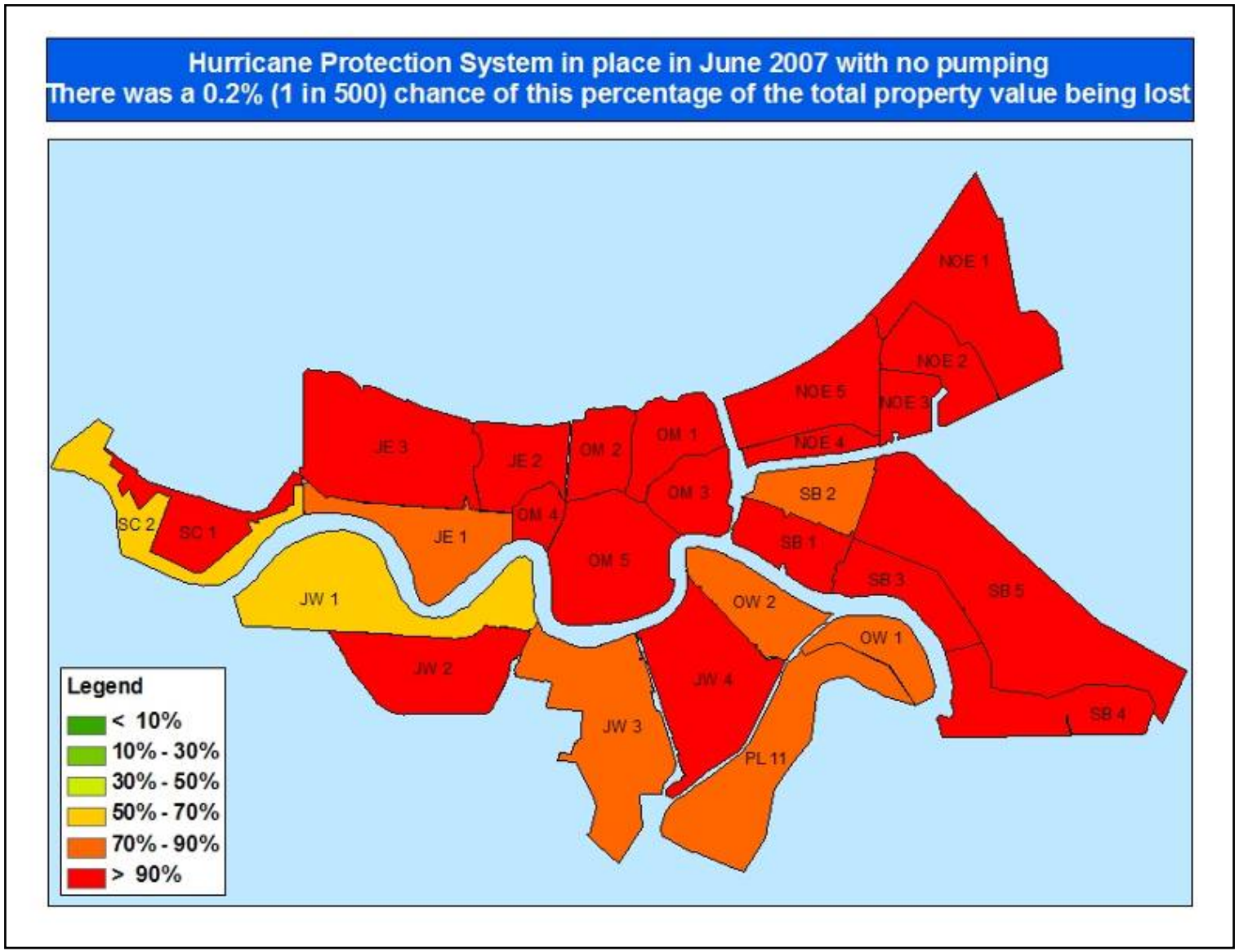

Figure 88. June 2007 % of total value lost (0.2% chance, no pumping).

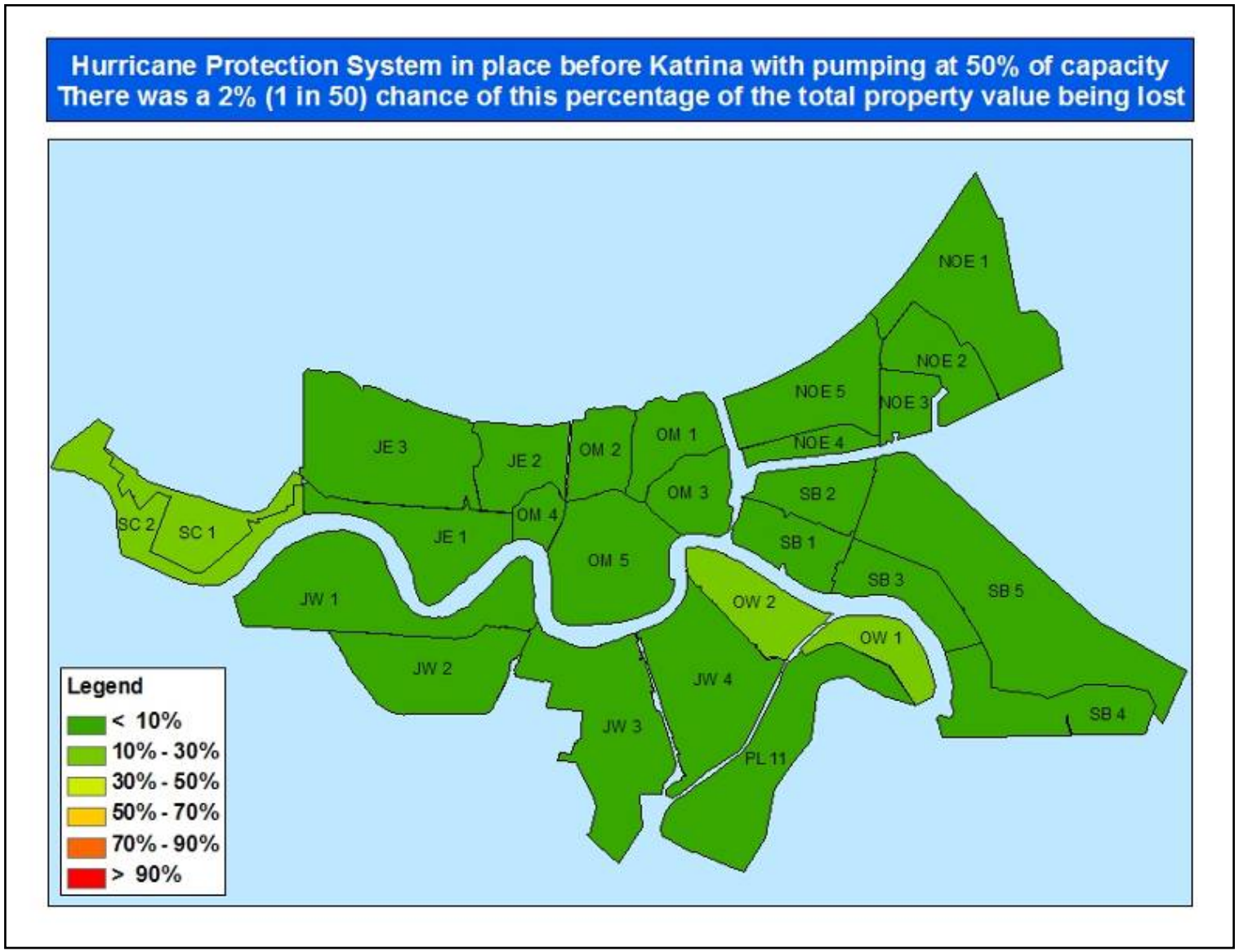

Figure 89. Pre-Katrina % of total value lost (2% chance, 50% pumping).

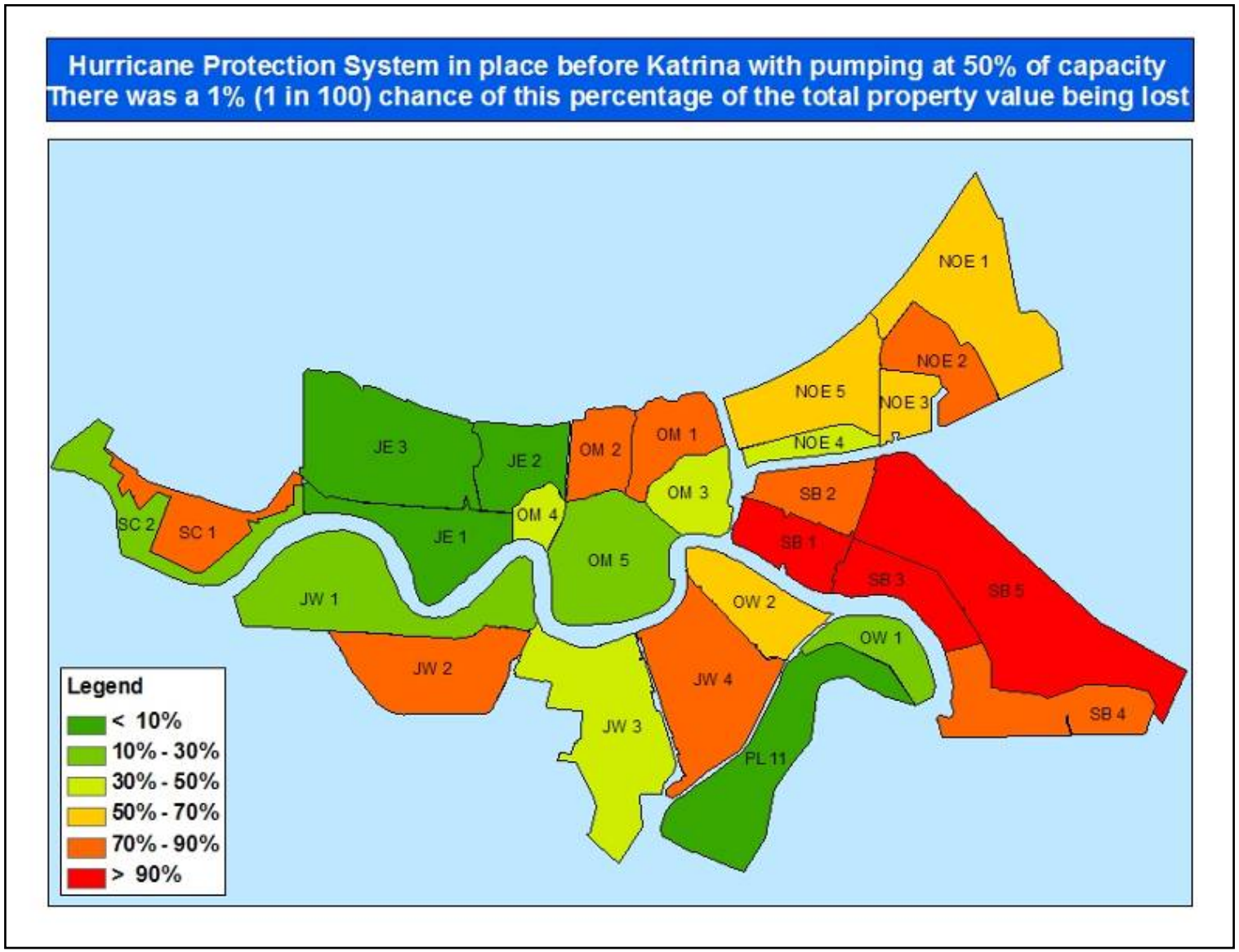

Figure 90. Pre-Katrina % of total value lost (1% chance, 50% pumping).

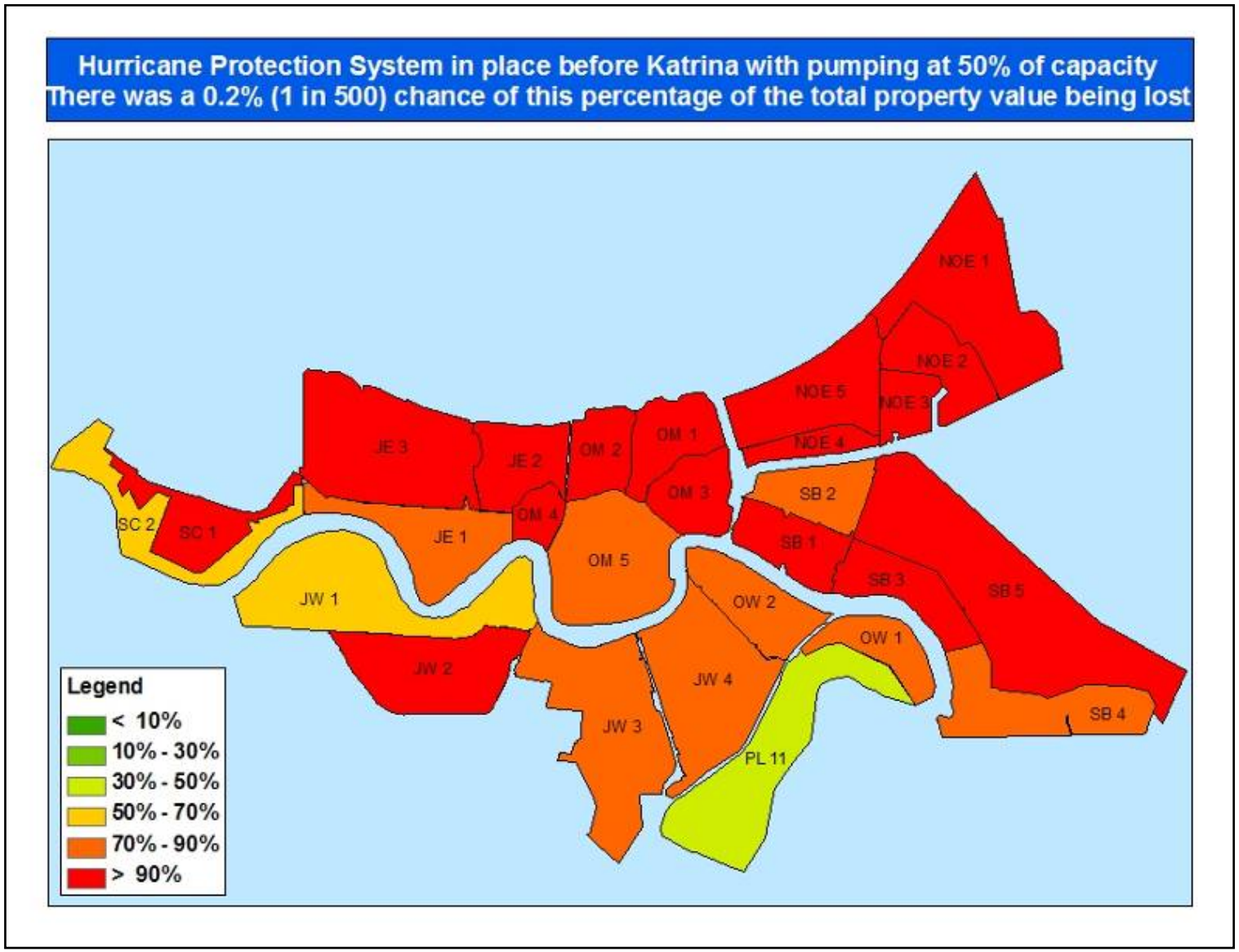

Figure 91. Pre-Katrina % of total value lost (0.2% chance, 50% pumping).

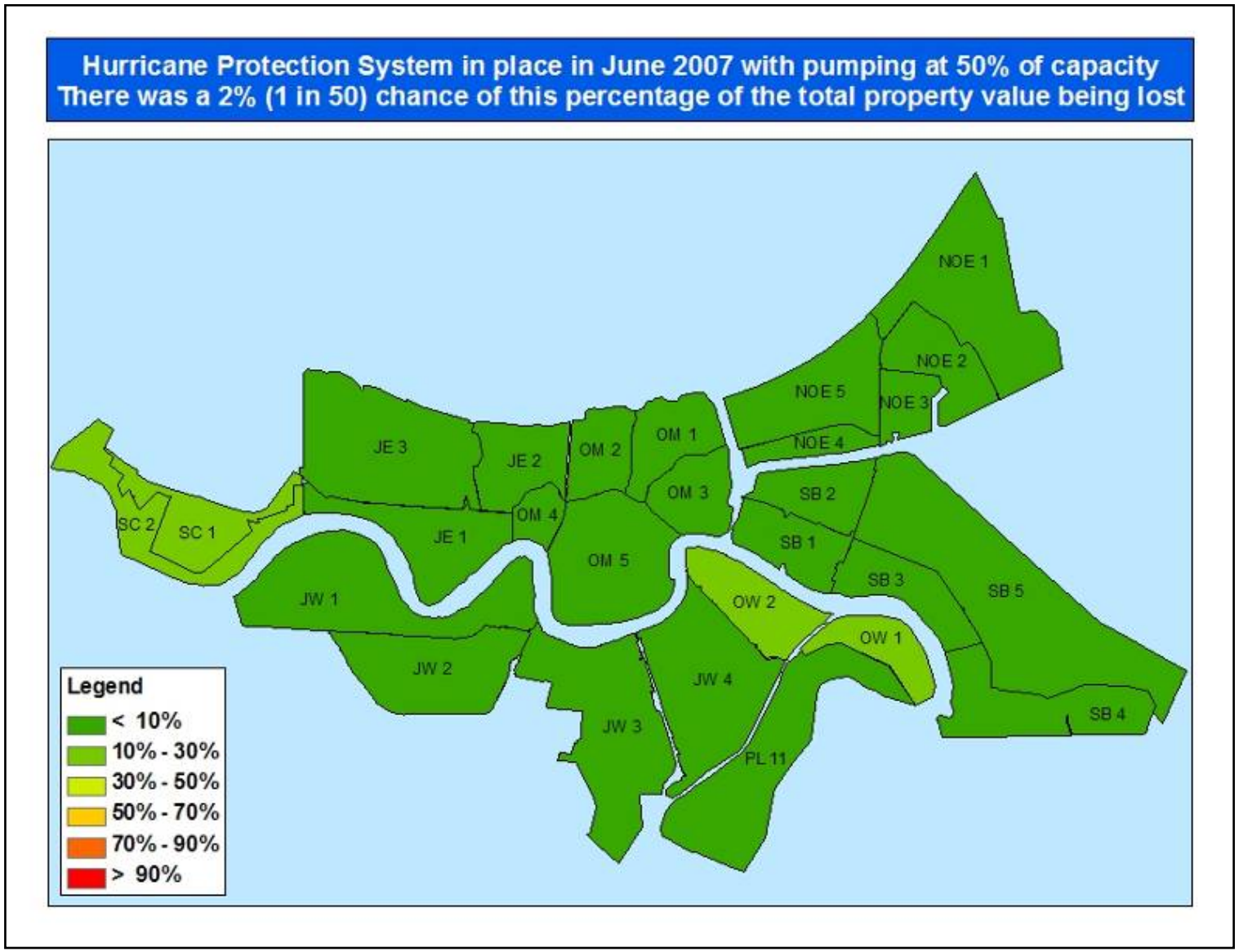

Figure 92. June 2007% of total value lost (2% chance, 50% pumping).

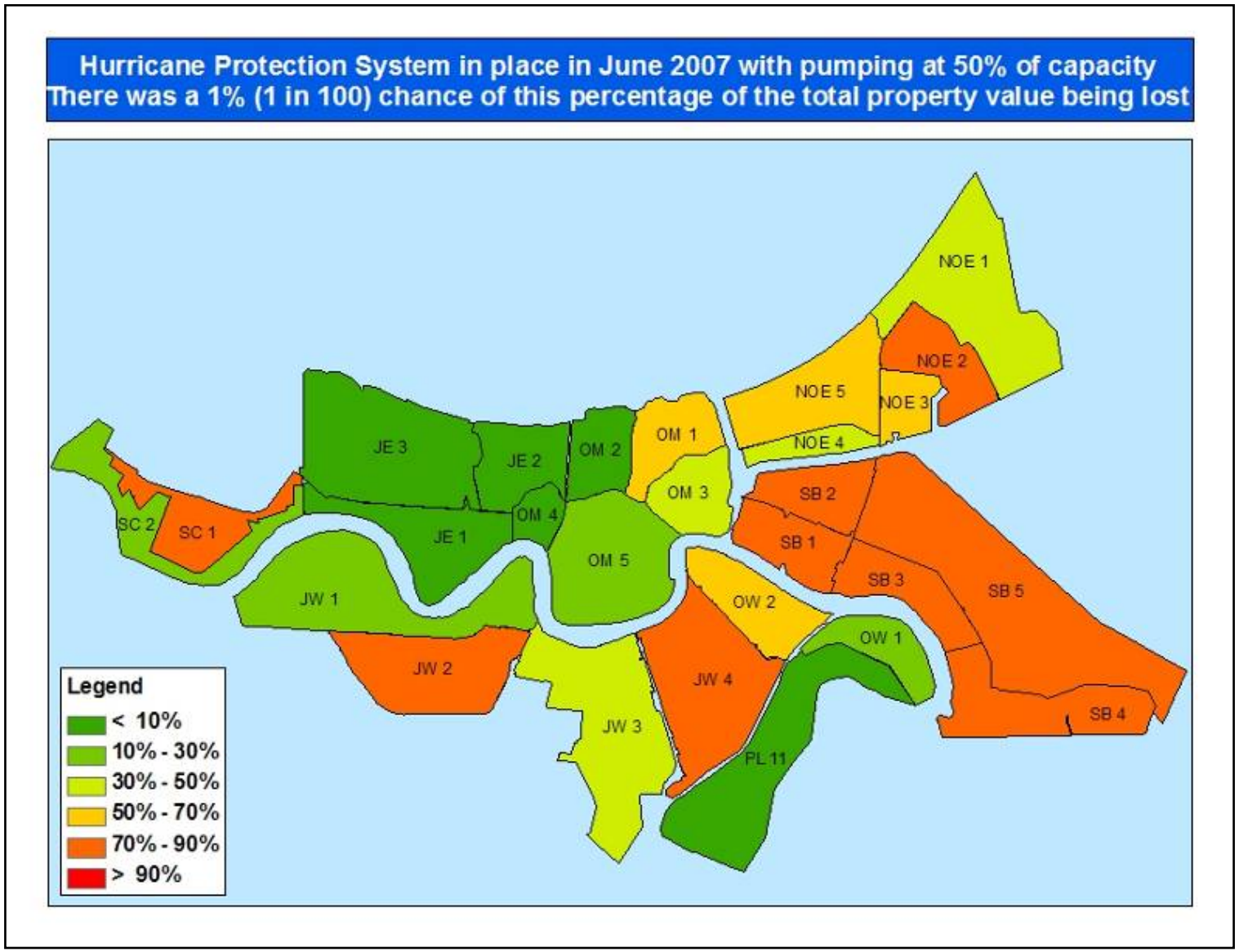

Figure 93. June 2007 % of total value lost (1% chance, 50% pumping).

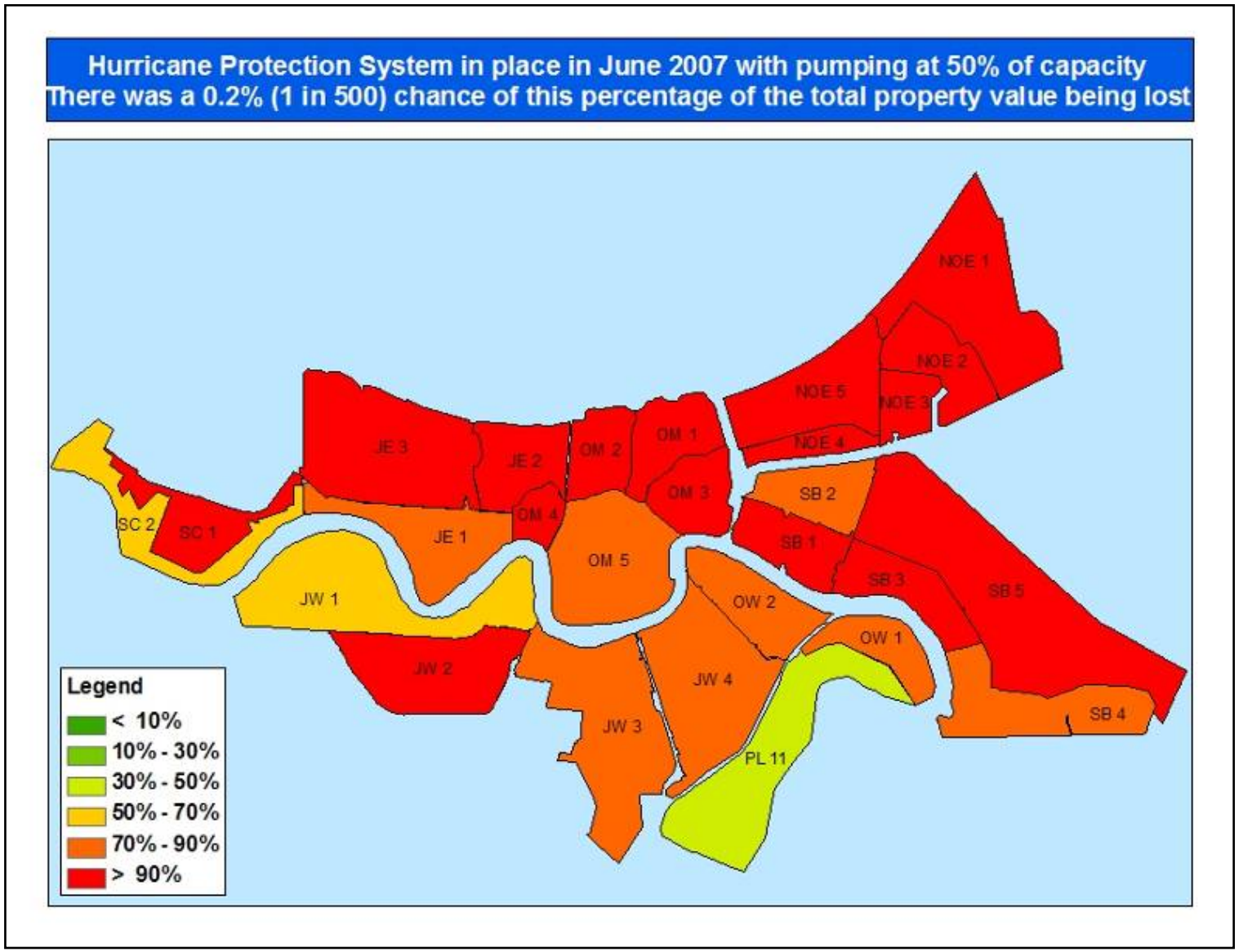

Figure 94. June 2007 % of total value lost (0.2% chance, 50% pumping).

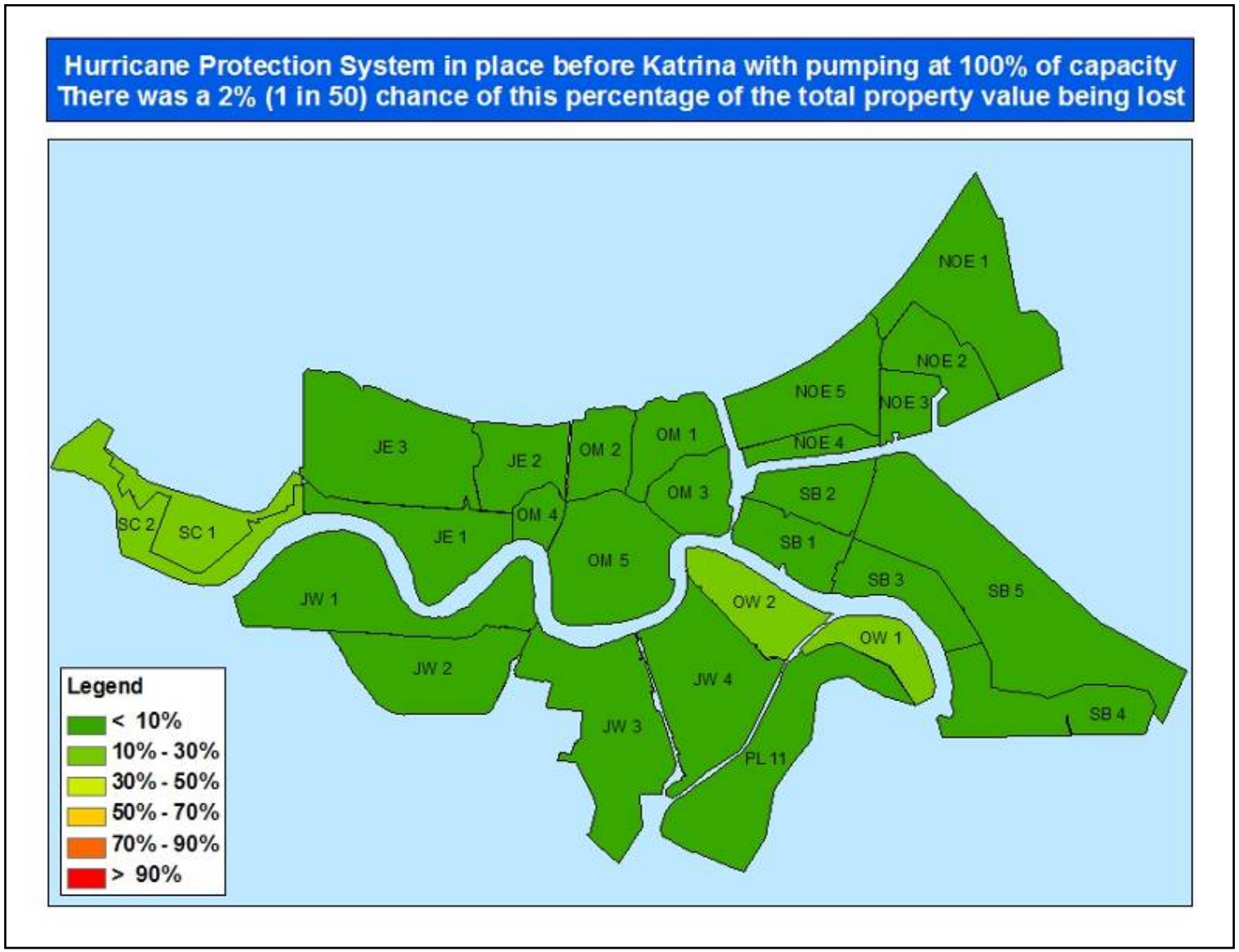

Figure 95. Pre-Katrina % of total value lost (2% chance, 100% pumping).

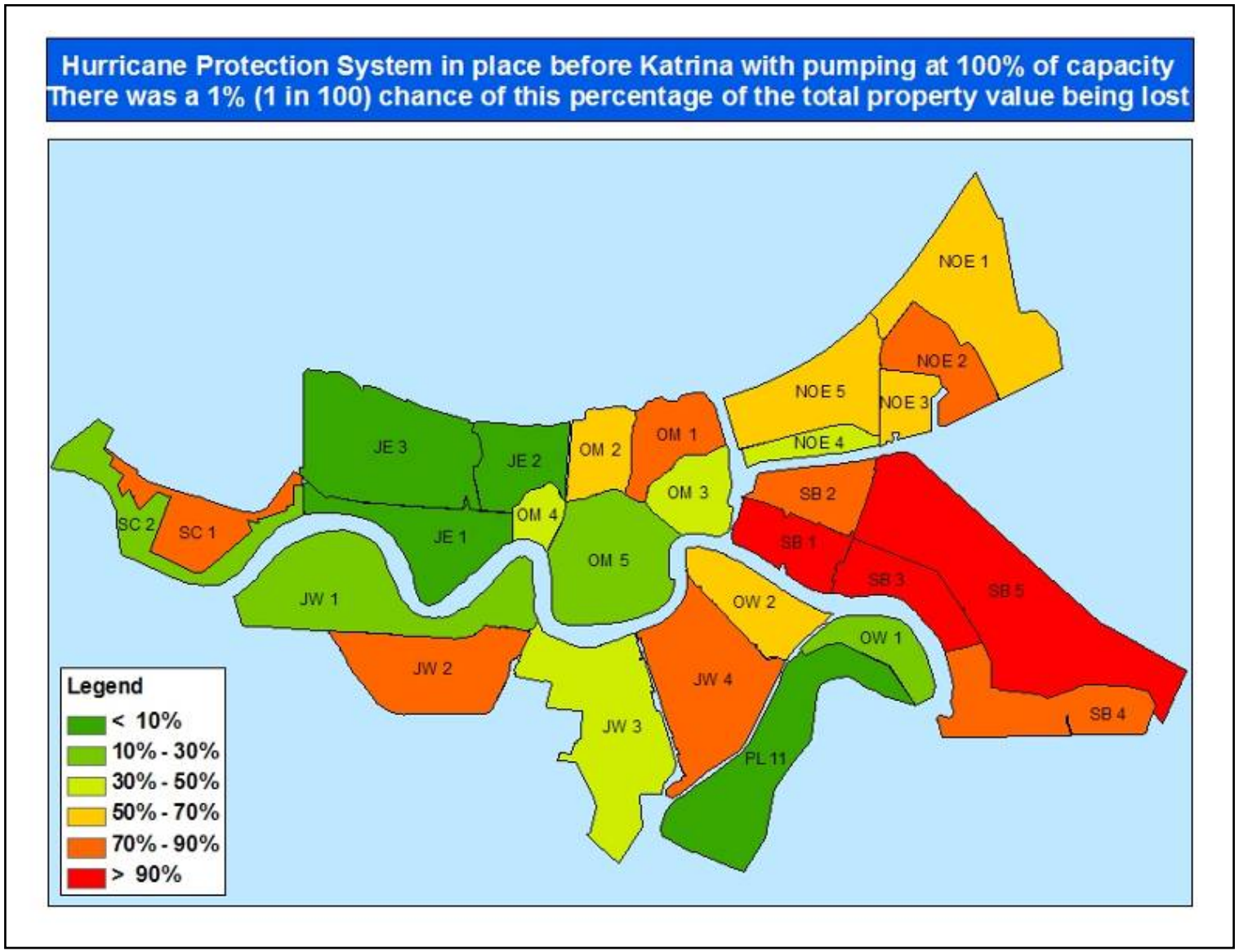

Figure 96. Pre-Katrina % of total value lost (1% chance, 100% pumping).

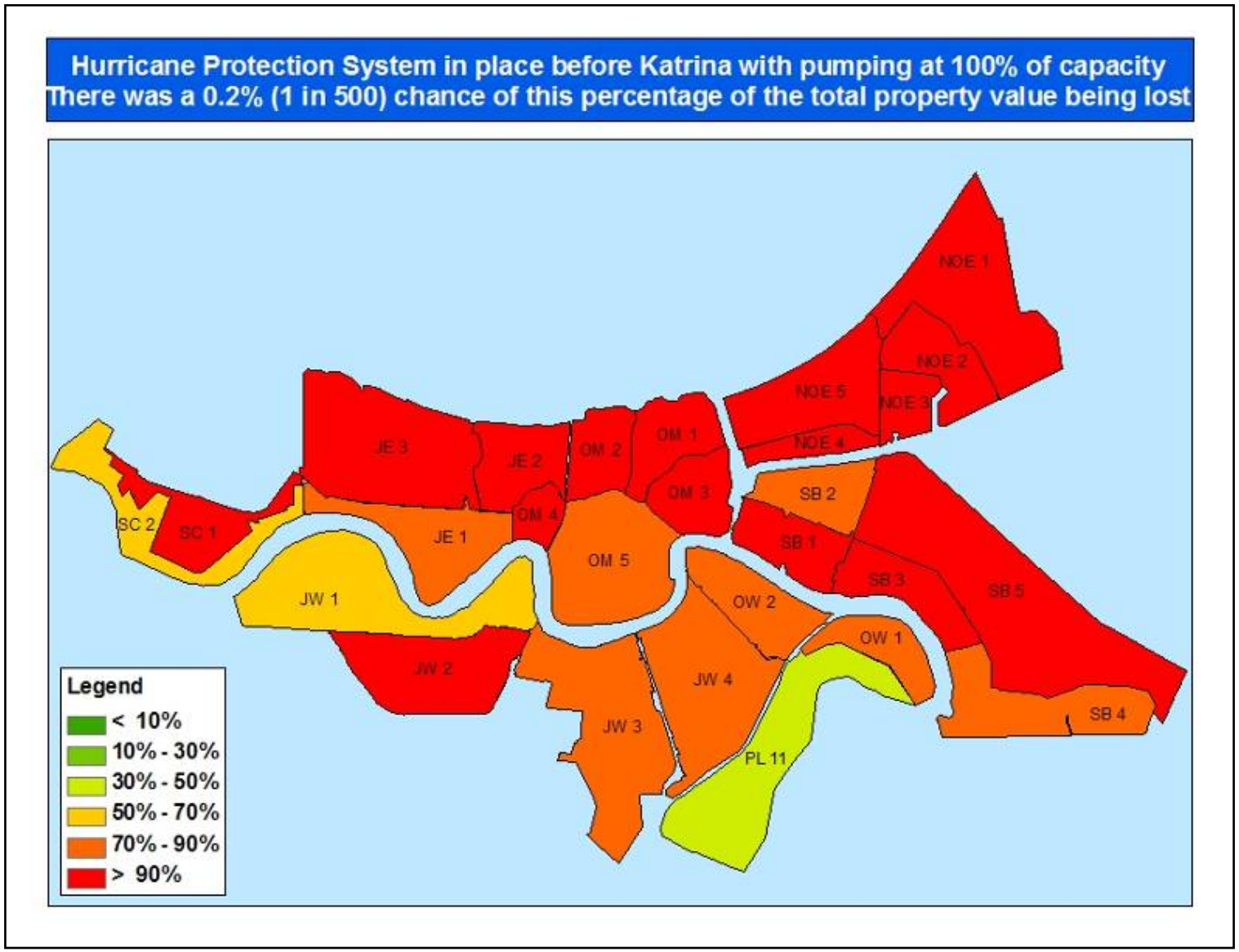

Figure 97. Pre-Katrina % of total value lost (0.2% chance, 100% pumping).

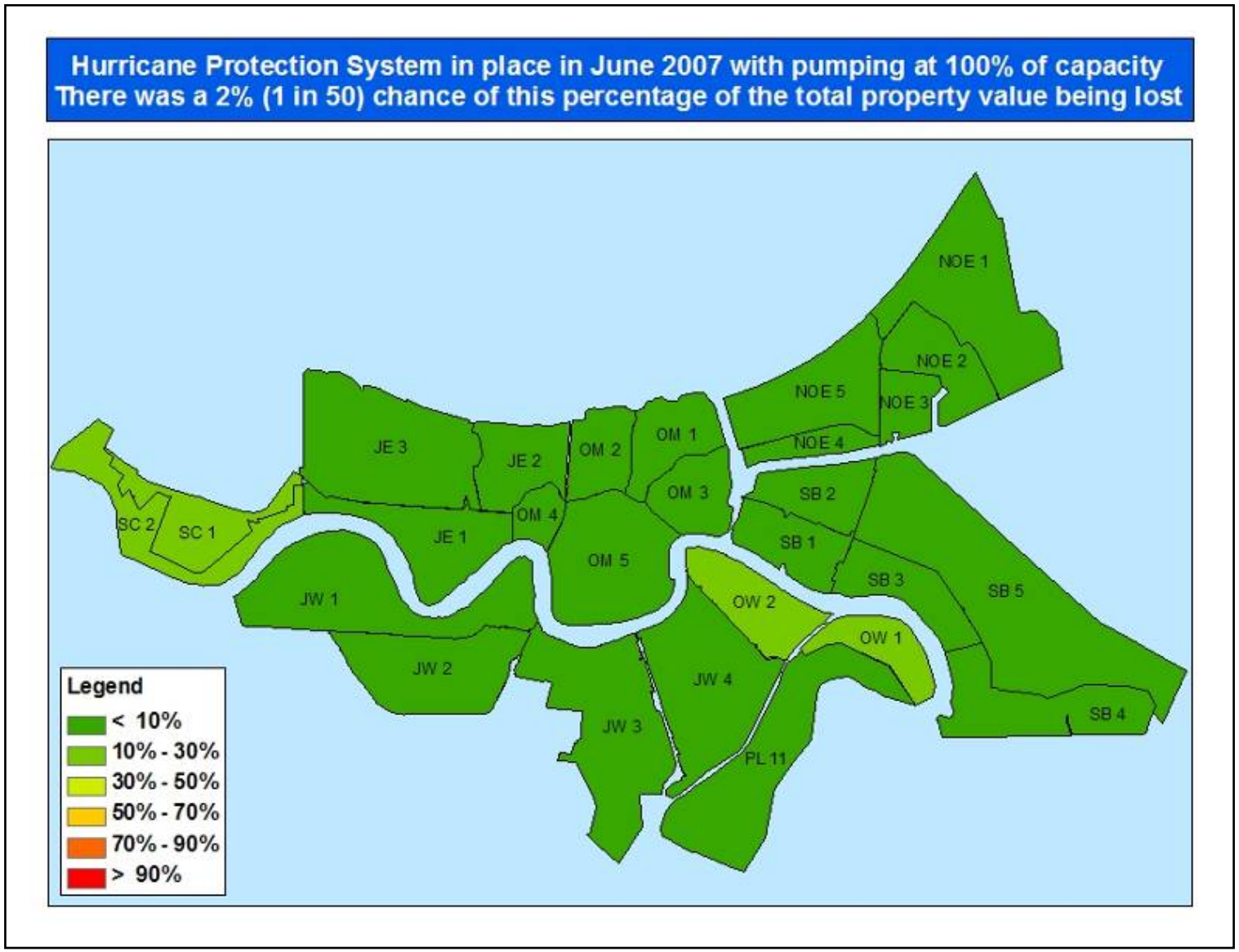

Figure 98. June 2007 % of total value lost (2% chance, 100% pumping).

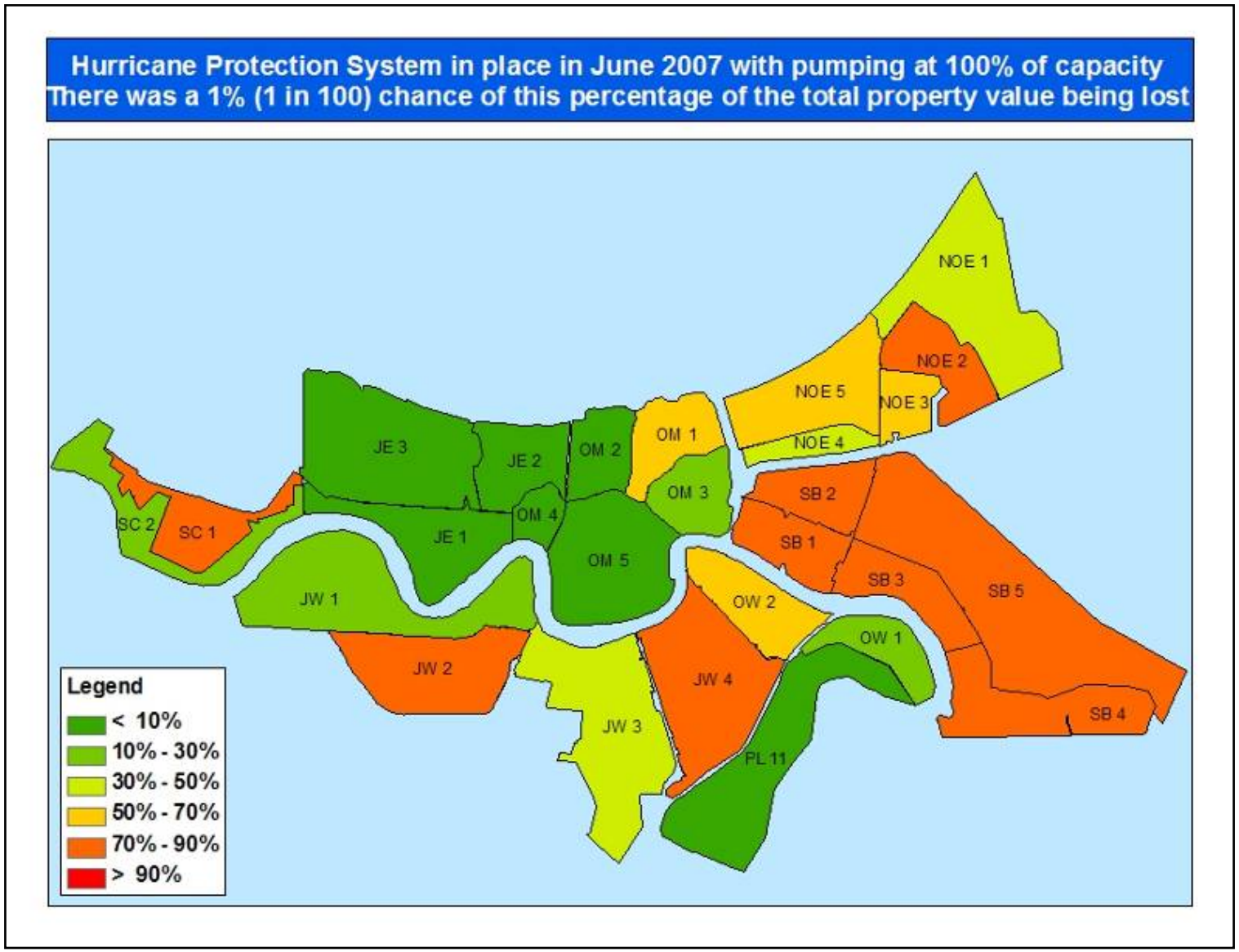

Figure 99. June 2007 % of total value lost (1% chance, 100% pumping).

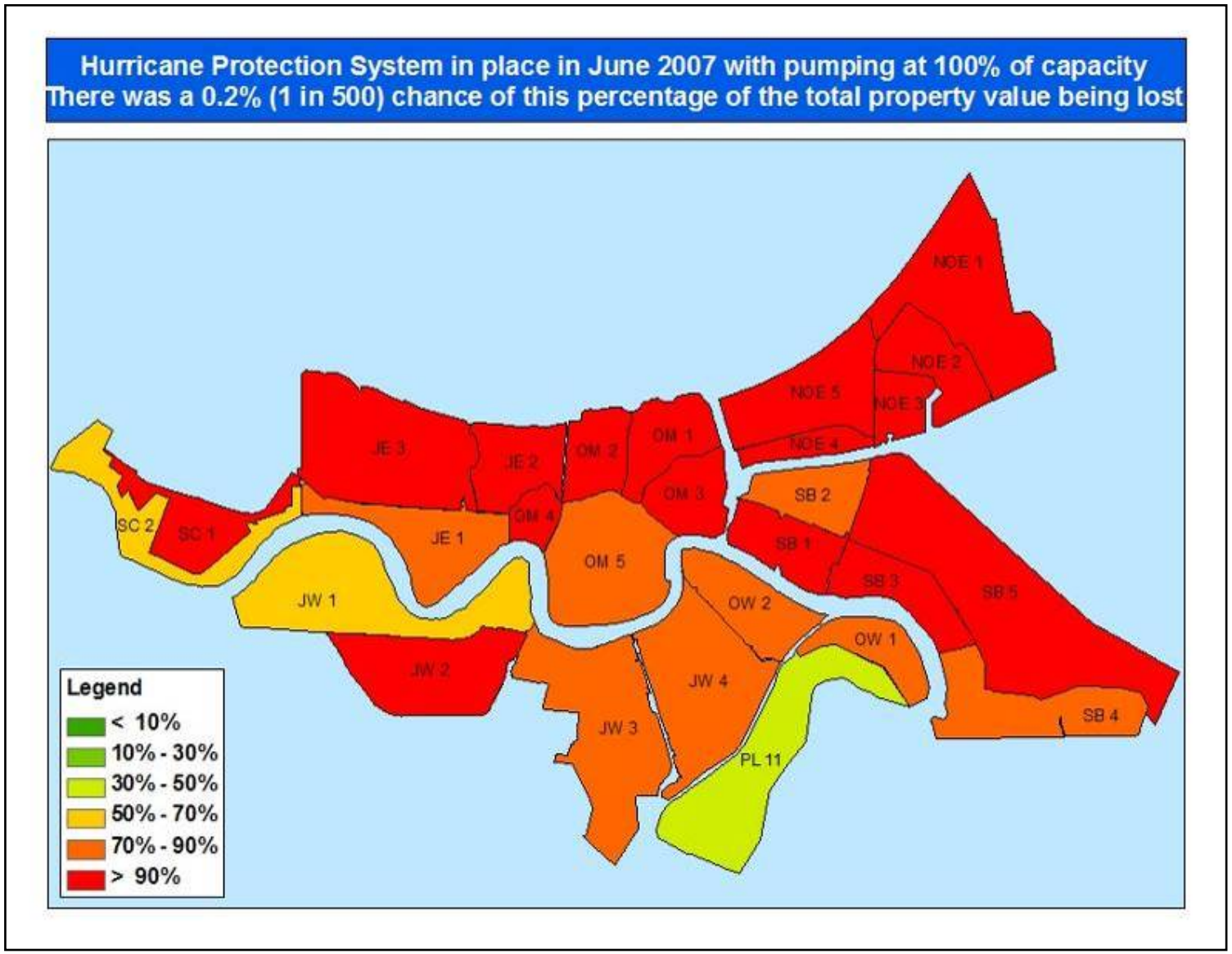

Figure 100. June 2007 % of total value lost (0.2% chance, 100% pumping).

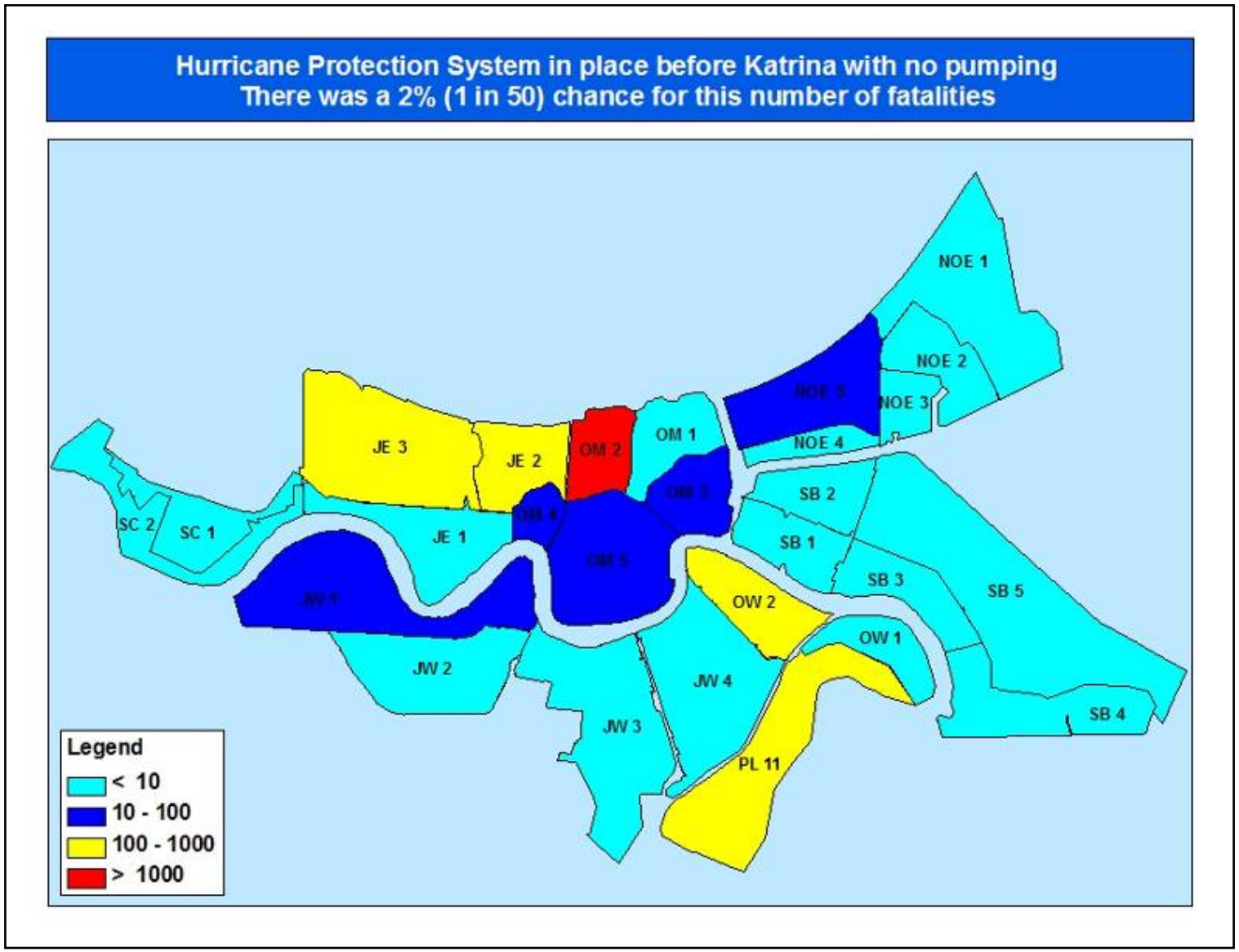

Figure 101. Pre-Katrina potential fatalities (2% chance, no pumping).

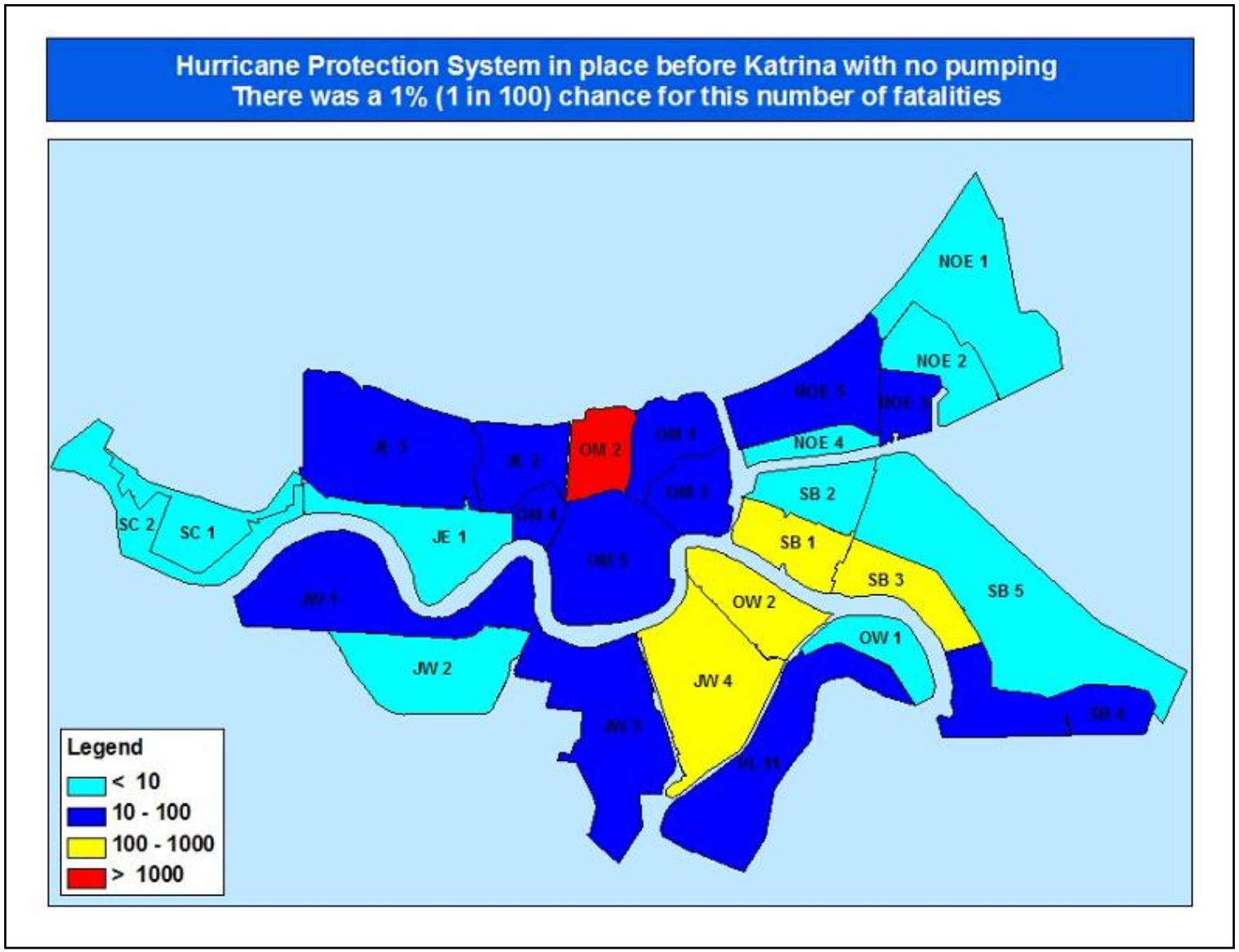

Figure 102. Pre-Katrina potential fatalities (1% chance, no pumping).

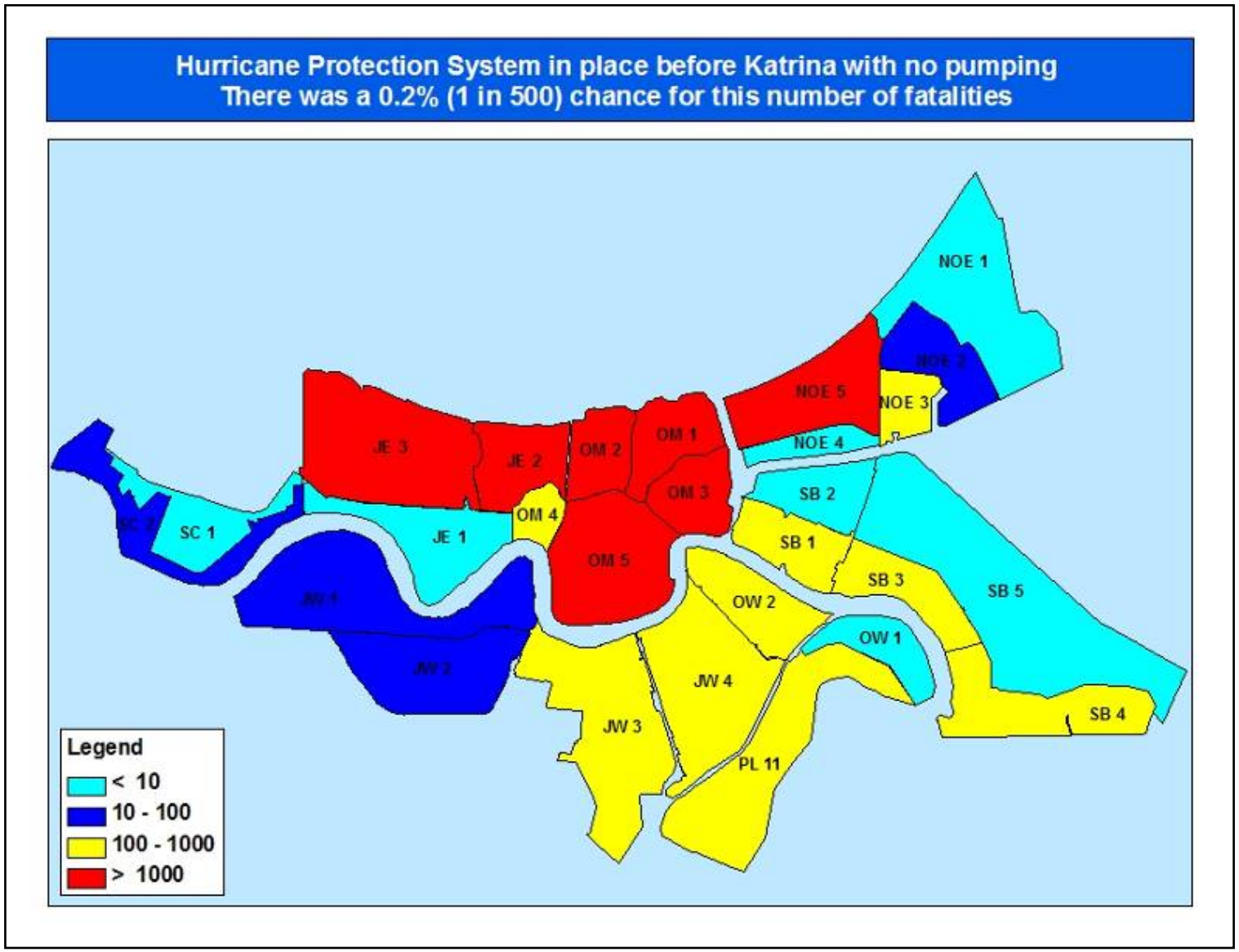

Figure 103. Pre-Katrina potential fatalities (0.2% chance, no pumping).

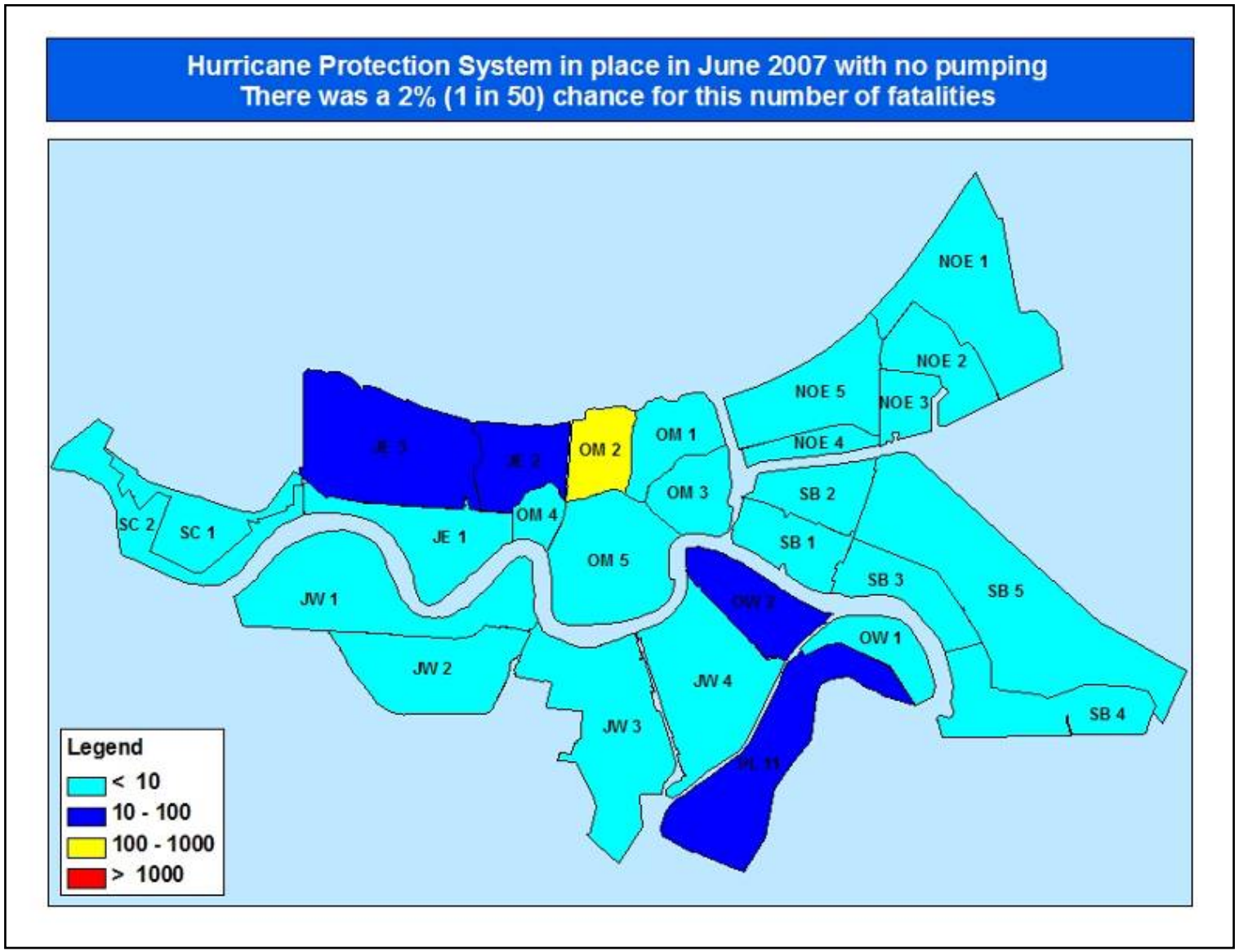

Figure 104. June 2007 potential fatalities (2% chance, no pumping).

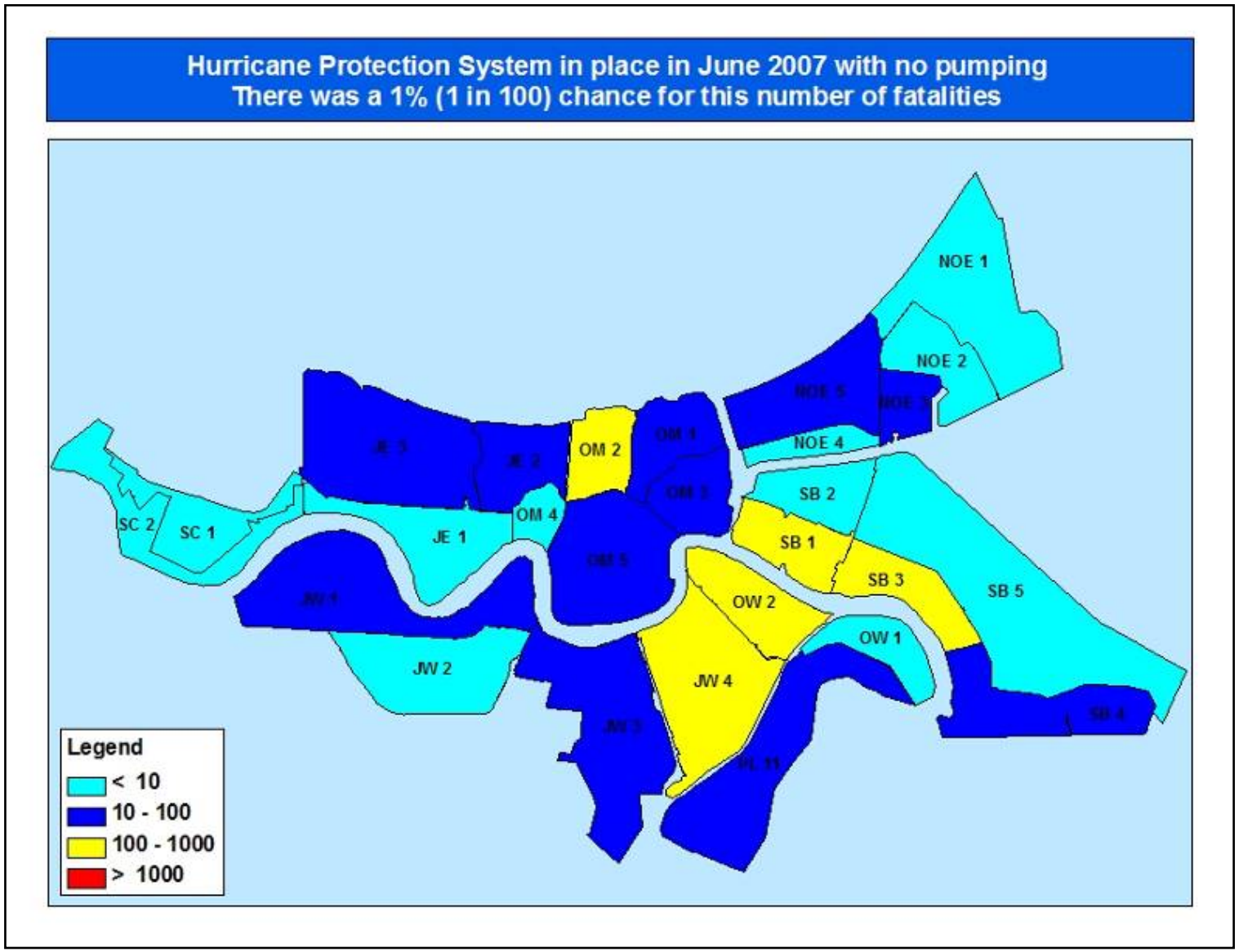

Figure 105. June 2007 potential fatalities (1% chance, no pumping).

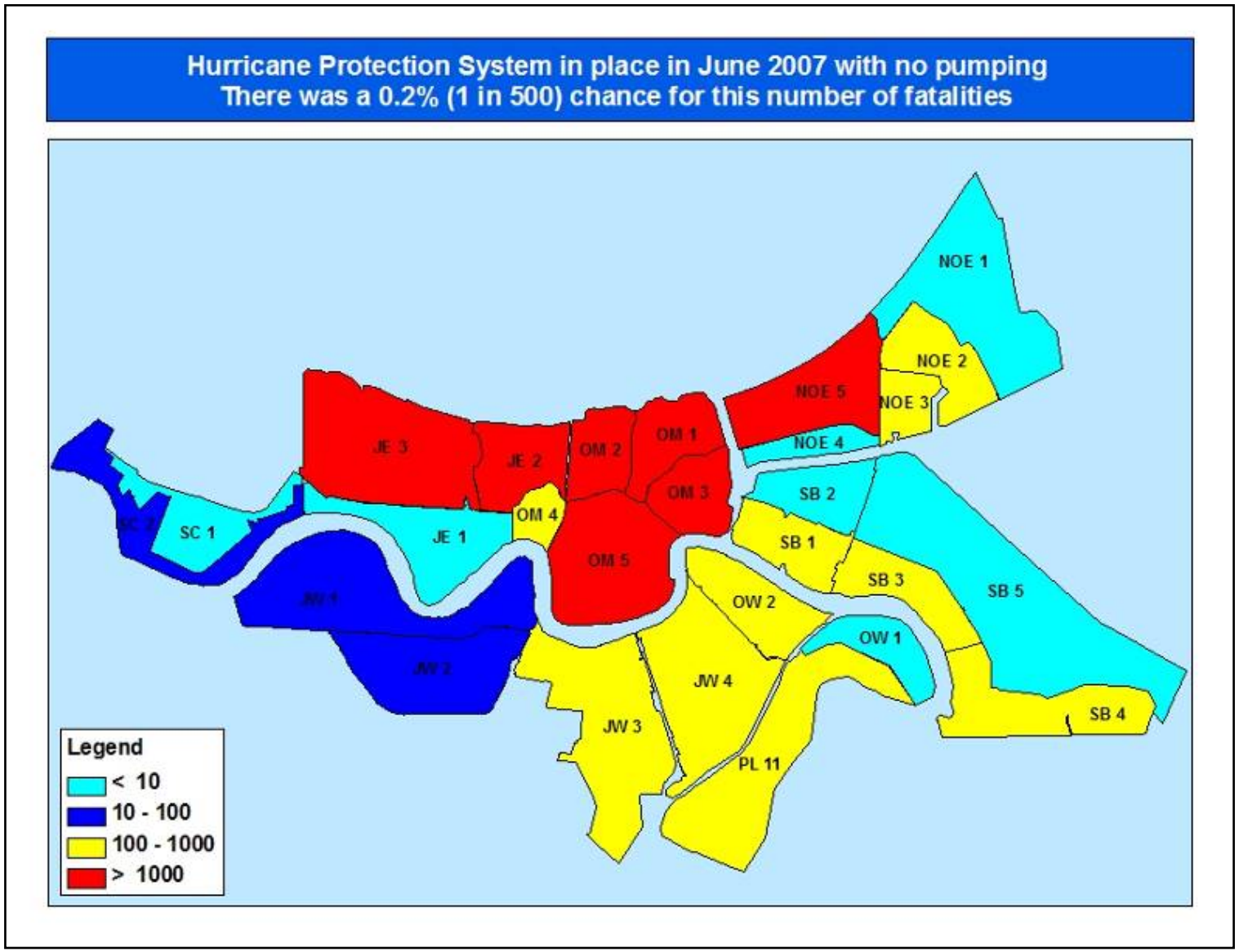

Figure 106. June 2007 potential fatalities (0.2% chance, no pumping).

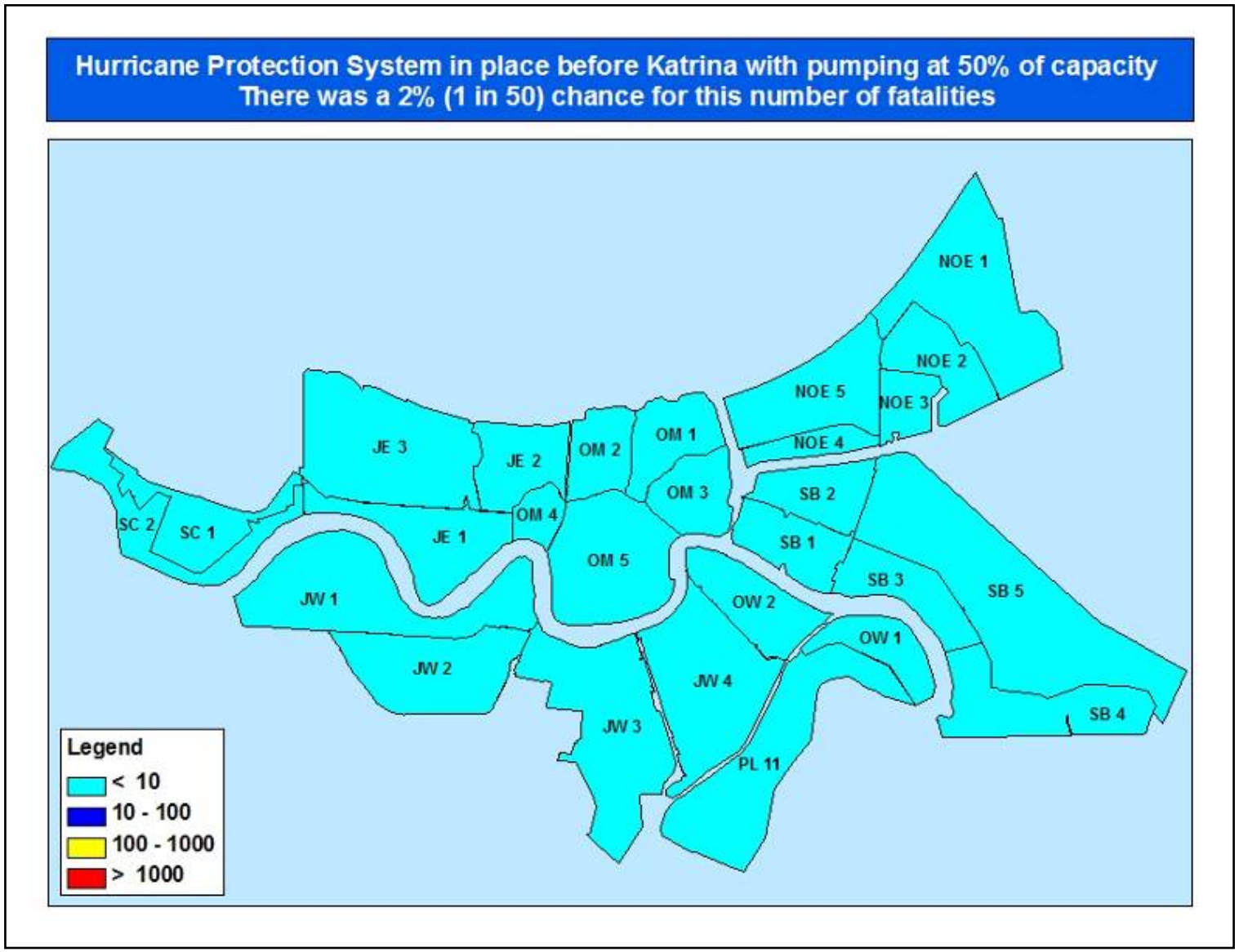

Figure 107. Pre-Katrina potential fatalities (2% chance, 50% pumping).

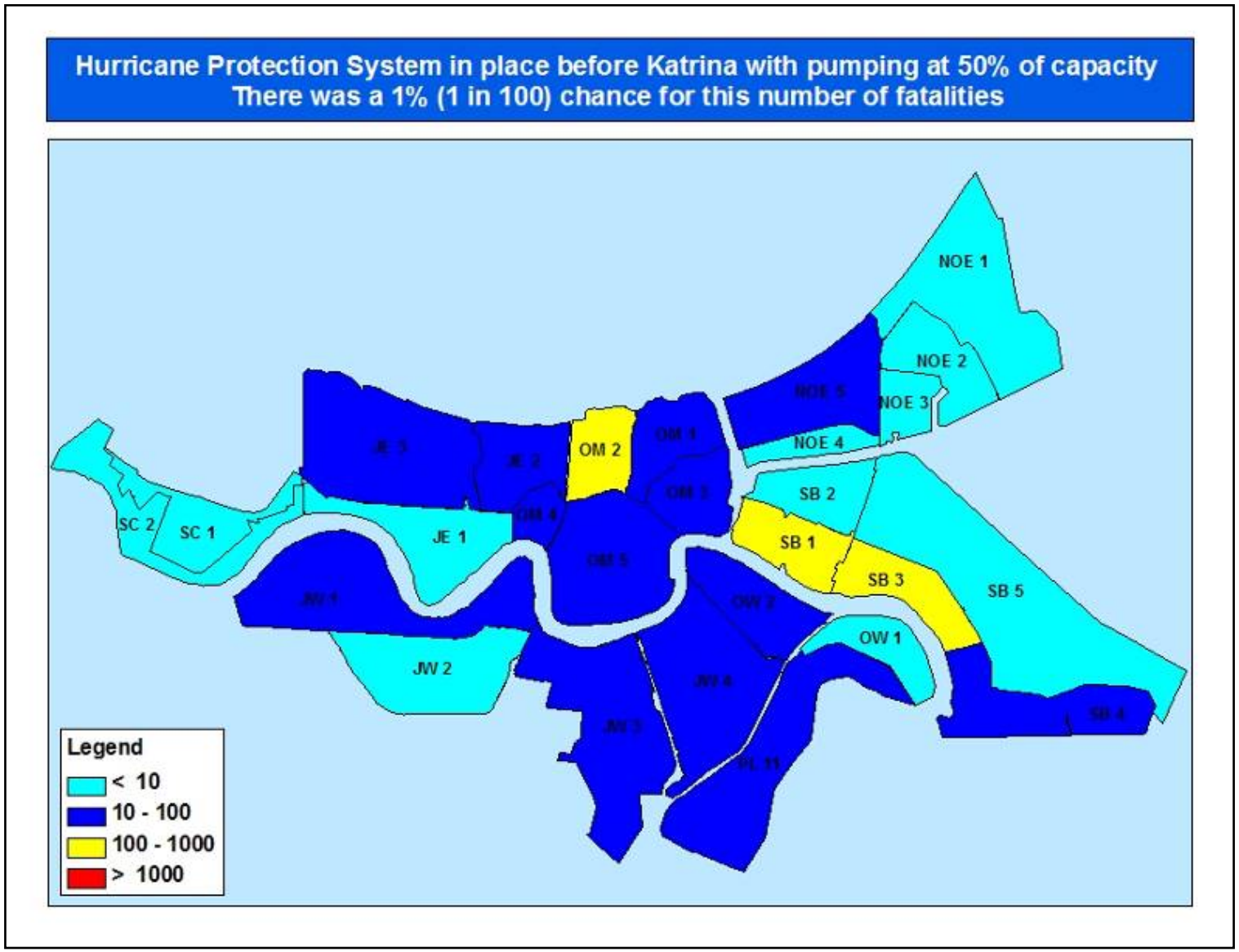

Figure 108. Pre-Katrina potential fatalities (1% chance, 50% pumping).

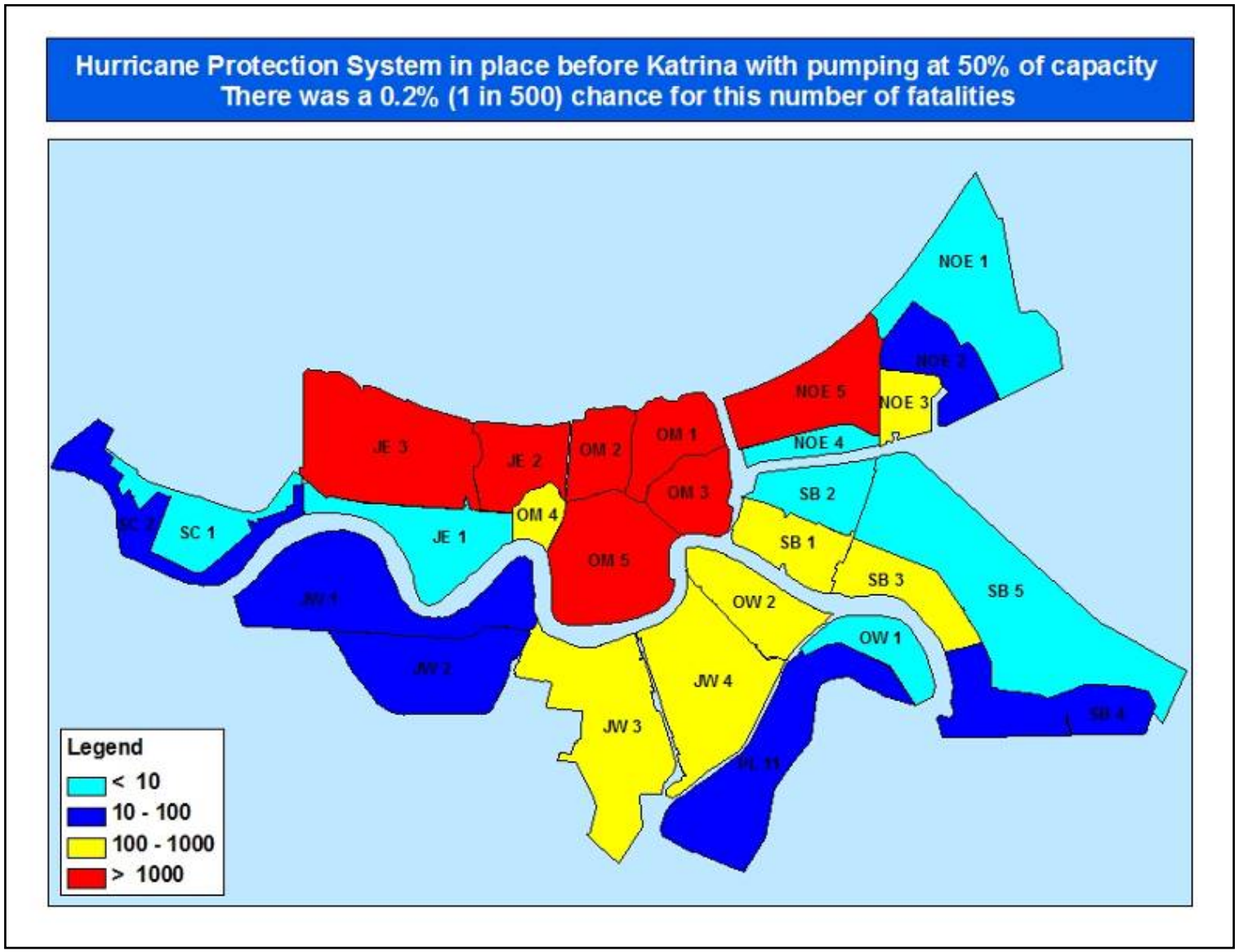

Figure 109. Pre-Katrina potential fatalities (0.2% chance, 50% pumping).

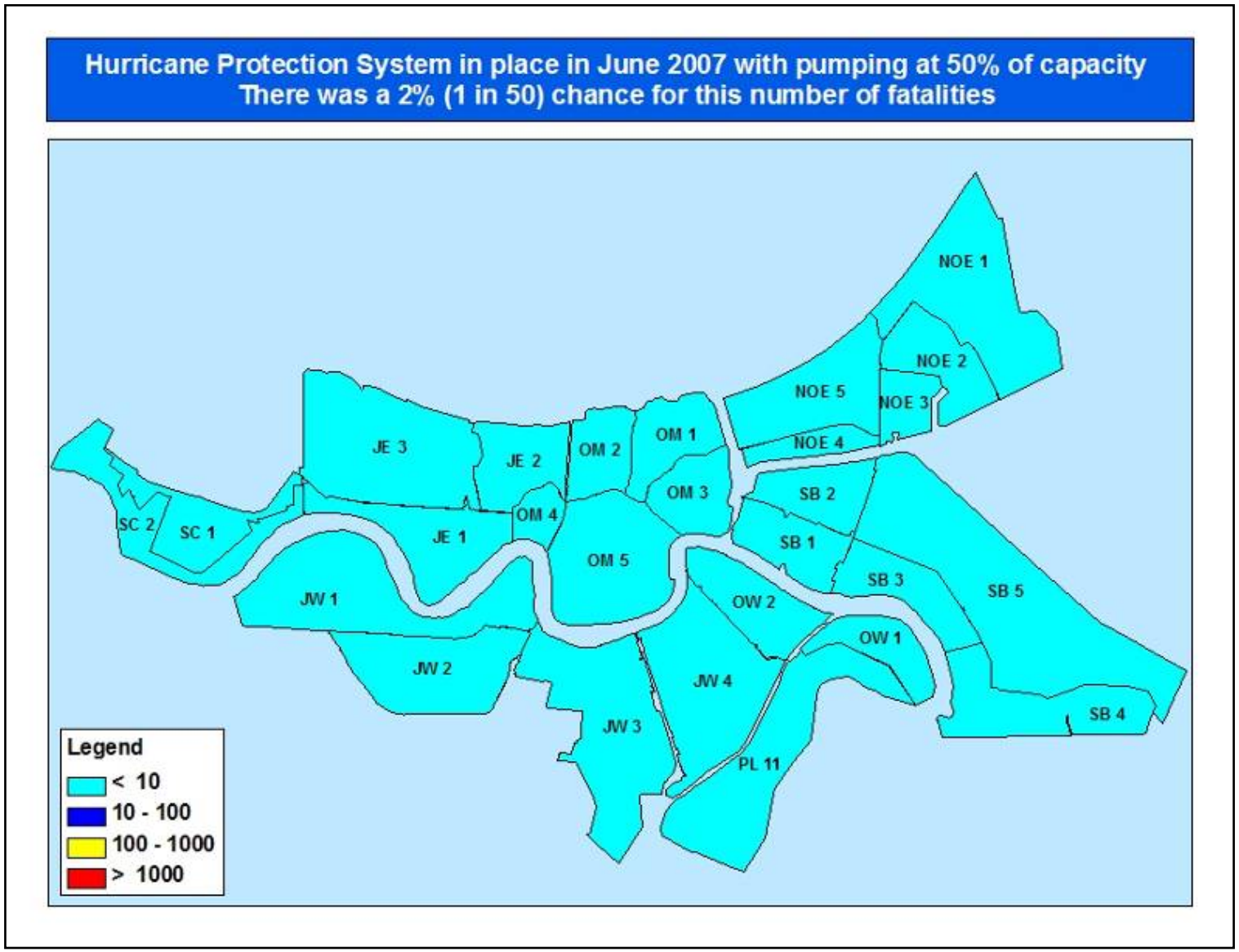

Figure 110. June 2007 potential fatalities (2% chance, 50% pumping).

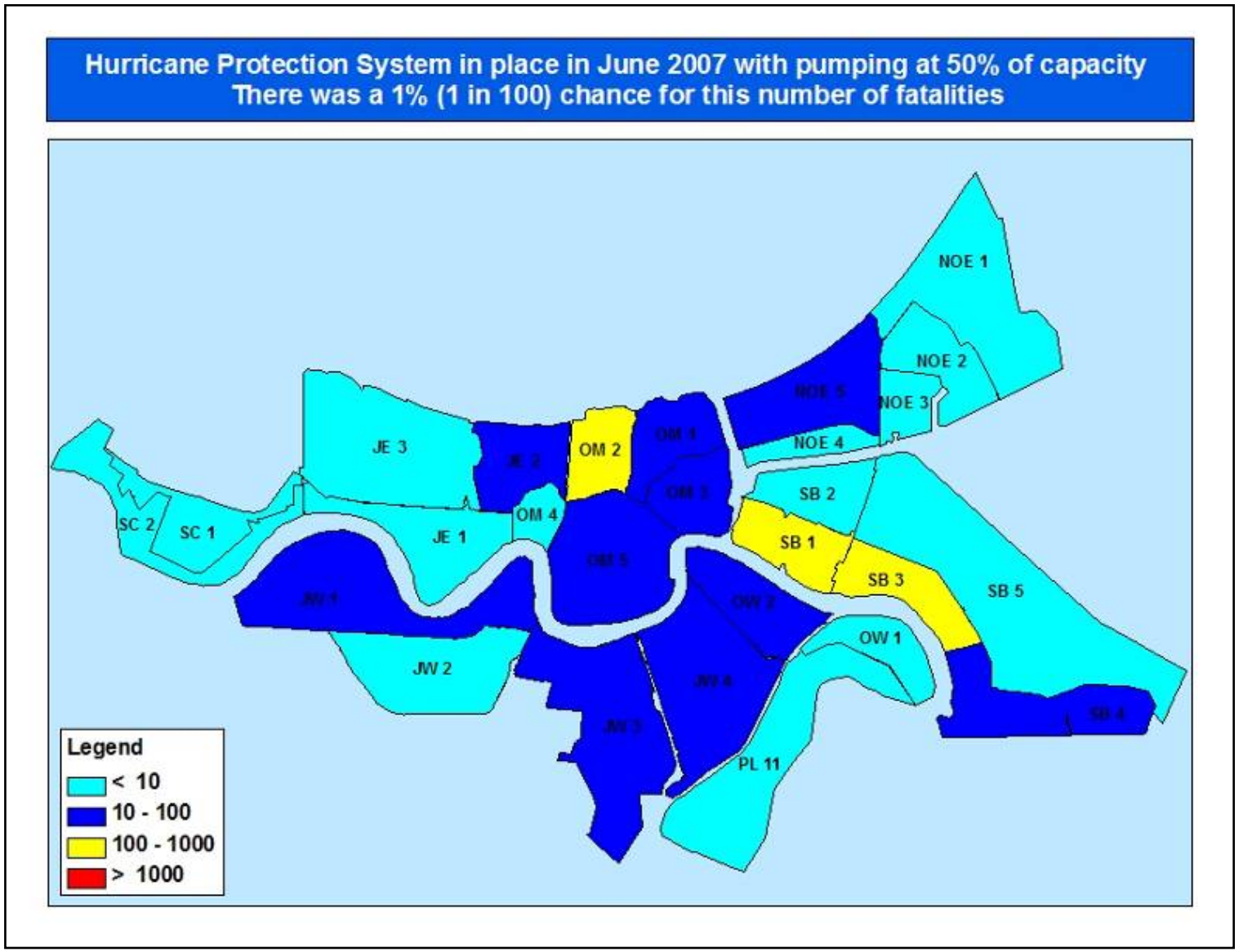

Figure 111. June 2007 potential fatalities (1% chance, 50% pumping).

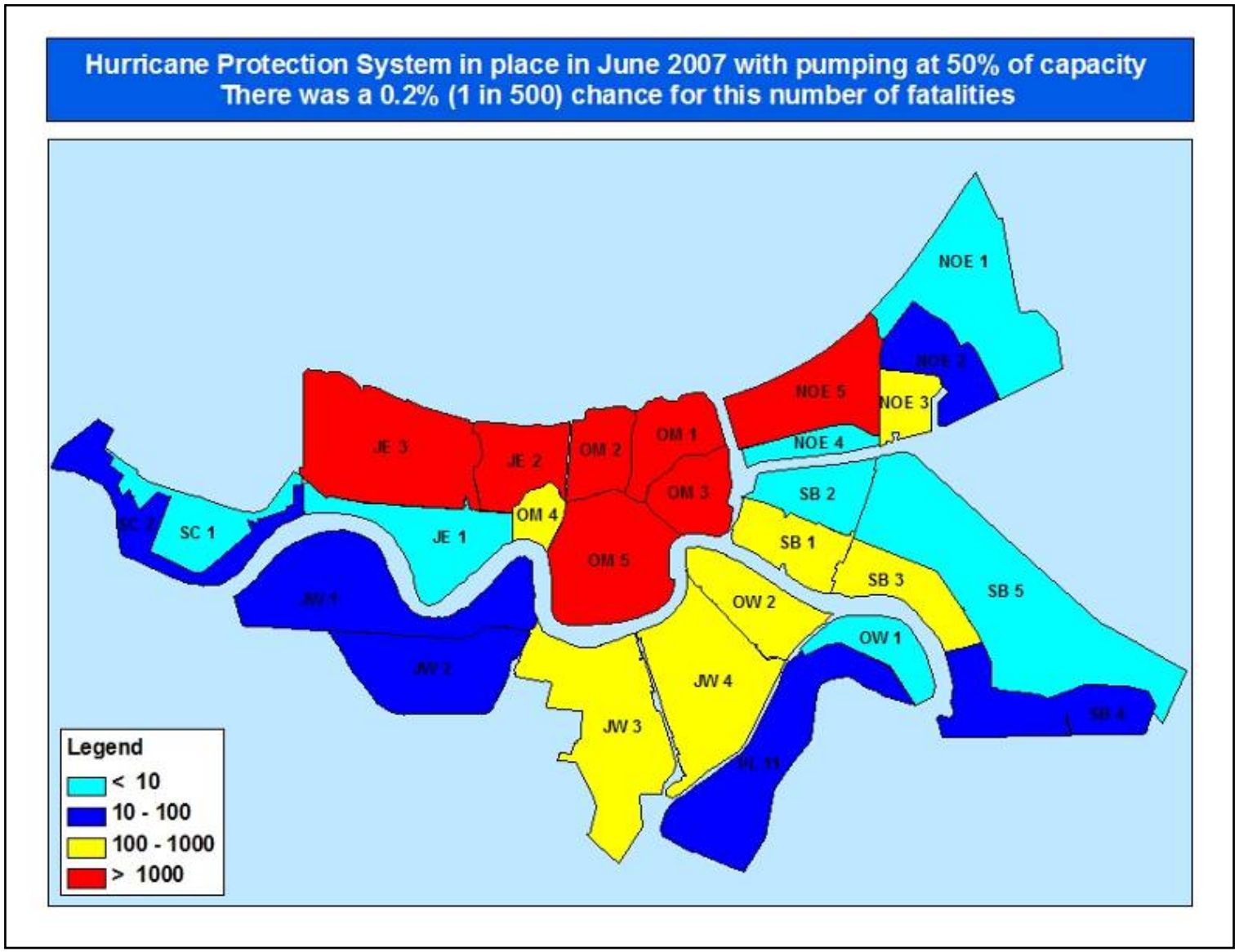

Figure 112. June 2007 potential fatalities (0.2% chance, 50% pumping).

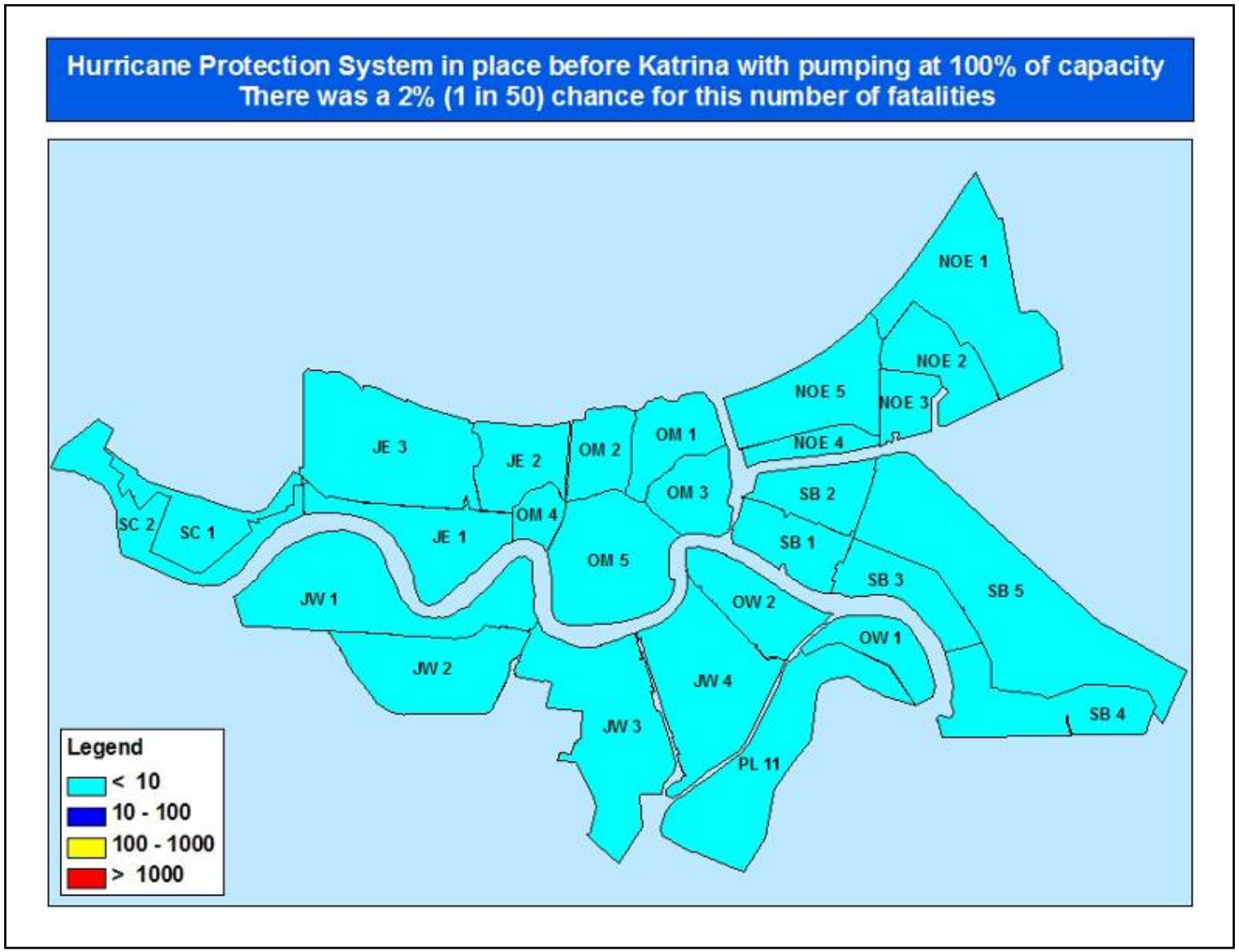

Figure 113. Pre-Katrina potential fatalities (2% chance, 100% pumping).

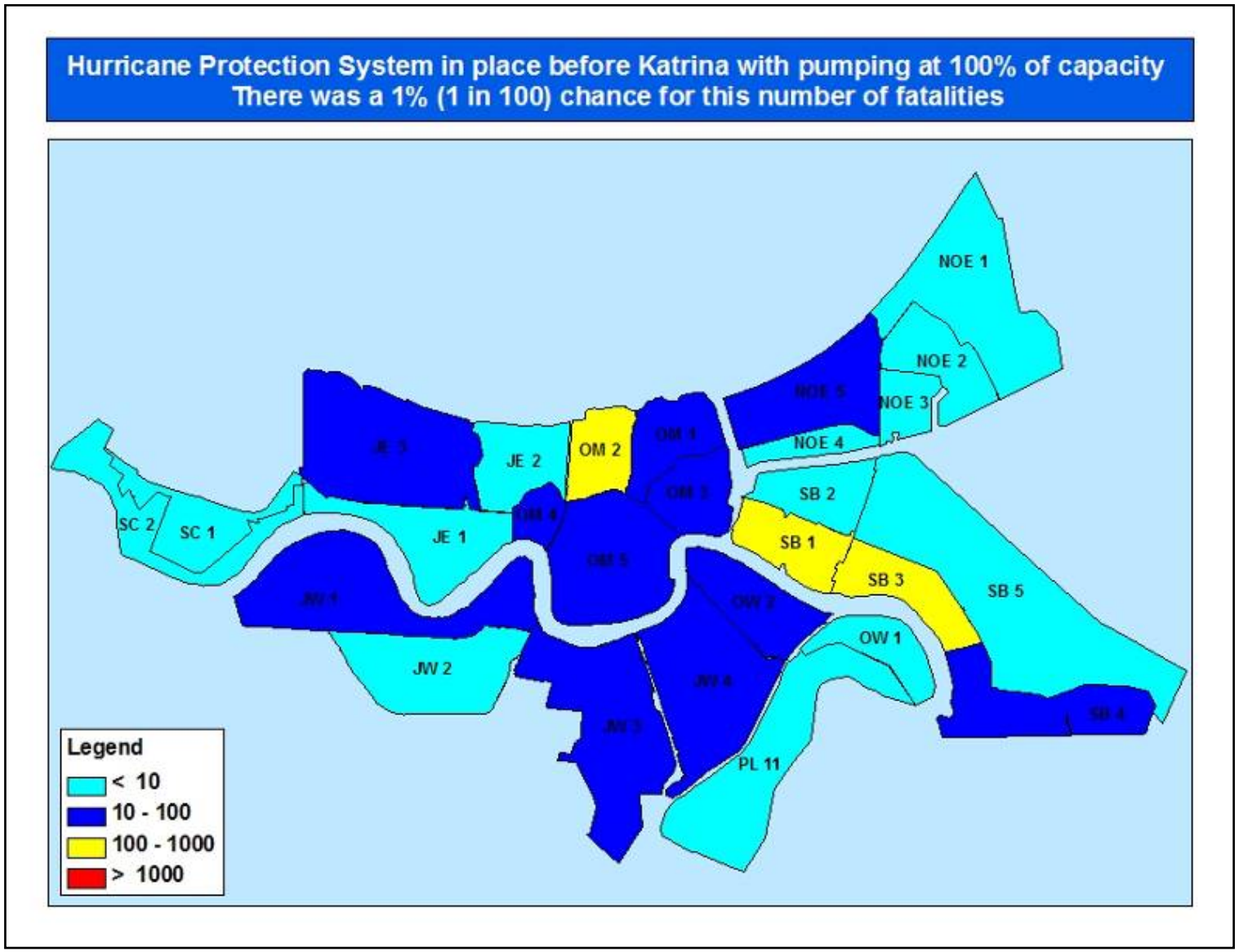

Figure 114. Pre-Katrina potential fatalities (1% chance, 100% pumping).

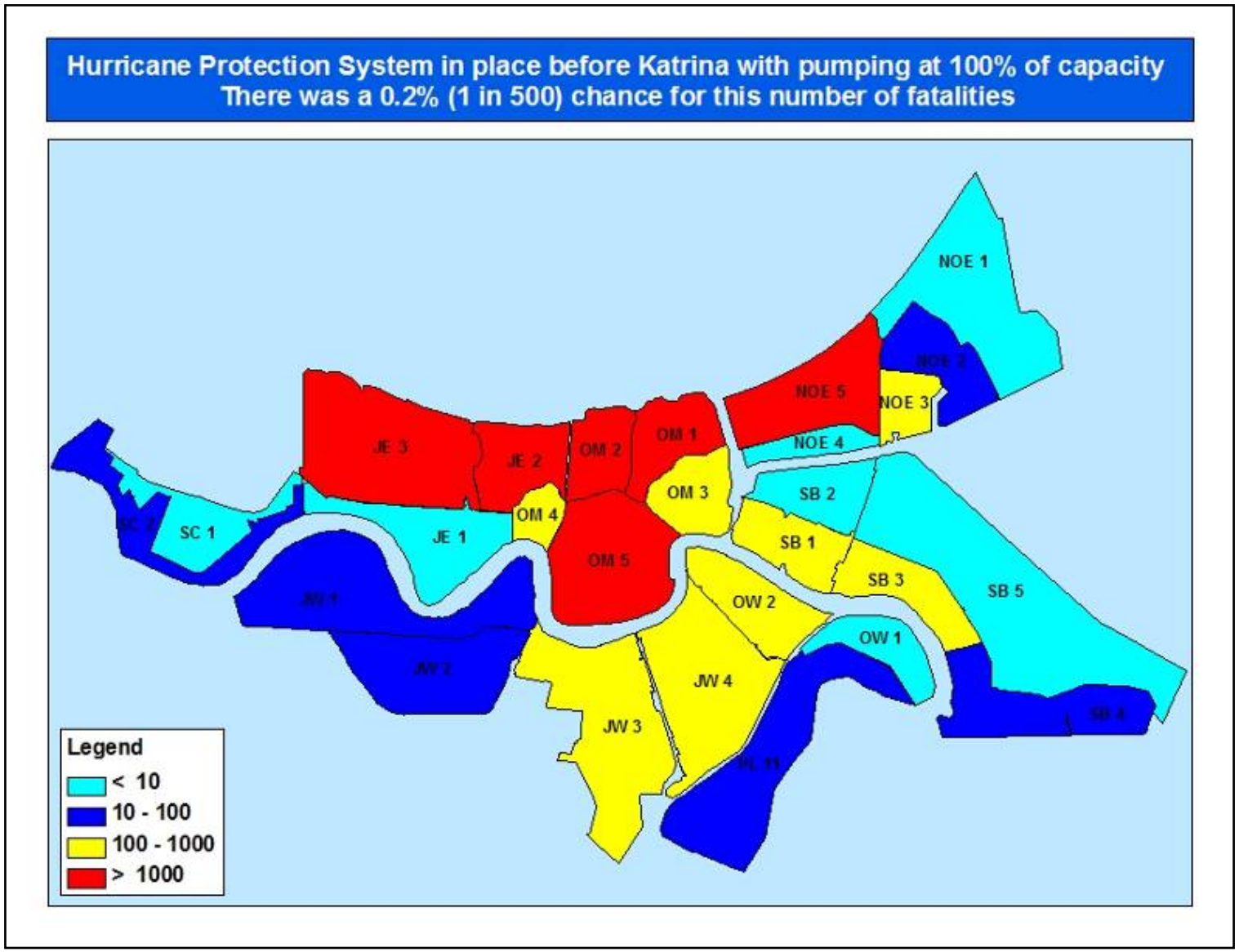

Figure 115. Pre-Katrina potential fatalities (0.2% chance, 100% pumping).

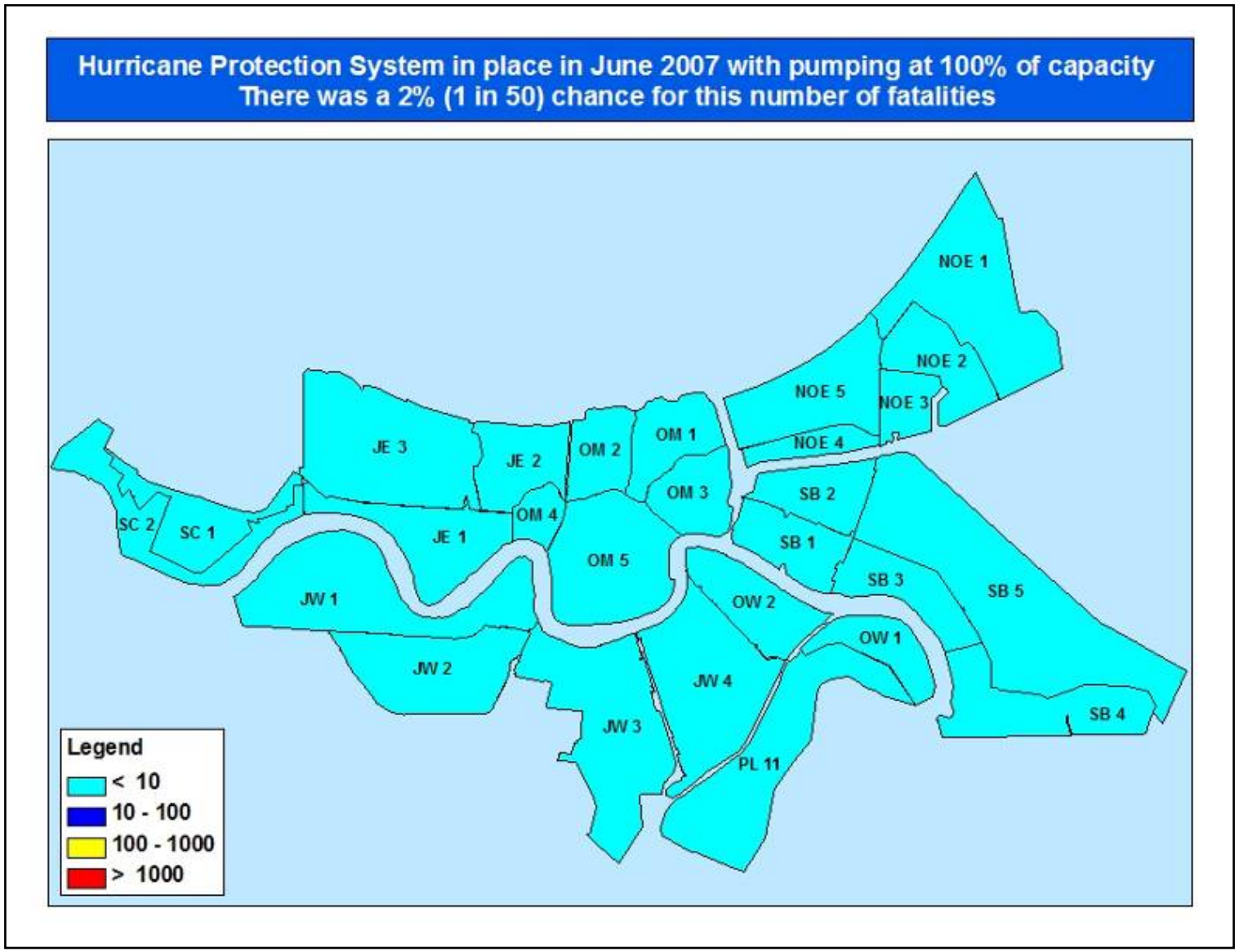

Figure 116. June 2007 potential fatalities (2% chance, 100% pumping).

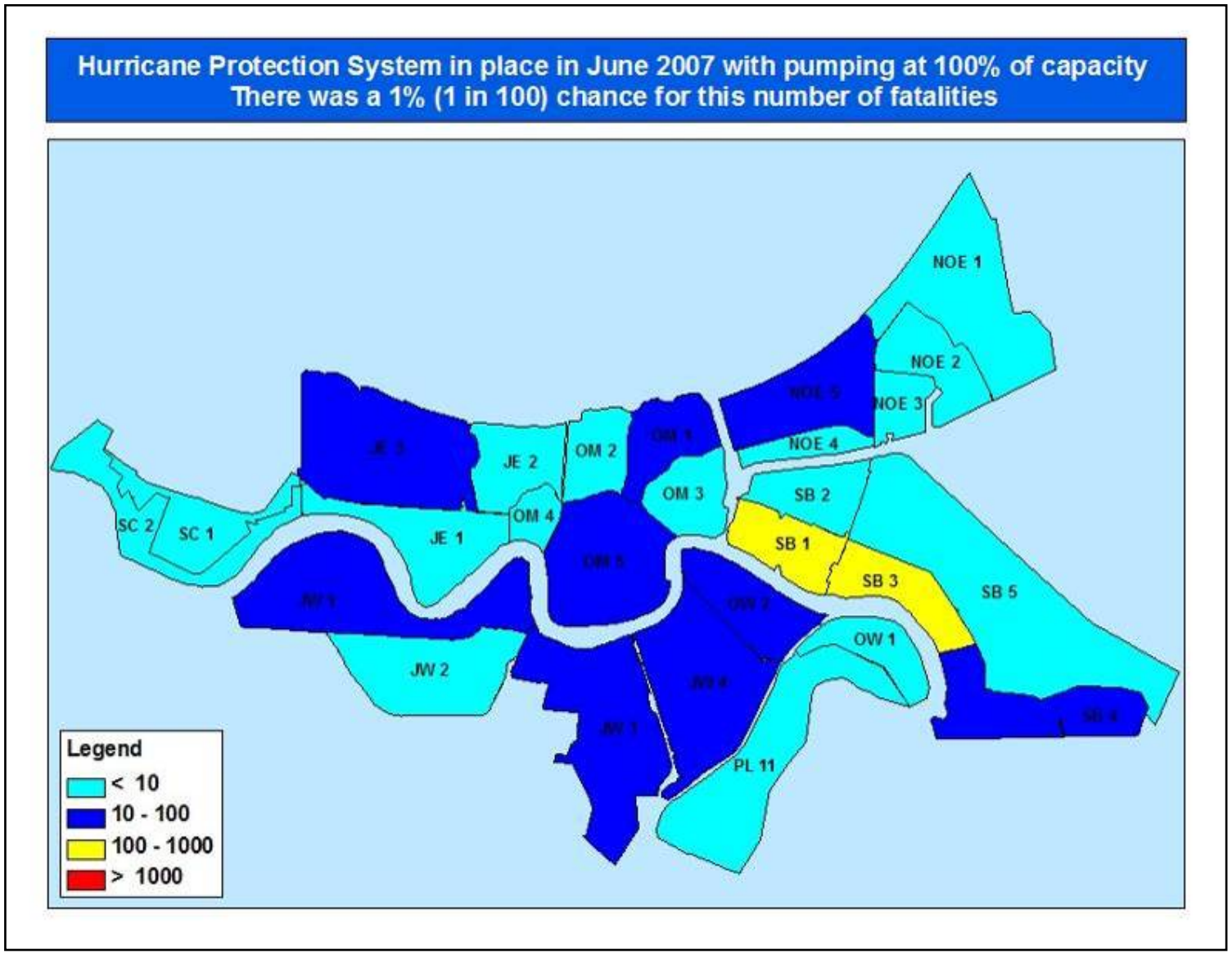

Figure 117. June 2007 potential fatalities (1% chance, 100% pumping).

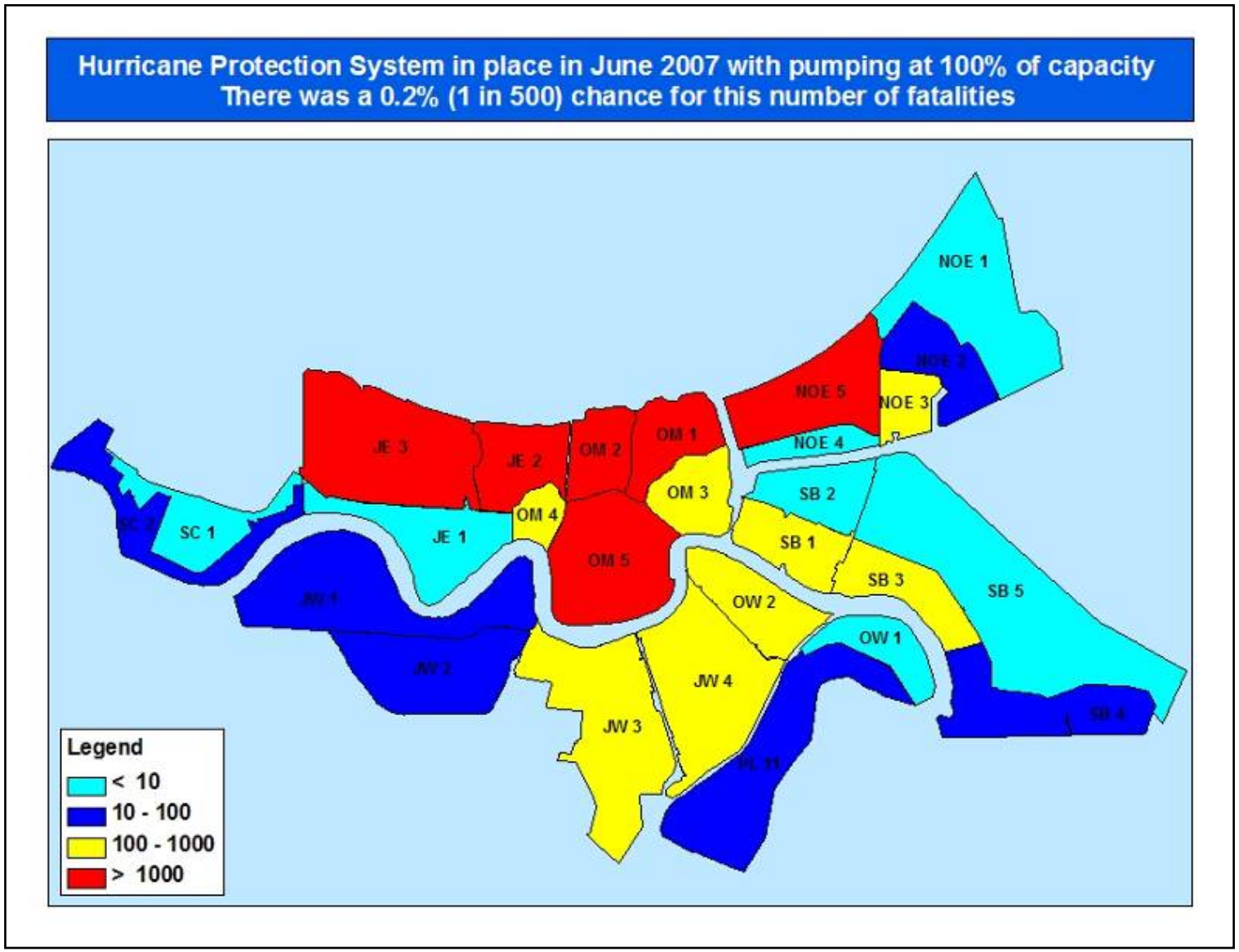

Figure 118. June 2007 potential fatalities (0.2% chance, 100% pumping).

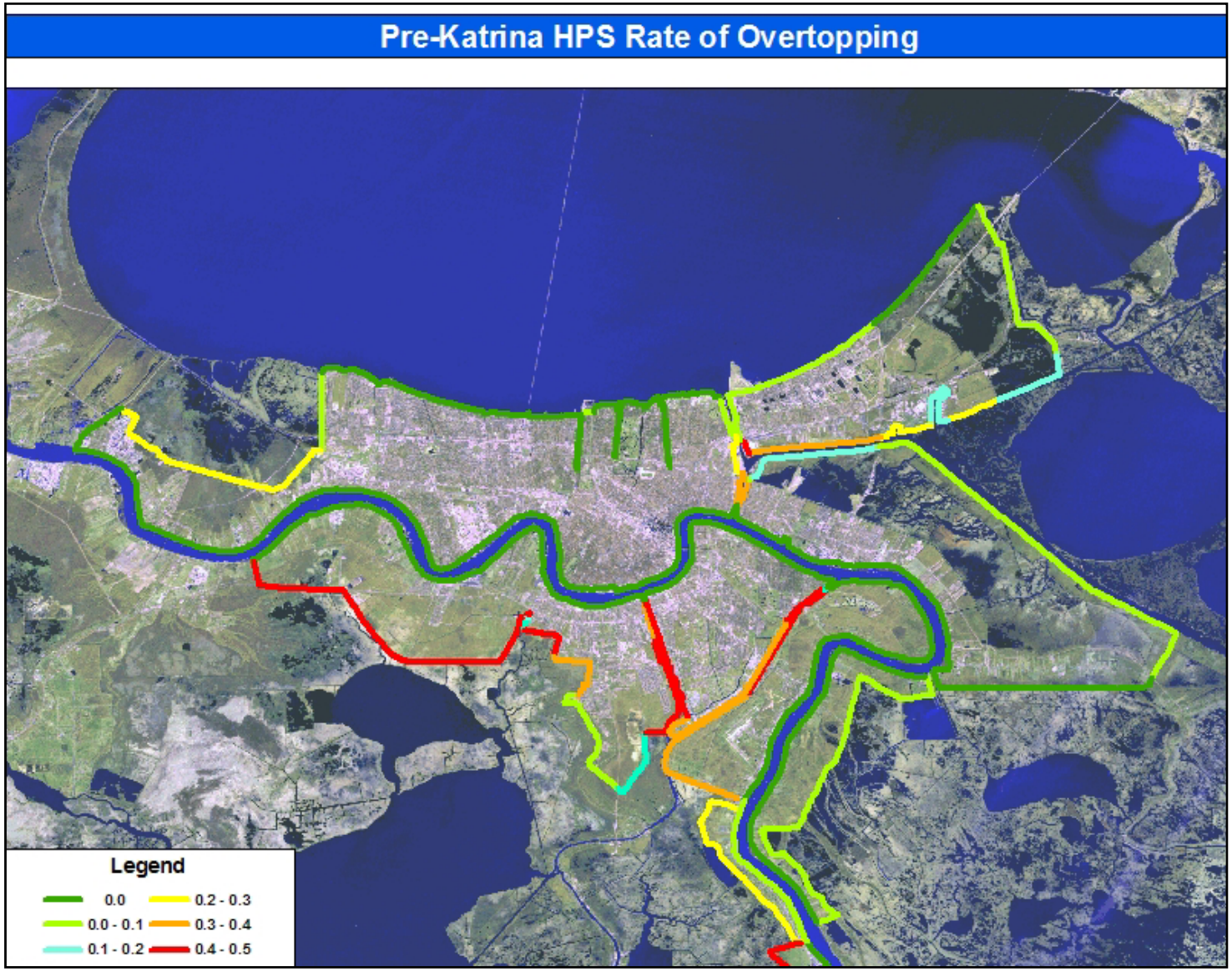

Figure 119. Pre-Katrina HPS rate of overtopping.

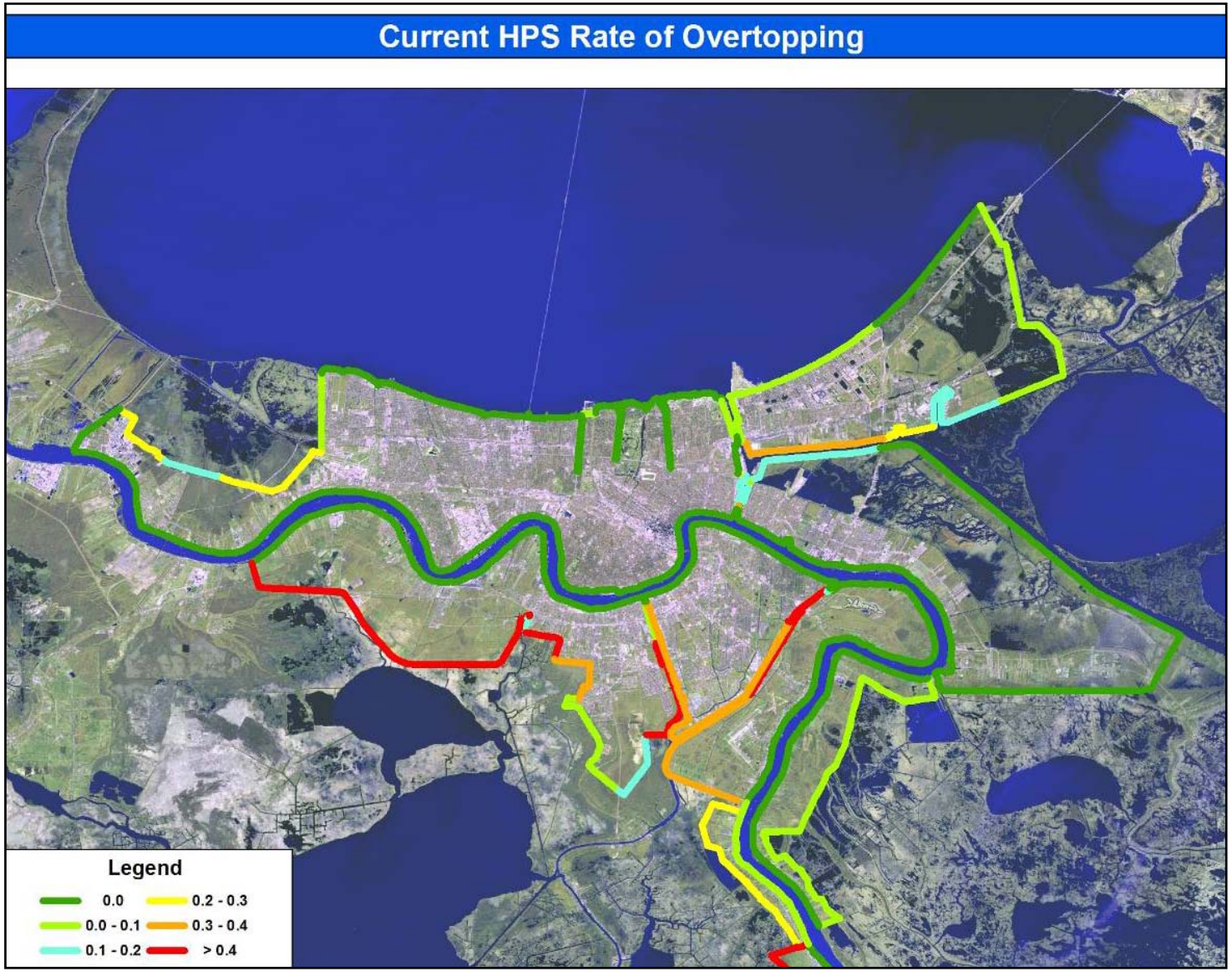

Figure 120. June 2007 HPS rate of overtopping.

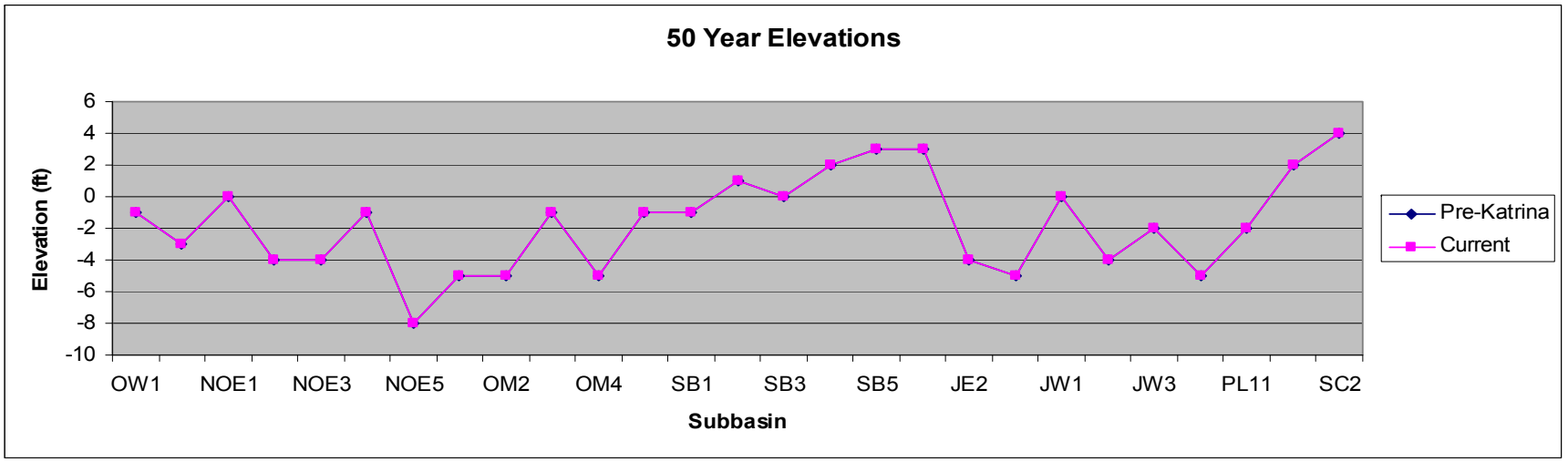

Figure 121. 50 Year Inundation Elevations for Pre-Katrina and June 2007 HPS.

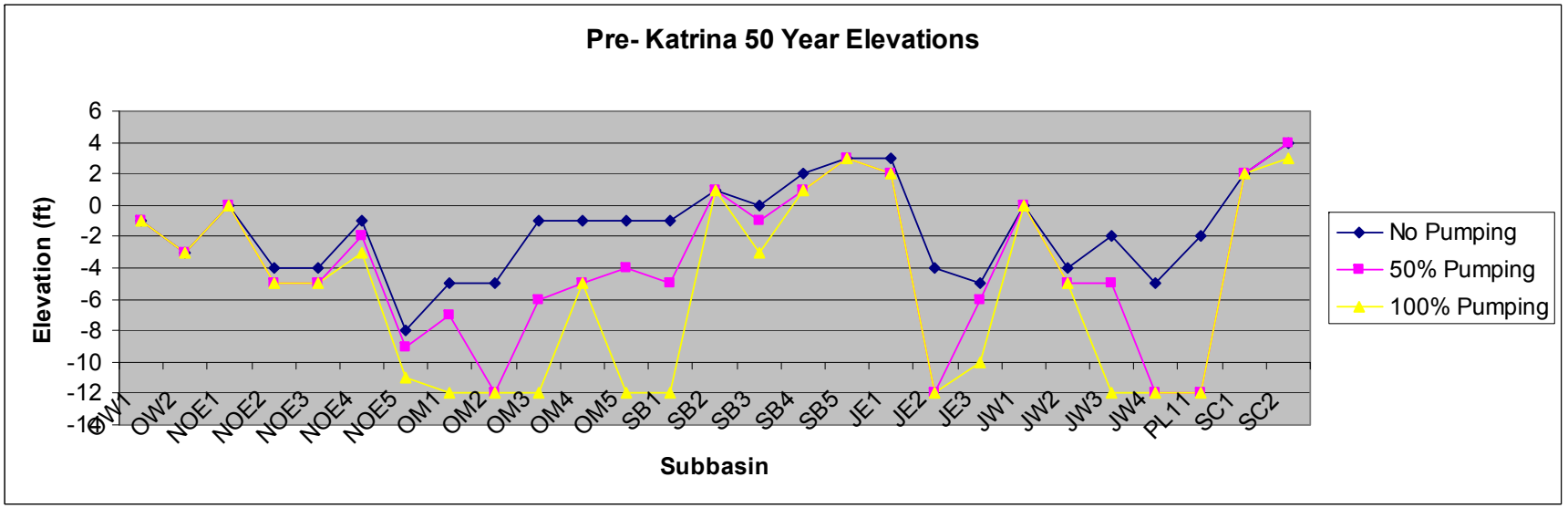

Figure 122. 50 Year Inundation Elevations for Pre-Katrina with Pumping.

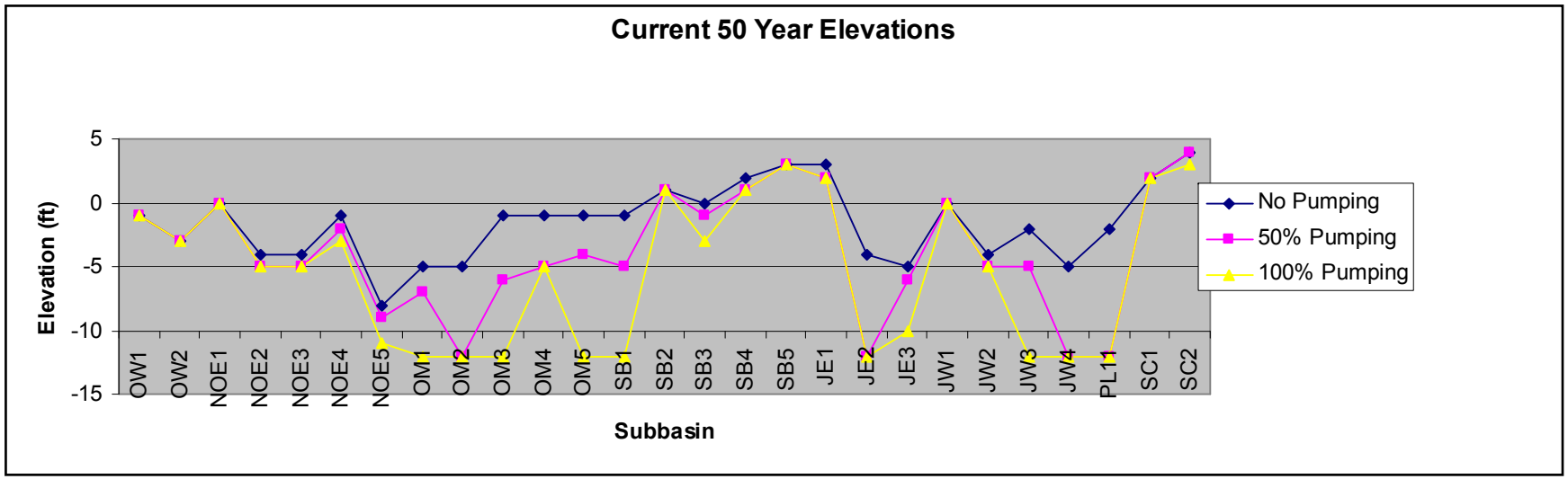

Figure 123. 50 Year Inundation Elevations for June 2007 with Pumping.

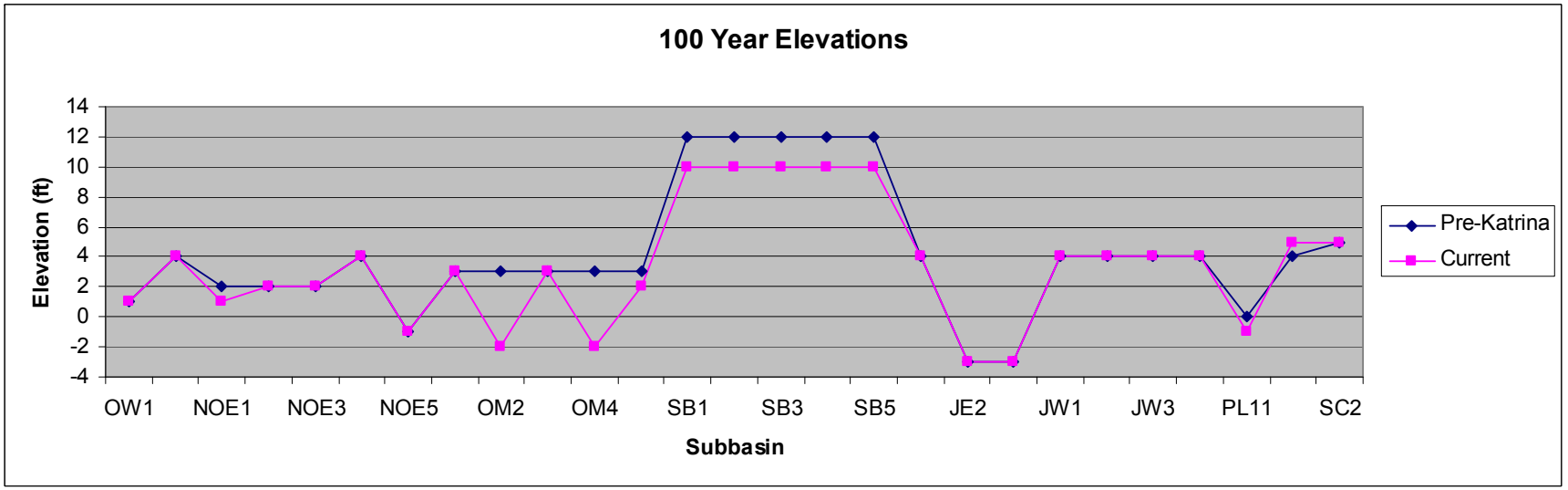

Figure 124. 100 Year Inundation Elevations for Pre-Katrina and June 2007 HPS

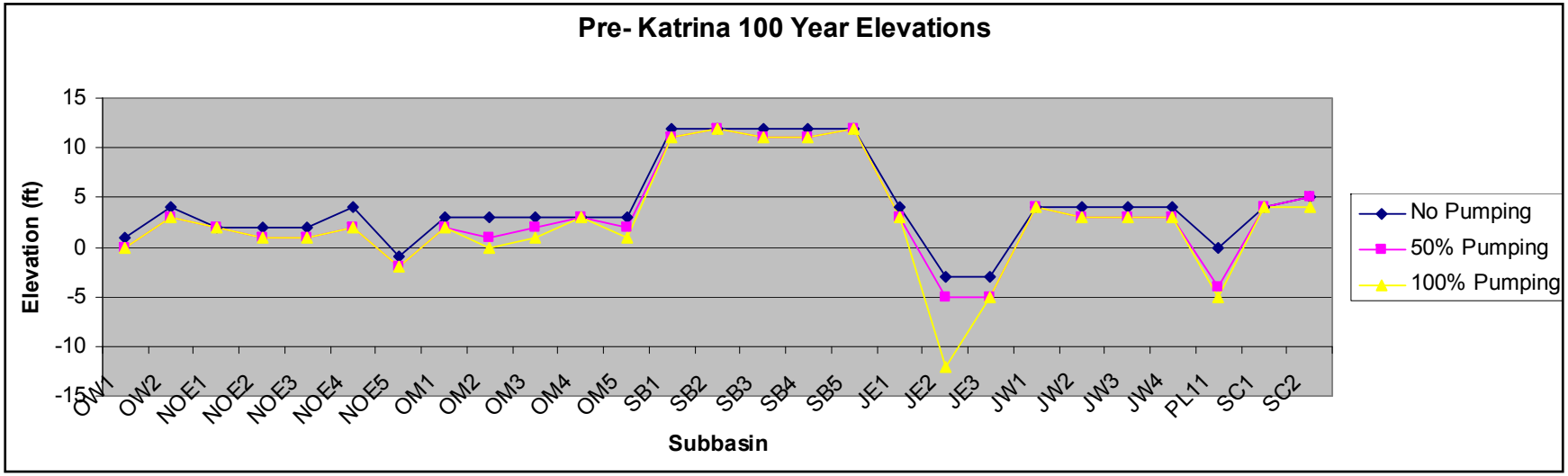

Figure 125. 100 Year Inundation Elevations for Pre-Katrina with Pumping.

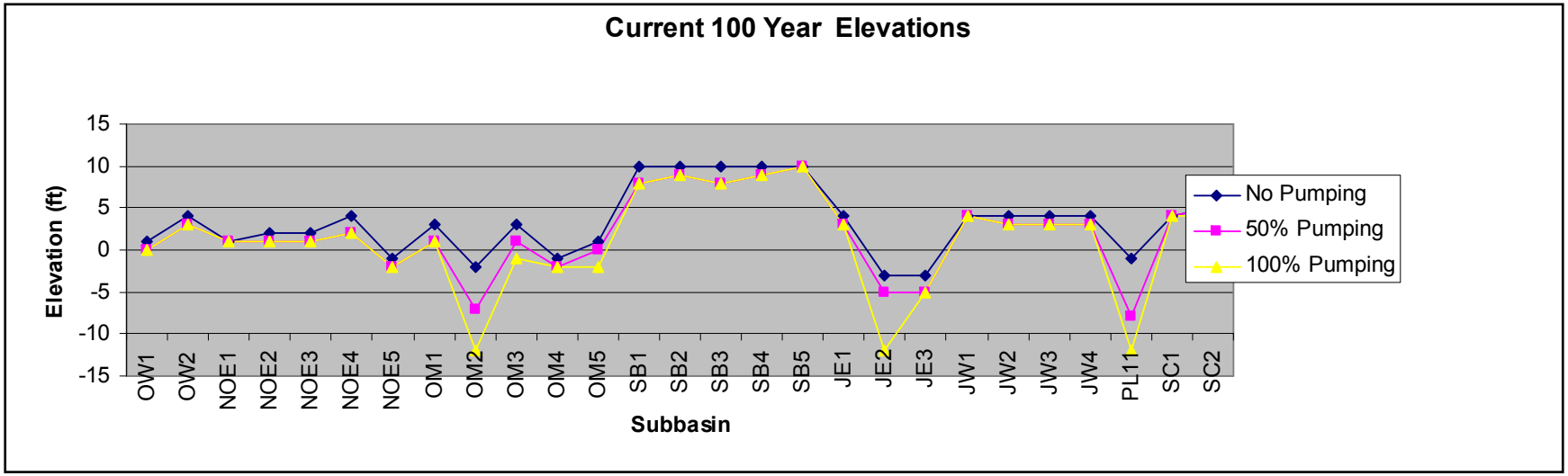

Figure 126. 100 Year Inundation Elevations for June 2007 with Pumping.

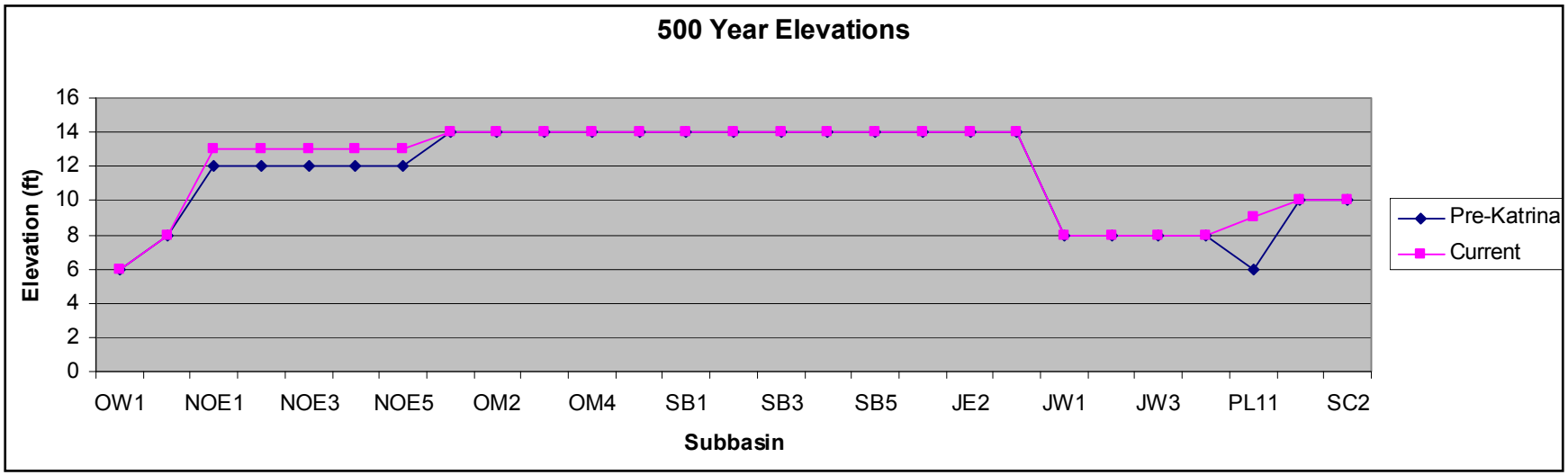

Figure 127. 500 Year Inundation Elevations for Pre-Katrina and June 2007 HPS

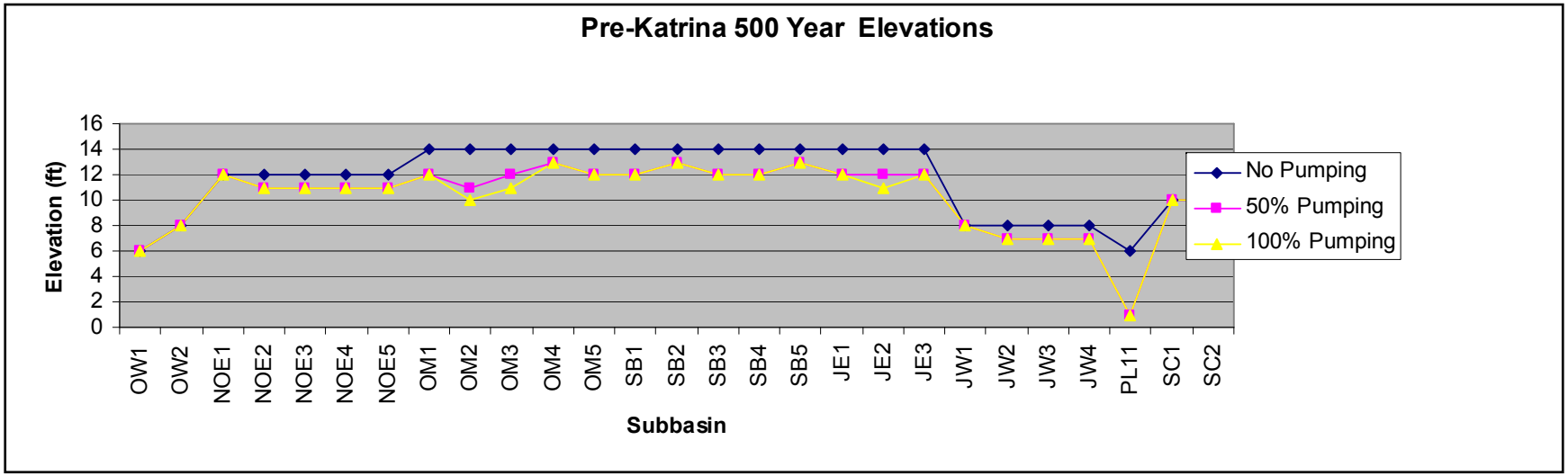

Figure 128. 500 Year Inundation Elevations for Pre-Katrina with Pumping.

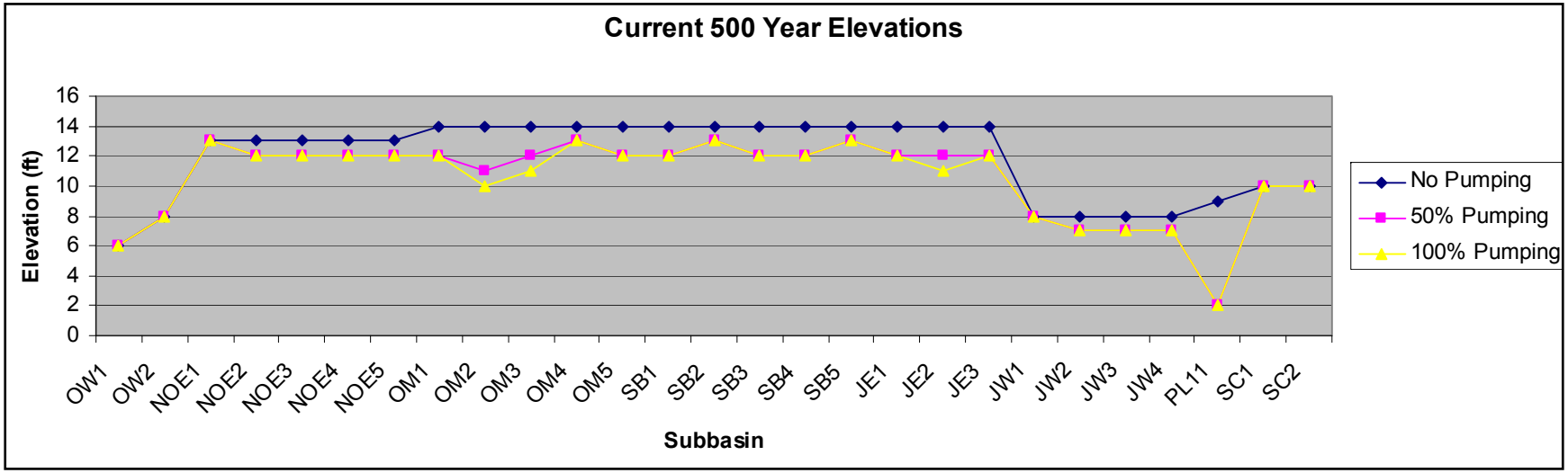

Figure 129. 500 Year Inundation Elevations for June 2007 with Pumping.

References

ADCIRC. 2006. Finite element hydrodynamic model for coastal oceans, inlets, rivers and floodplains. *http://www.nd.edu/~adcirc/index.htm*.

Ang, A.H-S., and W. H. Tang. 2007. *Probability concepts in engineering.* New York: John Wiley and Sons.

ASCE. 1996. *Minimum design loads for buildings and other structures*. ASCE 7-95. New York.

Ayyub, B. M. 2003. *Risk analysis in engineering and economics.* FL: Chapman & Hall/CRC Press.

Baecher, G. B., and J. T. Christian. 2003. *Statistics and reliability in geotechnical engineering.* London and NY: John Wiley and Sons.

Batts, M. E., M. R. Cordes, L. R. Russell, J. R. Shaver, and E. Simiu. 1980. *Hurricane wind speeds in the United States.* Rep. No. BSS-124. Washington, DC: Nat. Bureau of Standards, U.S. Department of Commerce.

Bedford, T., and R. Cooke. 2001. *Probabilistic risk analysis.* Cambridge: Cambridge University Press.

Bister, M., and K. A. Emanuel. 2002. Low frequency variability of tropical cyclone potential intensity. 1: Interannual to interdecadal variability. *J. Geoph. Res.* 107: 4801.

Borgman, L. E., M. Miller, L. Butler, and R. Reinhard. 1992. Empirical simulation of future hurricane storm histories as a tool in engineering and economic analysis. In *Proceedings* Fifth International Conference on Civil Engineering in the Ocean, ASCE, November, College Station, Texas.

Broccoli, A. J., and S. Manabe. 1990. Can existing climate models be used to study anthropogenic changes in tropical cyclone climate? *Geophys. Res. Lett.* 17: 1917-1920.

Cardone, V. J., W. J. Pierson, and E. G. Ward. 1976. Hindcasting the directional spectra of hurricane generated waves. *J. Petrol. Technol.* 28: 385-394.

Chan, J. C. L., and S. L. Liu. 2004. Global warming and Western North Pacific typhoon activity from an observational perspective. *J. Climate* 17: 4590-4602.

Chen, S., M. Lonfat, J. A. Knaff, and F. D. Marks, Jr. 2006. Effects of vertical wind shear and storm motion on tropical cyclone rainfall asymmetries deduced from TRMM. Submitted to *Monthly Weather Review*.

Chouinard, L. E., C. Liu, and C. K. Cooper. 1997. Model for severity of hurricanes in Gulf of Mexico. *J. Waterway, Port, Coastal and Ocean Engineering* 123(3): 120-129.

Chow, S. 1971. A study of the wind field in the planetary boundary layer of a moving tropical cyclone. MS thesis, New York University.

Collins, J. I., and M. J. Viehmann. 1971. A simplified model for hurricane wind fields. Paper 1346, Offshore Technology Conference, Houston, TX.

Cooke, R. 2006. *Uncertainty analysis with high dimensional dependence modeling.* London: John Wiley & Sons.

Dally, W. R., R. G. Dean, and R. A. Dalrymple. 1985. Wave height variation across beaches of arbitrary profile. *Journal of Geophysical Research* 90(6): 11,917-11,927.

Daugherty, R., J. Franzini, and E. Finnemore. 1985. *Fluid mechanics with engineering applications*. New York: McGraw-Hill Book Co.

DeGroot, D. J., and G. B. Baecher. 1993. Estimating auto covariance of in-situ soil properties. *Journal of the Geotechnical Engineering Division, ASCE, v.119*(GT1): 1247-1265.

Dixon, T. H., F. Amelung, and A. Ferretti. 2006. Subsidence and flooding in New Orleans. *Nature* 441: 587-588.

Dokka, R. K. 2006. Modern-day tectonic subsidence in coastal Louisiana. *Geology* 34(4): 281–284.

Eijgenraam, C. J. J. 2006. *Optimal safety standards for dike-ring areas*. CPB Netherlands Bureau for Economic Policy Analysis: CPB Discussion Paper 62.

Elsner, J. B. 2005. Hurricane science review: The next 5 years? Dept. of Geography, Florida State University. *http://garnet.fsu.edu/~jelsner/www*.

Elsner, J. B., and B. Kocher. 2000. Global tropical cyclone activity: A link to the North Atlantic oscillation. *Geophys. Res. Lett.* 27: 129-132.

Emanuel, K. A. 1987. The dependence of hurricane intensity on climate. *Nature* 326: 483-485.

Emanuel, K. A. 2000. A statistical analysis of tropical cyclone intensity. *Mon. Wea. Rev.* 128: 1139-1152.

Emanuel, K. A. 2005a. Increasing destructiveness of tropical cyclones over the past 30 years. *Nature* 436: 686-688.

Emanuel, K. A. 2005b. Anthropogenic effects on tropical cyclone activity. Dept. of Earth and Planetary Sciences, MIT. *http://wind.mit.edu/~emanuel/anthro2.htm*.

Federal Emergency Management Agency (FEMA). 2006. Mitigation Assessment Team Report: Hurricane Katrina in the Gulf Coast - Building performance observations, recommendations, and technical guidance (July 2006). *http://www.fema.gov/library/viewRecord.do?id=1857*

Free, M., M. Bister, and K. A. Emanuel. 2004. Potential intensity of tropical cyclones: Comparison of results from radiosonde and reanalysis data. *J. Climate* 17: 1722-1727.

Georgiou, P. N., A. G. Davenport, and B. J. Vickery. 1983. Design wind speed in regions dominated by tropical cyclones. *J. Wind Engrg. And Industrial Aerodynamics* 13(1): 139-152.

Goldenberg, S. B., C. W. Landsea, A. M. Mestas-Nunez, and W. M. Gray. 2001. The recent increase in Atlantic hurricane activity: Causes and implications. *Science* 293: 474-479.

Grossi, P., and H. Kunreuther. 2005. *Catastrophe modeling: A new approach to managing risk*. New York: Springer-Verlag.

Haarsma, R. J., J. F. B. Mitchell, and C. A. Senior. 1992. Tropical disturbances in a GCM. *Climate Dyn.* 8: 247-257.

Hallegatte, S. 2006. A cost-benefit analysis of the New Orleans Flood Protection System. AEI-Brookings Joint Center: Regulatory Analysis 06-02.

Hartford, D. N. D., and G. B. Baecher. 2004. *Risk and uncertainty in dam safety.* London: Thos. Telford Ltd.

Henderson-Sellers, A., H. Zhang, G. Berz, K. A. Emanuel, W. Gray, C. Landsea, G. Holland, J. Lighthill, S-L. Shieh, P. Webster, and K. McGuffie. 1998. Tropical cyclones and global climate change: A post-IPCC assessment. *Bull. Amer. Meteor. Soc.* 79: 9-38.

Ho, F. P., and V. A. Myers. 1975. *Joint probability method of tide frequency analysis applied to Apalachicola Bay and St. George Sound, Florida*. NOAA Tech. Rep. NWS 18, 43 p.

Ho, F. P., J. C. Su, J. L. Hanevich. R. J. Smith, and F. P. Richards. 1987. *Hurricane climatology for the Atlantic and Gulf Coasts of the United States*. NOAA Technical Report NWS 38. Washington, DC: U.S. Department of Commerce.

Holland, G. J. 1980. An analytic model of the wind and pressure profiles in hurricanes. *Monthly Weather Review* 108: 1212-1218.

Holland, G. J., and P. J. Webster. 2007. Heightened tropical cyclone activity in the North Atlantic: Natural variability or climate trend? Phil. Trans., R. Soc. A., doi:10.1098/rest.2087.2083.

Houghton, J. T., Y. Ding, D. J. Griggs, M. Noguer, P. J. van der Linden, and D. Xiaosu, eds. 2001. Climate Change 2001: The Scientific Basis: Contributions of Working Group I to the Third Assessment Report of the Intergovernmental Panel on Climate Change, Cambridge University Press.

Irish, J. L., Resio, D. T., and J. J. Ratcliff. 2008. The Influence of storm size on hurricane surge. *J. Phys. Oceanogr*., (In Press).

Jack R. Benjamin & Associates, Inc. 2005. *Preliminary seismic risk analysis associated with levee failures in the Sacramento – San Joaquin Delta.* Report to the California Bay-Delta Authority and California Department of Water Resources, Menlo Park.

Jarvinen, B. R., C. J. Neumann, and M. A. S. Davis. 1984. *A tropical cyclone data tape for the North Atlantic Basin 1886-1893: Contents, limitations and uses*. NOAA Tech. Memo. NWS-NHC-22. Washington, DC: U.S. Department of Commerce.

Kimball, S. K. 2006. A modeling study of hurricane landfalls in a dry environment. *Mon. Wea. Rev*. 134: 1901-1918.

Knudsen, J. K., and C. L. Smith. 2000. "Estimation of system failure probability uncertainty including model success criteria." Prepared for Idaho National Engineering Laboratory, Bechtel Corp., Idaho Falls.

Knutson, T. R., and R. E. Tuleya. 2004. Impact of CO_2-induced warming on simulated hurricane intensity and precipitation: Sensitivity to the choice of climate model and convective parameterization. *J. Climate* 17: 3477-3495.

Kurowicka, D., and R. Cooke. 2006. *Uncertainty analysis with high dimensional dependence modeling.* London: John Wiley & Sons.

Landsea, C. W., R. A. Pielke, Jr., A. M. Mestas-Nunez, and J. A. Knaff. 1999. Atlantic Basin Hurricanes: Indices of climatic changes. *Climatic Change* 42: 89-129.

Lighthill, J., G. J. Holland, W. M. Gray, C. Landsea, K. A. Emanuel, G. Craig, J. Evans, Y. Kurihara, and C. P. Guard. 1994. Global climate change and tropical cyclones. *Bull. Amer. Meteor. Soc.* 75: 2147-2157.

Linkov, I., and A. B. Ramadan. 2005. *Overcoming uncertainties in risk analysis: Trade-offs among methods of uncertainty analysis.* NATO Science Series: IV: Earth and Environmental Sciences. Netherlands: Springer-Verlag.

Lonfat, M., F. D. Marks, Jr., and S. S. Chen. 2004. Precipitation distribution in tropical cyclones using the tropical rainfall measuring mission (TRMM) microwave imager: A global perspective. *Mon. Wea. Rev.* 132: 1645-1660.

Luettich, R. A., J. J. Westerink, and N. W. Scheffner. 1992. *ADCIRC: An advanced three-dimensional circulation model for shelves, coasts and estuaries; Report 1: Theory and methodology of ADCIRC-2DDI and ADCIRC-3DL*. Technical Report DRP-92-6. Vicksburg, MS: Coastal Engineering Research Center, U.S. Army Engineer Waterways Experiment Station.

Melchers, R. 1999. *Structural reliability analysis and prediction.* New York: John Wiley and Sons.

Michaels, P. J., P. C. Knappenberger, and C. W. Landsea. 2005. Comments on "Impact of CO_2-induced warming on simulated hurricane intensity and precipitation: Sensitivity to the choice of climate model and convective parameterization." *J. Climate,* in press.

Modarres, M., M. Kaminskiy, and V. Krivstov. 1999. *Reliability engineering and risk analysis: A practical guide*. New York: Marcel Decker Inc.

Morgan, M. G., and M. Henrion. 1990. *Uncertainty: A guide to dealing with uncertainty in quantitate risk and policy analysis*. Cambridge: Cambridge University Press.

Muir-Wood, R., and W. Bateman. 2005. Uncertainties and constraints on breaching and their implications for flood loss estimation. *Philosophical Transactions of the Royal Society A: Mathematical, Physical, and Engineering Sciences* 363(1831): 1423-1430.

Myers, V. A. 1954. Characteristics of United States hurricanes pertinent to levee design for Lake Okeechobee, Florida. Hydromet. Rep. No. 32. Washington, DC: U.S. Weather Bureau.

Myers, V. A. 1975. *Storm tide frequencies on the South Carolina coast*. NOAA Tech. Rep. NWS-16.

Myers, V.A. 1954: Characteristics of United States hurricanes pertinent to levee design for Lake Okeechobee, Florida, Hydromet. Rep. No. 32, U.S. Weather Bureau, Washington, DC.

National Flood Insurance Program (NFIP). 2006. Flood insurance manual: May 2005 (Revised October 2006). *http://www.fema.gov/business/nfip/manual200610.shtm*

Neumann, C. J. 1991. *The National Hurricane Center Risk Analysis Program (HURISK)*. NOAA Tech. Memo. NWS-NHC-38. Washington, DC: U.S. Department of Commerce.

Paté-Cornell, E. 2002. Risk and uncertainty analysis in government safety decisions. *Risk Analysis 22*(3): 633-646.

Pielke, R. A., Jr., C. W. Landsea, M. Mayfield, J. Laver, and R. Pasch. 2005. Hurricanes and global warming. *Bull. Amer. Meteor. Soc.* November 2005: 1571-1575.

Powell, M., G. Soukup, S. Cocke, S. Gulati, N. Morisseau-Leroy, S. Hamid, N. Dorst, and L. Axe. 2005. State of Florida hurricane loss projection model: Atmospheric science component. *J. Wind Engineering and Industrial Aerodynamics* 93: 651-674.

Resio, D. T. 2007. "White paper on the joint probability method with optimal sampling. Coastal and Hydraulics Laboratory, ERDC, Vicksburg, MS.

Resio, D. T., and E. A. Orelup. 2006. Potential effects of climatic variability in hurricane characteristics on extreme waves and surges in the Gulf of Mexico, submitted to *J. Climate*.

Russell, L. R. 1971. Probability distribution for hurricane effects. *J. Wtrwy., Harb. and Coast. Engrg. Div., ASCE,* 97(1): 139-154.

Scheffner, N. W., L. E. Borgman, and D. J. Mark. 1996. Empirical simulation technique based storm surge frequency analyses. *J. Wtrwy., Port, Coast., and Oc. Engrg.* 122(2): 93-101.

Schwerdt, R. W., F. P. Ho, and R. R. Watkins. 1979. Meteorological criteria for standard project hurricane and probable maximum hurricane windfields, Gulf and East Coasts of the United States. Tech. Rep. NOAA-TR-NWS-23. National Oceanic and Atmospheric Administration.

Schwerdt, R. W., F. P. Ho, and R. R. Watkins. 1979. *Meteorological criteria for Standard Project Hurricane and Probable Maximum Hurricane Windfields, Gulf and East Coasts of the United States.* Tech. Rep. NOAA-TR-NWS-23. National Oceanic and Atmospheric Administration.

Simpson, J., R. F. Adler, and G. R. North. 1988. A proposed tropical rainfall measuring mission (TRMM) satellite. *Bulletin of the American Meteorological Society* 69:278-295.

TAW. 2002. "Technical Report Wave Run-up and Wave Overtopping at Dikes," Technical Advisory Committee of Flood Defence, The Netherlands Government, Delft.

Thompson, E. F., and V. J. Cardone. 1996. Practical modeling of hurricane surface wind fields. *ASCE J. Waterway, Port, Coastal, and Ocean Engineering* 122(4): 195-205.

U.S. Army Corps of Engineers (USACE). 1972. New Orleans East Lakefront Levee Paris Road to South Point, Lake Pontchartrain. Barrier Plan, DM 2 Supplement 5B, New Orleans District, June.

U.S. Army Corps of Engineers. 1984. *Shore protection manual.* Washington, DC: U.S. Government Printing Office.

U.S. Army Corps of Engineers. 1999. Risk-Based Analysis in Geotechnical Engineering for Support of Planning Studies. Technical Letter ETL 1110-2-556.

U.S. Army Corps of Engineers. 2000. Unwatering plan of the Greater Metropolitan Area of New Orleans, LA. USACE New Orleans District.

U.S. Army Corps of Engineers. 2006. Interagency Performance Evaluation Task Force Draft Report on "Performance Evaluation of the New Orleans and Southeast Louisiana Hurricane Protection System," Draft Volume VIII – Engineering and Operational Risk and Reliability Analysis, USACE, Washington, DC. (1 June 2006). *https://IPET.wes.army.mil*

U.S. Army Corps of Engineers. 2006a. Performance evaluation of the New Orleans and southeast Louisiana hurricane protection system draft final report of the Interagency Performance Evaluation Task Force. U.S. Army Corps of Engineers Report.

U.S. Army Corps of Engineers. 2006b. Louisiana Coastal Protection and Restoration (LACPR) preliminary technical report – Appendix B – History of hurricane occurrences. U.S. Army Corps of Engineers New Orleans District Report.

U.S. Navy (USN). 1983. *Hurricane havens handbook for the North Atlantic Ocean*. Naval Research Laboratory: NAVENVPREDRSCHFAC TR 82-03 (modified August 2005). *http://www.nrlmry.navy.mil/port_studies/tr8203nc/0start.htm*

U.S. Senate. 2006. Hurricane Katrina: A nation still unprepared. Report to the Committee on Homeland Security and Government Affairs, U.S. Senate, Washington, DC.

Van Gelder, M. 2000. Statistical methods for risk-based design of civil structures. PhD diss., Delft University of Technology, Report No. 00-1, The Netherlands.

Van Ledden, M. 2007. "Wave overtopping IPET (draft)," Memorandum M002MVLED, Royal Haskoning Inc.

Van Manen, S. E., and M. Brinkhuis. 2005. Quantitative flood risk assessment for polders. *Reliability Engineering & System Safety* 90: 229-237.

Vanmarcke, E. H. 1977. Reliability of earth slopes. *Journal of the Geotechnical Engineering Division, ASCE, v. 103* (GT11): 1247-1265.

Vickery, P. J., and L. A. Twisdale. 1995a. Prediction of hurricane wind speeds in the United States. *J. of Structural Engineering* 121(11): 1691-1699.

Vickery, P. J., and L. A. Twisdale. 1995b. Wind-field and filling models for hurricane wind-speed predictions. *J. of Structural Engineering* 121(11): 1700-1709.

Vickery, P. J., P. F. Skerlj, and L. A. Twisdale. 2000. Simulation of hurricane risk in the U.S. using empirical track model. *J. of Structural Engineering* 126(10): 1222-1237.

Voortman, H. 2003. Risk-based design of large scale flood defence systems. PhD diss., Delft University of Technology, Report No. 02-3, The Netherlands.

Webster, P. J., G. J. Holland, J. A. Curry, and H.-R. Chang. 2005. Changes in tropical cyclone number, duration, and intensity in a warming environment. *Science* 309: 1844-1846.

Westerink, J. J., R. A. Luettich, A. M. Baptista, N. W. Scheffner, and P. Farrar. 1992. Tide and storm surge predictions using finite element model. *J. Hydraul. Eng. ASCE*, 118(10),1373-1390.

Westerink, J. J., R. A. Luettich, J. C. Feyen, C. Atkinson, M. D. Dawson, J. P. Powell, H. J. Roberts, E. J. Kubatko, and H. Pourtaheri. 2007. A basin to channel scale unstructured grid hurricane storm surge model as implemented for southern Louisiana. *Monthly Weather Review*, 135.

White House. 2006. The federal response to Hurricane Katrina: Lessons learned. *http://www.whitehouse.gov/reports/katrina-lessons-learned/*

Willoughby, H. E., and M. E. Rahn. 2004. Parametric representation of the primary hurricane vortex. Part I: Observations and evaluation of the Holland (1980) model. *Monthly Weather Review* 132: 3033-3048.